



Attractive Steric Interactions

By

Adebayo Samuel AUGUSTUS

A thesis presented to University College London in
partial fulfilment of the requirements for the degree of
Doctor of Philosophy

(1999)

University College London
Department of Chemistry
20, Gordon Street
London WC1H 0AJ

ProQuest Number: 10609061

All rights reserved

INFORMATION TO ALL USERS

The quality of this reproduction is dependent upon the quality of the copy submitted.

In the unlikely event that the author did not send a complete manuscript and there are missing pages, these will be noted. Also, if material had to be removed, a note will indicate the deletion.



ProQuest 10609061

Published by ProQuest LLC (2017). Copyright of the Dissertation is held by the Author.

All rights reserved.

This work is protected against unauthorized copying under Title 17, United States Code
Microform Edition © ProQuest LLC.

ProQuest LLC.
789 East Eisenhower Parkway
P.O. Box 1346
Ann Arbor, MI 48106 – 1346

In majority of organic molecules a few pairs of atoms would be so close to each other to repel but most will be separated by more than the sum of their van der Waals radii as a result of which they will attract, albeit weakly, and help lower the enthalpy of formation of the molecule. This attractive steric interaction is one of the causes of folding in molecules and this thesis is devoted to the study of such interactions by NMR spectroscopy and force field calculations.

We synthesised and investigated attractive steric interactions, principally, in hexasubstituted-benzenes and with some attention to monosubstituted cyclohexanes. The three types of hexasubstituted-benzene systems investigated are:-

- (i) The 1,3,5-trisubstituted-2,4,6-trimethylbenzenes, where the groups in the 1, 3 and 5 positions are CH_2X ($\text{X} = \text{Cl}, \text{Br}, \text{I}$ and Me).
- (ii) The 1,3-disubstituted-2,4,5,6-tetramethylbenzenes, where the groups in the 1 and 3 positions are CH_2X or CH_2Z . Here X and Z ranged from a small atom or group such as $-\text{Cl}$, $-\text{CH}_3$, to bulky groups such as 1-adamantyl, *tert*-butyl, naphthyl, xylyl, phenyl, iodine e.t.c.. In some of the compounds, $\text{X} = \text{Z}$ and for others, $\text{X} \neq \text{Z}$.
- (iii) The 1,4-disubstituted-2,3,5,6-tetramethylbenzenes, where the groups in the 1 and 4 positions are CH_2X ($\text{X} = \textit{tert}$ -butyl, chlorine, bromine and iodine).

Each one of these compounds has two major conformations, the *syn* and the *anti*. In the *syn* conformation all or both the X groups as in (i) and (iii), and both the X and Z groups as in (ii), lie on the same side of the ring plane and a 180° rotation about a $\text{Ar-CH}_2\text{X}$ or $\text{Ar-CH}_2\text{Z}$ bond should give the *anti* form. In each of these compounds we were able to slow down rotation about both bonds on the NMR time scale and determine whether or not the more compact *syn* form is the more populated and therefore more stable relative to the *anti*. The barrier to rotation about the $\text{Ar-CH}_2\text{X}$ and $\text{Ar-CH}_2\text{Z}$ bonds is also discussed.

In majority of the compounds, with the exception of a few such as the 1-(halomethyl)-3-neopentyl-2,4,5,6-tetramethylbenzenes and the 1,4-disubstituted-2,3,5,6-tetramethylbenzenes, dynamic NMR spectroscopy show that the more compact *syn* conformations is more stable relative to the *anti*. The best results were obtained for the 1-neopentyl-2,4,5,6-tetramethylbenzenes {type (ii)}, where $\text{X} = \textit{tert}$ -butyl and $\text{Z} = \alpha$ -naphthyl, β -naphthyl or phenyl. In each of the three compounds, molecular mechanic calculations also show that the more compact *syn* form benefits substantially, relative to the *anti*, from the pair wise atom-atom van der Waals interactions between the X and Z groups.

In most of the compounds investigated calculation shows that the interlocking arrangement of the methyl and methylene groups on the main benzene ring, a process referred to as "gearing", favours one conformation over the other. Thus, in compounds where experiments indicate that the *syn* is the more stable, one has to be cautious in attributing the difference in enthalpy in its entirety to attractive steric interactions between the X and Z groups.

In the cyclohexylethynyl derivatives, the less compact *equatorial* conformation was found to be the more stable relative to the *axial* form, presumably, because the total of the attractive steric interactions between the methylene groups from the ring and the substituent is not high enough to offset the equatorial advantage from 1,3-diaxial interaction.

Dedication

Throughout my education, my family has been very supportive and has always been my source of inspiration, for which I am very grateful and it is to them that I dedicate this work.

Acknowledgements

Firstly, I would like to thank my supervisor, Dr J. E. Anderson for giving me the opportunity to undertake this project and for his support and guidance throughout the duration of this project.

Thanks are also due to the present and past members of the “Anderson’s group”, this includes Tony, Rima, Dorina and Jorge for their help and friendship. I also wish to acknowledge the contribution of Ms Dorina Voulgari who synthesised the 1,4-disubstituted-2,3,5,6-tetramethylbenzenes that were used in this work.

My thanks also to the “Ganellin’s group” for their friendship and for allowing me to use their instruments. I am especially indebted to Henny, for his useful advice on synthetic chemistry.

I wish to acknowledge with thanks, Dr Jonathan Steed of Kings College London for obtaining the X-ray crystallography structures that were used in this thesis.

Finally, I would like to thank the Engineering and Physical Sciences Research Council for the award of a postgraduate research studentship.

CONTENTS

Abstract	2
Acknowledgements	4

CHAPTER ONE

General Introduction

1.1	Introduction	9
1.1.1	van der Waals interactions	9
1.1.2	Preference of folded conformations in certain molecules	11
1.1.3	Axial vs equatorial in monosubstituted cyclohexanes	15
1.1.4	Determination of conformational population ratio using NMR	17
1.1.5	Molecular Mechanics Calculations	20
1.2	Aims and Objectives	22
1.2.1	Attractive steric interactions in highly substituted benzenes	22
1.2.2	Attractive steric interaction in monosubstituted-cyclohexanes	25

CHAPTER TWO

Attractive steric interactions in 1,3,5-tris(halomethyl)-2,4,6-trimethylbenzenes and 1,3,5-triethyl-2,4,6-trimethylbenzene

2.1	Introduction	28
2.2	Results and discussion	31
2.2-1	Conformational assignment of NMR signals at low temperature	31
2.2-2	MM3 Calculations	36
2.3	Conclusion	42
2.4	Synthesis	43

CHAPTER THREE

Attractive steric interactions in 1,3-disubstituted-2,4,5,6-tetramethylbenzenes, where the two substituents are identical

3	Introduction	48
	Section One (substituents:- neopentyl and halomethyl groups)	
3.1.1	Results and discussion	51
3.1.1-1	Conformational assignment of NMR signals at low temperatures	51
3.1.1-2	MM3 calculations	60
3.1.2	Conclusion	66
	Section Two (substituents:- ethyl, β -naphthylmethyl, benzyl and p-nitrobenzyl groups)	
3.2.1	Results and discussion	68
3.2.1-1	Conformational assignment of NMR signals at low temperatures	68
3.2.1-2	MM3 calculations	72

3.2.2	Conclusion	75
	Section three	
3.3	Synthesis	77

CHAPTER FOUR

Attractive steric interactions in 1,3-disubstituted-2,4,5,6-tetramethylbenzenes, where the two substituents are non-identical

4	Introduction	89
	Section One (one of the substituent is a neopentyl group)	
4.1.1	Results and discussion	92
	4.1.1-1 Conformational assignment of NMR signals at low temperatures	92
	4.1.1-2 MM3 calculations	104
	4.1.1-3 X-ray analysis {1-(α -naphthylmethyl)-3-neopentyl-2,4,5,6-tetramethylbenzene}	111
4.1.2	Conclusion	112
	Section Two (one of the substituent is a benzyl group)	
4.2.1	Results and discussion	115
	4.2.1-1 Conformational assignment of NMR signals at low temperatures	115
	4.2.1-2 MM3 calculations	120
4.2.2	Conclusion	124
	Section Three (one of the substituent is an ethyl group)	
4.3.1	Results and discussion	125
	4.3.1-1 Conformational assignment of NMR signals at low temperatures	125
	4.3.1-2 MM3 calculations	128
4.3.2	Conclusion	130
	Section Four	
4.4	Synthesis	132

CHAPTER FIVE

Attractive steric interactions in 1,4-dineopentyl-2,3,5,6-tetramethylbenzene and the 1,4-bis(halomethyl)-2,3,5,6-tetramethylbenzenes

5.1	Introduction	153
5.2	Results and discussion	154
	5.2.1 Conformational assignment of NMR signals at low temperatures	154
	5.2.2 MM3 calculations	159
	5.2.3 X-ray analysis (1,4-dineopentyl-2,3,5,6-tetramethylbenzene)	164
5.3	Conclusion	165
5.4	Synthesis	166

CHAPTER SIX

Barriers to rotation in hexasubstituted-benzenes

6.1	Introduction	171
6.2	Results	172
6.3	Conclusion	182

CHAPTER SEVEN

Attractive steric interactions in monosubstituted cyclohexanes

7.1	Introduction	185
7.2	Results and discussion	187
7.3	Conclusion	190

GENERAL INFORMATION

Experimental Considerations	198
Abbreviations	200
References	201

General Introduction

(1.1) Introduction

Organic chemists usually consider a molecule as being more stable when the bulkiest groups are as far apart as bond rotation will allow, for a molecule is best stabilised when repulsive interactions are at a minimum. With this approach little or no consideration is given to attractive steric interactions between the bulky groups. Attractive steric interactions are mainly van der Waals type interactions between closed shell atoms. Such interactions are a major cause of folding in molecules, so an understanding of how they operate is desirable.

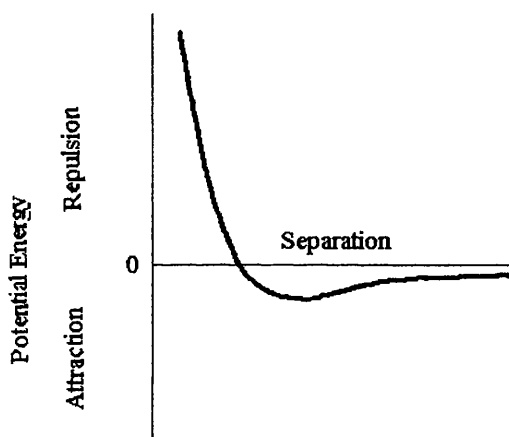


Figure 1.1. The Lennard-Jones potential energy level diagram for two atoms not bonding.

(1.1.1) van der Waals interactions¹

When two neutral atoms come close to one another the various interactions between the electrons(s) and the nucleus of one atom and the electron(s) and the nucleus of the other produces a potential energy of interaction that is best represented by the Lennard-Jones potential energy level diagram (figure 1.1).

When the atoms, which are not forming a bond, are in close proximity the repulsive force dominates the attractive force. With increased separation repulsion decreases more rapidly than attraction so beyond a certain intermediate distance the atoms attract and the potential of the interaction is negative. At large distances the attraction approaches zero. As shown in the diagram repulsion is short ranged whilst attraction is long ranged. Although the general shape of the curve shown in figure 1.1 is accepted as a true representation of van der Waals interactions, information such as the radius and depth of the well are not precisely known and that is one justification for carrying out

experiments. The non-bonded interactions between two or more atoms or molecules, are all ultimately electrostatic and are called **van der Waals** interactions. A number of terms are involved in the van der Waals interactions.

a. Dipole-Dipole interactions

Dipole-dipole interactions are found in species with permanent dipole moments. The energy of interaction of two dipoles in a fixed orientation is simply

$$E = -\frac{\mu_1 \mu_2 f}{4\pi \epsilon_0 R^3}, \quad \text{with } f = 1 - 3\cos^2 \theta$$

where μ_1 and μ_2 are the permanent dipole moments, R is the separation of the two dipoles and θ is the orientation angle of the dipoles. When the dipoles are free to rotate, the potential energy is proportional to R^{-6}

b. Dipole-Induced dipole interactions

The dipole moment μ of a polar species A, can create an electric field which then polarises an otherwise non-polar species B, generating an induced dipole moment of magnitude $\mu\alpha$ in specie B, where α is the polarizability of B. The potential energy of such interaction is given as

$$E = -\frac{4\alpha}{(4\pi \epsilon_0)^2} \mu^2 R^{-6}$$

c. Induced dipole-Induced dipole interactions

Even in species with no permanent dipole, instantaneous dipoles are generated because of fluctuation in the electron distribution. The electrons in the two (or more) non-polar species, synchronise their movements to minimise electron-electron repulsion and to maximise electron-nucleus attractions. The attractive force generated by these interactions, sometimes called London force or dispersion force are short ranged and weak. The potential energy of such attractive interactions is:

$$E = -\frac{2}{3} \alpha_1 \alpha_2 \frac{I_1 I_2}{I_1 + I_2} R^{-6}$$

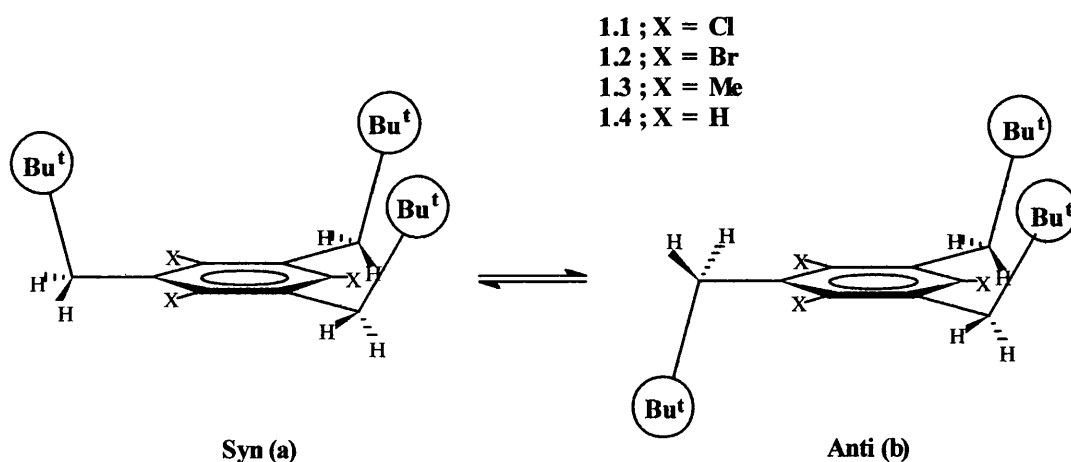
Where α_1 and α_2 are the polarisability volume and I_1 and I_2 are the first ionisation energies of the two atoms.

(1.1.2) Preference of folded conformations in certain molecules.

Attractive steric interaction is a feature of all but the smallest of molecules. In almost all molecules a few pairs of atoms will be so close to each other to repel but most will be separated by more than the sum of their van der Waals radii. All such pairs will thus weakly attract and help to lower the overall enthalpy of formation of the molecule. Clearly the sum of such attractive interactions will differ in different conformations. Due to recent developments in spectroscopic and computer techniques, it has become clearer that in certain molecular environment, the conformations in which bulky groups are near enough to maximise attractive interactions, but not so near as to repel each other may be preferred over another similar conformation in which the bulky groups are far apart, so that the attractive interactions are reduced.

Evidence of the stabilisation produced by attractive steric interactions is not often encountered in the literature. A literature survey has been carried out and a few examples are presented below. These all involve conformational equilibrium that can be slowed down on the NMR time-scale and so can be measured directly, and where the difference between the two sides of the equilibrium can be attributed to attraction.

The trineopentylbenzenes **1.1**, **1.2**, **1.3** and **1.4** each has two major conformations



the *syn* and *anti* conformations. In the *syn* conformer the three *tert*-butyl groups are on the same side of the ring plane whereas in the *anti* conformer two of the *tert*-butyl groups are situated on one side and the third on the other side of the ring plane.

Dynamic NMR analysis of **1.1**, **1.2** and **1.3** in chloroform-*d* and carbondisulfide showed separate signals for *syn* and *anti* just below room temperature and also revealed^{2,3} that in compounds **1.1-1.3** the more compact *syn* conformation, where the three *tert*-butyl groups are closer together, is more stable relative to the *anti*. The NMR results in chloroform-*d* are shown in table 1.1. It is worth pointing out that since there are six equivalent versions of the *anti* yet only two versions of *syn*, any conformation of the *anti* is three times more populated than any conformation of the *syn*. Therefore in order to show the extent of the dominance of the *syn* conformation in the equilibrium one has to multiply the population ratios given in the table by a factor of three.

Table 1.1. The conformational population ratio of the trineopentyl compounds in chloroform-*d*.

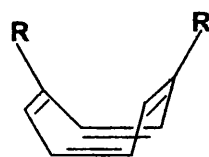
X	Temperature / °C	Population ratio ^a
Cl (1.1)	-20	2.1
Br (1.2)	-10	2.5
Me (1.3)	-40	3.2

^a The conformational population ratio is that between the *syn* and *anti*.

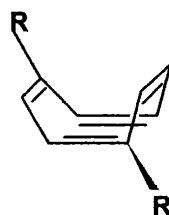
Investigation of **1.3** and **1.4** by molecular mechanics calculation revealed⁴ that the *syn* conformation is 1.4 and 0.91 kcal mol⁻¹ respectively more stable than the *anti* conformation. The extra stability of the *syn* conformer in the four molecules was attributed almost entirely to the stabilising intramolecular attractive forces between the three *tert*-butyl groups. These interactions are smaller in the *anti* conformation because here one of the *tert*-butyl groups is far from the other two.

X-ray crystallography determination of the molecular structure of **1.2** show⁵ evidence of intramolecular and intermolecular attractive steric interactions. Each unit cell consists of a 1:1 ratio of the *syn* and *anti* conformations.

It was recently shown^{6,7} that the 1,6-disubstituted cyclooctatetraenes (**a**) equilibrates with the 1,4-isomer (**b**) by a bond shift process slow enough on the NMR time scale to allow direct measurement of the relative populations of the two isomers. In the di-*t*-butyl compounds,⁶ the 1,6-isomer (**1.6a**) with the *t*-butyls close together in space is more stable than the 1,4-isomer (**1.6b**). The ratio of populations is 2.08:1 at 25 °C in deuterated chloroform solution, representing a free energy difference of 0.43 kcal mol⁻¹ in favour of (**1.5a**). For the corresponding dimethyl isomers (**1.5a**) and (**1.5b**), NMR analysis



(a)



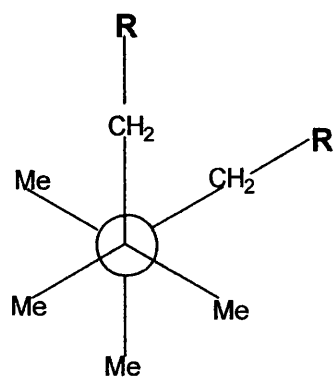
(b)

1.5 ; R = Me
1.6 ; R = C(CH₃)₃.

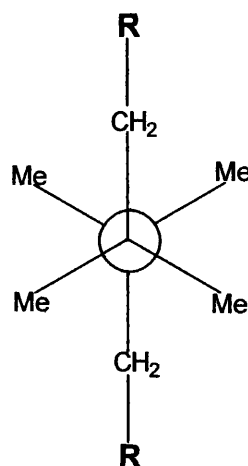
showed⁸ the 1,6-isomer to be 0.081 kcal mol⁻¹ more stable than the 1,4-isomer at 20 °C in perdeuteriobenzene solution.

Results from molecular mechanic calculations agree closely with the experimental results. The trend in magnitude of the van der Waals attractive interactions reflects the total number of interactions between the **R** groups: with two *t*-butyl substituents there are 169 (the square of the number of atoms) mutual interactions, while with two methyl substituents, there are 16 i.e. (4 x 4) mutual interactions. This was confirmed to be the case when the population of the isomers when **R** = Me, Et, ^{*i*}Pr or ^{*t*}Bu were measured and analysed⁹ by molecular mechanics calculations. The energy difference between the two isomers was found to be Me (0.08), Et (0.24), ^{*i*}Pr (0.36) and ^{*t*}Bu (0.43) kcal mol⁻¹ in favour of the 1,6-isomer.

The unforeseen folding observed in the series of molecules with the general formula RCH₂C(Me)₂-C(Me)₂CH₂R has also been attributed to long range attractive steric interactions.¹⁰ The bond of interest in the molecule is the central carbon-carbon bond. Experimental study of the equilibrium along this bond showed that the conformation with RCH₂ groups *gauche* to one another (1.7) is 0.08-0.2 kcal mol⁻¹ more stable than the *anti* conformation (1.8). Groups **R** are *anti* to the central bond to avoid repulsive interactions along that bond, but once they are *anti* then the larger groups CH₂R prefer to be *gauche*. The extra stability of the *gauche* conformation is attributed¹¹ to a greater level of attractive steric interactions between the two **R** groups when they are closer together but not too close to repel.

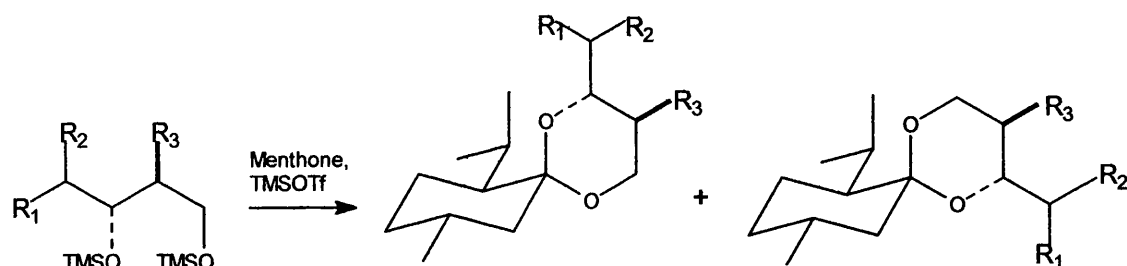


(1.7)



(1.8)

The products of the acetalization reaction of racemic bis(trimethylsilyl) ethers **1.9** with racemic menthone was shown¹² to be the spiroacetals **1.10** and **1.11**. The reaction was also shown to be thermodynamically controlled¹³ with high temperatures favouring the formation of **1.10** over **1.11**. But more interesting is the fact that while the reaction of the silyl ether when $R_1 = R_2 = R_3 = H$ was less selective, the stereoselectivities¹³ were increased with an increase in the size of R_1 and R_2 see table **1.2** The ratios being 4.1:1 ($R_1 = R_2 = Me, R_3 = H$); 5.4:1 ($R_1 = t\text{-Bu}, R_2 = R_3 = H$) and



(1.9)

(1.10)

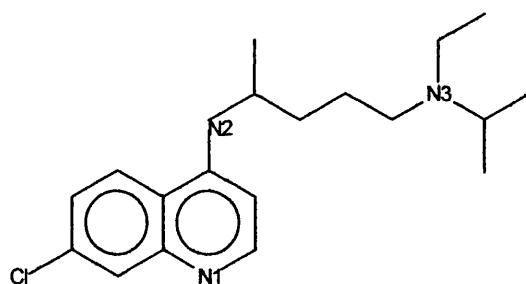
(1.11)

Table **1.2** acetalization of bis(trimethylsilyl) ethers **1.9a-d** with racemic menthone in methylene chloride and chloroform at -40°C .

Compound	R_1	R_2	R_3	Ratio (1.10:1.11)	
				CH_2Cl_2	CHCl_3
a	H	H	H	1.2	-
b	Me	Me	H	3.5	4.1
c	<i>t</i> -Bu	H	H	3.5	5.4
d	$-(\text{C}_2\text{H}_5)-$		Me	5.4	7.8

7.8:1 ($R_1 = R_2 = -(C_2H_5)-$, $R_3 = Me$) in favour of **1.10** in chloroform at $-40\text{ }^{\circ}C$. The correlation between the observed stereoselectivities and the size of the R groups was explained in terms of an enhanced attractive steric interactions between the substituents on the 1,3 dioxan ring and the menthane moiety in **1.10**. These interactions are much reduced in **1.11** because of the relatively higher interatomic distances. The results from force field calculations is in good agreement with the observed ratios. The calculated ratio of **1.10d:1.11d**, based on a Boltzmann distribution of the stable conformers at $-40\text{ }^{\circ}C$ is 6.0:1. For **1.10c:1.11c** and **1.10b:1.11b** the ratios were 5.2:1 and 3.8:1 respectively.

Determination of the spatial geometry of chloroquin (1.12) an antimalarial in acetone at $20\text{ }^{\circ}C$ by PMR revealed¹⁴ that the molecule exist in a compact conformation. The extent of the compactness is given by a N1-N3 separation of 7.39 \AA , a distance almost 7.0 \AA less than in the crystalline state of the diprotonated species. The difference



(1.12)

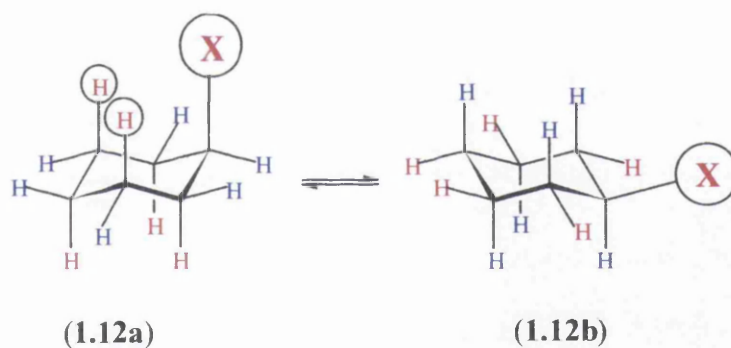
between the crystal and solution conformations is not surprising. Electrostatic repulsion between the positive charges would tend to force the molecule to adopt a more open structure in the crystal, hence the large N1-N3 separation. However, the small N1-N3 separation observed in solution was attributed mainly to intramolecular dipole-induced dipole attractive interaction between the N3 ethyl groups and the pi electrons of the quinoline ring.

(1.1.3) *Axial vs Equatorial* in monosubstituted cyclohexanes

Following van't Hoff's proposal of a tetrahedral geometry for methane¹⁵ in 1875, Sachse proposed two conformations for cyclohexane that are free of angle strain.¹⁶ One is a

flexible conformation capable of adopting the boat form and the other is a rigid chair conformation. He also predicted that the *axial* and *equatorial* hydrogens are in different molecular environments and that it should be possible to isolate the *axial* and *equatorial* isomers in monosubstituted cyclohexanes. But after several unsuccessful attempts to isolate the two isomers, in 1918, Mohr correctly advanced the idea that cyclohexane has a flexible conformation capable of interconverting one chair conformation with another via boat and twist,^{17,18} thus equilibrating the *axial* and *equatorial* protons.

Much modern work has focused on determining the conformational preference in monosubstituted cyclohexanes. In the vast majority of monosubstituted cyclohexanes, the **X** substituent has a preference to adopt the *equatorial* position. The lower stability of the *axial* orientation (see **1.12a**) is often rationalised in terms of an enhanced "1,3 diaxial interactions" between the *axial* substituent and the two *syn-axial* hydrogens at the three and five positions of the ring. These interactions are very low in the *equatorial* orientation (see **1.12b**).



The *axial*/*equatorial* population ratios for a wide range of substituents have been measured and tabulated,¹⁹ only six substituents where *axial* is preferred over *equatorial* is encountered in the literature, (see table **1.3**) and in all these compounds a mercury atom is directly bonded to the cyclohexane ring.

An *axial*/*equatorial* ratio of approximately zero was first reported for the bromomercury²⁰ and acetoxymcury groups.²¹ The former was measured by chemical equilibration of the *cis*- and *trans*-4-methylcyclohexylmercuric bromides in pyridine and the latter by direct ¹H NMR measurements at 194 K. The accuracy of this results were undermined by the decomposition of the bromomercury compound during the equilibration process and the use of low frequency ¹H NMR (100 MHz) machines which gives poorly resolved spectra. A re-investigation of these groups by Anet and Kitching

with a high field ^1H (251 MHz) and ^{13}C NMR at 183-193 K revealed a small but consistent preference for the *axial* conformer.²²

The *axial/equatorial* population ratio for HgCl ,²² HgCN ,²³ HgPh ,²³ and HgH ²⁴ groups (see table 1.3) have been determined and they all show a slight preference for the *axial* conformer.

Table 1.3. The free energy difference between the *axial* and *equatorial* conformations.

Substituents (X)	Solvent	ΔG^a (Temp/K)	Reference
HgOAc	Pyridine	-0.17 (183)	22
	CDCl_3	-0.30 (183)	22
HgCl	CDCl_3	-0.25 (183)	22
HgBr	Pyr	-0.09 (368)	22
HgCN	CD_2Cl_2	-0.14 (193)	23
HgH	Pyr/ CD_2Cl_2	-0.20 (193)	24
HgPh	Pyr/ CD_2Cl_2	-0.14 (193)	23

^a The energy difference in kcal mol^{-1} is in favour of the *axial* conformation.

The preference for the *axial* conformer in the cyclohexylmercuric equilibria was attributed to, firstly, a reduced 1,3 *diaxial* interactions in the *axial* conformation because of the long C-Hg bond and secondly to the van der Waals attractive interactions between the highly polarisable mercury atom and the methylene groups on the cyclohexane ring. These attractive interactions are much more reduced in the *equatorial* conformer because here the *equatorial* mercury atom is far from the methylene groups on the ring. Putting it another way the *equatorial* conformation is elongated while the *axial* is somewhat folded.

(1.1.4) Determination of conformational population using NMR spectroscopy

Often the different conformers of a molecule in equilibrium will have distinct physical and spectral properties that may be used to determine their relative population. NMR, infrared, X-ray and electron diffraction, together with dipole moments are all techniques that may be used to study dynamic processes. An account of the uses of these techniques in the determination of conformational population is given in some textbooks.²⁵ NMR is the most widely used and will be discussed in this chapter.

a. *Direct ^1H and ^{13}C NMR measurements:* When the rate of interconversion between conformers in equilibrium is rapid on the NMR time scale, as is often the case with processes involving rotation about single bonds at ambient temperature, only one set of signals is observed. The observed chemical shifts (δ) and coupling constants (J) are averaged over all conformations:²⁶

$$\delta = \sum n_i \delta_i \quad \dots\dots\dots(\text{I})$$

$$J = \sum n_i J_i \quad \dots\dots\dots(\text{II})$$

δ_i and J_i are the chemical shifts and coupling constants of the i th conformer and n_i the corresponding mole fraction. However, if the interconversion process is "slow on the NMR time scale," as often happens at low temperatures, separate sets of signals are observed for each of the different conformational isomers. A process is said to be "slow on the NMR time scale" when the frequency of interconversion between conformers or rotamers is less than the frequency separation of the signals originating from the individual conformers. It is also feasible that when the interconversion barrier is high the spectral lines for each conformer will appear separately at ambient, in which case it will be necessary to warm the sample to get the spectral lines to coalesce.

At temperatures well below the coalescence point the population ratio of the conformers may be determined directly from the relative signal intensities of the conformers. And with knowledge of the conformational population, the equilibrium constant (K) and the difference in Gibbs free energy (ΔG) for the process may be calculated using the equation:

$$\Delta G = - R T \ln K \quad \dots\dots\dots(\text{III})$$

The energy barriers to rotation about single bonds or to ring inversion, i.e. the energy of activation (ΔG^\ddagger /cal mol⁻¹) may be calculated at any of a range of temperatures where the separation shows kinetic broadening, but most easily at the temperature (T_c /K) at which signals just coalesce using the equation:

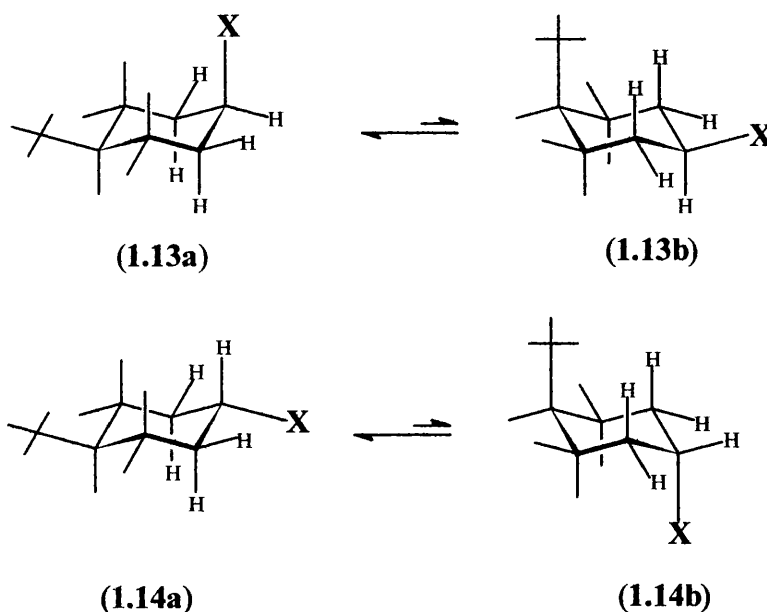
$$\Delta G^\ddagger = 1.987 T_c (23.788 + \ln T_c - \ln k_c) \quad \text{.....(IV)}$$

$$\text{where } k_c = \frac{\pi \Delta \nu}{\sqrt{2}} \quad \text{.....(V)}$$

k_c is the rate constants at the coalescence point and $\Delta \nu$ in Hz is the frequency of separation of the two emerging signals originating from the different conformers. Equation (V) assumes the two conformations in equilibrium are equally populated.

b. *Indirect methods using chemical shifts and coupling constants:* It is desirable to measure ΔG at 25 °C, because most physical, spectral and pharmacological properties are dealt with around this temperature. When separate sets of well-resolved signals are observed for each of the different conformers (well below the coalescence), the chemical shifts for nuclei and the coupling constants between two appropriate nuclei can be determined for the individual conformers. In principle, with knowledge of the coupling constants and the chemical shifts of the individual conformers, application of equation (I) and (II) to the averaged spectrum seen well above the coalescence temperature should give the conformational composition. However, chemical shifts are sensitive to changes in temperature in a way that may be difficult to allow for reliable result from equation (I). And attempting a temperature extrapolation is not often successful because it is usually the case that reliable chemical shifts for the individual conformers can only be obtained over a short range of temperatures. On the other hand, the sensitivity of coupling constants from individual conformers to changes in temperature is usually negligible, thus the application of equation (II) to circumstances well above the coalescence temperature gives reliable results.

Coupling constants for individual conformers have also been obtained indirectly from "conformationally locked" model compounds. These are compounds confined to a single conformation. A popular example is in the conformational analysis of monosubstituted cyclohexane derivatives, where the 4-*tert*-butyl-substituted compounds (1.13a) and (1.14a) are used as model compounds.²⁷



The presence of the 4-*tert*-butyl group virtually locks the conformational equilibrium in favour of the isomers where the butyl group occupies the *equatorial* position. The methine *eq-eq* and *eq-ax* proton-proton coupling constants may be obtained from **1.13a** whereas the methine *ax-eq* and *ax-ax* may be obtained from the **1.14a** isomer. The assumption in this method is that the *tert*-butyl group has no intrinsic effect on the coupling constants being measured.

Some important generalities in the study of cyclohexyl derivatives using ^1H NMR spectroscopy²⁸ are that the *equatorial* protons generally resonate downfield from the *axial* protons and because of the operation of the Karplus relationship,²⁹ the *axial* protons generally show larger splitting than *equatorial* protons, this is because unlike *equatorial* protons, *axial* protons generally have other protons anti-periplanar to them, and thus show a large 180° coupling.

(1.1.5) Molecular Mechanics Calculations

Molecular mechanics calculations provide a practical method for exploring the conformations adopted by a wide range of molecules. It gives the energies associated with each conformation as well as other information such as bond length distance between pair of atoms. The Allinger approach³⁰ gives the "excess energy" of a molecule. The excess energy also called "steric energy" or "strain energy" is the difference between the energy of the real molecules and that of a hypothetical strain-free molecule. In this project the force

field program that will be used for calculating structures is the "MM3 94 program"³¹, that was developed by Allinger.

In MM3 94, the computer program is set to take the total steric energy (E_T) of a molecule as the sum of the following terms: the total energy due to bond stretching and compression energy ($\Sigma E_{stretch}$), the total energy due to bond angle deformations (ΣE_{bend}), the total energy increment due to changes in torsional angles from their optima ($\Sigma E_{torsion}$), the total energy (van der Waals type) due to interactions between non bonded atoms (ΣE_{vdw}) and the total energy arising from the interaction of dipoles. This may be expressed mathematically as:

$$E_T = \Sigma E_{stretch} + \Sigma E_{bend} + \Sigma E_{torsion} + \Sigma E_{vdw} + \Sigma E_{dipolar} + \text{Cross terms} \dots (I)$$

The assessment of the individual terms in the equation is by the "empirical force field method". Reliable simple mathematical equations are derived to express each of these different energy terms. To obtain the force field a few simple molecules whose structures and vibrational energies are well known are selected and the equation is parameterised in such a way that the program reproduces the energies obtained experimentally for these structures.

If the potential energy of a molecule is to be determined, a rough set of geometrical co-ordinates for each of the atoms in the molecule is fed to the computer. The computer then calculates the magnitude of each of the components in equation (I) and then sums these to obtain the steric energy of the initial structure. The computer then goes through a minimisation process by continuously changing the geometry slightly and then selecting the one that gives the lowest energy. The process continues until all further distortions in geometry results in an increase in the total steric energy. The total steric energy and the atomic co-ordinates at this point are then computed.

A problem that may arise is that the structure exploration may end up in a local minima which doesn't represent the lowest minima of the molecule. To overcome this problem, the computer may be deliberately driven to perform rotation about an appropriate bond in the minimised structure and to find a deeper minimum.

It is worth pointing out at this stage that the difference in steric energies between two conformations, is effectively the difference between their standard enthalpy of

formation (ΔH°). ΔH is related to the difference in Gibbs free energy (ΔG) by equation (II), where T is the temperature and ΔS is the difference in entropy. Whilst calculation

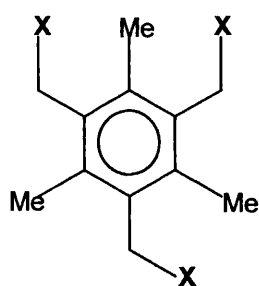
$$\Delta G = \Delta H - T\Delta S \quad \dots\dots\dots\text{(II)}$$

leads to ΔH° , results from NMR using the conformational population ratio leads to ΔG .

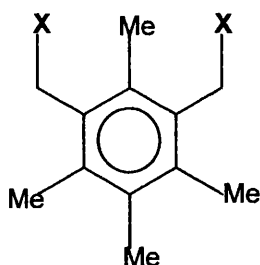
(1.2) Aims and Objectives

We seek to investigate attractive steric interactions in two systems, principally the hexa-substituted benzenes but with some attention to monosubstituted cyclohexanes. In this project, an attempt is made to quantify attractive steric interactions and to compare the experimental results with those obtained from force field calculations.

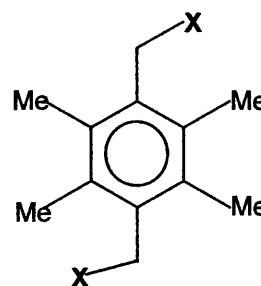
(1.2.1) Attractive steric interactions in hexa-substituted-benzenes



(1.15)



(1.16)



(1.17)

The series of molecule (1.15), (1.16) and (1.17) would be expected to exist in two major conformations, the *syn* and *anti* (see figure 1.2). In the *syn* conformation all the X groups, three in the case of the 1,3,5-trisubstituted and two in the cases of the 1,3-disubstituted and 1,4-disubstituted compounds all lie on the same side of the ring plane. A 180° rotation about any of the C-CH₂X bonds should give the *anti* conformation. In this project we report which of the two conformations is more stable and how the nature of X and solvent polarity affect this.

An important factor that may affect the *syn/anti* equilibrium is the direct steric interaction between the X groups. These groups seem to be too far apart to have repulsive steric interactions so there should be small stabilising attractions. Therefore in compounds 1.15, 1.16, and 1.17 the more compact *syn* conformation, where the three X groups are closer together for better mutual attraction, would be expected to be relatively more stable than the *anti* conformation.

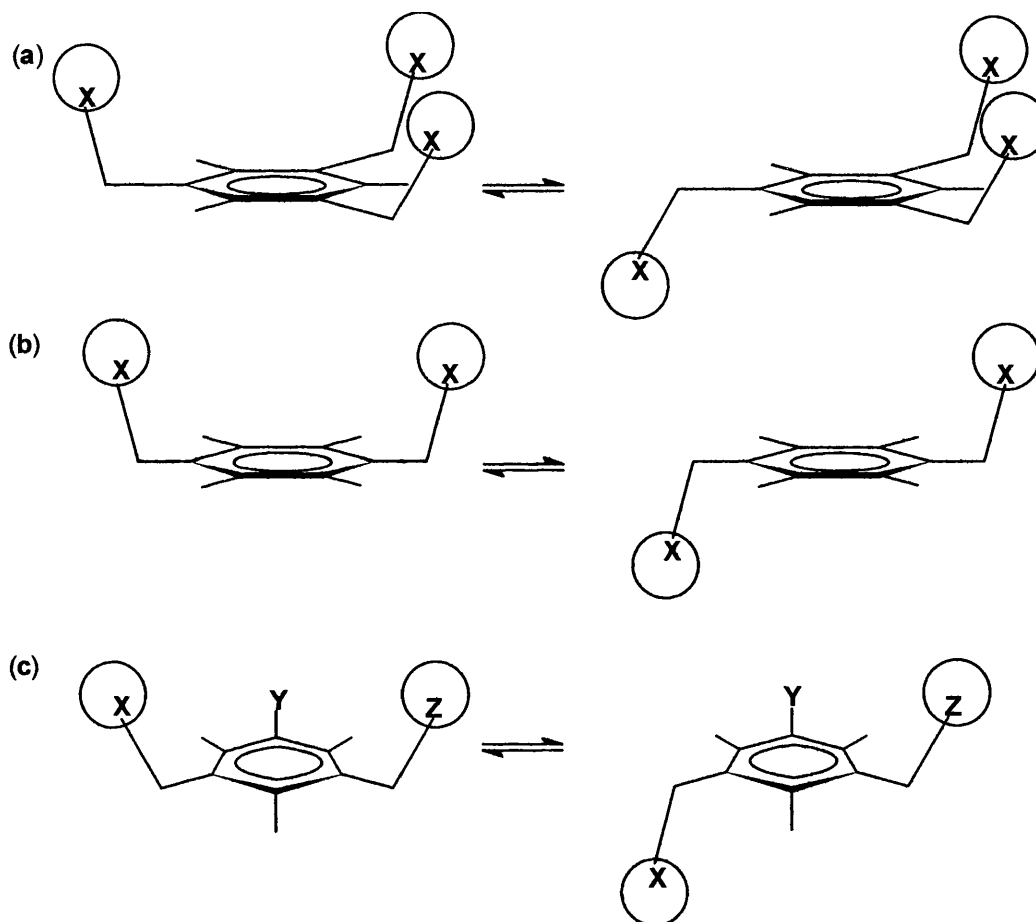


Figure 1.2. The *syn* and *anti* conformations of 1.15, 1.16 and 1.17.

It has been shown that the preferred conformation in hexamethylbenzene³² and hexaethylbenzene³³ has successive up and down arrangement of C-X bonds (X is either H or Me), see figure 1.3, with the CH₂X group meshed together to minimise repulsive interactions a process referred to as *gear effect*. It is plausible to speculate that such 'self organisation' should have an effect on the *syn/anti* equilibrium of the molecules under investigation.

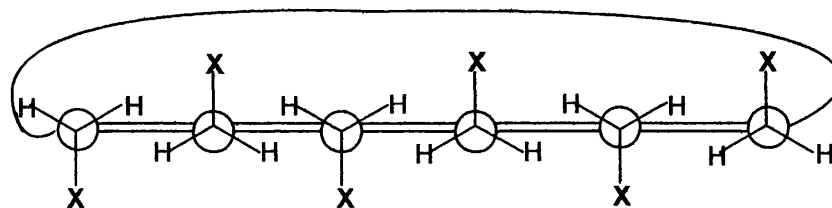


Figure 1.3 Diagram showing the preferred conformation adopted by hexamethylbenzene ($X = H$) and hexaethylbenzene ($X = Me$).

The remaining factor that may affect the *syn/anti* equilibrium is the repulsive interactions between the C-X bonds. If the C-X bonds are polarised, the *syn* arrangement of any two C-X bonds be they 1,3 or 1,4 is disfavoured, although the dipoles are somewhat less than parallel and are not necessarily anti-parallel when they are *anti*. Thus a polarised C-X bond would be expected to destabilise the *syn* conformation relative to the *anti*.

It is worth pointing out at this stage that the observed equilibrium constant (K) depends on entropy difference (ΔS) as well as enthalpy difference (ΔH) between conformations. In molecules containing six rotamers it is thus important to be aware of rotational entropy, this particularly the case for methyl groups. Rotation of these will be different in the two conformations in a way that is not easy to predict, but there is no doubt that because of the molecular structure, rotational freedom is considerably restricted in both conformations.

Using Allinger's MM3 94 program, we hope to calculate the minimum-energy structure and relative energy of the *syn* and *anti* conformations for the series of compound with the general formulae 1.15, 1.16 or 1.17. Considering for example the *syn* and *anti* conformations of 1.16, it may seem that such calculations should give reliable results for such simple molecules, but a little consideration suggest that this may be problematic.

Since the X, groups are not close to each other, their interactions are small yet the differences between conformations depend on correct calculations of these weak interactions. Insofar as dipole moment can be calculated and measured, polar interactions of benzylic halogen atoms ought to be reproducible, but there are problems. There are many small interactions that make up the total meshing network of six substituents around the benzene ring. The differences between *syn* and *anti* conformations plausibly involve many small contributions of similar size, and an overall

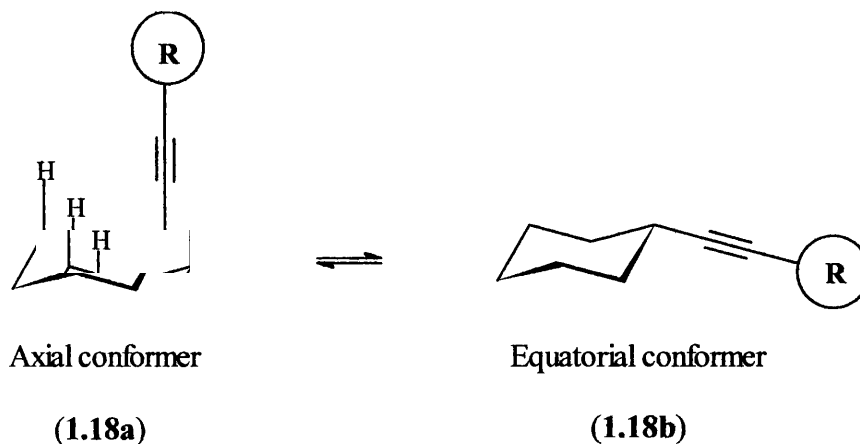
experimental energy difference which is small compared with many of these gearing interactions. That being so, the small difference between two quite large total sums may not be reliably reproduced by calculations.

Finally, there is the matter of the small attractive interactions between the X groups. There is no experimental evidence for the correct parameterisation of such interactions beyond a general feeling for what the format should be. The shortcomings of the MM3 program for calculating conformational situations involving such weak interactions of the attractive type and others of similar magnitude but repulsive of the buttressing type have already been demonstrated³⁴.

All these reservations about calculation's ability to distinguish small conformation effects mean that calculations are much more likely to predict the structure of *syn* and *anti* conformations reasonably correctly, than they are to predict the relative energies of the two conformations. We may hope however that we will learn something about the calculations by comparing them with our experimental measurements

(1.2.2) Attractive steric interactions in monosubstituted cyclohexane

In the majority of monosubstituted cyclohexanes, the *equatorial* conformer is more stable than the *axial* conformer. This trend is often rationalised in terms of the presence of 1,3 diaxial interactions in the *axial* conformer. This interaction is much more reduced in the *equatorial* conformer. Part of the aim of the project is to synthesise and investigate monosubstituted cyclohexanes, where the compact *axial* conformer is more stable.



The cyclohexane molecule is substituted in such a way that the atoms of the various groups to be investigated R are far (more than the sum of their van der Waals radii)

from the atoms of the cyclohexane ring. To achieve this, an acetylenic group is inserted between the ring and the **R** group. Because the group of atoms in the **R** group and those making up the cyclohexane ring are not so close to be repelling, one would expect the nature of their interaction to be one of attraction. Attractive steric interactions are stabilising forces and should reduce the enthalpy of formation of the conformations. However, the levels of attractive interactions are different in the two conformations.

The *axial* conformer is "L" shaped, with the **R** group positioned above or below the plane of the ring. In this arrangement, the atoms in the **R** group and those in the cyclohexane ring are closer together for better mutual attractive interactions. By contrast, attractive steric interactions are less in the *equatorial* conformation because here the two sets of atoms are too far apart.

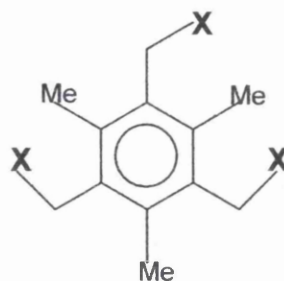
The axial conformation **1.18a** which favours attraction has nonetheless destabilising interactions of the acetylenic group with the 1,3-diaxial hydrogens. This is known^{35,36} to amount to 0.41-0.51 kcal mol⁻¹ in cyclohexaneacetylene. The question therefore is whether attraction between the **R** group and the cyclohexane ring in **1.18a** can even be great enough to counterbalance this repulsion.

Attractive Steric Interactions in 1,3,5-
tris(Halomethyl)-2,4,6-
trimethylbenzenes and 1,3,5-Triethyl-
2,4,6-trimethylbenzene.

(2.1) Introduction

Figure 2.1.

X	compound
Cl	2.1
Br	2.2
I	2.3
Et	2.4



Rotation about the $\text{Ar-CH}_2\text{X}$ bond in **2.1**, **2.2**, **2.3** and **2.4** should give rise to two major conformations, the *syn* and the *anti*. In the *syn* conformer the three X groups lie on the same side of the ring plane, whereas in the *anti* conformer two X groups lie on one side and the third on the other side of the ring plane. A total of eight rotamers in equilibrium are expected for each of these compounds. As shown in figure 2.2 there are two equivalent forms of the *syn* conformer and six forms of the *anti* conformer.

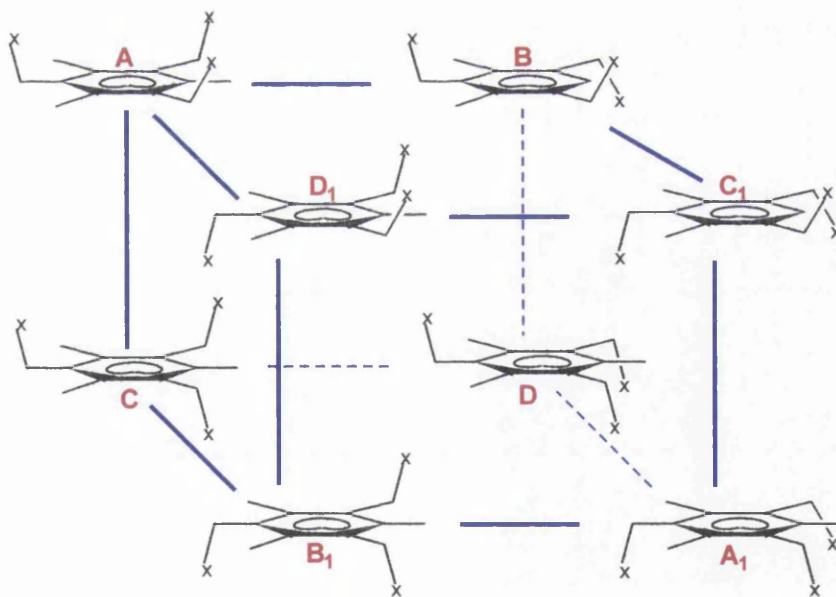
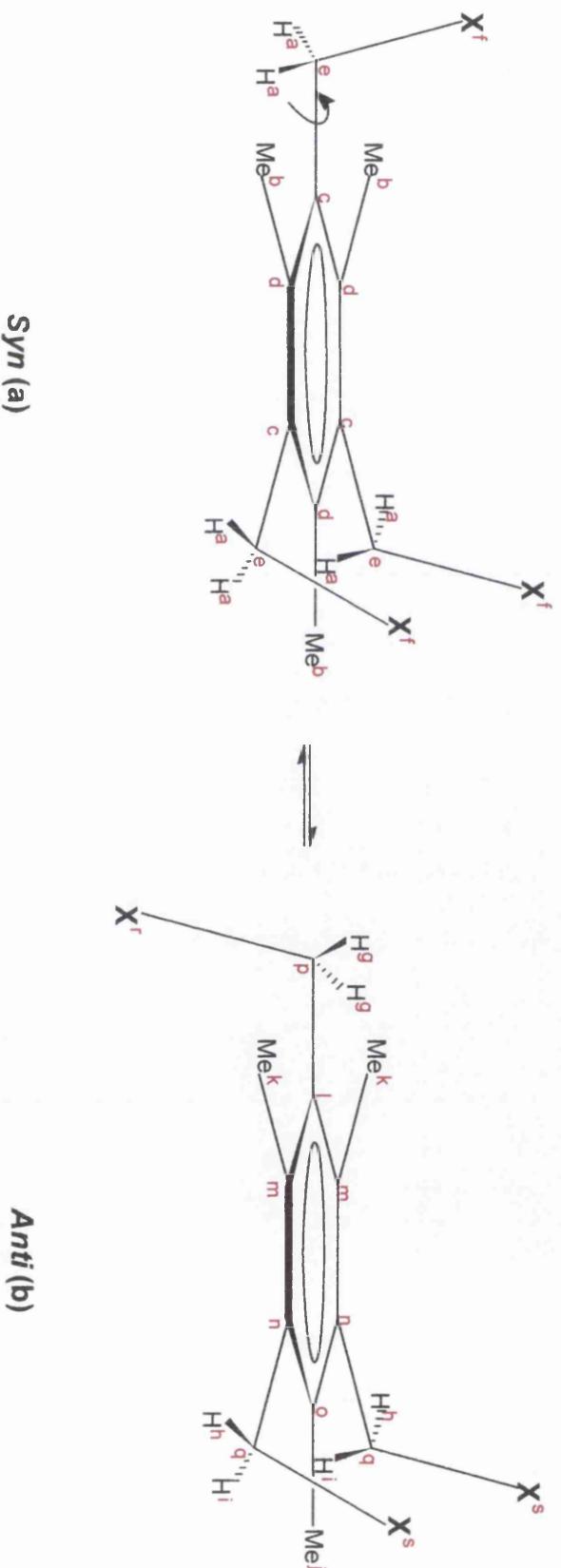


Figure 2.2. The rotamer inter-conversion scheme for compounds **2.1-2.4**. It is assumed that rotation about the $\text{C}_{\text{Ar}}\text{-CH}_2\text{X}$ bond happens independently. There are two equivalent versions of the *syn* conformation and six equivalent versions of the *anti* conformation. One of the methyl groups in rotamers **B** and **C₁** are omitted for clarity.



2.1; X = Cl
 2.2; X = Br
 2.3; X = I
 2.4; X = Me

Figure 2.3. Diagram showing the *syn* and *anti* conformations. The letters in red denotes the chemical environment of the proton and carbon atoms in the molecule.

Thus, a useful comparison between the relative populations of a *syn* and an *anti* conformation may only be made when the population of the *anti* conformation obtained experimentally has been divided by three. The corrected *syn/anti* ratio may then be used for calculating the equilibrium constant and the change in Gibbs free energy. Free energy differences quoted henceforth are always between one *syn* and one *anti*.

We hope to investigate by dynamic NMR which of the two conformations *syn* or *anti* is the more stable and how the nature of X and solvent polarity would affect this. We also intend to compare the experimental results with those obtained from molecular mechanics calculations.

NMR spectroscopy

The *syn* and *anti* conformations of **2.1**, **2.2** and **2.3** are shown in figure 2.3. The letters in red denotes the environments of the proton and carbon atoms in the molecules. In the *syn* conformation the six methylene protons *a* are equivalent and should appear as a singlet in the proton NMR. The methylene protons of the *anti* conformation are in three different environments *i*, *h* and *g*. The pair of protons, *i* and *h* are diastereotopic and should be mutually coupled to give an AB system. The protons *g* are not coupled to anything and should therefore give a singlet. At temperatures well below the coalescence point, the methylene region of **2.1**, **2.2** and **2.3**, where X is a halogen atom should consist of an AB system and a singlet of intensity ratio 2:1 from the *anti* conformation, together with a second singlet signal from the *syn* conformation.

As for the triethyl-compound (**2.4**), the three pairs of methylene protons *a* from the *syn* conformation and the pair *g* from the *anti* conformation are each coupled to their adjacent methyl protons, therefore should each give rise to a quartet. The protons *i* and *h* from the *anti* conformation are expected to have a complex splitting pattern because they are coupled to one another but in addition they are coupled to their adjacent methyl protons.

In the decoupled ^{13}C NMR spectrum of **2.1-2.4**, at temperatures well below the coalescence point, each of the signals that appear at room temperature should each split into three peaks. Two of the three peaks should be of relative intensity 2:1 and come from the *anti* and the third peak of unrelated intensity should come from the *syn* conformation.

It is also worth pointing out that at low temperatures some signals may overlap meaning that separate signals are not seen for the two isomers.

(2.2) Results and Discussion

(2.2-1) Conformational assignment of NMR signals at low temperatures

(a) NMR spectra of the tris halomethyl trimethylbenzenes **2.1**, **2.2** and **2.3**

For the chloride (**2.1**) at room temperature an average spectrum of the two conformations is observed, but on cooling to $-95\text{ }^{\circ}\text{C}$ rotation about the Ar-CH₂Cl bonds is slow on the NMR time scale so two sub-spectra representing the two conformations are observed. The proton NMR chemical shifts are shown in table **2.1**. The methylene region of the proton NMR of the chloride (**2.1**) in CD₂Cl₂ is shown in figure **2.4a** as expected, it consist of two singlets and an AB system. The AB system centred at 4.65 and 4.70 ppm together with the singlet signal at 4.72 ppm, which appears to be half the intensity of the AB quartet, are from the *anti* conformation. The more intense of the singlets resonating at 4.62 ppm is from the *syn* conformation.

Table **2.1**. The proton NMR chemical shifts^a of compounds **2.1-2.4** at temperatures below the coalescence point.

Compound ↓	Chemical shifts/ppm		
R/temp	CH ₂ CH ₃	Ar-CH ₃	CH ₂ R ^b
Cl / $-95\text{ }^{\circ}\text{C}$ (CD ₂ Cl ₂)		2.41	4.62 (s, H ^a); 4.65 (AB, J = 12.1 Hz, <i>anti</i>)
		-	4.70 (AB, J = 12.1 Hz, <i>anti</i>); 4.72 (s, H ^b)
Br / $-90\text{ }^{\circ}\text{C}$ (CD ₂ Cl ₂)		2.4	4.52 (s, H ^a); 4.54 (AB, J = 11.2 Hz, <i>anti</i>)
		-	4.61 (AB, J = 11.2 Hz, <i>anti</i>); 4.72 (s, H ^b)
Br / $-80\text{ }^{\circ}\text{C}$ (CD ₃ COCD ₃)		2.43 (1H, <i>anti</i>)	4.75 (AB, J = 11.2 Hz, <i>anti</i>); 4.77 (s, H ^a)
		2.437 (<i>syn</i>)	4.84 (s, H ^b); 4.87 (AB, J = 11.2 Hz, <i>anti</i>)
		2.442 (2H, <i>anti</i>)	
I / $-40\text{ }^{\circ}\text{C}$ (CD ₂ Cl ₂)		2.23	4.37 (s, H ^a); 4.38 (AB, J = 9.4 Hz, <i>anti</i>)
		2.24	4.47 (s, H ^b); 4.48 (AB, J = 9.4 Hz, <i>anti</i>)
Me / $-120\text{ }^{\circ}\text{C}$ (CCl ₂ F ₂)	1.07 (1H, <i>anti</i>)	2.28	2.68 (H ^a)
	1.10 (2H, <i>anti</i>)	2.31	2.72 (H ⁱ , H ^h)
	1.13 (<i>syn</i>)		2.74 (H ^b)

^a The signal from the *syn* conformation is shown in red.

^b The superscript letters denotes the chemical environments see figure **2.3**.

The decoupled ^{13}C NMR spectrum of the chloride (**2.1**) at $-95\text{ }^{\circ}\text{C}$ has two sub-spectra representing the *syn* and *anti* conformations. The chemical shifts are shown in table 2.2. Figure 2.4b is the $\text{C}_{\text{Ar}}\text{-Me}$ region of the spectrum, it consists of three signals of intensity ratio 1:2:2. The two peaks at 132.69 ppm and 132.36 ppm of intensity ratio 1:2 are from the *anti* and the third signal at 132.16 ppm is from the *syn* conformation. From this spectrum the *syn/anti* intensity ratio was found to be 3:2 and more importantly the ratio of a *syn* conformer to any of the *anti* conformations is 2.0:1. This represents a free energy difference of $0.25\text{ kcal mol}^{-1}$ in favour of a *syn* conformation.

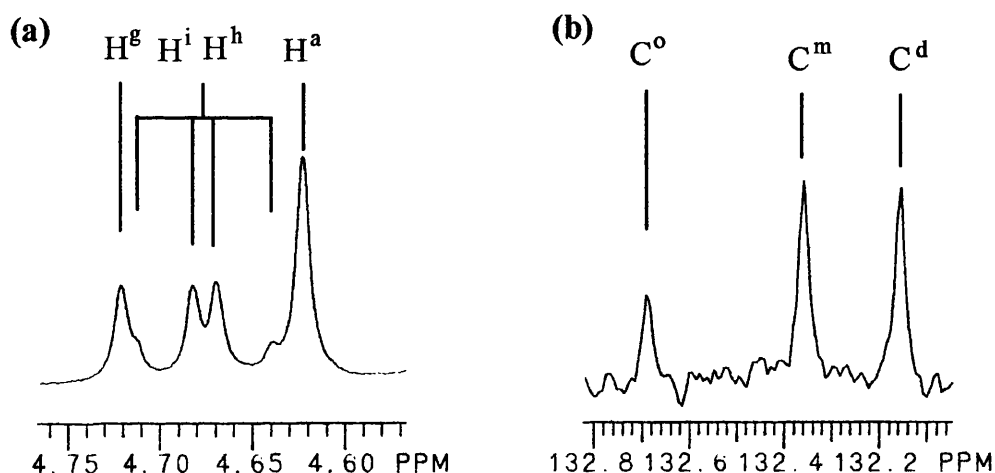


Figure 2.4.

(a) Is the methylene region of the proton NMR of the bromide (**2.1**) at $-95\text{ }^{\circ}\text{C}$.

(b) Is the C-Me region of the decoupled ^{13}C NMR of the bromide (**2.1**).

The superscript letters denotes the chemical environments see figure 2.3.

The features of the proton and ^{13}C NMR of the bromide (**2.2**) and iodide (**2.3**) below de-coalescence are similar to those of the chloride (**2.1**). The proton and ^{13}C NMR chemical shifts are summarised in tables 2.1 and 2.2 respectively. The methylene region of the proton NMR of the bromide (**2.2**) at $-80\text{ }^{\circ}\text{C}$ in acetone- d_6 is shown in figure 2.5a. The AB system centred at 4.75 and 4.87 ppm together with the singlet at 4.84 ppm are from the *anti* conformation whilst the obscured singlet at 4.77 ppm is from the *syn* conformation.

The $\text{C}_{\text{Ar}}\text{-Me}$ region of the ^{13}C NMR is shown in figure 2.5b. The two most downfield signals of intensity ratio 1:2 are from the *anti* and the most upfield signal is from the *syn* conformation. From this spectrum a *syn/anti* population ratio of 0.80:1

Table 2.2. The ^{13}C NMR chemical shifts for 2.1-2.4. The shifts shown in red are from the *syn* conformation.

R/temp (solvent)	Chemical shifts / ppm ^a				
	$\text{CH}_2\text{-CH}_3$	Ar-CH_3	CH_2R	C-Me^b	$\text{C-CH}_2\text{R}$
Cl / -95°C (CD_2Cl_2)		15.04	41.85	132.16 (C^d)	137.43 (2C, <i>anti</i>)
		15.08	41.94	132.36 (2C, C^m)	137.48 (1C, <i>anti</i>)
		15.34	-	132.69 (1C, C^o)	137.74 (<i>syn</i>)
Br / -90°C (CD_2Cl_2)		15.09	30.76	132.23 (C^d)	137.12 (2C, <i>anti</i>)
		15.18	30.86	132.53 (2C, C^m)	137.26 (1C, <i>anti</i>)
		15.32	-	132.96 (1C, C^o)	137.67 (<i>syn</i>)
Br / -80°C (CD_3COCD_3)		15.21 (2C, <i>anti</i>)	31.72 (<i>syn</i>)	133.56 (C^d)	138.66 (2C, <i>anti</i>)
		15.47 (<i>syn</i>)	31.7 (2C, <i>anti</i>)	133.70 (2C, C^m)	138.66 (1C, <i>anti</i>)
		15.59 (1C, <i>anti</i>)	31.81 (1C, <i>anti</i>)	134.11 (1C, C^o)	138.93 (<i>syn</i>)
I / -40°C (CD_2Cl_2)		5.16 (<i>syn</i>)	15.51 (2C, <i>anti</i>)	133.54 (C^d)	135.74 (2C, <i>anti</i>)
		5.33 (2C, <i>anti</i>)	15.58 (<i>syn</i>)	134.08 (2C, C^m)	135.81 (1C, <i>anti</i>)
		5.45 (1C, <i>anti</i>)	15.61 (1C, <i>anti</i>)	134.57 (1C, C^o)	136.46 (<i>syn</i>)
Me / -140°C (CCl_2F_2)	13.8	24.79	14.84	131.96 (1C, C^o)	139.17(<i>syn</i>)
	-	-	14.97	132.03 (C^d)	139.34 (2C, <i>anti</i>)
	-	-	15.10	132.14 (2C, C^m)	139.73 (1C, <i>anti</i>)

^a The number of entries for each carbon is indicative of the number of signals observed.

^b The superscript letters denotes the chemical environments see figure 2.3.

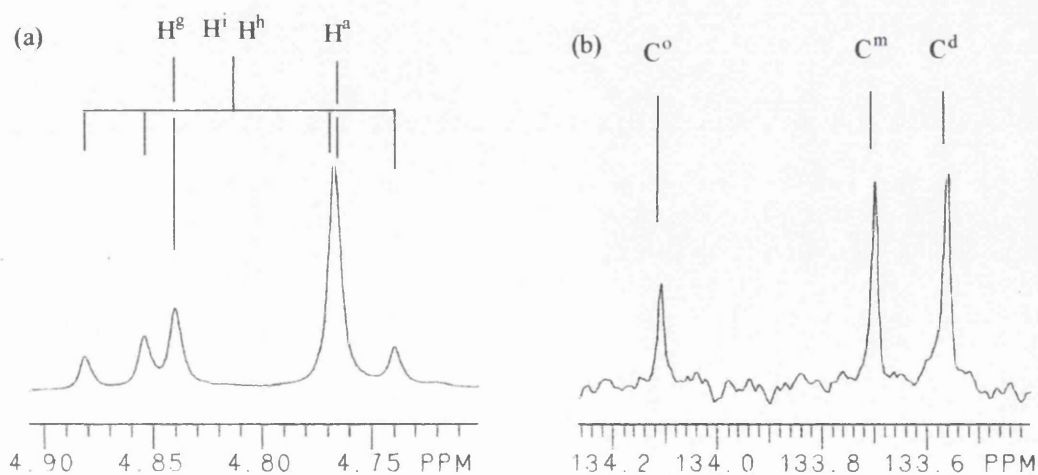


Figure 2.5

(a) Is the methylene region of the proton NMR and of the bromide (2.2) in acetone- d_6 at -80°C

(b) Is the decoupled ^{13}C NMR spectrum showing the C-Me region of the same compound. The superscript letters denotes the chemical environments see figure 2.3.

(2.4:1 when corrected for symmetry differences) is obtained, this equates to an energy difference of $0.34 \text{ kcal mol}^{-1}$ in favour of the *syn* conformation. The same molecule in methylene chloride- d_2 gave a lower energy difference, the corrected *syn/anti* ratio being 1.5:1 at -90°C representing a free energy difference of $0.15 \text{ kcal mol}^{-1}$ in favour of the *syn* conformation.

The methylene region of the proton NMR of the *tris* iodomethyl in methylene chloride d_6 at -40°C is shown in figure 2.6. The obscured singlet at 4.37 ppm is from the *syn* conformation whilst the AB system centred at 4.38 and 4.48 ppm together with the other obscured singlet at 4.47 ppm are from the *anti* conformation. From this spectrum a *syn/anti* population ratio of 0.30:1, equivalent to 0.91:1 when corrected for symmetry differences is obtained. It therefore follows that in contrast to the previous two compounds, the *anti* is slightly more stable than the *syn* by $0.04 \text{ kcal mol}^{-1}$.

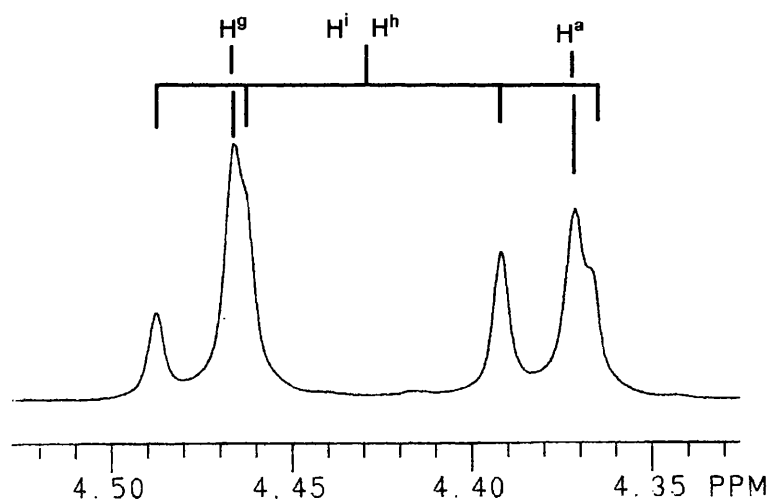


Figure 2.6. The methylene region of the proton NMR of the iodide (2.3) at -40°C in CD_2Cl_2 . Note the two singlets are being obscured by the AB system. The superscript letters denote the chemical environments see figure 2.3.

(b) NMR spectra of the triethyl-compound (2.4)

The methylene region of the proton NMR of the triethyl-compound (2.4) in $\text{CHClF}_2:\text{CD}_2\text{Cl}_2$ (~4:1) at -120°C , a temperature well below the coalescence point, is resolved as a broad multiplet, however on decoupling at the CH_2CH_3 proton the simplified spectrum shown in figure 2.7a is obtained. The simplified spectrum should theoretically consist of two singlets and an AB system just like in the *tris*-halomethylbenzene molecules. However, unlike in the trishalomethylbenzenes, where the assignment of signals, especially in the methylene region is unambiguous, in the

triethyltrimethylbenzene none of the signals in the methylene region has the appearance of an AB quartet as a result of which distinguishing between the signals arising from the *syn* and *anti* conformations is virtually impossible.

The phenyl region of the decoupled ^{13}C NMR of **2.4** at -130°C in CCl_2F_2 contained two sets of three peaks. The three peaks originating from CCH_2Me (see figure 2.7b) is of intensity ratio 1:2:3.9. This could be interpreted as a *syn/anti* population ratio of 3.9:3 which is equivalent to an energy difference of $0.39\text{ kcal mol}^{-1}$ in favour of *syn* or a *syn/anti* ratio of 1:5.9 that is equivalent to $0.19\text{ kcal mol}^{-1}$ in favour of *anti*. However, the latter is highly unlikely because results from force field calculations

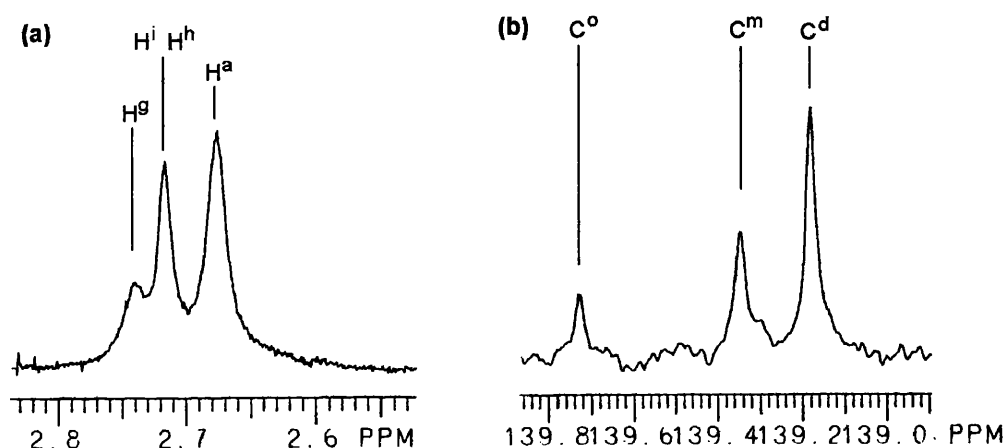


Figure 2.7.

- (a) The methylene region of the proton NMR of the triethyl-compound (**2.4**) at -120°C on irradiating the CH_2CH_3 signal.
- (b) The CCH_2Me region of the ^{13}C NMR of **2.4** at -130°C . The superscript letters denotes the chemical environments see figure 2.3.

suggest that *syn* is substantially more stable than *anti*, the calculated enthalpy difference being $0.86\text{ kcal mol}^{-1}$.

Assuming that the *syn* is the more stable, the signals in both the ^1H and ^{13}C NMR spectra have been assigned accordingly. In the proton NMR, the most intense and the most upfield of the signals at 2.68 ppm is from the *syn* and the other two signals centred at 2.72 and 2.74 ppm are from the *anti* conformation. However, the more intense of the *anti* signals at 2.72 ppm, which has the appearance of a singlet, is an unresolved AB system from the *anti* conformation. In the C-Me region of the ^{13}C NMR (see figure 2.7b), the two peaks at 131.96 and 132.14 ppm are from the *anti* whilst the peak at 132.03 ppm is from the *syn* conformation. The free energy difference was found to be $0.39\text{ kcal mol}^{-1}$ in favour of the *syn* conformation.

A closer look at the low temperature proton NMR of the 1,3,5-trisubstituted compounds, revealed that the chemical shifts of the methylene protons seems to be dependent on their position in relation to the ring. In the *syn* conformation, the three pairs of methylene protons are *cis* to one another (i.e. they are on the side of the ring plane) whereas in the *anti*, two pairs are *cis* and the third pair is *trans* (i.e. on opposite side of the ring plane). In the *syn* conformation of the 1,3,5-trisubstituted molecules, the signals from the three pairs of *cis* methylene protons always resonated relatively upfield to those originating from the *anti* albeit *cis* or *trans*. Furthermore, in the *anti* conformation, the mean of the A and B chemical shifts for the AB system from the two pairs of *cis* methylene protons, also resonates relatively upfield to the singlet from the pair that is *trans*.

(2.2-2) MM3 calculations

The printout from molecular mechanics calculations includes the van der Waals energy of interactions between all the non-bonding pairs of atoms together with the energies associated with the interactions between pairs of polar bonds i.e. dipole-dipole interaction. Table 2.3 is a summary of the contributions to the steric energies of the *syn* and *anti* conformations of 2.1-2.4. In every one of these molecules calculation revealed that the more compact *syn* conformation is the more stable. The factors that may account for the energy differences between the *syn* and *anti* conformations are discussed below.

In the chloride (2.1), the difference between the total van der Waals energy term for the *syn* and *anti* conformations is $0.79 \text{ kcal mol}^{-1}$. This difference is partly due to the presence of a greater level of attractive steric interactions among the chlorine atoms in the *syn* conformation. These interactions are less in the *anti* conformation because unlike in the *syn* conformation where the three chlorine atoms are closer together, in the *anti* one of the chlorine atom is far away from the other two. The van der Waals attractive energy between a pair of chlorine atoms on the same side of the ring plane is about $0.036 \text{ kcal mol}^{-1}$, on the other hand, when the two atoms are on opposite sides of the ring plane the attractive energy is hardly much less at $0.021 \text{ kcal mol}^{-1}$. The total of the three way attractive steric interactions among the three chlorine atoms in the *syn* and *anti* conformations are 0.110 and 0.080 respectively. Thus, according to MM3 the degree of stabilisation gained in the form of attractive steric

Table 2.3. A summary of the contributions to the final steric energy (kcal mol⁻¹) for the *syn* and *anti* conformations of 2.1-2.4

	Chloride (2.1)		Bromide (2.2)		Iodide (2.3)		Ethyl-compound (2.4)	
	<i>Syn</i>	<i>anti</i>	<i>syn</i>	<i>Anti</i>	<i>syn</i>	<i>anti</i>	<i>syn</i>	<i>anti</i>
Compression	1.9044	2.0348	2.0623	2.1731	1.9629	2.0820	2.3470	2.4514
Bending	3.0087	3.3074	3.0446	3.3437	4.2401	4.5445	2.8520	3.0824
Bend-bend	-0.3744	-0.3722	-0.3774	-0.3735	-0.7428	-0.7423	-0.2194	-0.2115
Stretch-bend	-0.3749	-0.3897	-0.3743	-0.3918	-0.3545	-0.3738	-0.3861	-0.4017
van der Waals								
1,4 energy	8.8925	8.8155	8.8412	8.8078	8.4317	8.3596	12.1907	12.1372
Other	5.1880	6.0504	5.6305	6.2213	5.0552	5.6702	6.2400	6.8192
Torsional	-4.8348	-4.9620	-5.5686	-5.6072	-21.8106	-21.7363	-11.8979	-11.8852
Torsion-stretch	0.0000	0.0000	0.0000	0.0000	0.0000	0.0000	-0.0011	-0.0012
Dipole-dipole	5.1672	4.6788	5.5686	5.2241	5.7265	5.4316	7.8096	7.8012
Total Steric Energy	18.5768	19.1630	18.9022	19.3973	2.5084	3.2355	18.9347	19.7917
Enthalpy difference (-ΔH)	0.5862		0.4951		0.7271		0.8570	

interactions, by having the three chlorine atoms on the same face of the ring is very small, about $0.030 \text{ kcal mol}^{-1}$. In the other molecules **2.2-2.4**, the stabilisation energy from such interactions are (Br, 0.071); (I, 0.106) and (Me, $0.044 \text{ kcal mol}^{-1}$). The increase on going from the chloride (**2.1**) to the bromide (**2.2**) and then the iodide (**2.3**) is best explained in terms of the polarisability of the halogen atoms. The more polarisable the halogen atom, the higher is the magnitude of mutual attraction.

The interactions between polar C-X bonds in the halides probably accounts for the difference between the total dipole-dipole terms in the final steric energy contributions for the *syn* and *anti* conformations. Take the chloride for example, the sum of the three (C-Cl)-(C-Cl) dipole-dipole interactions, extracted from MM3 printout, destabilises the *syn* conformation by about $0.76 \text{ kcal mol}^{-1}$ and the *anti* by $0.27 \text{ kcal mol}^{-1}$, a difference of $0.49 \text{ kcal mol}^{-1}$. There seems to be a direct correlation between this value and the difference in energy between the *syn* and *anti*'s total dipole-dipole contributions which also amounted to $0.49 \text{ kcal mol}^{-1}$ (see table **2.3** and **2.4**). This relationship is not exclusive to the chloride, it also applies to the bromide and iodide. The sum of the (C-X)-(C-X) dipole-dipole interactions for the halides are summarised in table **2.4**.

The destabilisation energy between two dipoles from "2-up" C-X bonds, albeit from the *syn* or *anti* conformation, is about (Cl, 0.25); (Br, 0.18) and (I, $0.16 \text{ kcal mol}^{-1}$) but from "1-up, 1-down" C-X bonds, the repulsive energy is significantly reduced at about (Cl, 0.02); (Br, 0.01 - 0.02) and (I, $0.03 \text{ kcal mol}^{-1}$). The energies associated with the interaction of dipoles from two C-X bonds in the halides, when it is "2-up" and "1-up, 1-down" is summarised in table **2.4**.

Table 2.4 The sum of the (C-X)-(C-X) dipole-dipole interactions for the halides.

Bond	Dipole-dipole interaction energy / kcal mol^{-1}							
	"3-up"			sum	"2-up, 1-down"			sum
C-Cl	+0.2530	+0.2532	+0.2532	+0.7594	+0.0232	+0.2517	+0.0204	+0.2953
C-Br	+0.1803	+0.1803	+0.1802	+0.5408	+0.0098	+0.1788	+0.0180	+0.2066
C-I	+0.1617	+0.1616	+0.1616	+0.4849	+0.0271	+0.1612	+0.0322	+0.2205

Another factor that may account for a large part of the difference between the total van der Waals energy terms of the *syn* and *anti* conformations of the 1,3,5-trisubstituted molecules, is the fact that there is a higher level of gearing (self-organisation) among the halomethyl and methyl groups in the *syn* conformation. Figure 2.8 shows the structure calculated to be preferred by the two conformers of 2.1-2.4. In the *syn* conformation, there is a successive up and down arrangement of C-Z bonds (Z = Cl, Br, I, Me or H) and in addition these bonds lie more or less perpendicular to the plane of the ring. In the *anti* conformation, in contrast, a C-H bond from one of the two methyl groups flanking the unique C-X bond is more or less in the plane of the ring rather than perpendicular to it. The organisation of the methyl and halomethyl groups in the *syn* conformation is similar to that observed for the most stable conformations of hexamethyl-³⁰ and hexaethyl-benzenes³¹. In these conformations adjacent C-Y bonds (Y = H or Me) are arranged alternatively in an up and down fashion all the way round the ring, and any other conformation that breaks this arrangement is less stable.

In order to analyse gearing in both conformations of the 1,3,5- trisubstituted compounds, a dissection of the van der Waals energy of the 1,3,5-*tris*(chloromethyl)-trimethylbenzene was attempted. This molecule should serve as a model for other compounds in the series. The six CH₂Z (Z = Cl or H) groups attached to the ring were given numbers from one to six and the sum of the van der Waals energy of interaction between neighbouring CH₃ and CH₂Cl groups were calculated and tabulated see table 2.5

Table 2.5. The van der Waals energy of interaction between adjacent methyl and CH₂Cl groups in 2.1.

Methyl-CH ₂ Cl	Methyl-CH ₂ Cl energy of interaction /kcal mol ⁻¹	
	<i>anti</i>	<i>syn</i>
1-2	+2.026	+1.717
2-3	+1.691	+1.724
3-4	+2.094	+1.752
4-5	+1.716	+1.667
5-6	+1.775	+1.728
6-1	+1.775	+1.714
Total →	+11.077	+10.302

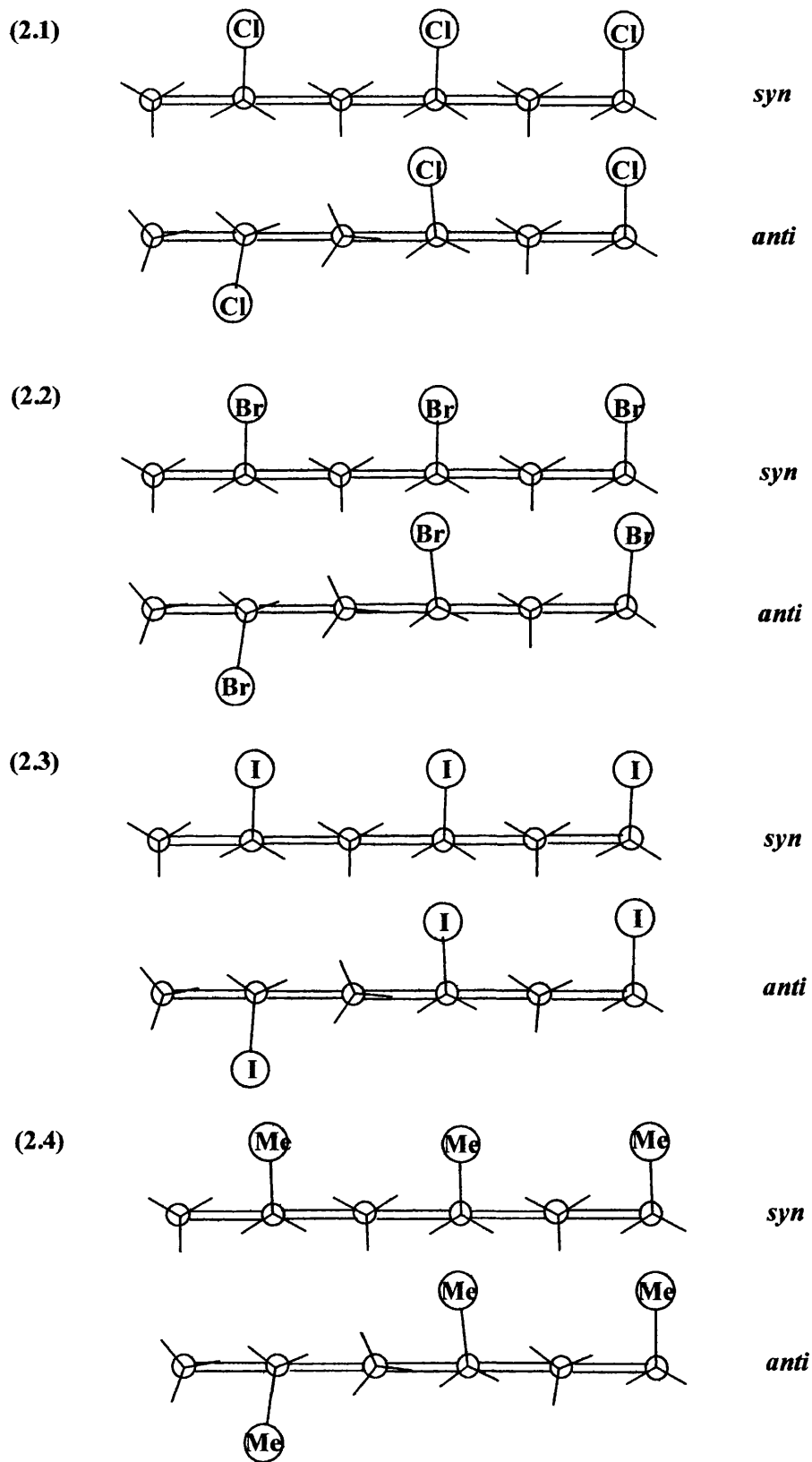


Figure 2.8. Diagram showing the conformation adopted by the methyl and halomethyl groups in 2.1, 2.2, 2.3 and 2.4. N.B. the diagram was constructed using the torsional angles from MM3 calculations.

As shown in table 2.5 the net interaction between the CH_2Z groups ($\text{Z} = \text{H}$ or Cl) is not the same in both conformations. In the *anti* conformation the net $\text{CH}_3\text{-CH}_2\text{Cl}$ interaction is $+11.08 \text{ kcal mol}^{-1}$, a value which is $0.78 \text{ kcal mol}^{-1}$ more than the figure obtained for the *syn*. The high value from the *anti* is mainly down to a relatively higher repulsive steric interactions between the two methyl groups that each has a C-H bond in the plane of the ring (i.e. “eclipsing”) and one of their flanking CH_2Cl groups (specifically the one that is closer to the “eclipsing” C-H bond). The energy of such $\text{CH}_3\text{-CH}_2\text{Cl}$ interactions is about $0.3 \text{ kcal mol}^{-1}$ higher than any other $\text{CH}_3\text{-CH}_2\text{Cl}$ interactions in the *syn* or *anti* conformation.

The data from MM3 calculations, specifically the list of torsional angles for the ring carbons reveals that the benzene rings are deformed. This explains the fact that the six carbons bonded to the benzene ring are not all in the same plane. The lack of planarity in the ring carbons and the outer methyl and methylene carbons is, presumably, to reduce the clashing of adjacent methyl and halomethyl groups on the ring.

The torsional angles for the ring carbons in both conformations of the 1,3,5-trisubstituted molecules are shown in table 2.6. There is a succession of positive and negative angles in the *syn* conformation of the chloride, this is characteristic of a chair conformation. The pattern observed for the *anti* is characteristic of a boat conformation.

Table 2.6. The torsional angles of the of the benzene ring carbons.

Torsional angles	Chloride (2.1)		Bromide (2.2)		Iodide (2.3)		Ethyl (2.4)	
	<i>Syn</i>	<i>Anti</i>	<i>Syn</i>	<i>Anti</i>	<i>Syn</i>	<i>Anti</i>	<i>Syn</i>	<i>Anti</i>
1-2-3-4	+1.9	-0.7	+2.2	-1.1	+0.4	+0.2	+0.9	-0.7
2-3-4-5	-1.6	-2.4	-2.2	-2.1	-0.4	-1.7	-1.0	-1.9
3-4-5-6	+1.6	+4.3	+2.2	+4.4	+0.4	+2.0	+1.4	+3.2
4-5-6-1	-1.8	-3.0	-2.1	-3.3	-0.5	-0.8	-1.6	-1.9
5-6-1-2	+2.0	-0.2	+2.1	-0.1	+0.5	-0.7	+1.5	-0.6
6-1-2-3	-2.0	+2.0	-2.2	+2.2	-0.5	+1.0	-1.2	+1.9

(2.3) Conclusion

Dynamic NMR analysis showed that in the chloride (2.1), bromide (2.2) and the ethyl-compound (2.4) the more compacted *syn* conformation is more stable than the *anti*. The dynamic NMR and MM3 calculation results are summarised in table 2.7.

Table 2.7. Summary of results from experiments and calculations

R	solvent	Temperature	Equilibrium constant	$-\Delta G_{exp}$	$-\Delta H_{calc}$
		$^{\circ}\text{C}$		kcal mol $^{-1}$	kcal mol $^{-1}$
Cl	CD ₂ Cl ₂	-95	2.0	0.25	0.59
Br	CD ₂ Cl ₂	-90	1.5	0.15	0.53
	Acetone-d ₆	-80	2.4	0.34	
I	CD ₂ Cl ₂	-40	0.91	-0.04	0.73
Me	CHClF ₂	-130	3.9	0.39	0.86

One has to be cautious in attributing the energy differences in favour of *syn* in these compounds entirely to attractive steric interactions between the X groups, which is supposedly high in the *syn* conformation and much more reduced in the *anti*. This is because MM3 calculations suggest that the position of the *syn-anti* equilibrium is not solely determined by attractive steric interaction among the X groups, but other factors such as dipole-dipole interactions and the difference in the nature of gearing in the two conformations, both affect the position of the equilibrium.

Experiment also show that in the halomethyl compounds, the extra stability of the *syn* conformation over the *anti* increased in the order iodide < bromide < chloride. This trend is the reverse of that obtained from MM3 calculations, when only the van der Waals interaction among the three X groups are being considered. The trend observed experimentally also supports the idea that attractive steric interactions among the X groups does not solely determine the position of the equilibrium for if this was the case one would expect the *syn/anti* ratio to increase in the order chloride < bromide < iodide, because an iodine atom is more polarisable than a bromine atom which in turn is more polarisable than a chlorine atom and the more polarisable the halogen atom the greater is the level of mutual attraction.

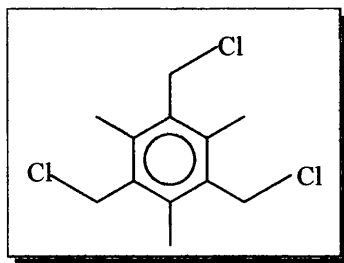
Surprisingly, results from NMR spectroscopy indicate that the *anti* conformation of the iodide (2.3) is slightly more stable, about 0.04 kcal mol $^{-1}$ more stable than the

syn, this result is in contrast to calculations, where the *syn* was found to be substantially the more stable.

With the exception of the iodide, MM3 calculations agrees with experimental results as to the extra stability of the *syn* conformation over the *anti* but failed in all cases to predict the magnitude of the energy difference between the two conformations. The failure of calculations to predict that the *syn* is more stable in the iodide and to accurately predict the magnitude of the energy difference between the two conformations in all the molecules is probably due to an overestimation of the energy gained from gear effect in the *syn* conformation.

Finally, the effect of changing the solvent from methylene chloride- d_2 to a more polar solvent (acetone- d_6) in the bromide was to increase the relative stability of the *syn* conformation. The solvent probably binds to the less sterically hindered face of the solute's benzene ring by the interaction of its π electron cloud and the acidic proton of the solvent thereby stabilising the *syn* conformation in the process. However, because the protons in acetone are more acidic than those from methylene chloride the former should form a stronger complex with the solute. A more comprehensive solvent study carried out on the 1,3-bis(halomethyl)-2,4,5,6-tetramethylbenzene series of compounds will be discussed in the next chapter.

(2.4) Synthesis



1,3,5-tris(Chloromethyl)-2,4,6-trimethylbenzene. (2.1)

Commercially available 1,3,5-*tris*(chloromethyl)-2,4,6-trimethylbenzene was used for the analysis.

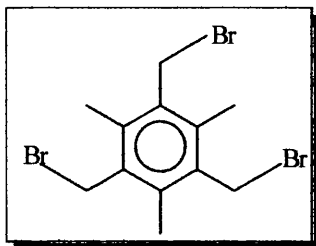
NMR spectroscopy

300 MHz ^1H NMR (CDCl_3) δ /ppm 2.49 (s, 9H, ArCH_3); 4.68 (s, 6H, CH_2Cl).

100.6 MHz ^{13}C NMR (CDCl_3) δ/ppm 15.38 (ArCH_3); 41.62 (CH_2Cl); 133.16 (CCH_3); 138.00 (CCH_2Cl).

Elemental analysis

Found: C, 54.51; H, 5.64; Cl, 40.32 %. $\text{C}_{12}\text{H}_{15}\text{Cl}_3$ requires C, 54.26; H, 5.70; Cl, 40.04 %.



1,3,5-tris(Bromomethyl)-2,4,6-trimethylbenzene.³⁷ (2.2)

Under an inert atmosphere of argon, a solution of hydrogen bromide (15 ml, 5.7 M in acetic acid, 86 mmol) was added to a stirring mixture of paraformaldehyde (2.5 g, 83 mmol) and mesitylene (2.4 g, 20 mmol) in glacial acetic acid (50 ml) at 120°C . The mixture was stirred at the same temperature for 24 h and then poured into water (100 ml). The mixture was filtered and the white solid was dried and collected. The solid was purified by recrystallisation from petroleum spirit (b.p. $60\text{--}80^\circ\text{C}$). A white crystalline solid (6 g) m.p. $48\text{--}49^\circ\text{C}$ (lit³⁸, 49°C) was obtained.

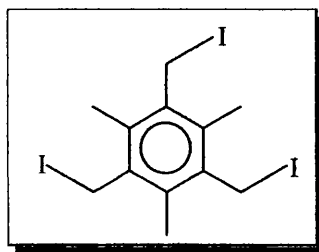
NMR spectroscopy

400 MHz ^1H NMR (CDCl_3) δ/ppm 2.45 (s, 9H, ArCH_3); 4.56 (s, 6H, CH_2Br).

100.6 MHz ^{13}C NMR (CD_2Cl_2) δ/ppm 15.43 (ArCH_3); 29.94 (CH_2Br); 133.27 (CCH_3); 137.92 (CCH_2Br).

Elemental analysis

Found: C, 36.22; H, 3.63; Br, 60.44 %. $\text{C}_{12}\text{H}_{15}\text{Br}_3$ requires C, 36.12; H, 3.80; Br, 30.10 %.



1,3,5-Tris(iodomethyl)-2,4,6-tetramethylbenzene.³⁸ (2.3)

Under anhydrous conditions a mixture of 1,3,5-tris(bromomethyl)-2,4,6-tetramethylbenzene (1.0 g, 2.51 mmol) and excess sodium iodide (6 g, 42 mmol) in acetone (15 ml) was stirred at 20 °C for 3 h. The solvent was removed using a rotary evaporator. Dichloromethane (30 ml) and water (20 ml) were added to the solid. The organic layer was separated and the aqueous layer was washed with dichloromethane (3 x 10 ml). The combined organic layer was washed with sulphurous acid to remove iodine and then with water (3 x 5 ml). The solution was dried with anhydrous magnesium sulfate and the solvent was removed under reduced pressure leaving a solid. The crude product was then re-crystallised from acetone to give slightly off white solid (0.9 g) m.p. 214-215 °C.

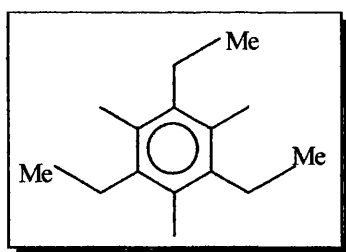
NMR spectroscopy

400 MHz ¹H NMR (CD₂Cl₂) δ/ppm 2.39 (s, 9H, ArCH₃); 4.77 (s, 6H, CH₂I).

100.6 MHz ¹³C NMR (CD₂Cl₂) δ/ppm 4.78 (CH₂I); 15.78 (ArCH₃); 134.72 (CCH₃); 136.35 (CCH₂I).

Elemental analysis

Found: C, 27.00; H, 2.66 %. C₁₆H₂₅I requires C, 26.69; H, 2.81; I, 70.50 %.



1,3,5-Triethyl-2,4,6-tetramethylbenzene.³⁹ (2.4)

The entire reaction was carried out under argon. A solution of lithium dimethylcuprate was prepared by adding a solution of metyllithium (13.6 ml, 1.0 M sol. in THF, 13.6 mmol) to a stirred mixture of copper iodide (1.29 g, 6.77 mmol) in ether (16 ml) at 0 °C. The mixture immediately turned yellow then colourless. The resultant mixture was stirred at 0 °C for 20 min.

1,3,5-tris(chloromethyl)-2,4,6-trimethylbenzene (0.60 g, 2.25 mmol) dissolved in ether (30 ml) was added to the lithium dimethylcuprate solution at 0 °C. The resultant yellow mixture was stirred at ambient temperature for 5 h. The reaction was quenched by carefully adding 3 M hydrochloric acid sol. (20 ml). The mixture was

filtered to remove insoluble materials. The organic layer was separated and the aqueous phase was extracted with ether (3 x 10 ml). The combined organic phase was washed with water (3 x 10 ml) and the dried over anhydrous magnesium sulfate. The solvent was removed under reduced pressure leaving a white solid. The crude product was purified by flash column chromatography using pet. spirit (b.p. 30-40 °C) as the eluting solvent. The product (210 mg) was obtained as a white solid m.p. 57-58 °C.

NMR spectroscopy

400 MHz ¹H NMR {CHCl₂F:CHClF₂:CD₂Cl₂ (~2:2:1)} δ/ppm 1.21 (t, J = 7.5 Hz, 9H, CH₂Me); 2.40 (s, 9H, ArCH₃); 2.83 (q, J = 7.5 Hz, 6H, CH₂CH₃).

100.6 MHz ¹³C NMR {CHCl₂F:CHClF₂:CD₂Cl₂ (~2:2:1)} δ/ppm 14.49 (CH₂CH₃); 15.85 (CH₂Me); 24.78 (ArCH₃); 132.90 (CCH₃); 140.72 (CCH₂Me).

Elemental analysis

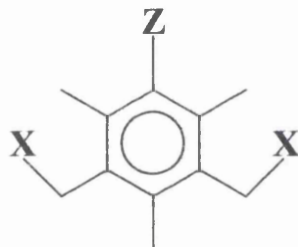
Found: C, 88.25; H, 11.95 %. C₁₆H₂₅ requires C, 88.15; H, 11.85 %.

Attractive Steric Interactions in 1,3-
Disubstituted-2,4,5,6-
tetramethylbenzenes,
where the two substituents are identical

(3) Introduction

Having investigated attractive steric interactions in the 1,3,5-trisubstituted-2,4,6-trimethylbenzenes we shall now look at 1,3-disubstituted-2,4,5,6-tetramethylbenzenes, see figure 3.1, where $Z = \text{Me}$ and the two substituent X , are the same together with the 1,3-bis(bromomethyl)-2,4,6-trimethylbenzene (i.e. 5-nor-bromo-compound).

Figure 3.1



In all these molecules with the exception of 3.4, where Z is H , $Z = \text{Me}$.

- | | | | |
|------------------------------|--|---|-------------------------------|
| 3.1; $\text{X} = t\text{Bu}$ | 3.4; $\text{X} = \text{Br}$; $Z = \text{H}$ | 3.7; $\text{X} = \text{Ph}$ | 3.10; $\text{X} = \text{OMe}$ |
| 3.2; $\text{X} = \text{Cl}$ | 3.5; $\text{X} = \text{I}$ | 3.8; $\text{X} = p\text{-C}_6\text{H}_4\text{NO}_2$ | |
| 3.3; $\text{X} = \text{Br}$ | 3.6; $\text{X} = \text{Me}$ | 3.9; $\text{X} = 2\text{-Naphthyl}$ | |

Rotation about the two $\text{C-CH}_2\text{X}$ bonds, one at a time, should give rise to four rotamers a , b , c and d (see figure 3.2). The two rotamers a and c , where both X groups lie on the same side of the ring plane are assigned *syn* conformation. A 180° rotation

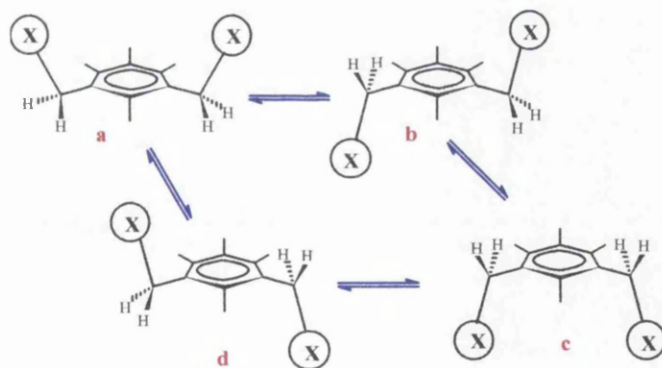


Figure 3.2. The rotamer interconversion scheme for compounds 3.1 – 3.10. It is assumed that rotation about the $\text{C-CH}_2\text{X}$ bonds occurs one at a time.

about a $\text{C-CH}_2\text{X}$ bond should give the *anti* rotamers b or d . The energy barriers to rotation about these bonds will be discussed in chapter six. It is interesting to know that when the two X groups are on the same side of the ring plane, the conformation contains an internal plane of symmetry and is therefore achiral. And a careful inspection

of the *syn* rotamers, *a* and *c*, also reveals that they are identical. On the other hand, the *anti* rotamers, *b* and *d*, are not superimposable, in fact they are mirror images of one another, in other words they are enantiomeric rotamers.

In this chapter, the results from dynamic NMR and molecular mechanics calculations are reported. The effect of different solvents of various polarities on the *syn/anti* equilibrium of these compounds, particularly **3.3**, is also treated. It is envisaged that the more compact *syn* conformation will be more stable than the *anti* because, unlike the *anti* where the X groups are far away from one another, in the *syn* conformation these groups are closer together so as to maximise attractive steric interactions and lower the enthalpy of formation. Perhaps just like the 1,3,5-trisubstituted-2,4,6-trimethylbenzenes "gear effect" will preferentially stabilise the *syn* conformations of the 1,3-disubstituted-methylbenzenes.

This chapter is divided into three sections. In the first section the dineopentyl (**3.1**) and the halomethyl compounds (**3.2** - **3.5**) where the *syn* and *anti* sub-spectra can be easily distinguished by using a chiral shift reagent are discussed. In the second section, the other 1,3-disubstituted-tetramethylbenzenes (**3.6** - **3.10**), where assignment of the *syn* and *anti* signals is ambiguous are treated. And in the final section the synthesis of these compounds (**3.1** - **3.10**) are discussed.

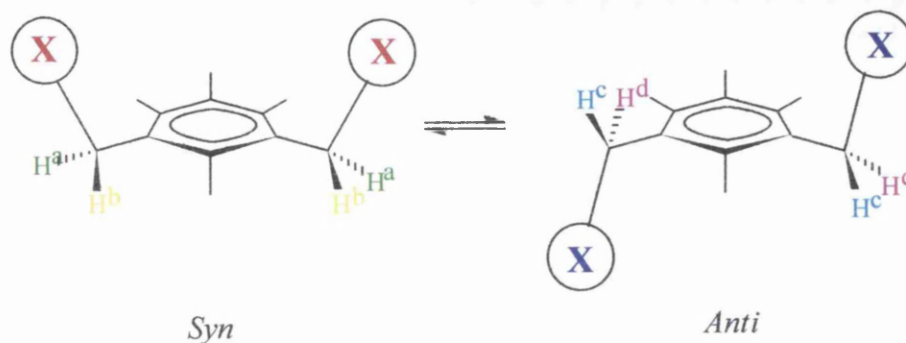
NMR spectroscopy

Below the coalescence temperature, the NMR spectrum of **3.1** - **3.10** should consist of two sub-spectra representing the *syn* and *anti* conformations. Considering the methylene region of the proton NMR of these compounds at temperatures below the coalescence point, it should consist of two sets of AB system. An AB set should come from the mutually coupled diastereotopic *a* and *b* protons from the *syn* conformation and the other quartet should come from the mutually coupled *c* and *d* protons in the *anti* conformation (see figure **3.2**).

In the ^{13}C NMR, each of the signals appearing at room temperature is expected to split into two, representing the *syn* and *anti* conformations.

It is worth pointing out that because of the similarity between the two sub-spectra in both the ^1H and ^{13}C NMR of the 1,3-disubstituted-methylbenzenes, it is virtually impossible distinguishing between the signals arising from the *syn* and *anti* conformations. But there is a solution to this problem. We know that the *anti* conformation is chiral whilst the *syn* is achiral. Now consider the interaction between a

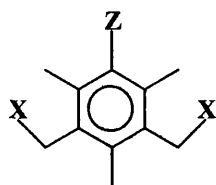
Figure 3.2



chiral shift reagent and the two conformations of the 1,3-disubstituted-methylbenzenes. The chiral *anti* conformation should interact, reversibly, with a chiral shift reagent to give the two corresponding diastereomers whose signals, hopefully, would be shifted to different extent, therefore leading to doubling of the signals arising from the *anti* conformation. By contrast, the achiral *syn* conformation is unable to form diastereomers, therefore only one set of signals is obtained.

Chiral shift reagents are mild Lewis acids capable of interacting with the basic sites in a substrate to form a complex. The Lewis acid, the substrate and the complex exist in equilibrium. And in a chiral shift experiment there is the need to drive the equilibrium towards formation of the complex by using excess of the chiral shift reagent. But having too much of it may lead to crystallisation and loss of resolution in the NMR spectrum, especially when it involves the sample being cooled.

SECTION ONE

(3.1.1) Results and Discussion of 3.1-3.5

With the exception of **3.4**,
where Z is H, Z = Me.

	X
3.1	^t Bu
3.2	Cl
3.3	Br

	X
3.4	Br (Z = H)
3.5	I

(3.1-1) Conformational assignment of NMR signals at low temperatures(a) *NMR of the 1,3-dineopentyl-tetramethylbenzene (3.1)*

The dynamic NMR spectrum of the dineopentyl compound (**3.1**) was carried out in methylene chloride- d_2 , acetone- d_6 and a mixture of $\text{CHClF}_2:\text{CHCl}_2\text{F}:\text{CD}_2\text{Cl}_2$ (~2:2:1). At ambient temperature an average spectrum of the two conformations is observed but on cooling, the *tert*-butyl signals de-coalesced at about -5°C before eventually sharpening up at lower temperatures. The NMR spectrum in methylene chloride- d_2 at ambient temperature and -40°C , a temperature well below the coalescent point, are shown in figure **3.4a** and **b** respectively. At -40°C , the $\text{C}(\text{CH}_3)_3$ signal together with one of the methyl signals has each split into two peaks of unequal intensity. The methylene region of the same spectrum (see figure **3.4c**) consists of an AB system centred at 2.720 and 2.763 ppm together with a singlet resonating at 2.753 ppm. The singlet is undoubtedly from a pair of diastereotopic methylene protons that coincidentally come into resonance at the same frequency.

To assign the two sub-spectra, an NMR spectrum of a mixture of **3.1** and seven fold excess of a chiral shift reagent, (*R*)-1-(9-anthryl)-2-2-2-trifluoroethanol, at -40°C was obtained. In the methylene region of the spectrum, the signal that originally appeared as a singlet has split into two, although with some degree of overlap, as a result of the chiral *anti* conformation being reversibly converted to the corresponding diastereomers while the AB system remained virtually unchanged. It therefore follows that the singlet is from the chiral *anti* conformation whilst the AB quartet is from the achiral *syn* conformation. Thus, the more intense of the signals from the *tert*-butyl and methyl groups are from the *syn* conformation. The ^1H and ^{13}C NMR chemical shifts at low temperatures are summarised in tables **3.1** and **3.2** respectively.

Table 3.1. The proton NMR chemical shifts for the dineopentyl-compound (3.1), chloride (3.2), 1,3-bis(bromomethyl)-2,4,5,6-tetramethylbenzene (3.3), 1,3-bis(bromomethyl)-2,4,6-tetramethylbenzene (3.4) and the iodide (3.5). (The chemical shifts from the more intense signals are shown in red which happens to come from the *syn*.)

Compound	Solvent	Chemical shifts /ppm				
		C(CH ₃) ₃	CH ₃	2 CH ₃	CH ₃	CH ₂ X
(3.1) 'Bu (-40 °C)	CD ₂ Cl ₂	0.84 (s, <i>anti</i>)	2.12 (s, <i>syn</i>)	2.19	2.24	2.720 (AB, J = 14.4 Hz, <i>syn</i>); 2.753 (s, <i>anti</i>)
		0.87 (s, <i>syn</i>)	2.13 (s, <i>anti</i>)			2.763 (AB, J = 14.4 Hz, <i>syn</i>)
(-40 °C)	Freons	0.95 (s, <i>anti</i>)	2.22 (s, <i>syn</i>)	2.29	2.37	2.844 (AB, J = 14.4 Hz, <i>syn</i>); 2.871 (s, <i>anti</i>)
		0.97 (s, <i>syn</i>)	2.31 (s, <i>anti</i>)			2.884 (AB, J = 14.4 Hz, <i>syn</i>)
(-40 °C)	CD ₃ COCd ₃	0.85 (s, <i>anti</i>)	2.11 (s, <i>syn</i>)	2.180	2.26 (s, <i>anti</i>)	2.745 (AB, J = 14.4 Hz, <i>syn</i>); 2.783 (s, <i>anti</i>)
		0.88 (s, <i>syn</i>)	2.12 (s, <i>anti</i>)		2.27 (s, <i>syn</i>)	2.778 (AB, J = 14.4 Hz, <i>syn</i>)
(3.2) Cl (-92 °C)	CD ₂ Cl ₂		2.13 (s, <i>syn</i>)	2.27	2.37	4.65 (AB, J = 12 Hz, <i>syn</i>); 4.68 (AB, J = 12 Hz, <i>syn</i>)
			2.14 (s, <i>anti</i>)			4.71 (s, <i>anti</i>)
(-90 °C)	CD ₃ COCd ₃		2.11 (s, <i>syn</i>)	2.27	2.40 (s, <i>syn</i>)	4.81 (AB, J = 12 Hz, <i>syn</i>); 4.84 (AB, J = 12 Hz, <i>syn</i>)
			2.13 (s, <i>anti</i>)		2.43 (s, <i>anti</i>)	4.84 (AB, J = 12 Hz, <i>anti</i>); 4.90 (AB, J = 12 Hz, <i>anti</i>)
(3.3) Br (-75 °C)	CD ₂ Cl ₂		2.15 (s, <i>syn</i>)	2.275 (s, <i>syn</i>)	2.28	4.56 (AB, J = 10.4 Hz, <i>syn</i>); 4.58 (AB, J = 10.4 Hz, <i>syn</i>)
			2.17 (s, <i>anti</i>)	2.281 (s, <i>anti</i>)		4.61 (AB, J = 10.9 Hz, <i>anti</i>); 4.65 (AB, J = 10.9 Hz, <i>anti</i>)
(-90 °C)	CD ₃ COCd ₃		2.13 (s, <i>syn</i>)	2.270 (s, <i>syn</i>)	2.39 (s, <i>syn</i>)	4.76 (AB, J = 11 Hz, <i>syn</i>); 4.78 (AB, J = 11 Hz, <i>syn</i>)
			2.14 (s, <i>anti</i>)	2.275 (s, <i>anti</i>)	2.41 (s, <i>anti</i>)	4.78 (AB, J = 10.9 Hz, <i>anti</i>); 4.87 (AB, J = 10.9 Hz, <i>anti</i>)

Continued on the next page

Table 3.1. *continued*

compound	Solvent	Chemical shifts /ppm				
		C(CH ₃) ₃	CH ₃	2 CH ₃	CH ₃	CH ₂ X
(-80 °C)	CD ₃ COD		2.23 (s, <i>syn</i>) 2.24 (s, <i>anti</i>)	2.34	2.40 (s, <i>syn</i>) 2.42 (s, <i>anti</i>)	4.68 (AB, J = 11 Hz, <i>syn</i>); 4.72 (AB, J = 11 Hz, <i>syn</i>) 4.74 (AB, J = 11 Hz, <i>anti</i>); 4.80 (AB, J = 11 Hz, <i>anti</i>)
(-90 °C)	Toluene- <i>d</i> ₆		1.47 (s, <i>anti</i>) 1.61 (s, <i>syn</i>)	1.84 (s, <i>syn</i>) 1.85 (s, <i>anti</i>)	^a	3.86 (m)
(3,4) Br ^b	CD ₂ Cl ₂		2.32	2.36		4.523 (s); 4.537 (AB, J = 10.6 Hz, <i>syn</i>) 4.615 (AB, J = 10.6 Hz, <i>syn</i>);
	CD ₃ COCOD ₃			2.33 (s, <i>anti</i>) 2.34 (s, <i>syn</i>)	2.40	4.71 (AB, J = 11 Hz, <i>anti</i>); 4.72 (AB, J = 11 Hz, <i>syn</i>) 4.76 (AB, J = 11 Hz, <i>syn</i>); 4.84 (AB, J = 11 Hz, <i>anti</i>)
(3,5) I	CD ₂ Cl ₂		2.18	2.220 (s, <i>anti</i>) 2.224 (s, <i>syn</i>)	2.25 (s, <i>syn</i>) 2.26 (s, <i>anti</i>)	4.39 (AB, J = 10.5 Hz, <i>syn</i>); 4.42 (AB, J = 10.5 Hz, <i>syn</i>) 4.42 (AB, J = 10.5 Hz, <i>anti</i>); 4.50 (AB, J = 10.5 Hz, <i>anti</i>)

^a One of the signals from the methyl group is being obscured by the solvent peak.^b The signal in the aromatic region of the proton NMR is not shown.

Table 3.2. The ^{13}C NMR chemical shifts for the dineopentyl- (3.1), chloride (3.2), 1,3-bis(bromomethyl)-2,4,5,6-tetramethylbenzene (3.3), 1,3-bis(bromomethyl)-2,4,6-tetramethylbenzene (3.4) and the iodide (3.5). (The chemical shifts from the more intense signals are shown in red.)

X (T/ $^{\circ}\text{C}$) solvent	Chemical Shifts /ppm					Aromatic Carbons			
	CH_3	2CH_3	CH_3	$(\text{CH}_3)_3$	$\text{C}(\text{CH}_3)_3$	CH_2X			
^tBu /(-60 $^{\circ}\text{C}$)	17.56 (<i>anti</i>)	19.64 (<i>syn</i>)	20.35 (<i>anti</i>)	30.38 (<i>syn</i>)	35.28	41.41 (<i>syn</i>)	133.87 (<i>syn</i>)	134.48 (<i>syn</i>)	135.00 (<i>anti</i>)
CD_2Cl_2	17.62 (<i>syn</i>)	19.97 (<i>anti</i>)	20.76 (<i>syn</i>)	30.62 (<i>anti</i>)	35.56	41.57 (<i>anti</i>)	134.05 (<i>anti</i>)	134.57 (<i>anti</i>)	135.26 (<i>syn</i>)
								135.82 (<i>syn</i>)	
Cl /(-92 $^{\circ}\text{C}$)	14.66 (<i>anti</i>)	16.02	16.30			42.58 (<i>syn</i>)	131.12 (<i>syn</i>)	133.31 (<i>anti</i>)	133.80 (<i>anti</i>)
CD_2Cl_2	14.81 (<i>syn</i>)					42.62 (<i>anti</i>)	131.32 (<i>anti</i>)	133.53 (<i>syn</i>)	133.91 (<i>syn</i>)
								136.42 (<i>anti</i>)	136.56 (<i>syn</i>)
Br /(-75 $^{\circ}\text{C}$)	14.75 (<i>anti</i>)	16.15	16.15 (<i>syn</i>)			31.88 (<i>syn</i>)	131.42 (<i>syn</i>)	133.47 (<i>anti</i>)	133.99 (<i>anti</i>)
CD_2Cl_2	14.90 (<i>syn</i>)		16.43 (<i>anti</i>)			31.94 (<i>anti</i>)	131.69 (<i>anti</i>)	133.73 (<i>syn</i>)	134.12 (<i>syn</i>)
						32.80	132.42 (<i>syn</i>)	134.21 (<i>anti</i>)	134.95 (<i>anti</i>)
$\text{CD}_3\text{COCOD}_3$	15.21 (<i>syn</i>)						132.71 (<i>anti</i>)	134.37 (<i>syn</i>)	135.09 (<i>syn</i>)
								137.53 (<i>syn</i>)	
I /(-60 $^{\circ}\text{C}$) ^a	15.27	16.66	16.80			6.66	132.32	133.11	134.20
CD_2Cl_2	15.42	16.62	16.89			6.83	132.91	133.04	134.30
								135.81	

^a. The signal intensity ratio cannot be distinguished from 1:1.

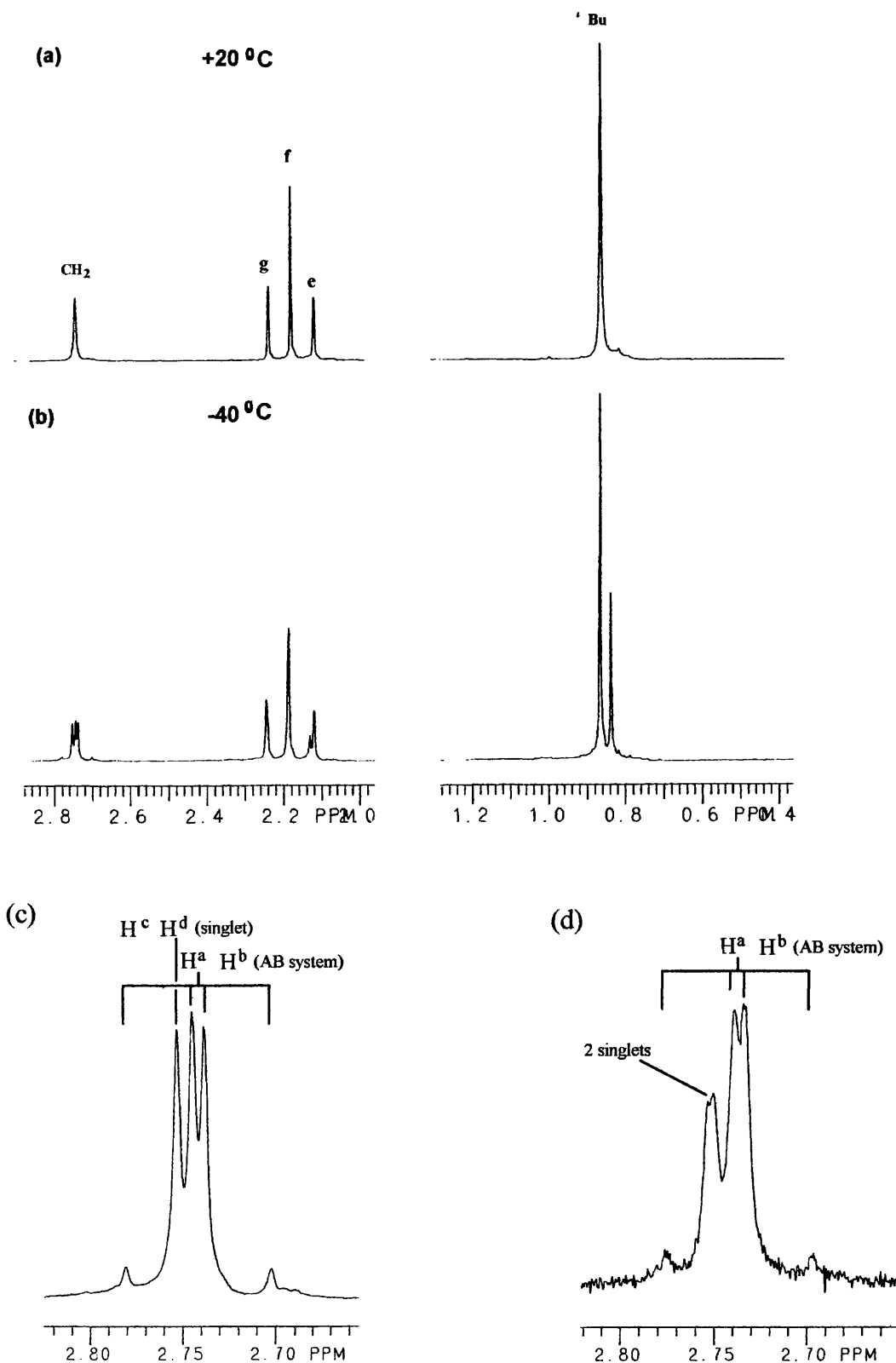


Figure 3.4.

- (a) The proton NMR spectrum of the dineopentyl-compound (3.1) in CD_2Cl_2 at $+20^\circ\text{C}$.
 (b) The proton NMR spectrum of the same sample but at -40°C .
 (c) An expansion of the methylene region of the spectrum shown in (b)
 (d) The methylene region of the proton NMR spectrum of (3.1) in the presence of excess shift reagent in CD_2Cl_2 at -40°C . The AB quartet persists unsplit and the singlet has now split into two.

From the relative intensities of the $\text{C}(\text{CH}_3)_3$ peaks a *syn/anti* conformational population ratio of 2.2:1 is obtained, this ratio is constant over the temperature range, -40 to -80 $^{\circ}\text{C}$. But in the more polar solvent mixture of $\text{CHClF}_2:\text{CHCl}_2\text{F}:\text{CD}_2\text{Cl}_2$ ($\sim 2:2:1$), a slightly higher temperature-independent ratio of 2.4:1 over the range -40 to -100 $^{\circ}\text{C}$ is observed. The ratios obtained with the two solvents, methylene chloride- d_2 (100 %) and freon, at -40 $^{\circ}\text{C}$ equates to energy differences of 360 and 410 kcal mol^{-1} respectively in favour of the *syn* conformation.

In contrast to methylene chloride- d_2 (100 %) and the mixture of freons, in acetone- d_6 , the *syn/anti* ratio is slightly temperature dependent, with the ratios rising from 2.2 to 2.7:1 on cooling from -20 to -80 $^{\circ}\text{C}$. The ratios obtained with the three solvents at various temperatures together with the energy differences at -40 $^{\circ}\text{C}$ are summarised in table 3.3. The proton NMR chemical shifts in the three solvents at low temperature are shown in table 3.1.

Table 3.3. The equilibrium constant of 1,3-dineopentyl-tetramethylbenzene (3.1) in three different solvents at various temperatures.

Solvent	Temperature / $^{\circ}\text{C}$	Equilibrium Constant ^a	ΔG / cal mol^{-1}
CD_2Cl_2	-40	2.2	-360
	-60	2.2	
	-80	2.2	
Freons ^b	-40	2.4	-410
	-60	2.4	
	-80	2.4	
	-100	2.4	
CD_3COCD_3	-20	2.2	-390
	-40	2.3	
	-60	2.4	
	-80	2.7	

^a This is the *syn/anti* ratio.

^b The solvent is $\text{CHClF}_2:\text{CHCl}_2\text{F}:\text{CD}_2\text{Cl}_2$ ($\sim 2:2:1$).

(b) NMR of the 1,3-bis(halomethyl)-benzene-compounds (3.2, 3.3, 3.4 and 3.5)

The features of the ^1H and ^{13}C NMR spectra of the halomethyl compounds at ambient and lower temperatures are similar. In the four halides, rotation about the $\text{C}-\text{CH}_2\text{X}$

bonds are slow on the NMR time scale at temperatures lower than -60°C . The energy barriers to rotation about these bonds will be discussed in chapter six. The ^1H and ^{13}C NMR chemical shifts at low temperatures are summarised in tables 3.1 and 3.2 respectively.

For the dichloro-compound (3.2), the methylene region of the ^1H NMR spectrum in methylene chloride- d_2 at -92°C consists of an AB system centred at 4.65 and 4.68 ppm together with a singlet at 4.71 ppm, see figure 3.5a. But in the presence of a shift

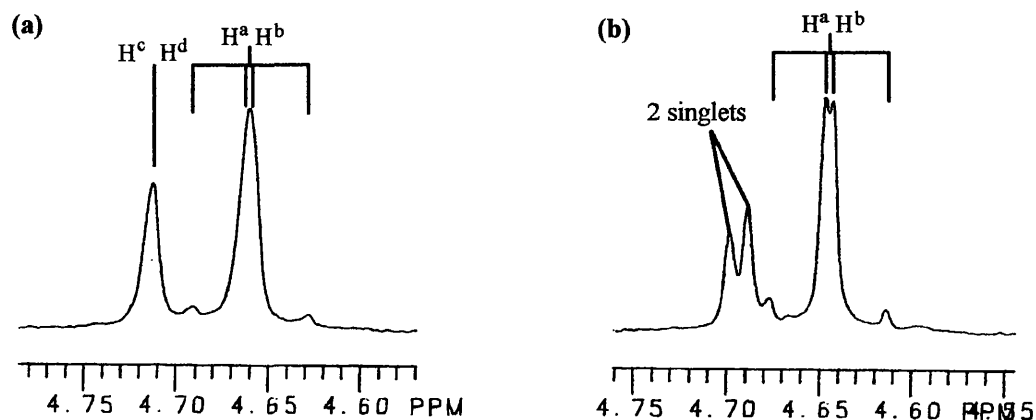


Figure 3.5.

- (a) The methylene region of the ^1H NMR of the chloride (3.2) in methylene chloride- d_6 at -92°C . The letters in superscript denotes the environment of the protons, see figure 3.2.
- (b) The methylene region of the proton NMR of the chloride in the presence of excess shift reagent at -92°C . The singlet has now split into two whilst the AB system remain unchanged.

reagent there is splitting of the singlet signal into two due to the formation of diastereomers from the interaction of the *anti* conformer with the shift reagent, see figure 3.5b. Thus, the AB system is from the *syn* conformation whilst the singlet is from the *anti* conformation. From the relative intensities of the AB quartet and singlet, the *syn/anti* population ratio was found to be 1.8:1, an energy difference of $0.21\text{ kcal mol}^{-1}$. The observed conformational population ratio is also substantiated by ^{13}C NMR spectroscopy. The ^{13}C NMR spectrum of the aromatic region at -92°C is shown in figure 3.6 as expected each of the four signals that appeared at room temperature has all split into two signals of unequal intensities.

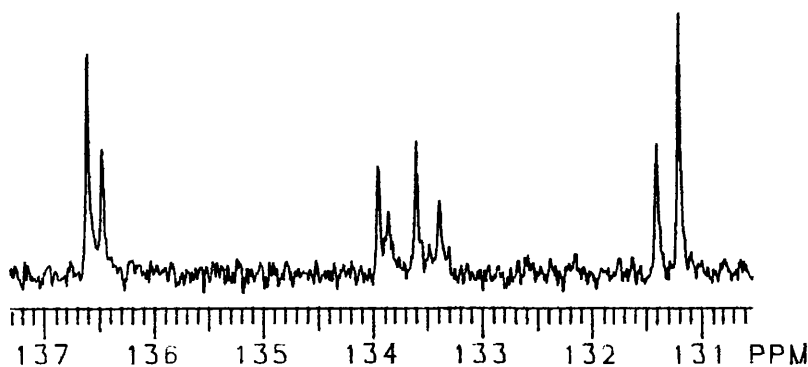


Figure 3.6. The aromatic region of the ^{13}C NMR of the chloride (3.2) in methylene chloride- d_6 at -85°C .

In acetone- d_6 at -90°C , the *syn/anti* ratio is slightly higher at 2.0:1, an energy difference of $0.25\text{ kcal mol}^{-1}$ in favour of the *syn* conformation.

The NMR spectrum of the bromide (3.3) was carried out in four different solvents, methylene chloride- d_2 , acetone- d_6 , toluene- d_8 and methanol- d_4 . Figure 3.7 is the methylene region of the ^1H NMR of 3.3 in methylene chloride- d_2 at -80°C . Unlike

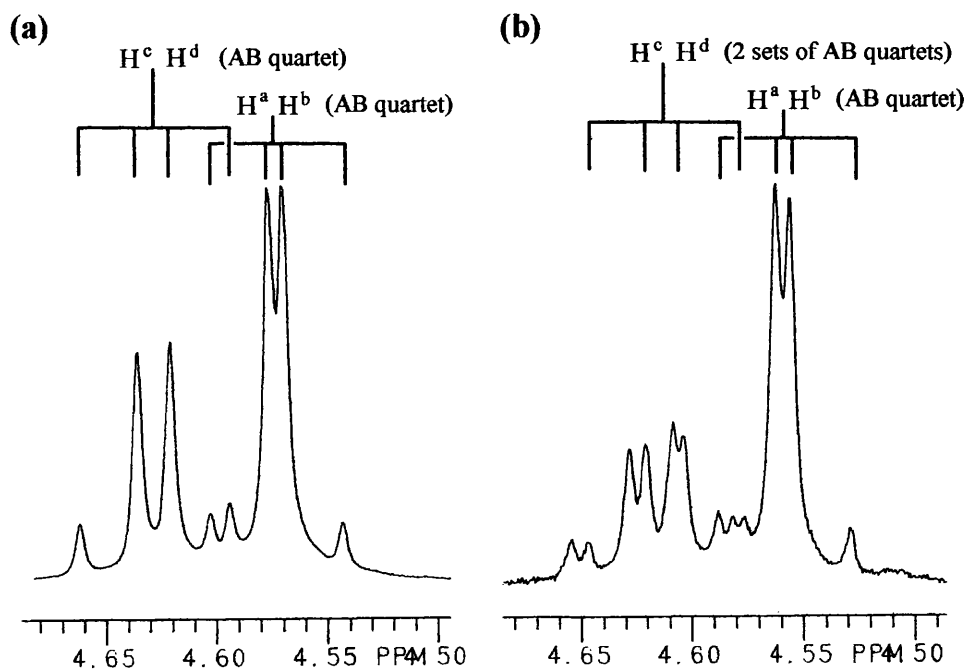


Figure 3.7.

(a) The methylene region of the proton NMR of the bromide (3.3) in CD_2Cl_2 at -80°C ,

(b) The methylene region of the same sample but with about three fold excess of a shift reagent. The more downfield of the quartets have now split into two whilst the more upfield remained unsplit.

the dineopentyl- and dichloro-compounds, the two sets of AB quartets in the dibromo-compound are well resolved. The set centred at 4.61 and 4.65 ppm did split into two in the presence of a shift reagent, while the other set at 4.56 and 4.58 ppm remained unaffected. Thus the more intense of the AB system is from the *syn* conformation. Using the relative intensities of the signals in the methylene region, a *syn/anti* population ratio of 1.5:1 equating to an energy difference of 0.15 kcal mol⁻¹ at -80 °C in favour of the *syn* conformation is observed.

In the more polar solvents, acetone-*d*₆ and methanol-*d*₄, a slightly higher population ratios of 1.7:1, equating to free energy differences of 0.19 kcal mol⁻¹ (at -90 °C in acetone) and 0.20 kcal mol⁻¹ (at -80 °C in methanol) both in favour of *syn* are observed. The lowest energy difference between the two conformations of the bromide (3.3) is obtained when a relatively non-polar solvent, toluene, is being used. The observed *syn/anti* population ratio in toluene is 1.3:1 at -90 °C, an energy difference of 0.10 kcal mol⁻¹.

As for, bis-1,3-(bromomethyl)-2,4,6-trimethylbenzenes (i.e. 5-nor-dibromo-), the spectrum was carried out in two deuterated solvents, methylene chloride-*d*₂ and acetone-*d*₆. The methylene region of the ¹H NMR in methylene chloride-*d*₂ at -85 °C consists of two sets of AB systems. From the quartets, the *syn/anti* conformational population ratio was found to be moderately lower at 1.2:1 (0.066 kcal mol⁻¹ in favour of *syn*), in comparison to that of the other bromide (3.3) with one more methyl group. Here, the *syn/anti* ratio is 1.5:1 (0.15 kcal mol⁻¹ in favour of *syn* at -80 °C). This trend is also reflected in their free energy differences.

In a more polar solvent, acetone-*d*₆, at -90 °C, the ratio is unchanged at 1.2:1 an energy difference of 0.068 kcal mol⁻¹. And once again, if one compares the results for both bromides in acetone-*d*₆, the magnitude of the energy differences is much higher in the tetramethyl-benzene derivative (3.3)

Considering the proton NMR spectrum of the diiodo-compound (3.5) in CD₂Cl₂ at -60 °C. The methylene region of the spectrum (see figure 3.8a) contains two sets of AB quartets of intensity ratio 1.1:1. But in the presence of a shift reagent the more down-field and less intense AB system, centred at 4.42 and 4.50 ppm did split into two whilst the up-field and more intense quartet remained unaffected (see figure 3.8b). Thus, the more intense AB system is from the *syn* conformation. The observed ratio

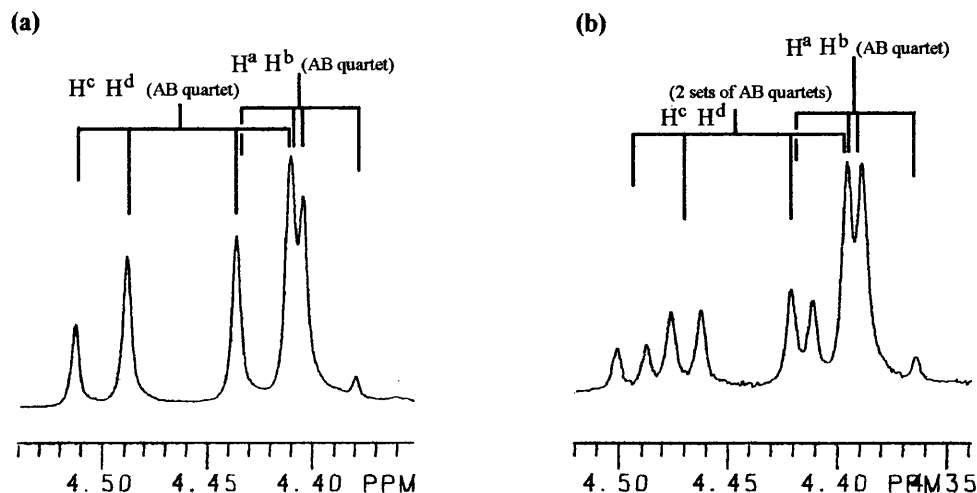


Figure 3.8.

(a) The methylene region of the proton NMR of the iodide (**3.5**) in CD_2Cl_2 at -60°C .

(b) The methylene region of the proton NMR of a sample of **3.5** containing about seven fold excess of a shift reagent.

equates to an energy difference of $0.040 \text{ kcal mol}^{-1}$ in favour of the *syn* conformation

It is worth pointing out that in all the dineopentyl and halomethyl compounds considered in this chapter, the proton NMR signals arising from the methylene protons of the *anti* always resonates downfield to those from the *syn* conformation. This observation also applies to the 1,3,5-trisubstituted-trimethylbenzenes discussed in the preceding chapter. Likewise, in the ^{13}C NMR spectra of the halomethyl-compounds the pattern observed as regards the relative shift of the *syn* and *anti* signals is the same in both the dichloro- and dibromo-compounds (for the diiodo-compound the *syn* and *anti* signals are indistinguishable). However, no clear pattern is observed for the methyl signals in the proton NMR.

(3.1.1-2) MM3 calculations

MM3 calculations were carried out on the dineopentyl- (**3.1**), dichloro- (**3.2**), dibromo- (**3.3**), 5-nor-dibromo- (**3.4**) and the diiodo- (**3.5**) compounds. A breakdown of the energies together with the difference in steric energies between the *syn* and *anti* conformations ($\Delta H_{\text{calc.}}$) are summarised in table 3.4a. The prediction for each of **3.1** - **3.5** is that the *syn* conformation is the more stable.

Table 3.4a The contributions to the final steric energies (kcal mol⁻¹) for the dineopentyl-compound (3.1), chloride (3.2), 1,3-bis(bromomethyl)-2,4,5,6-tetramethylbenzene (3.3), 1,3-bis(bromomethyl)-2,4,6-tetramethylbenzene (3.4) and the iodide (3.5)

	Dineopentyl comp. (3.1)		Chloride (3.2)		Bromide (3.3)		Bromide (3.4)		Iodide (3.5)	
	<i>Syn</i>	<i>Anti</i>	<i>Syn</i>	<i>Anti</i>	<i>Syn</i>	<i>anti</i>	<i>syn</i>	<i>anti</i>	<i>syn</i>	<i>anti</i>
Compression	2.6655	2.7950	1.8351	1.9698	1.9400	2.0482	1.4564	1.5033	1.8778	1.9949
Bending	3.5569	3.6722	2.7355	3.0658	2.7682	3.0731	2.3223	2.4515	3.5680	3.8731
Bend-bend	-0.1896	-0.1855	-0.3097	-0.3088	-0.3101	-0.3095	-0.2426	-0.2386	-0.5526	-0.5564
Stretch-bend	-0.5969	-0.6210	-0.3847	-0.3987	-0.3842	-0.4003	-0.2799	-0.2859	-0.3720	-0.3914
van der Waals										
1,4 energy	19.1027	18.9283	9.0343	8.9600	9.0033	8.9801	8.0112	8.0082	8.7257	8.6678
Other	2.8975	3.6463	5.3413	5.9587	5.3958	5.9270	2.4286	2.6240	5.0464	5.5758
Torsional	-14.8828	-15.0962	-5.3413	-5.5097	-5.7745	-5.8576	-5.4871	-5.5421	-16.6447	-16.5273
Torsion-stretch	0.0000	0.0000	0.0000	0.0000	0.0000	0.0000	0.0000	0.0000	0.0000	0.0000
Dipole-dipole	16.0837	16.1900	5.7821	5.5341	6.1239	5.9456	5.5978	5.4371	6.2430	6.0939
Total Steric Energy (<i>H</i>)	28.6370	29.3291	18.4599	19.2713	18.7625	19.4065	13.8069	13.9574	7.8916	8.7304
-Δ <i>H</i>	0.6921		0.8114		0.6440		0.1505		0.8388	

The sum of the pair wise van der Waals interaction from the two **X** groups in both conformations, are summarised in table 3.4b, such interactions favours the *syn* conformation in the five compounds.

For the dineopentyl-compound, the difference in total enthalpy ($\Delta H_{\text{calc.}}$) was calculated to be $0.69 \text{ kcal mol}^{-1}$ in favour of the *syn* conformation. However, when only the 169 i.e. (13 x 13) mutual atom-atom van der Waals interaction of the two *tert*-butyl groups in both conformations are extracted from the calculation, the more compact *syn* conformation is about $0.25 \text{ kcal mol}^{-1}$ more stable i.e. $0.44 \text{ kcal mol}^{-1}$ of the overall $0.69 \text{ kcal mol}^{-1}$ comes from elsewhere. The $0.25 \text{ kcal mol}^{-1}$ advantage for the *syn* conformation is actually in spite of there being a $0.095 \text{ kcal mol}^{-1}$ repulsive interaction between the nearest pair of hydrogen atoms from the two *tert*-butyl groups in the *syn* conformer.

Table 3.4b. The sum of the atom-atom van der Waals interaction (kcal mol^{-1}) between the two **X** groups in 3.1 – 3.5.

	Neopentyl-compd. (3.1)	Chloride (3.2)	Bromide ^a (3.3)	Bromide ^b (3.4)	Iodide (3.5)
<i>Syn</i>	-0.4190	-0.0375	-0.0721	-0.0739	-0.1067
<i>Anti</i>	-0.1680	-0.0213	-0.0364	-0.0391	-0.0507
Diff. ^c	-0.2510	-0.0162	-0.0357	-0.0348	-0.0560

^a The bis (bromomethyl) tetramethylbenzene.

^b The bis (bromomethyl) trimethylbenzene.

^c The difference between the *syn* and *anti*

The remainder of $\Delta H_{\text{calc.}}$, about $0.41 \text{ kcal mol}^{-1}$, may only be explained in terms of gearing. Presumably, there is less strain in the geared system that is in operation in the *syn* conformation. The conformation adopted by the groups on the ring is calculated to be as in figure 3.9, which shows torsional angles as calculated rather than stylised. All groups except methyl in the 5 position show more or less distortion from being orthogonal to the ring plane.

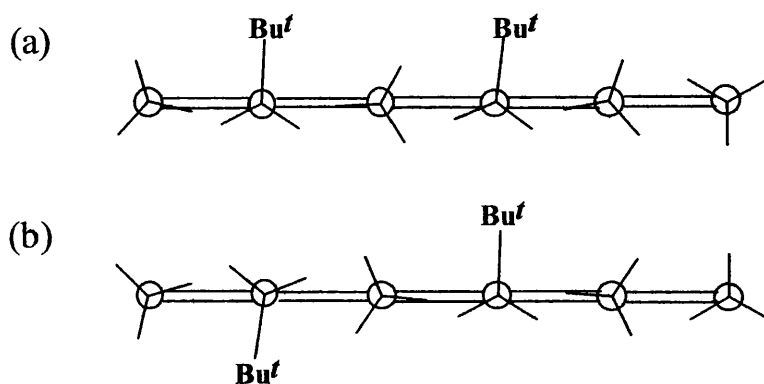


Figure 3.9. The conformations adopted by the groups on the benzene ring in the *syn* and *anti* conformations of the dineopentyl compound (3.1). Note the diagram was constructed using the individual torsional angles from the MM3 print out.

In all the halomethyl-benzenes the magnitude of the relative stabilisation energy gained by the *syn* conformation in having the two halogen atoms on the same face of the ring is small and it increased in the order $\text{Cl} < \text{Br} < \text{I}$, the energies being (3.2 ; 16), (3.3 ; 36), (3.4 ; 35) and (3.5 ; 56 cal mol^{-1}) see table 3.4b.

Considering the dipole-dipole interaction between the polar C-X bonds in the halides, in the *syn* conformation, where the dipoles are closer to being aligned in the same direction, the destabilising energy is significantly higher than in the *anti*, where the two dipoles are more or less *anti* parallel. Comparing individual C-X/C-X dipole-dipole interaction values, the net effect is that the *syn* conformations are relatively destabilised by (3.2 ; 0.23), (3.3 ; 0.16), (3.4 ; 0.17) and (3.5 ; 0.12 kcal mol^{-1}) see table 3.5. There seems to be a correlation between these values and the overall dipole-dipole

Table 3.5. The energy in kcal mol^{-1} associated with the interaction of the two dipoles from the C-X bonds in 3.1 – 3.5.

	Chloride (3.2)	Bromide ^a (3.3)	Bromide ^b (3.4)	Iodide (3.5)
<i>Syn</i>	+0.2527	+0.1802	+0.1788	+0.1617
<i>Anti</i>	+0.0184	+0.0169	+0.0083	+0.0316
Diff. ^c	+0.2343	+0.1633	+0.1725	+0.1201

^a The bis (bromomethyl) tetramethylbenzene.

^b The bis (bromomethyl) trimethylbenzene.

^c The difference between the *syn* and *anti*

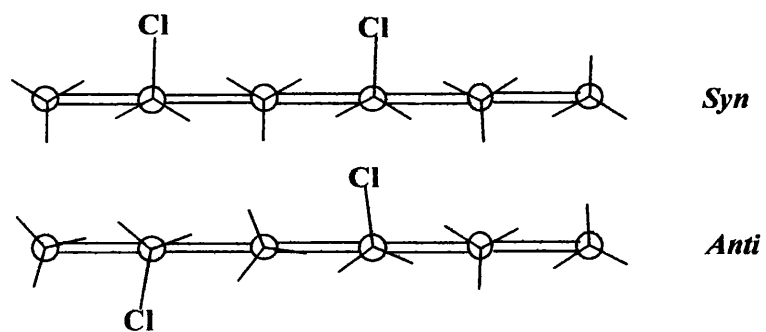
contributions to the final steric energies. In the dineopentyl-compound the destabilisation energy from dipole-dipole interactions is negligible since the C-X bond is relatively non-polar.

In the halides, the calculated *syn* advantage from X-X van der Waals interaction is small compared to the overall calculated ΔH advantage of *syn*. Furthermore, the *anti* conformation is favoured by dipole-dipole interactions, so there must be a further factor that strongly favours *syn*. This is concluded to be a high level of unfavourable interactions between the methyl and halomethyl groups in the *anti* conformation. Such unfavourable interactions are reduced in the *syn* conformation because, unlike in the *anti*, the methyl and halomethyl groups attached to the benzene ring are nicely “geared”.

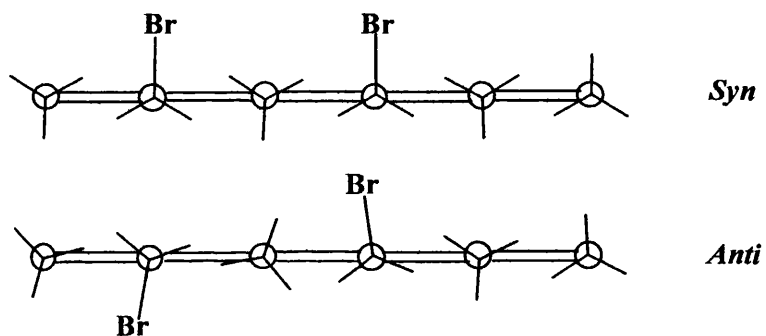
Figure 3.10 shows the arrangement of both groups in the *syn* and *anti* conformations of the halides. In each and every one of the *syn* conformations, with the exception of the trimethyl-benzene derivative of the bromide, a C-H bond from each of the four methyl groups together with the two C-X (X = Cl, Br or I) bonds, are more or less perpendicular to the plane of the ring, furthermore, these bonds are arranged in an up and down manner all the way round the ring. The up and down arrangement of bonds is similar to that observed for the most stable conformations of hexamethyl-³¹, hexaethyl-benzenes³². By contrast, in the *anti* conformation, a C-H bond from two of the methyl groups both lie in the plane of the ring.

It is also interesting how in the dineopentyl-compound, the two tert-butyl groups are so demanding of space that no up and down gearing of substituents is possible. To shed more light on the role played by “gear effect”, compare the ΔH_{calc} values for both bromides i.e. 3.3 and 3.4. The calculated value for (3.3) is significantly higher than that for the 5-nor-dibromo-compound. Presumably, because the later, in comparison to the former, has one fewer methyl group, therefore, less steric crowding as a result of which the contribution from gear effect is less pronounced.

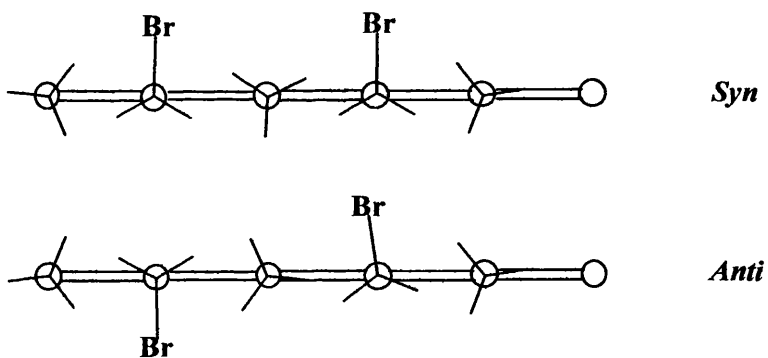
(3.2)



(3.3)



(3.4)



(3.5)

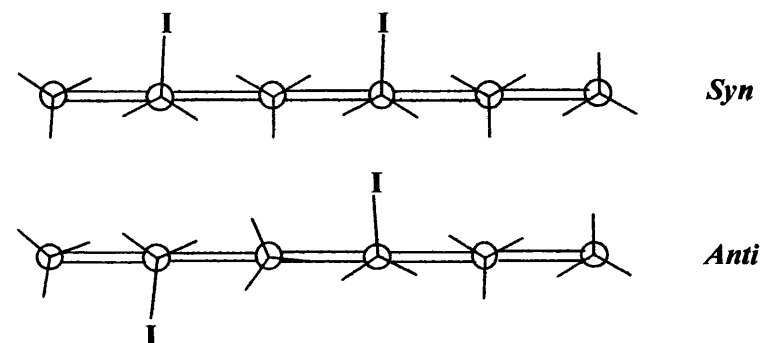


Figure 3.10. The interlocking arrangement of the halomethyl and methyl groups in the *syn* and *anti* conformations of the halides (3.2 – 3.5). The diagram was constructed using the calculated torsional angles.

(3.1.2) Conclusion

In 3.1 - 3.5, NMR spectroscopy showed that the more compact *syn* conformation is more stable than the *anti* a trend also supported by MM3 calculations. The ΔG_{exp} and ΔH_{calc} values are summarised in table 3.6. One has to be cautious in attributing the whole of the free energy difference (ΔG_{exp}) to attractive steric interactions between the two X groups because:

Table 3.6 Summary of the results from NMR spectroscopy and calculation.

X	solvent	Temperature /°C	Equilibrium constant	$-\Delta G_{exp}$ /cal mol ⁻¹	$-\Delta H_{calc}$ /cal mol ⁻¹
^t Bu ^a	CD ₂ Cl ₂	-40	2.2	360	660
	Freon	-40	2.4	410	
	Acetone- <i>d</i> ₆	-40	2.3	390	
Cl	Acetone- <i>d</i> ₆	-90	2.0	250	810
	CD ₂ Cl ₂	-92	1.8	210	
Br (3.3)	Acetone- <i>d</i> ₆	-90	1.7	190	640
	Methanol- <i>d</i> ₆	-80	1.7	200	
	CD ₂ Cl ₂	-80	1.5	150	
	Toluene- <i>d</i> ₈	-90	1.3	95	
Br (3.4)	Acetone- <i>d</i> ₆	-90	1.2	66	150
	CD ₂ Cl ₂	-85	1.2	68	
I	CD ₂ Cl ₂	-60	1.1	40	840

^a The *syn/anti* ratio is temperature dependent in acetone but not in freon and methylene chloride.

Firstly, if this was the case, ΔG_{exp} would be expected to be equal in both bromides i.e. 3.3 and 3.4, after all, the X groups in both compounds are the same. But in actual fact the ΔG_{exp} obtained for the more strained 3.3 is about 0.1 kcal mol⁻¹ greater than that of the 5-nor-dibromo-compound. One possible explanation for the observed result in light of the prediction from calculation is that the interlocking of methyl and

halomethyl groups stabilises the *syn* conformation of the hexa-substituted-benzene (3.3) to a greater extent in comparison to the penta-substituted-benzene (3.4).

Secondly, calculations for the hexa-substituted-benzenes (3.2, 3.3 and 3.5) indicate that dipole-dipole interactions between polar C-X bonds, also affect the magnitude of ΔH_{calc} by destabilising the *anti* relative to the *syn*.

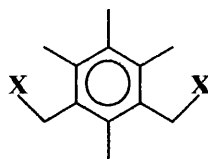
In summary, as for the dineopentyl compound (3.1), calculations shows that a significant amount of the energy difference between the *syn* and *anti* could be attributed to attractive steric interactions between the *tert*-butyl groups. But for the halides, the attraction between the halogen atoms, even when they are closer together is so small suggesting that a substantial amount of the calculated *syn/anti* energy difference originates from steric interaction between neighbouring halomethyl and methyl groups on the ring. Such interactions destabilise the *anti* form relative to the *syn*. In the dineopentyl compound, the role played by such destabilising steric interactions, is not as clear-cut as in the halides because in neither the *syn* or *anti* conformations is the up and down arrangement of bonds preserved. The *tert*-butyl group is so bulky that it prevents C-H bonds in adjacent methyl groups from being perpendicular to the ring plane.

The magnitude of ΔG_{exp} in a particular solvent in the hexa-substituted-benzenes (3.2, 3.3 and 3.5), increases in the order iodide < bromide < chloride a trend MM3 fails to predict just like in the 1,3,5-tris(halomethyl)-2,4,6-trimethylbenzenes (see chapter two). An explanation for this is that MM3 poorly reproduces the steric strain associated with these molecules.

The magnitude of ΔG_{exp} increases slightly but consistently with increasing solvent polarity in the bromide (3.3) and chloride (3.2). Presumably, the *syn* forms a more stable CH/ π interaction type complex with the solvent because unlike the *anti*, in the *syn*, one side of the ring plane is free of steric hindrance. Here, the polar C-H bonds and π electrons are provided by the solvent and solute respectively and the more polar the solvent the more polar are their C-H bonds and therefore the more stable are their complexes.

The calculations certainly encourage caution in interpreting the experimental results.

SECTION TWO

(3.2.1) Results and Discussion of 3.6-3.10

	X
3.6	Me
3.7	Ph
3.8	<i>p</i> -C ₆ H ₄ -NO ₂

	X
3.9	β -Naphthyl
3.10	OMe

(3.2.1-1) Conformational assignment of NMR signals at low temperature.(a) *NMR spectra of the diethyl compound (3.6)*

In 1,3-diethyl-2,4,5,6-tetraethylbenzene (**3.6**), proton NMR spectroscopy at low temperatures did not yield much useful information because the signals were strongly overlapping one another.

The aromatic region of the ¹³C NMR spectrum at +22 °C contains four peaks. But on cooling, the most downfield of the signals which comes from the ring carbon bearing the ethyl group, broadened and then de-coalesces at about -103 °C before finally splitting into two signals of intensity ratio 2.2:1 at -120 °C. The aromatic region of the ¹³C NMR spectrum in CHFC1₂:CD₂Cl₂ (~4:1) is shown in figure 3.9.

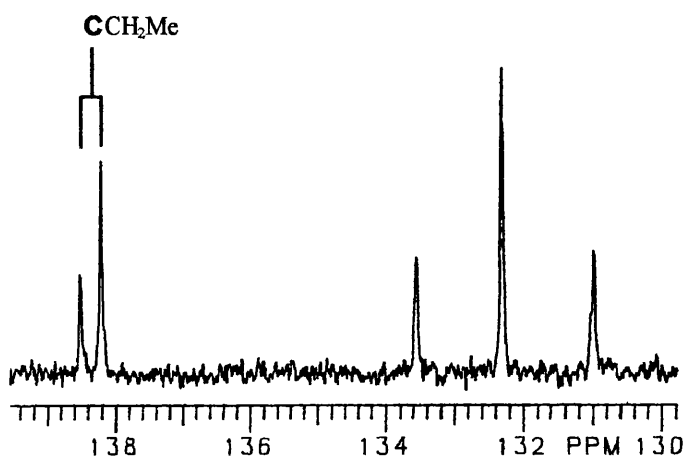


Figure 3.9. The aromatic region of the ¹³C NMR spectrum of the diethyl compound (**3.6**)

We were unable to differentiate between the signals from the *syn* and *anti* conformations in either the ¹H or ¹³C NMR spectra, but since in the *tri*-substituted analogue i.e. 1,3,5-triethyl-2,4,6-trimethylbenzene, (see chapter 2 for the discussion of

this compound) the *syn* conformation is the more stable by about $0.24 \text{ kcal mol}^{-1}$, it is plausible to suggest that by analogy the *syn* conformation of diethyl compound (3.6) would also be the more stable and the more populated. Thus, the observed ratio corresponding to an energy difference of $0.24 \text{ kcal mol}^{-1}$ in favour of the *syn* conformation.

(b) *NMR spectra of 3.7 – 3.9*

As for the *di*-phenyl compound (3.7), at $+22^\circ\text{C}$ rotation about the $\text{C-CH}_2\text{Ph}$ bonds is fast on the NMR time scale as a result of which an average spectrum representing the both conformations is observed in the $400 \text{ MHz } ^1\text{H}$ and $100.6 \text{ MHz } ^{13}\text{C}$ NMR spectra. However, on cooling the sample, the singlet signal in the methylene region broadened and then de-coalesces at about -105°C before eventually sharpening at lower temperatures. At -130°C , the singlet has split into an AB quartet and a singlet, with the singlet marginally upfield the midpoint of the AB system, see figure 3.10a. Because of strong overlapping of signals in both the methylene and methyl regions, it is not possible to extract the conformational population ratio from the proton NMR spectrum. Nevertheless, in the methylene region, the singlet was found to be more intense than the AB system.

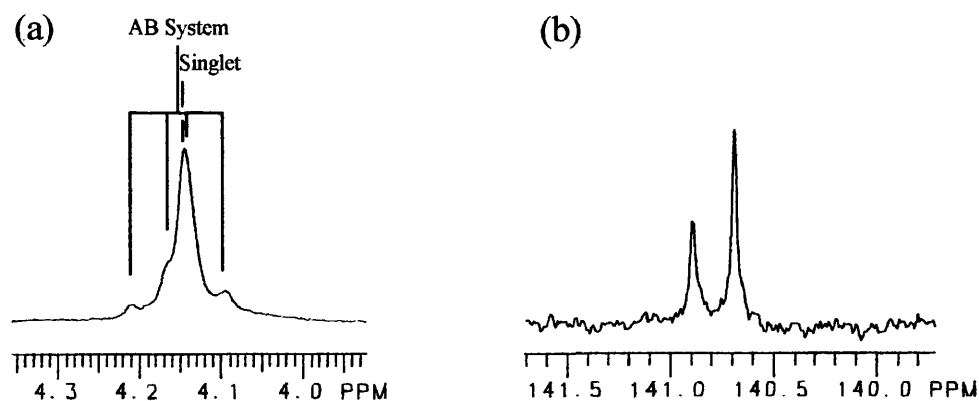


Figure 3.10.

- (a) The methylene region of the proton NMR spectrum of the *di*-phenyl compound (3.7) at -130°C .
(b) The signal from the CCH_2Ph aromatic carbon at -130°C .

In the ^{13}C NMR spectrum at $+22^\circ\text{C}$, the most downfield peak that comes from the ring carbon bearing the CH_2Ph group is well separated from other signals. On cooling to -130°C , this isolated ring carbon signal has split into two peaks of intensity

ratio 2.2:1, this equates to an energy difference of $0.18 \text{ kcal mol}^{-1}$. The signal from the CCH_2Ph aromatic carbon at -130°C is shown in figure 3.10b.

For the *di*-nitro (3.8) compound, in the aromatic region of the $100 \text{ MHz } ^{13}\text{C}$ NMR spectrum at -120°C , a population ratio of 1.7:1 is obtained from the signal of the ring carbon bearing the NO_2 group. They are the most down field in the spectrum, resonating at 149.45 and 149.34 ppm, the pair of peaks of interest are shown in figure 3.11b. The intensity ratio of these peaks equates to an energy difference of $0.16 \text{ kcal mol}^{-1}$.

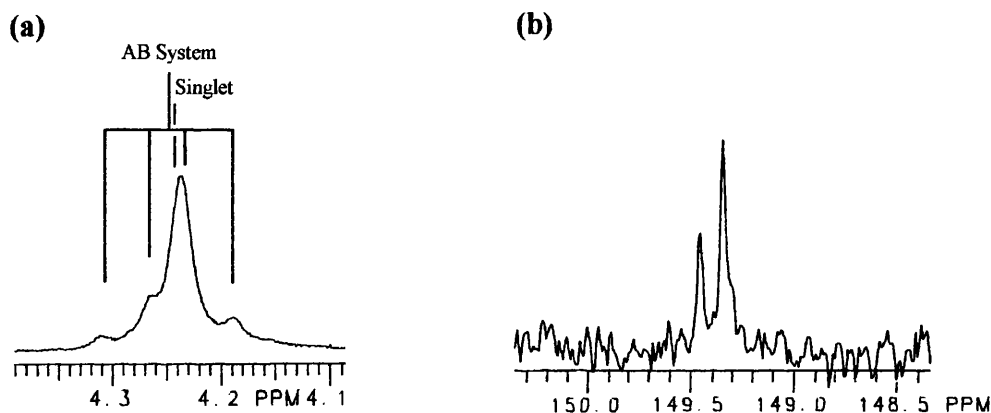


Figure 3.11.

- (c) The methylene region of the proton NMR spectrum of the *di*-nitro compound (3.8) at -120°C .
(d) The signal from the CCH_2Ph aromatic carbon at -120°C .

As regards the *di*-naphthyl compound (3.9), the ^{13}C NMR spectrum at temperatures below -120°C did not yield much useful information as to the population ratio of the two conformations because of the complex nature of the spectrum. Nevertheless, the ratio was extracted from the methyl region of the proton NMR spectrum albeit at the expense of precision. The methyl region of the proton NMR spectrum at -120°C is shown in figure 3.12, from the methyl signals a population ratio of about 1.3 is obtained. This represents an energy difference of $0.080 \text{ kcal mol}^{-1}$.

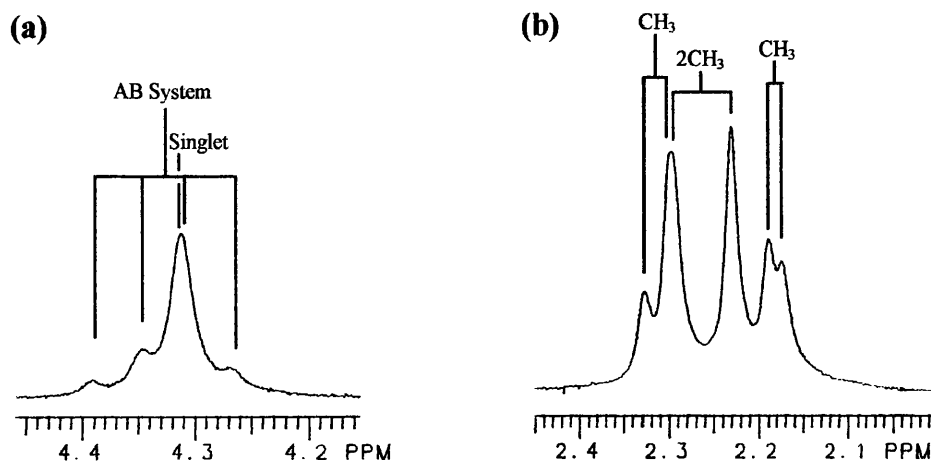


Figure 3.12.

(a) The methylene region of the proton NMR spectrum of the *di*-naphthyl compound (3.9) at -120°C .
 (b) The methyl region of the same spectrum.

The methylene region of the 400 MHz proton NMR spectrum of the *di*-phenyl (3.7), *di*-nitro (3.8) and *di*-naphthal (3.9) compounds are similar, see figures 3.10a, 3.11a and 3.12a, in that they each contain a singlet and an AB system with the former resonating marginally upfield the midpoint of the latter. And in the three compounds, the singlet is more intense than the AB system. There is a problem with signal assignment, in the sense that it is impossible to establish which of the two conformers is the more populated in the *syn/anti* equilibrium. The chiral shift experiment that was used extensively to solve this problem in the compounds investigated in the first section of this chapter was attempted on one of the compounds in the series. The *nitro* compound (3.8), being the most polar was selected for this experiment. The NMR spectrum of a mixture of 3.8 and four fold excess of the chiral shift reagent in CD_2Cl_2 at -110°C on a 500 MHz spectrometer did not yield any information as to which of the signals are from the *anti* conformation.

However, assuming that as in the series of compounds investigated in the first section of this chapter and chapter two, the signals from the *anti* always resonates downfield to those from the *syn* in the methylene region, it is reasonable to conclude on these basis that the *syn* is the more populated and therefore the more stable in 3.7-3.9.

(c) NMR spectra of the dimethoxy-compound (3.10)

On cooling a sample of 1,3-dimethoxy-2,4,5,6-tetramethylbenzene (3.10) to -130°C the signals did not show any sign of dynamic broadening presumably because rotation

about the H₂C-OMe bonds does not become slow on the NMR time scale at temperatures above -130 °C. This led to the conclusion that the compound is not suitable for dynamic NMR studies.

(3.2.1-2) MM3 calculations

The essential data needed to perform calculations on the dinitro-compound (3.8) is not available on the MM3 program. The results for the dimethyl- (3.6), diphenyl- (3.7) and dinaphthyl- (3.9) compounds are summarised in table 3.7. In each of these three compounds, calculations show that the *syn* conformation is the more stable.

Table 3.7. A summary of the contributions to the final steric energies (kcal mol⁻¹) for 3.6, 3.7 and 3.9.

	Diethyl- (3.6)		Diphenyl- (3.7)		Dinaphthyl- (3.9)	
	<i>Syn</i>	<i>Anti</i>	<i>Syn</i>	<i>anti</i>	<i>syn</i>	<i>anti</i>
Compression	2.1354	2.2370	2.6655	2.7950	3.1089	3.1873
Bending	2.6571	2.8892	3.5569	3.6722	4.5325	4.6256
Bend-bend	-0.2051	-0.1989	-0.1896	-0.1855	-0.2546	-0.2517
Stretch-bend	-0.3914	-0.4068	-0.5969	-0.6210	-0.7892	-0.8100
van der Waals						
1,4 energy	11.22946	11.1722	19.1027	18.9283	26.1472	26.0102
Other	5.7927	6.3732	2.8975	3.6463	1.0607	1.9687
Torsional	-10.0946	-10.1077	-14.8975	-15.0962	-25.3198	-25.1752
Torsion-stretch	-0.0007	-0.0007	0.0000	0.0000	0.0000	0.0000
Dipole-dipole	7.8185	7.8113	16.0837	16.1900	17.1772	17.1987
Total Steric Energy (H)	18.9412	19.7687	28.6370	29.3291	25.6628	26.7537
-ΔH	0.8275		0.6921		1.0909	

When only the van der Waals interactions between the two X groups are being considered (see table 3.8) in the dinaphthyl-compound, the benefit by the molecule in having the two X groups *syn* rather than *anti* were found to be substantially high, the energy being 0.64 kcal mol⁻¹. In the diphenyl-compound, this energy is lower at 0.25 kcal mol⁻¹, reflecting the fact that the X group has fewer atoms. And in the diethyl-compound, the energy is negligible, see table 3.8.

Table 3.8. The van der Waals energy in kcal mol⁻¹ associated with the interaction between the atom(s) of the X groups in both conformations of 3.6, 3.7 and 3.9.

	Diethyl- (3.1)	Diphenyl- (3.2)	Dinaphthyl- (3.4)
<i>Syn</i>	-0.0251	-0.4074	-0.7439
<i>Anti</i>	-0.0124	-0.1542	-0.1081
Diff.	-0.0127	-0.2532	-0.6358

It is worth pointing out that unlike the X group in the diethyl-compound, those in the dinaphthyl- and diphenyl-compounds do not behave like a sphere in that rotation about the C-X bonds can generate other *syn* and *anti* conformations with different final steric energies, depending on the value of the torsional angles ϕ_1 and ϕ_2 (see figure 3.13a). However, the energies being discussed in this section are those originating from structures where ϕ_1 and ϕ_2 have been optimised to give the most stable

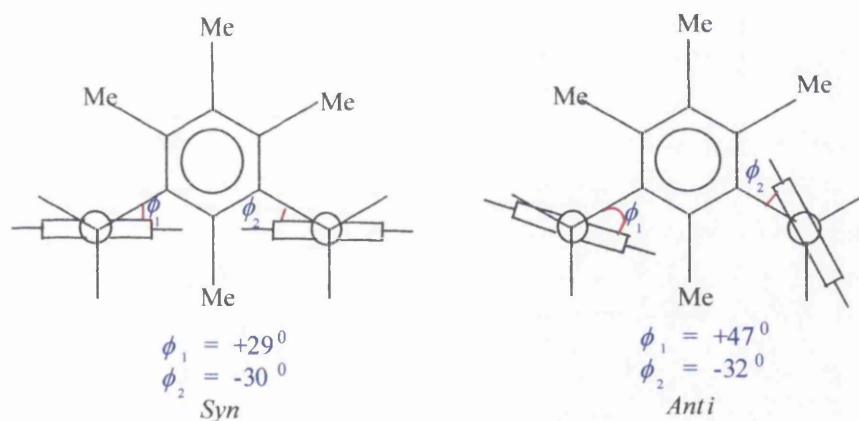


Figure 3.13a. Diagram illustrating the conformation about the C-X bonds in the diphenyl-compounds.

conformation. As for the dinaphthyl-compound, the calculated structure is shown in figure 3.13b.

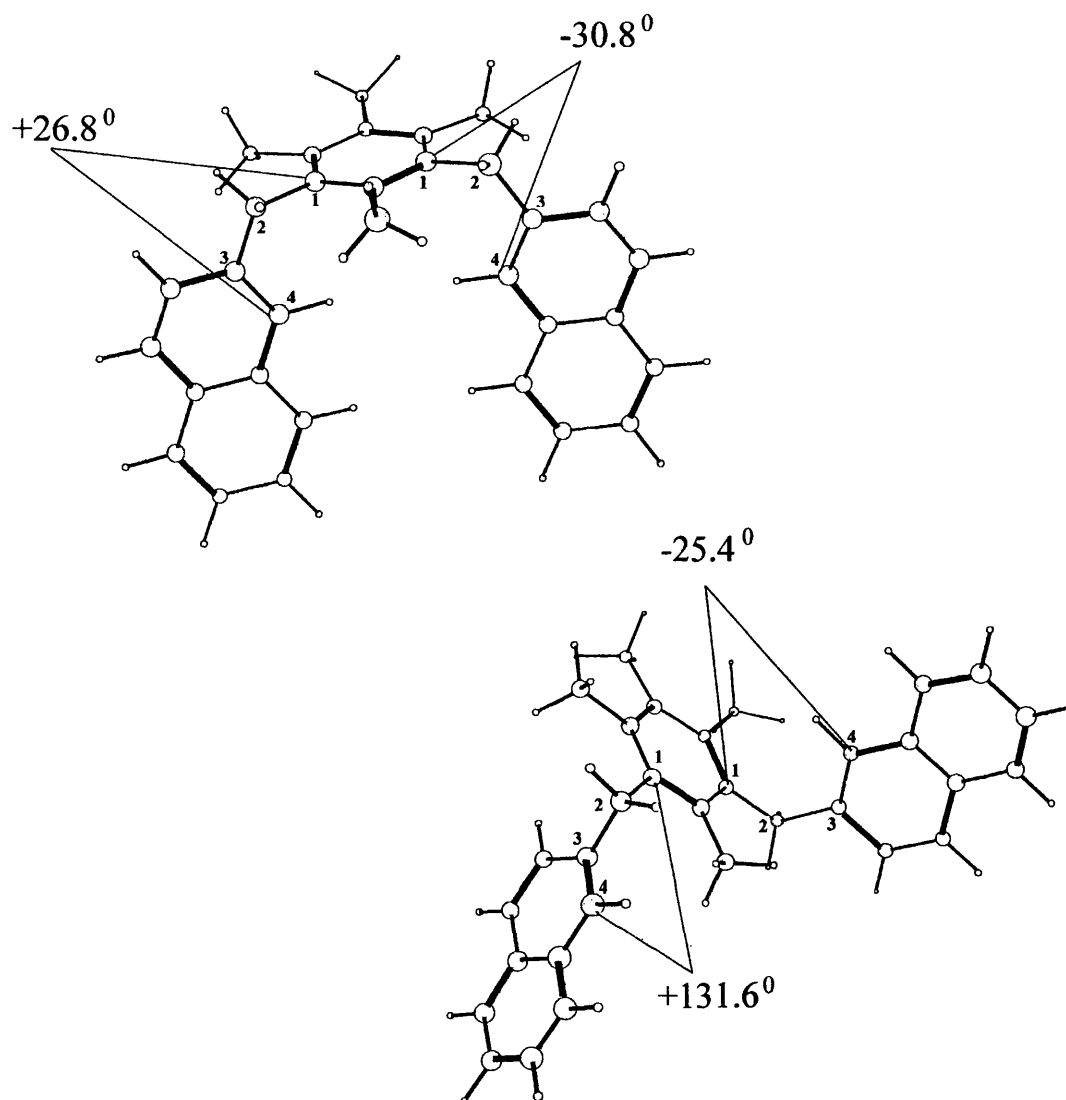


Figure 3.13b. The *syn* and *anti* conformations of the dinaphthyl-compound (3.9) as calculated by MM3.

As regards the arrangement of the methyl and CH_2X groups in the three compounds, the successive up and down arrangement of C-H or C-X bonds, is preserved in the *syn* conformation but not in the *anti*, see figure 3.14. The gear system in the *syn* undoubtedly keeps steric repulsion between the methyl and CH_2X groups at a minimum and this presumably, partly explains the extra stability of the *syn* conformation in the three compounds.

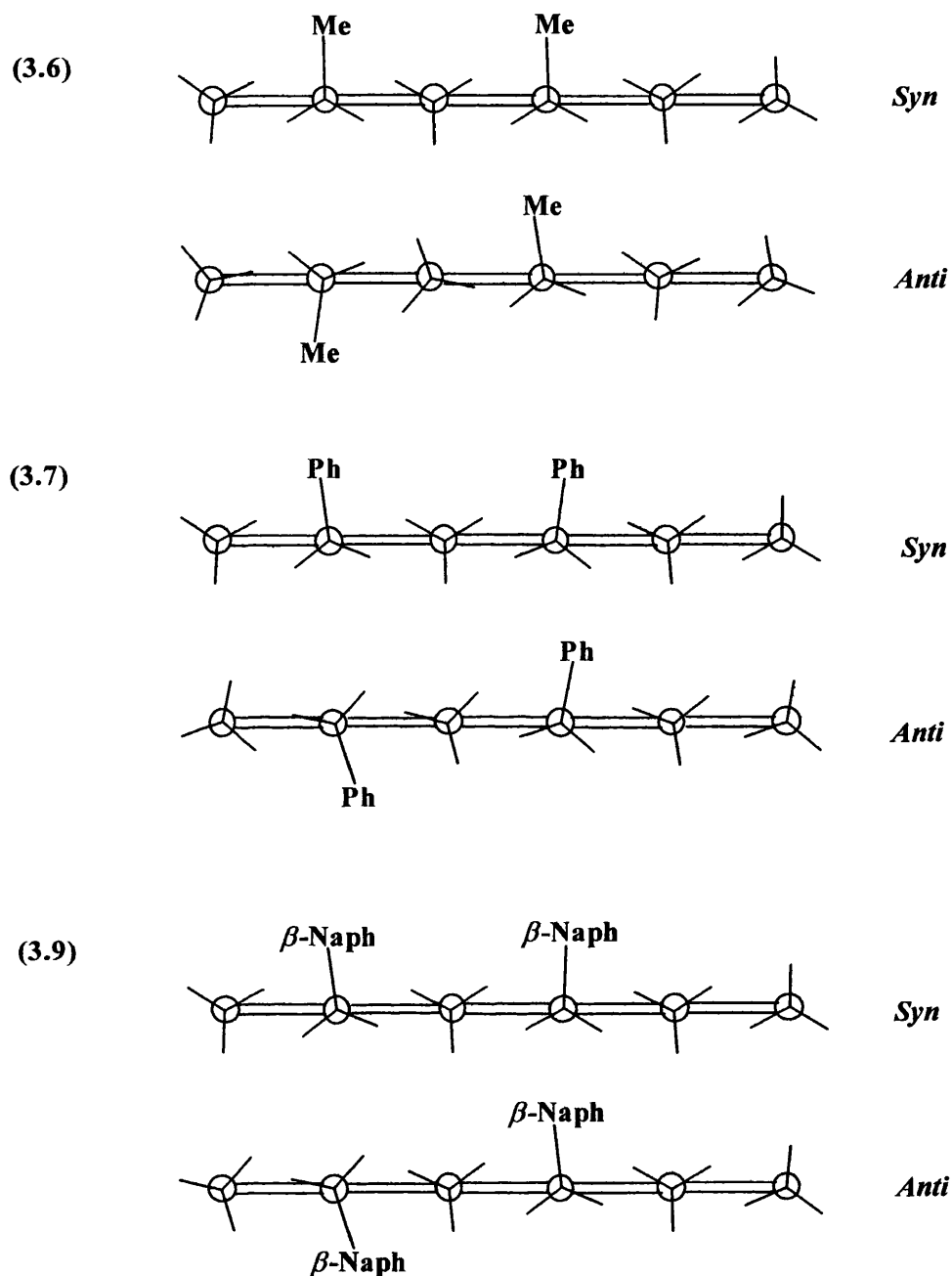


Figure 3.14. Diagram showing the arrangement of the groups attached to the main benzene ring. Note the diagram was constructed using a list of the torsional angles from the MM3 print out.

(3.2.2) Conclusion

The results from dynamic NMR spectroscopy and calculations are summarised in table 3.9. Calculations show that in the diethyl- (3.6), diphenyl- (3.7) and dinaphthyl- (3.9) compounds, the *syn* conformation is more stable than *anti*. It also suggests that attractive steric interactions between the two X groups do not solely determine the

magnitude of the differences in enthalpy (ΔH_{calc}) and that other factor(s), presumably gearing, also stabilises the *syn* conformations of these compounds.

Table 3.9. The free energy differences and the calculated difference in enthalpies for 3.6 – 3.9.

X	T/°C	Equilibrium constant	$-\Delta G_{exp}$ kcal mol ⁻¹	$-\Delta H_{calc}$ kcal mol ⁻¹
Me (3.6)	-120	2.2	0.24	0.83
Ph (3.7)	-130	1.6	0.18	0.69
<i>p</i> -C ₆ H ₄ NO ₂ (3.8)	-120	1.7	0.16	^a
2-Naphthyl (3.9)	-120	1.3	0.08	1.09

^a Not available

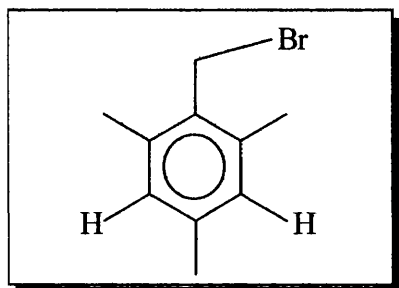
We are unable to unequivocally distinguish between the set of signals from the *syn* and *anti* conformations of the diethyl- (3.6), diphenyl- (3.7), dinitro- (3.8) and dinaphthyl- (3.9) compounds using the chiral shift reagent, however, we have been able to make the following conclusions:

Bearing in mind the closeness in magnitudes of the Gibbs free energies of the 1,3-bis(halomethyl)-2,4,5,6-tetramethylbenzenes and the corresponding 1,3,5-bis(halomethyl)-2,4,6-tetramethylbenzenes, it is reasonable to propose that since the *syn* conformation was found to be significantly more stable than the *anti* in the 1,3,5-triethyl-2,4,6-trimethylbenzene, by analogy the same trend would be reproduced in the diethyl-compound. Thus, the observed energy difference in diethyl-compound is in favour of the *syn*, this trend is also supported by calculation.

In the methylene region of the diphenyl- dinitro- and dinaphthyl- compounds, the midpoint of the AB system resonates slightly downfield the more intense singlet signal, see figures 3.10a, 3.11a and 3.12a. Based on the assumption that the more downfield signal in the methylene regions is always to be attributed to the *anti*, it is reasonable to suggest that the *syn* conformation is the more populated and therefore the more stable in these compounds.

SECTION THREE**(3.3) Synthesis**

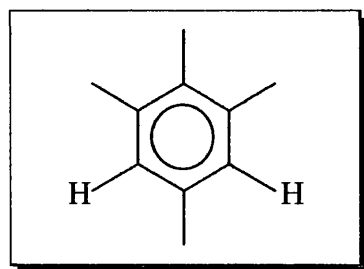
The *mono*-bromomethylation of mesitylene described below will serve as a general procedure for the preparation of various bromomethylbenzenes.

**1-(Bromomethyl)-2,4,6-trimethylbenzene.³⁷ (3.1a)**

To a mixture of paraformaldehyde (12.20 g, 407 mmol), mesitylene (48 g, 400 mmol) and glacial acetic (200 ml) at 50 °C was added 30 %wt of HBr in acetic acid (80 ml). The mixture was stirred at the same temperature for 5 h and then allowed to cool. The mixture was poured into water (400 ml) and the white precipitate was collected by suction filtration. The crude product was dried and then purified by crystallisation from petroleum spirit (b.p. 60-80 °C) to give the product (48.1 g) as colourless needle crystals m.p. 47-48 °C.

NMR spectroscopy

300 MHz ¹H NMR (CDCl₃) δ/ppm 2.26 (s, 3H, CH₃); 2.37 (s, 6H, CH₃); 4.56 (s, 2H, CH₂Br); 6.85 (s, 2 H, arom.).

**1,2,3,5-Tetramethylbenzene.⁴⁰ (3.1b)**

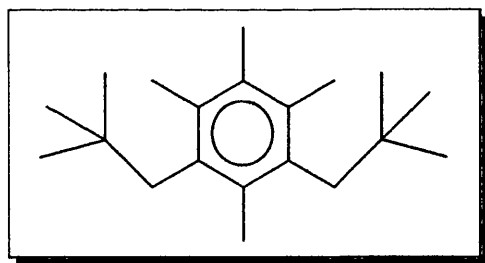
Because commercially available isodurene (3.1b) is less than 85 % pure, the impurity being durene, it was deemed necessary to synthesise pure isodurene.

The LiAlH_4 solution used in this reaction was prepared as follows: Freshly distilled THF (200 ml) was added to LiAlH_4 (11.5 g). The mixture was stirred for 3 h and then filtered using a sintered glass funnel packed with celite, under a slight positive pressure of argon. A clear solution of LiAlH_4 in THF of approximately 1.3 M was obtained.

With the aid of a syringe, a solution of 1-(bromomethyl)-2,4,6-trimethylbenzene (**3.1a**) (44.1 g, 206 mmol) in THF (180 ml) was added to a solution of LiAlH_4 (170 ml, 1.3 M in THF, 221 mmol) dissolved in THF (80 ml) at 22 $^\circ\text{C}$. After stirring for 2.5 h, the reaction was quenched by adding ethylacetate (40 ml) and then 3 M hydrochloric acid until all the solid had dissolved. The organic layer was separated and the aqueous layer was washed with ether (5 x 50 ml). The combined organic extracts were dried over anhydrous magnesium sulfate and the solvent was removed leaving a colourless liquid. The crude product was purified by distillation and the product (19.95 g,) was obtained as a colourless liquid b.p. 78 $^\circ\text{C}$ at 9 mm Hg pressure.

NMR spectroscopy

300 MHz ^1H NMR (CDCl_3) δ /ppm 2.12 (s, 3H, CH_3); 2.33 (s, 9 H, CH_3); 6.82 (s, 2H, Ar-H);



1,3-Dineopentyl-2,4,5,6-tetramethylbenzene.⁴¹ (**3.1**)

The reaction was carried out under argon. A 0.02 M solution of the lithium tetrachlorocuprate catalyst was prepared by adding THF (50 ml) to a mixture of lithium chloride (0.086 g, 2.03 mmol) and CuCl_2 (0.136 g, 1.01 mmol). The mixture was stirred at ambient temperature for 10 min.

1,3-bis(bromomethyl)-2,4,5,6-tetramethylbenzene (**3.2**) (1.0 g, 3.13 mmol) dissolved in THF (30 ml) was added to a stirring solution of *tert*-butylmagnesium chloride (18.8 ml, 1.0 M in THF, 18.8 mmol) in THF (20 ml) at 30 $^\circ\text{C}$. To the mixture was added a portion of the catalyst (0.3 ml). The resultant mixture was stirred at the

same temperature for 14 h. The reaction was quenched by the addition of 2 M hydrochloric acid (20 ml). The organic phase was separated and the aqueous phase was extracted with ether (4 x 10 ml). The combined organic phase was dried over anhydrous magnesium sulfate and the solvent was removed using a rotary evaporator. The resultant white solid was purified by flash column chromatography using petroleum spirit (b.p. 30-40 °C) as the eluting solvent. The product (54 mg) was obtained as a white solid m.p. 67-68 °C.

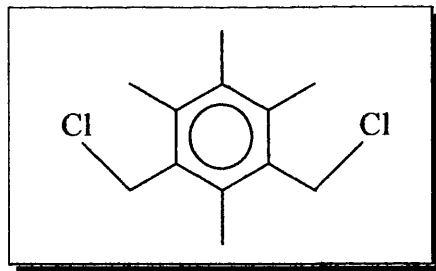
NMR spectroscopy

300 MHz ^1H NMR (CDCl_3) δ /ppm 2.79 (s, 4H, ArCH_2); 2.30 (s, 3H, CH_3); 2.23 (s, 6H, CH_3); 2.17 (s, 3H, CH_3) 0.91 {s, 9H, $\text{C}(\text{CH}_3)_3$ }.

100.6 MHz ^{13}C NMR (CD_2Cl_2) δ /ppm 17.40 (1C, ArCH_3); 19.32 (2C, ArCH_3); 20.43 (1C, ArCH_3); 30.51 { $\text{C}(\text{CH}_3)_3$ }; 34.84 { $\text{C}(\text{CH}_3)_3$ }; 41.37 (CH_2); 132.12, 133.71, 134.73, 134.80 (arom. C).

Elemental analysis

Found: C, 87.48; H, 12.74 %. $\text{C}_{20}\text{H}_{34}$ requires C, 87.51; H, 12.50 %.



1,3-Bis(chloromethyl)-2,4,5,6-tetramethylbenzene.⁴²(3.2)

The reaction was carried out under anhydrous conditions. To a mixture of 1,3-bis(bromomethyl)-2,4,5,6-tetramethylbenzene (0.5 g, 1.56 mmol) and excess lithium chloride (0.74 g,) was added acetone (15 ml). The mixture was refluxed for 2 days and the solvent was removed using a rotary evaporator. To the residue was added water (15 ml) and dichloromethane (15 ml). The organic phase was separated and the aqueous layer was extracted with dichloromethane (3 x 10 ml). The combined organic layer was washed with water (3 x 10 ml) and then dried over anhydrous magnesium sulfate. The solvent was removed under reduced pressure leaving a white residue.

Using the residue and the same quantities of lithium chloride and acetone, the procedure was repeated four times so as to get a full conversion of the bromine atoms to chlorine. The product (180 mg) was obtained as a white solid m.p. 114-116 °C.

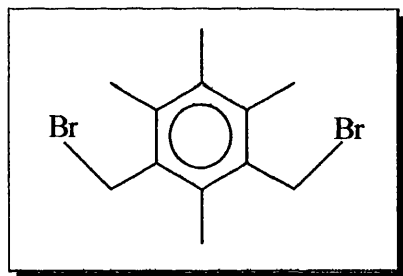
NMR spectroscopy

300 MHz ^1H NMR (CDCl_3) δ /ppm 4.70 (s, 4H, CH_2Cl); 2.47 (s, 3H, CH_3); 2.35 (s, 6H, CH_3); 2.21 (s, 3H, CH_3).

100.6 MHz ^{13}C NMR (CD_2Cl_2) δ /ppm 15.21 (1C, CH_3); 16.47 (2C, CH_3); 16.76 (1C, CH_3); 42.87 (CH_2Cl); 132.54 (2C, CCH_3); 134.51 (2 x CCH_3); 137.30 (CCH_2Cl).

Elemental analysis

Found: C, 62.04; H, 6.99; Cl, 30.70 %. $\text{C}_{12}\text{H}_{16}\text{Cl}_2$ requires C, 62.32; H, 6.93; Cl, 30.69 %.



1,3-Bis(bromomethyl)-2,4,5,6-tetramethylbenzene.³⁷ (3.3)

The general procedure described for the *mono*-bromomethylation of mesitylene was used except that a mixture of 1,2,3,5-tetramethylbenzene (**3.1b**) (2.68 g, 20 mmol), paraformaldehyde (1.23 g, 41 mmol) and 30 wt% HBr (8 ml) was stirred at 80 °C for 8h. After purification by recrystallisation a white crystalline solid (4.85 g) m.p. 141–142 °C was obtained.

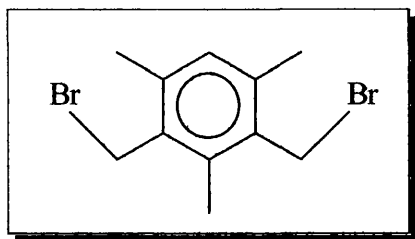
NMR spectroscopy

300 MHz ^1H NMR (CDCl_3) δ /ppm 4.60 (s, 4H, CH_2Br); 2.43 (s, 3H, CH_3); 2.33 (s, 6H, CH_3); 2.21 (s, 3H, CH_3).

100.6 MHz ^{13}C NMR (CD_2Cl_2) δ /ppm 15.20 (1C, CH_3); 16.49 (2C, CH_3); 16.78 (1C, CH_3); 31.65 (CH_2Br); 132.60 (2C, arom.); 134.55, 134.61 (1C, arom.); 137.34 (CCH_2Br).

Elemental analysis

Found: C, 45.08; H, 5.03; Br, 49.72 %. $C_{12}H_{16}Br_2$ requires C, 45.01; H, 5.00; Br, 49.95 %.

1,3-Bis(bromomethyl)-2,4,6-trimethylbenzene.³⁷ (3.4)

The method described for the bromomethylation of mesitylene was followed but using mesitylene (2.00 g, 16.6 mmol), paraformaldehyde (1.00 g, 33.3 mmol) and a solution of hydrogen bromide (6.0 ml, 5.6 M in acetic acid, 33.6 mmol). The mixture was heated at 80 °C for 8 h.

The product (4.3 g) was obtained as a white solid m.p. 134-135 °C.

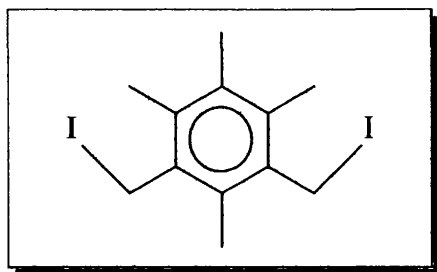
NMR spectroscopy

300 MHz 1H NMR ($CDCl_3$) δ /ppm 2.37 (s, 6H, CH_3); 2.43 (s, 3H, CH_3); 4.57 (s, 4H, CH_2Br); 6.89 (s, 1H, arom.).

75 MHz ^{13}C NMR (CD_2Cl_2) δ /ppm 14.63 (2C, CH_3); 19.43 (1C, CH_3); 29.70 (CH_2Br); 130.65 (1C, arom.); 132.57, 137.12 (2C, arom.); 138.01 (1C, arom.).

Elemental analysis

Found: C, 43.28; H, 4.48; Br, 52.06 %. $C_{11}H_{14}Br_2$ requires C, 43.15; H, 4.61; Br, 52.24 %.

1,3-Bis(iodomethyl)-2,4,5,6-tetramethylbenzene.³⁸ (3.5)

A mixture of 1,3-bis(bromomethyl)-2,4,5,6-tetramethylbenzene (**3.3**) (0.30 g, mmol) and excess NaI (0.6 g,) in acetone (15 ml) was stirred at 20 °C for 3 h under anhydrous conditions. The solvent was removed using a rotary evaporator. Dichloromethane (20 ml) and water (20 ml) were added to the solid. The organic layer was separated and the aqueous layer was extracted with dichloromethane (3 x 5 ml). The combined organic layer was washed with sulphurous acid to remove iodine and then with water (3 x 5 ml). The solution was dried with anhydrous magnesium sulfate and the solvent was removed under reduced pressure leaving a white solid (0.31 g).

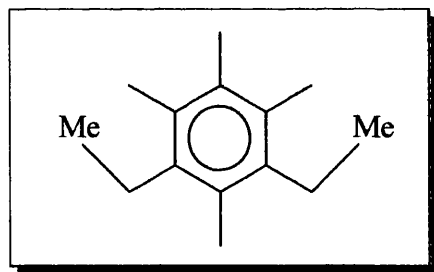
NMR spectroscopy

300 MHz ^1H NMR (CDCl_3) δ /ppm 4.46 (s, 4H, CH_2Br); 2.27 (s, 3H, CH_3); 2.23 (s, 6H, CH_3); 2.20 (s, 3H, CH_3).

100.6 MHz ^{13}C NMR (CD_2Cl_2) δ /ppm 7.95 (CH_2I); 16.98 (1C, CH_3); 18.17 (2C, CH_3); 18.37 (1C, CH_3); 134.90 (br, 1C, CCH_3); 135.04 (br, 2C, CCH_3); 137.77 (CCH_2I).

Elemental analysis

Found: C, 34.82; H, 3.79; I, 61.47 %. $\text{C}_{12}\text{H}_{16}\text{I}_2$ requires C, 34.79; H, 3.90; I, 61.47 %.



The procedure described below will serve as a general procedure for the synthesis of ethylbenzenes from bromomethylbenzenes.

1,3-Diethyl-2,4,5,6-tetramethylbenzene.³⁹ (**3.6**)

The reaction was carried out under argon. A solution of lithium dimethylcuprate was prepared by adding a solution of methyllithium (6.65 ml, 1.6 M in THF, 10.8 mmol) to a stirred mixture of copper iodide (1.03 g, 5.4 mmol) in ether (16 ml) at 0 °C. The mixture immediately turned yellow then colourless. The resultant mixture was stirred at 0 °C for 20 min.

The 1,3-bis(bromomethyl)-2,4,5,6-tetramethylbenzene (**3.3**) (0.80 g, 2.5 mmol) dissolved in ether (30 ml) was added to the lithium dimethylcuprate solution at 0 °C.

The resultant yellow mixture was stirred at ambient temperature for 5 h. The reaction was quenched by carefully adding 3 M hydrochloric acid (20 ml) and the mixture was filtered to remove insoluble materials. The organic layer was separated and the aqueous phase was extracted with ether (3 x 10 ml). The combined organic phase was washed with water (3 x 10 ml) and then dried over anhydrous magnesium sulfate. The solvent was removed under reduced pressure leaving a white solid. The crude product was purified by flash column chromatography using petroleum spirit (b.p. 30-40 °C) as the eluting solvent. The product (230 mg) was obtained as a white solid mp 37-38 °C.

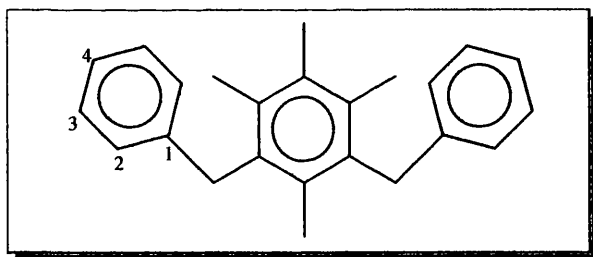
NMR spectroscopy

400 MHz ^1H NMR (CD_2Cl_2) δ /ppm 1.17 (t, $J = 7.6$, 6H, CH_2CH_3); 2.27 (s, 3H, ArCH_3); 2.31 (s, 6H, ArCH_3); 2.35 (s, 3H, ArCH_3); 2.79 (q, $J = 7.6$ Hz, 4H, CH_2Me);

100.6 MHz ^{13}C NMR (CD_2Cl_2) δ /ppm 14.53 (CH_2CH_3); 15.78 (1C, ArCH_3); 16.58 (2C, ArCH_3); 17.17 (1C, ArCH_3); 24.42 (CH_2CH_3); 131.89 (1C, arom.); 132.88 (2C, arom.); 134.09 (1C, arom.) 139.60 (CCH_2Me).

Elemental analysis

Found: C, 88.22; H, 11.88 %. $\text{C}_{14}\text{H}_{22}$ requires C, 88.33; H, 11.66 %.



1,3-Bis(phenylmethyl)-2,4,5,6-tetramethylbenzene.³⁹ (3.7)

The method described for the synthesis of 1,3-diethyl-2,4,5,6-tetramethyl (3.5) was followed but using phenyllithium solution (1.7 ml, 1.8 M in cyclohexane/ether 7:3, 3.1 mmol), copper (I) bromide (0.45, 3.1 mmol) instead of copper (I) iodide, and 1,3-bis(bromomethyl)-2,4,5,6-tetramethylbenzene (3.3) (0.48 g, 1.5 mmol).

The product (210 mg) was obtained as a white solid m.p. 120-122 °C

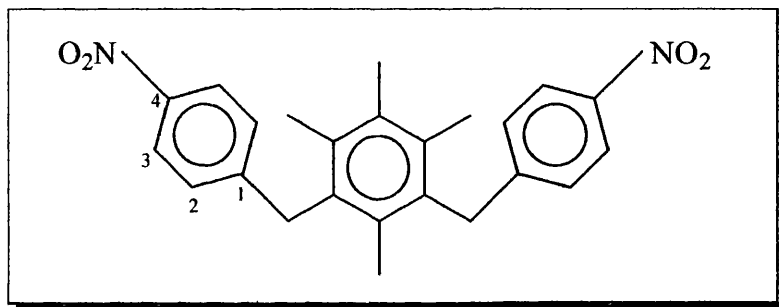
NMR spectroscopy

300 MHz ^1H NMR (CDCl_3) δ/ppm 2.11 (s, 3H, CH_3); 2.19 (s, 6H, CH_3); 2.24 (s, 3H, CH_3); 4.12 (s, 4H, CH_2Ph); 7.03 (m, 4H, 4Ar-H^2); 7.14 (m, 2H, Ar-H^4); 7.23 (m, 4H, Ar-H^3).

100.6 MHz ^{13}C NMR (CD_2Cl_2) δ/ppm 17.38 (2 x CH_3); 17.50 (2C, CH_3); 37.24 (CH_2Ph); 126.89 (arom. C^4); 129.29 (4C, arom.); 129.63 (4C, arom.); 134.62 (1C, arom.); 134.93 (1C, arom.); 135.37, 135.87 (2C, arom.); 142.24 (CCH_2Ph).

Elemental analysis

Found: C, 90.82; H, 8.49 %. $\text{C}_{24}\text{H}_{26}$ requires C, 91.64; H, 8.35 %.



1,3-Bis(p-nitrobenzyl)-2,4,5,6-tetramethylbenzene.⁴³ (3.8)

The reaction was carried out under an inert atmosphere of argon. A solution of aluminium chloride (1.50 g, 11.2 mmol) in nitromethane (5 ml) was added to a stirred solution of isodurene (3.1b) (1.50 g, 11.2 mmol) in nitromethane (5 ml). The solution immediately turned brown and it was then cooled down to -5°C .

A solution of 4-nitrobenzylchloride (1.92 g, 11.2 mmol) dissolved in nitromethane (5 ml) was added to the brown mixture whilst cooling. The mixture was left stirring at 22°C for 24 h. The reaction was quenched by the addition of 2 M hydrochloric acid solution (10 ml). The organic layer was separated and the aqueous layer was extracted with dichloromethane (3 x 6 ml). The organic phases were combined and washed with water (3 x 15 ml). The solvent was removed using a rotary evaporator to give a black viscous liquid. The crude product was then made purer by flash column chromatography using petroleum spirit [b.p. $30-40^\circ\text{C}$]:dichloromethane (9:1) as the eluent. The product was crystallised from chloroform to give an off white solid (3.10 g) m.p. 124°C .

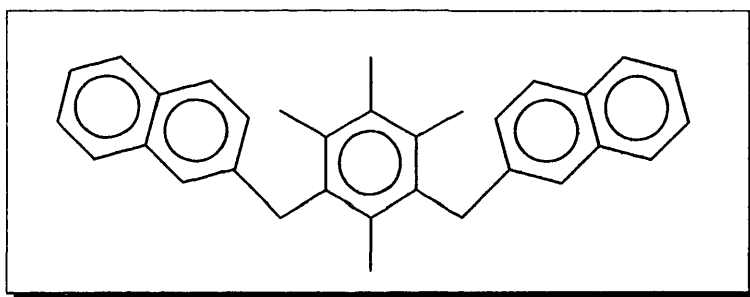
NMR spectroscopy

300 MHz ^1H NMR (CDCl_3) δ /ppm 2.03 (s, 3H, CH_3); 2.17 (s, 6H, CH_3); 2.26 (s, 3H, CH_3); 4.21 (s, 4H, ArCH_2); 7.16 (d, $J = 8.68$ Hz, 4H, Ar-H^2); 8.10 (s, $J = 8.68$ Hz, 4H, Ar-H^3);

100.6 MHz ^{13}C NMR (CD_2Cl_2) δ /ppm 17.40 (1C, CH_3); 17.50 (1C, CH_3); 17.59 (2C, CH_3); 37.32 (ArCH_2); 124.85 (arom. C^3); 129.94 (arom. C^2); 134.64 (1C, arom.); 134.69 (2C, arom.); 135.37 (1C, arom.); 136.00, 147.91 (2C, arom.); 150.19 (arom. C-NO_2);

Elemental analysis

Found: C, 70.54; H, 6.17; N, 6.61 %. $\text{C}_{24}\text{H}_{24}\text{N}_2\text{O}_4$ requires C, 71.26; H, 5.99; N, 6.92; O, 15.82 %.



1,3-Bis(2-naphthyl)-2,4,5,6-tetramethylbenzene.⁴⁴ (3.9)

The reaction was carried out under an inert atmosphere of argon.

A 0.2 M solution of the lithium tetrachlorocuprate catalyst was prepared by adding THF (50 ml) to a mixture of lithium chloride (0.85 g, 20 mmol) and copper (II) chloride (1.35 g, 10 mmol). The mixture was then stirred for 10 min.

The Grignard was prepared by adding a solution of 2-bromonaphthalene (1 g, 4.8 mmol) in THF (10 ml) to a stirred mixture of magnesium turnings (0.12 g, 4.9 mmol) in THF (10 ml), and a crystal of iodine. The iodine acts as an initiator. The mixture was refluxed for 5 h and then cooled to 0 $^{\circ}\text{C}$.

A mixture containing a solution of 1,3-bis(iodomethyl)-2,4,5,6-tetramethylbenzene [3.5] (1.0 g, 2.4 mmol) in THF (20 ml) and the lithium tetrachlorocuprate catalyst (0.6 ml) was added dropwise over a period of 15 min to the Grignard mixture at 0 $^{\circ}\text{C}$. The mixture was stirred at the same temperature for 2 h and then at 22 $^{\circ}\text{C}$ for 24 h. The reaction was then quenched by the addition of 2 M hydrochloric acid solution (20 ml).

The organic and aqueous phases were separated and the latter was extracted with ether (3 x 15 ml). The organic phases were combined and then washed with a saturated solution of sodium sulfite to remove iodine. The organic phase was dried over anhydrous magnesium sulfate and the solvent was removed under reduced pressure. The crude product was purified by flash column chromatography using petroleum spirit [b.p. 30-40 °C]:dichloromethane (9:1) as the mobile phase. The product (410 mg) was obtained as a white solid m.p. 179-181 °C.

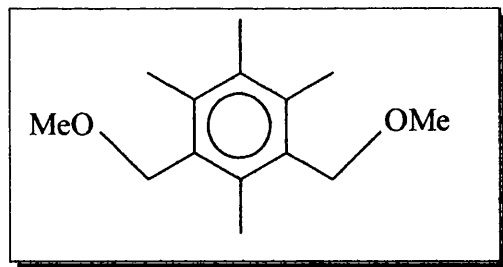
NMR spectroscopy

300 MHz ^1H NMR (CDCl_3) δ /ppm 2.16 (s, 3H, CH_3); 2.24 (s, 6H, CH_3); 2.28 (s, 3H, CH_3); 4.29 (s, 4H, ArCH_2); 7.28-7.43 (m, 8H, arom.); 7.67-7.79 (s, 6H, arom.)

100.6 MHz ^{13}C NMR (CD_2Cl_2) δ /ppm 17.44 (1C, CH_3); 17.48 (1C, CH_3); 17.57 (2C, CH_3); 37.50 (ArCH_2); 126.39, 127.04, 127.10, 128.51, 128.78, 128.80, 129.12, 133.58 (arom C); 134.76, 135.14 (1C, arom C); 135.26, 135.58, 135.76, 139.85 (arom C).

Elemental analysis

Found: C, 91.57; H, 7.32 %. $\text{C}_{32}\text{H}_{30}$ requires C, 91.64; H, 8.35 %.



1,3-Dimethoxy-2,4,5,6-tetramethylbenzene (3.10)

A mixture of 1,3-bis(bromomethyl)-2,4,5,6-tetramethylbenzene (3.3) (0.50 g, 1.57 mmol) and methanol:chloroform (1:1) was refluxed for 6 h. The solvent was removed on a rotary evaporator leaving the product (32 mg), a slightly off white solid m.p. 38 – 40 °C.

500 MHz ^1H NMR (CDCl_3) δ /ppm 2.1 (s, 3H, CH_3); 2.28 (s, 6H, CH_3); 2.39 (s, 3H, CH_3); 3.39 (s, 4H, ArCH_2); 4.48 (s, 6H, OCH_3).

100.6 MHz ^{13}C NMR (CD_2Cl_2) δ/ppm 15.39 (1C, CH_3); 16.43 (3C, CH_3); 58.06 (OCH_3); 69.41 ($\text{CH}_2\text{O}-$); 131.90 (2C, arom.); 133.12, 134.90 (1C, arom.); 136.46 (2C, arom.).

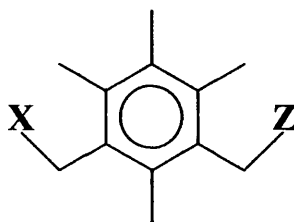
Elemental analysis

Found: C, 75.40; H, 9.84 %. $\text{C}_{14}\text{H}_{22}\text{O}_2$ requires C, 75.62; H, 9.99; O, 14.39 %.

Attractive Steric Interactions in 1,3-
Disubstituted-2,4,5,6-
tetramethylbenzenes,
where the two substituents are non-
identical

(4) Introduction

In the two preceding chapters we investigated attractive steric interactions between bulky groups that are identical. In this chapter, attractive steric interactions between two non-identical bulky groups **X** and **Z**, in the series of compounds (**4.1** - **4.16**), are discussed. This chapter is divided into four sections, those where **X** is a *tert*-butyl group are treated in the first section. Those where **X** is a phenyl ring and a methyl group are discussed in the second and third sections respectively. The final section deals with the synthesis of these compounds. Note the barrier to rotation about bonds will be discussed in chapter six.



	X	Z
4.1	<i>t</i> -Butyl	Cl
4.2	<i>t</i> -Butyl	Br
4.3	<i>t</i> -Butyl	I
4.4	1-Adamantyl	Br
4.5	<i>t</i> -Butyl	α -Naphthyl
4.6	<i>t</i> -Butyl	β -Naphthyl
4.7	<i>t</i> -Butyl	Ph
4.8	<i>t</i> -Butyl	Xylyl
4.9	<i>t</i> -Butyl	Me

	X	Z
4.10	Ph	Cl
4.11	Ph	Br
4.12	Ph	I
4.13	Ph	Me
4.14	<i>p</i> -C ₆ H ₄ NO ₂	<i>p</i> -C ₆ H ₄ NH ₂
4.15	Me	Cl
4.16	Me	Br
4.17	Me	I

Assuming rotation about the C-CH₂X and C-CH₂Z bonds happens one at a time, the compounds **4.1** - **4.17** should each have four major rotamers *a*, *b*, *c* and *d* see figure **4.1**. In *a* and *c* the two groups, **X** and **Z** are on the same face of the ring plane and are assigned “*syn*”. A 180 °C rotation about either the C-CH₂X or C-CH₂Z bond in rotamers *a* or *c* should give rise to the *anti* rotamers *b* and *d*. The pairs of rotamers *a*, *c* and *b*, *d* are conformational enantiomers. It is worth pointing out that when **X** = **Z**, like the compounds treated in the preceding chapter, the *anti* is chiral whilst the *syn* conformation is achiral whereas when **X** ≠ **Z**, the two conformations are chiral.

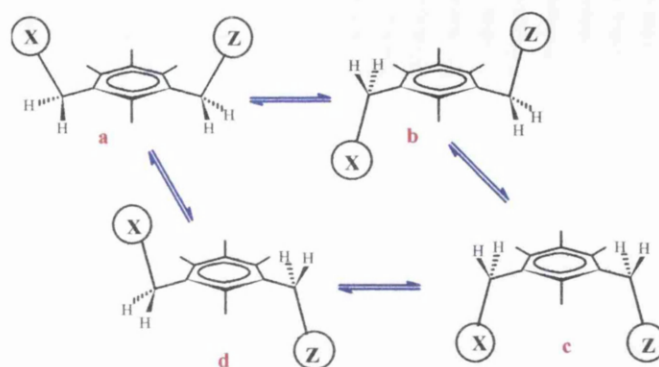


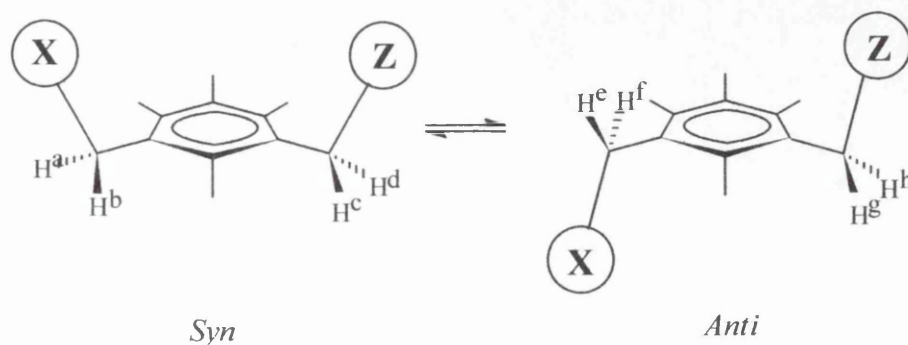
Figure 4.1. The four rotamers of **4.1** – **4.17** obtained by a 180° rotation about the C-CH₂X and C-CH₂Z bonds assuming rotation about this bonds happens one at a time.

The atoms of the **X** and **Z** groups in the *syn* and *anti* conformers are not so close to be repelling hence they should attract as a result of which the overall enthalpy of formation of the structure is reduced. However, it is envisaged that the more compact *syn* conformation that has the atoms of **X** and **Z** groups closer together so as to maximise attractive steric interactions will be more stable and the more populated.

NMR spectroscopy

As regards the proton and ¹³C NMR spectrum of **4.1** - **4.17** at room temperature. The four CH₃ groups on the benzene ring should each appear as a singlet in the proton NMR spectrum. The signals from the CH₂X and CH₂Z groups should resonate at different frequency. When rotation about both C-CH₂X and C-CH₂Z bonds are fast on the NMR time scale the *geminal* protons from the CH₂X group, like those from the CH₂Z group, should be *enantiotopic* and therefore *isochronous* i.e. indistinguishable by NMR. But as

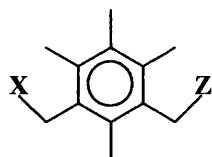
Figure 4.2



soon as rotation about one of these bonds becomes slow on the NMR time scale, the geminal protons should become diastereotopic and therefore mutually couple to give an AB system for each CH_2 's. Only when rotation about both bonds is slow should we get two subspectra representing the *syn* and *anti* conformers, in which case two sets of AB systems would be seen for each CH_2 's.

All other signals in the proton NMR spectrum, like those in the ^{13}C NMR will remain as singlets until both rotations are slow on the NMR time scale. But exceptions to these predictions are in compounds where X or Z is a methyl group, at temperatures well below the point of de-coalescence, the signals from the CH_2CH_3 protons will be expected to be complex because these protons are coupled to one another and to adjacent methyl protons.

SECTION ONE

(4.1.1) Results and Discussion of 4.1 - 4.9.

	X	Z		X	Z
4.1	<i>t</i> -butyl	Cl	4.6	<i>t</i> -butyl	β -Naphthyl
4.2	<i>t</i> -butyl	Br	4.7	<i>t</i> -butyl	Ph
4.3	<i>t</i> -butyl	I	4.8	<i>t</i> -butyl	Xylyl
4.4	Ad	Br	4.9	<i>t</i> -butyl	Me
4.5	<i>t</i> -butyl	β -Naphthyl			

(4.1.1-1) Conformational analysis of signals in the NMR spectra at low temperatures(a) *NMR analysis of the halides (4.1 – 4.4).*

The features of the NMR spectra of the halides (4.1 – 4.3) when rotation about both C-CH₂Z (Z = Cl, Br or I) and C-CH₂Me₃ bonds becomes slow on the NMR scale are similar, the proton and ¹³C chemical shifts are summarised in tables 4.1 and 4.2 respectively. Although, it is straight forward to obtain the conformational population ratio by dynamic NMR spectroscopy, a basic proton or ¹³C dynamic NMR analysis did not yield much information as to which of the two conformations is the more populated. This problem was solved by carrying out a Nuclear Overhauser Enhancement (NOE) difference experiment on the bromide (4.2) and since the halides (4.1 – 4.3) are analogues, we assumed that the relative shift of the *syn* and *anti* signals in the proton and ¹³C NMR spectrum of the bromide will be reproduced in the chloride and iodide.

In this project, the conformational assignment of signals in the chloride (4.1) iodide (4.3) and 1-(1-adamantanemethyl)-3-bromomethyl-2,4,5,6-tetramethylbenzene (4.4) were based on that of the bromide (4.2). A description of the results from dynamic NMR and NOE difference experiments carried out on the bromide is now presented.

Dynamic NMR of the bromide was carried out in two different solvents, methylene chloride-*d*₂ and acetone-*d*₆. In methylene chloride, at +22 °C, an average of the two conformations is observed with the CH₂Br and CH₂C(CH₃)₃ protons appearing as singlets, although, the signal from the former is exchange broadened. But at –80 °C when rotation about both C-CH₂Br and C-CH₂Me₃ bonds is slow on the NMR time scale, two sets of AB quartets were seen in the CH₂Br region. And in the CH₂Me₃ region, an AB system together with a singlet is observed. The signals for some of the

Table 4.1. The proton NMR chemical shifts of the chloride (4.1), bromo-neopentyl-compound, (4.2) Iodide (4.3) and bromo-adamantyl-compound (4.4) at low temperature. The chemical shifts of the more intense signals which happens to come from the *anti* are depicted in red ink.

Z (T/ ^o C)	Chemical Shifts /ppm									
Solvent	C(CH ₃) ₃	CH ₃	CH ₃	CH ₃	CH ₃	CH ₃	CH ₂ CMe ₃	CH ₂ Z		
(4.1) Cl (-80 ^o C)		2.12	2.18	2.27	2.31		2.70 (AB, J = 14.6 Hz); 2.74 (s)	4.70 (AB, J = 11.6 Hz); 4.70 (AB, J = 11.6 Hz)		
CD ₂ Cl ₂	0.81	2.13		2.28	2.32		2.75 (AB, J = 14.6 Hz)	4.74 (AB, J = 11.6 Hz); 4.75 (AB, J = 11.6 Hz)		
(4.2) Br (-80 ^o C)	0.79	2.12	2.18	2.25	2.30		2.698 (AB, J = 14.3 Hz); 2.729 (s)	4.602 (AB, J = 10.5 Hz); 4.613 (AB, J = 10.5 Hz)		
CD ₂ Cl ₂	0.81	2.13		2.27			2.748 (AB, J = 14.3 Hz)	4.651 (AB, J = 10.5 Hz); 4.676 (AB, J = 10.5 Hz)		
(-80 ^o C)	0.817	2.10	2.17	2.25	2.35		2.751 (s); 2.748 (AB, J = 14.5 Hz);	4.745 (AB, J = 10.5 Hz); 4.761 (AB, J = 10.5 Hz)		
CD ₃ COCD ₃	0.823	2.11	2.19		2.36		2.791 (AB, J = 14.5 Hz).	4.780 (AB, J = 10.5 Hz); 4.807 (AB, J = 10.5 Hz)		
(4.3) Br (-80 ^o C)	-	2.147	2.360	2.293	2.337		2.593 (AB, J = 14.3 Hz); 2.612 (AB, J = 14.3 Hz);	4.613 (AB, J = 9.7 Hz); 4.626 (AB, J = 9.7 Hz);		
CD ₂ Cl ₂	-			2.298	2.355		2.643 (AB, J = 14.3 Hz); 2.663 (AB, J = 14.3 Hz).	4.663 (AB, J = 9.7 Hz); 4.689 (AB, J = 9.7 Hz).		
(4.4) I (-65 ^o C)	0.81	2.13	2.17	2.20	2.25		2.710 (AB, J = 15.0 Hz); 2.718 (AB, J = 15.0 Hz)	4.446 (AB, J = 9.6 Hz); 4.473 (AB, J = 9.6 Hz)		
CD ₂ Cl ₂	0.82	2.14	2.18	2.21			2.752 (AB, J = 15.0 Hz); 2.762 (AB, J = 15.0 Hz)	4.514 (AB, J = 9.6 Hz); 4.555 (AB, J = 9.6 Hz).		

Table 4.2. The ^{13}C NMR chemical shifts of the chloride (4.1), bromo-neopentyl-compound (4.2) and iodide (4.3) in CD_2Cl_2 at temperatures well below the coalescent point. The chemical shifts of the more intense signals which happens to come from the *anti* are depicted in red ink.

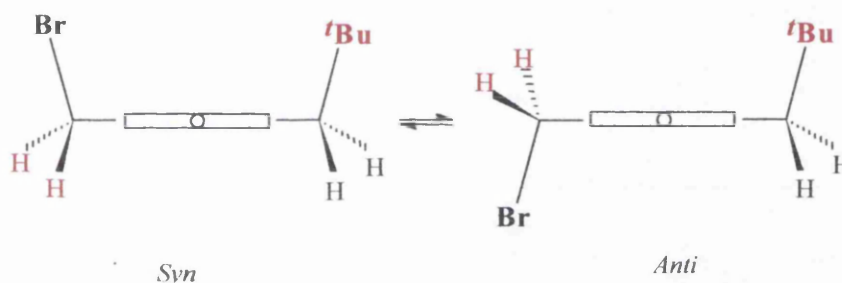
Z														Chemical shifts /ppm									
(T/ ^o C)	CH ₃	CH ₃	CH ₃	CH ₃	C(CH ₃) ₃	C(CH ₃) ₃	CH ₂ Me	CH ₂ Z	Ring Carbons														
(4.1) Cl	15.69	16.55	17.06	19.22	29.17	34.20	39.90	43.59	130.85	132.77	133.28	133.79	133.79	137.06									
(80 ^o C)		16.78	17.50			34.49	40.14	43.96	130.89	132.88	134.38	134.09		137.43									
(4.2) Br (80 ^o C)																							
					29.12	33.43	34.16	39.86	130.74	132.75	133.27	133.81	133.84	137.11									
						33.91	34.47	40.05	130.86	132.89	133.40	134.14		137.58									
(4.3) I (45 ^o C)																							
	15.85	16.79	17.44	19.43	29.54	34.39	40.34	9.14	131.81	132.48	133.50	133.63	134.47	136.71									
	15.94	16.95	17.72	19.51	29.63	34.69	40.50	9.82	132.14	132.69	133.70	133.97	134.74	137.34									

^a This part of the spectrum is not well resolved

other protons also do split, see table 4.1 for the chemical shifts. From the intensities of the $\text{C}(\text{CH}_3)_3$ signals, a population ratio of 2.0:1 is obtained.

To establish which of the two conformations is the more populated in the equilibrium, a NOE difference experiment was carried out at -60°C on a 500 MHz spectrometer. Considering the distance between the CH_2Br protons and the *tert*-butyl group, as shown in figure 4.2, they are undoubtedly closer together in the *anti* conformation. Thus, irradiating the *tert*-butyl signal in the proton NMR should lead to a higher enhancement of the *anti* CH_2Br signal relative to the corresponding *syn* bromomethylene signal.

Figure 4.3



On irradiating the $\text{C}(\text{CH}_3)_3$ protons, the signals from two of the CH_3 groups (~ 2.18 and ~ 2.30 ppm) showed positive NOEs, suggesting that the methyl groups in question are those flanking the CH_2CMe_3 group. In addition, the signals from the CH_2Br protons were also enhanced, albeit only marginally, but of more significance is the fact that the more intense of the AB systems, in the CH_2Br region, that is centred at 4.60 and 4.67 ppm, showed a relatively higher positive NOE, see figure 4.4a and b. A plausible inference that may be drawn from this is that the more intense of the quartets is from the *anti* conformation. Thus, the observed conformational ratio of 2:1 is in favour of the *anti* form, this equates to an energy difference of $0.26 \text{ kcal mol}^{-1}$ at -80°C .

It is also worth pointing out that if one considers the relative chemical shift of the midpoint of the two AB systems for the bromide (4.2), the NOE result is consistent with the assumption, which applies to analogue compounds discussed in chapter two, where $\text{X} = \text{Z}$, in that the *anti* signals always resonates downfield the *syn* signals in the methylene region.

In a more polar solvent, acetone- d_6 , at -80°C , the *syn/anti* ratio did not change at 1:2.0, an energy difference of $0.26 \text{ kcal mol}^{-1}$.

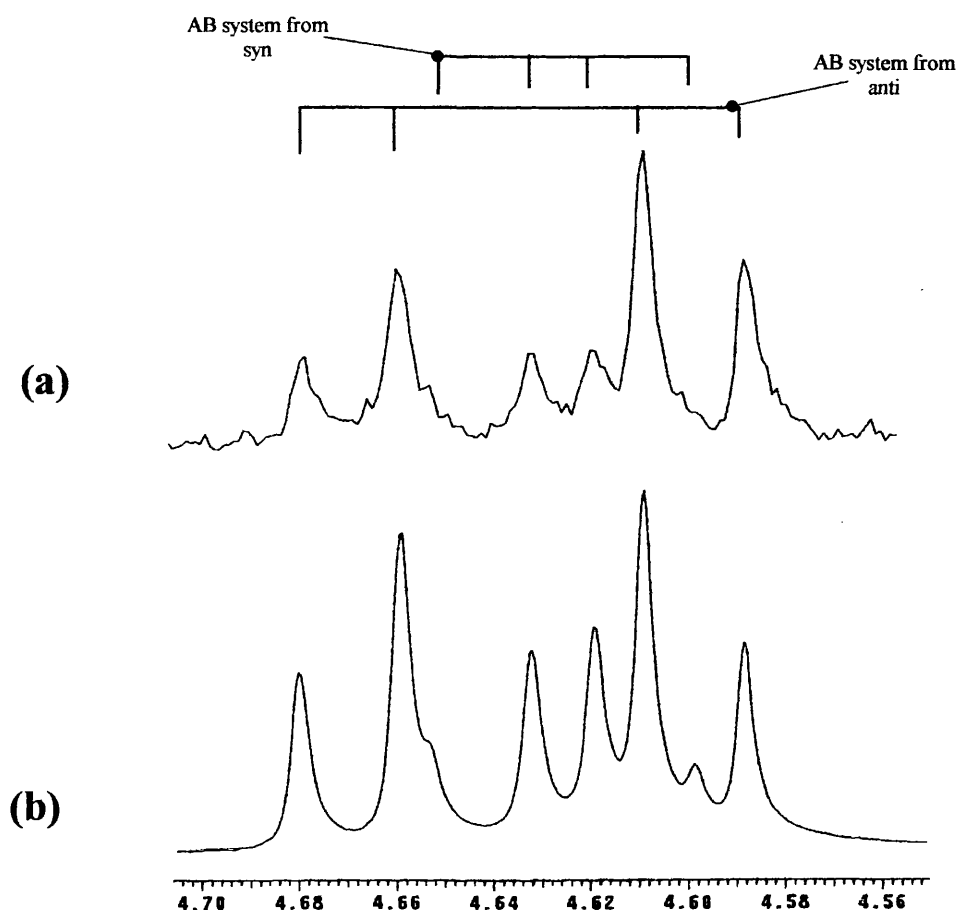


Figure 4.4.

- (a) The methylene region of the 500 MHz proton NMR spectrum of the bromide (4.2) at -60°C on irradiating at the $\text{CH}_2(\text{CH}_3)_3$ signal.
- (b) The methylene region of a normal proton NMR spectrum of the bromide at -60°C .

As for a sample of the chloride (4.1) in methylene chloride- d_2 , at $+22^{\circ}\text{C}$, the CH_2Cl and $\text{CH}_2\text{C}(\text{Me})_3$ signals both appeared as singlets in the proton NMR but unlike the bromide, at about -20°C , not one, but both singlets have de-coalesced into an AB system ($J = 11.6\text{ Hz}$). And on cooling further to -80°C , two sets of AB systems are observed in the CH_2Cl region, whilst in the $\text{CH}_2\text{C}(\text{Me})_3$ region, an AB quartet together with a singlet are seen. From the $\text{C}(\text{CH}_3)_3$ signals at 0.79 and 0.81 ppm, see figure 4.4b, a conformational population ratio of 2.3:1 is obtained. The pattern observed as regards the relative shift of the major and minor signals in both the proton and ^{13}C NMR spectra of the chloride, in comparison to that of the bromide, is consistent with the more intense signals coming from the *anti* conformation (see tables 4.1 and 4.2). Thus, the observed ratio of 1:2.3, representing an energy difference of $0.34\text{ kcal mol}^{-1}$ is in favour of the *anti* conformation.

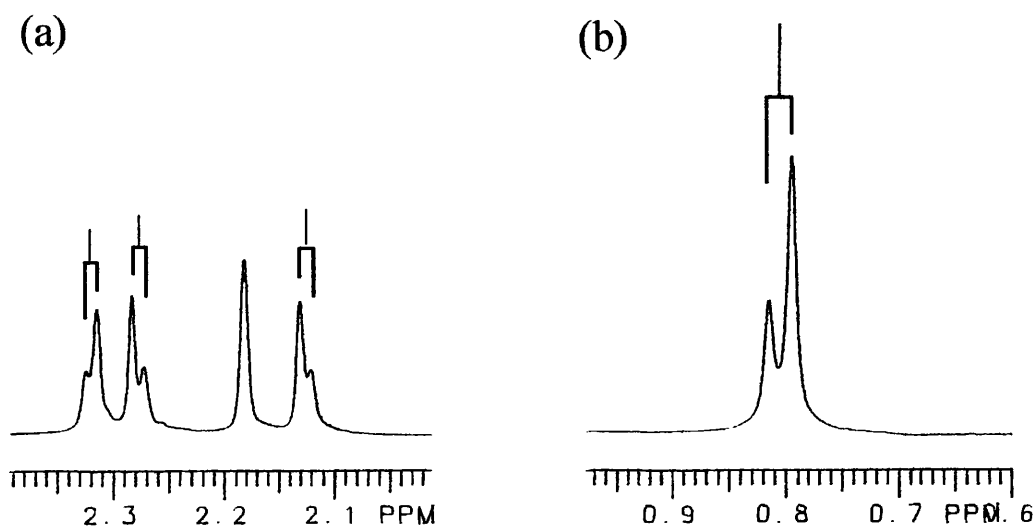


Figure 4.4.

(a) The Ar-CH₃ region of the proton NMR spectrum of the chloride (4.1) at -80 °C.

(b) The CH₂(CH₃)₃ region of the proton NMR spectrum of the chloride at -80 °C.

In the proton NMR spectrum of the iodide at room temperature, the CH₂I protons appears as a broad signal that de-coalesces at about +10 °C. And at -65 °C, the signal had split into two sets of AB systems, the CH₂I region of the spectrum is shown in figure 4.5. Comparing the relative shift of the major and minor signals from both the

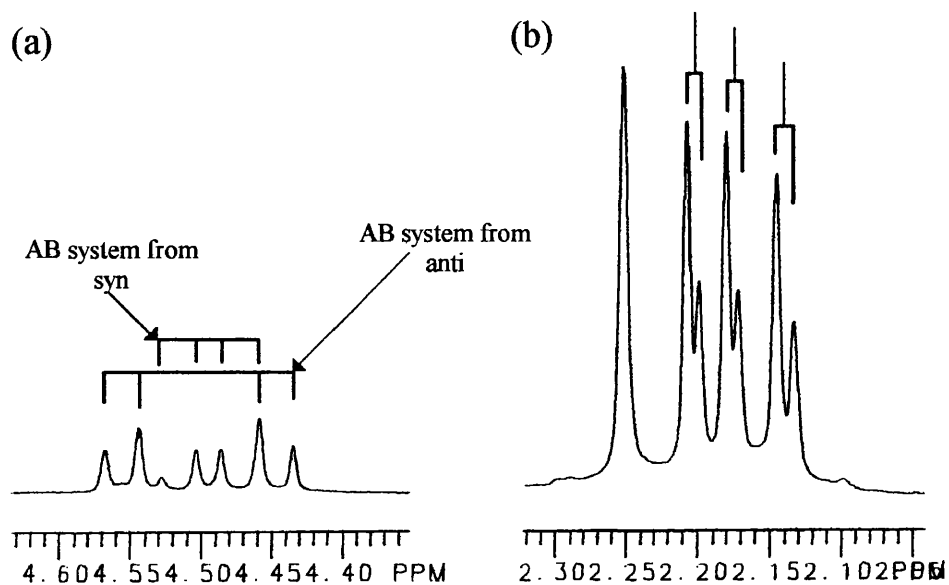


Figure 4.5.

(a) The methylene region of the proton NMR spectrum of the iodide (4.3) at -65 °C.

(b) The Ar-CH₃ region of the same spectrum.

proton and ¹³C NMR spectra of the iodide, with the relative shift of the *syn* and *anti* signals in the NMR spectra of the bromide, it is consistent with the *anti* being the more

populated in the iodide. Thus, the ratio of 1:2.0 at -65°C , obtained from the CH_2I signals, that equates to a free energy difference of $0.28 \text{ kcal mol}^{-1}$ is in favour of the *anti* conformation, the chemical shifts are summarised in tables 4.1 and 4.2.

Likewise for 1-(1-adamantanemethyl)-3-bromomethyl-2,4,5,6-tetramethylbenzene (4.4), the relative shifts of the major and minor peaks in the ArCH_3 and methylene regions of the proton NMR spectrum also resembles that of the other bromide (4.2), see table 4.1. This is not surprising bearing in mind the similarities which undoubtedly exist between a *tert*-butyl and an adamantyl group. After comparing the methylene regions of their proton NMR spectra, see figures 4.4a and 4.6a, the two sets of AB system in the adamantyl-compound were assigned accordingly:

The major set centred at 4.61 and 4.65 ppm is from the *anti* whilst the slightly obscured and less intense set, centred at 4.60 and 4.68 ppm is from the *syn*. The ArCH_3 and CH_2Br regions of the spectrum are shown in figures 4.6a and b respectively. From the relative intensity of the most downfield methyl signal that did split into two, a *syn/anti* conformational population ratio of 1:2.8 is obtained, this equates to an energy difference of $0.39 \text{ kcal mol}^{-1}$.

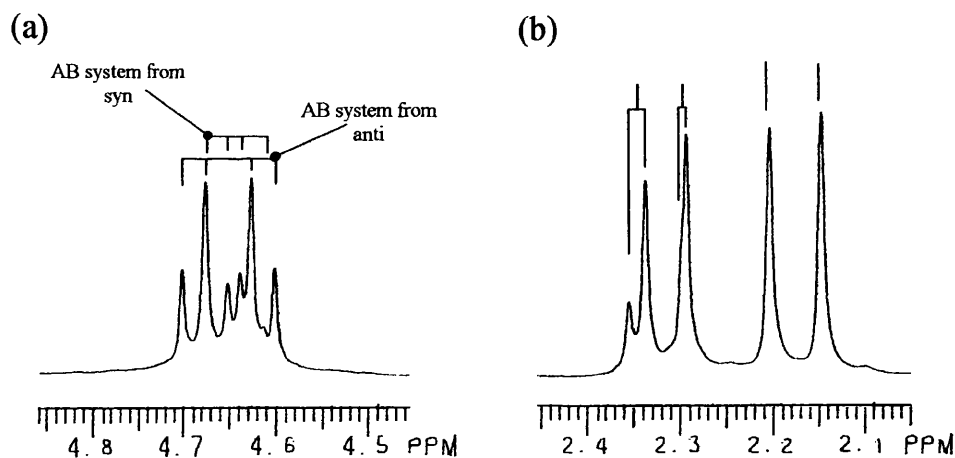


Figure 4.6.

- (a) The CH_2Br region of the proton NMR spectrum of the adamantyl-compound at -80°C .
 (b) The ArCH_3 region of the same spectrum.

(b) NMR spectra of 4.5 - 4.8

In the proton NMR spectra of 4.5 – 4.7 in $\text{CHCl}_2\text{F}:\text{CHClF}_2:\text{CD}_2\text{Cl}_2$ ($\sim 2:2:1$), the signals in the aromatic region are obscured by those from the solvent and at low temperatures the *tert*-butyl signals do not split, presumably, because the *tert*-butyl peaks from the two

conformations coincidentally come into resonance at the same frequency. The proton NMR chemical shifts for 4.5 – 4.7 are summarised in table 4.3.

A detailed description of the CH_2CMe_3 region of the 400 MHz proton NMR spectrum of phenyl-compound (4.7) at various temperatures is now presented. The NMR spectra between $+22\text{ }^\circ\text{C}$ and $-120\text{ }^\circ\text{C}$ are shown in figure 4.8, For the CH_2CMe_3 region of the spectrum at $-130\text{ }^\circ\text{C}$ see figure 4.7.

In the proton NMR spectrum, the signals from the $^t\text{BuCH}_2$ and PhCH_2 groups each appeared as a singlet at room temperature. But at $0\text{ }^\circ\text{C}$, when rotation about the $^t\text{Bu-CH}_2$ bond become slow, the $^t\text{BuCH}_2$ signal de-coalesces into an AB system ($J = 14.4\text{ Hz}$) whilst the PhCH_2 signal remained unchanged as a singlet. But on cooling further to $-40\text{ }^\circ\text{C}$, the PhCH_2 signal also do split into an AB system ($J = 16.6\text{ Hz}$).

At $-120\text{ }^\circ\text{C}$, when rotation about both the $^t\text{Bu-CH}_2$ and Ph-CH_2 bonds have become slow on the NMR time scale, an AB system together with a singlet are observed in the $^t\text{BuCH}_2$ region. And in the PhCH_2 region, only one set of AB system is seen, presumably, because the two sets from the *syn* and *anti* conformations coincidentally overlap. From the $^t\text{BuCH}_2$ signal at $-130\text{ }^\circ\text{C}$ (see figure 4.7), the intensity ratio of the AB system, centred at 2.78 and 2.86 ppm to the singlet at 2.88 ppm, was found to be 3.1:1 equating to an energy difference of $0.32\text{ kcal mol}^{-1}$.

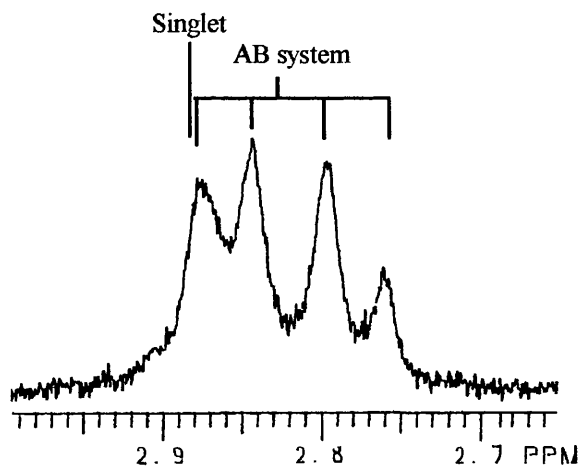


Figure 4.7. The $^t\text{BuCH}_2$ region of the proton NMR spectrum of the phenyl-compound (4.7) at $-130\text{ }^\circ\text{C}$.

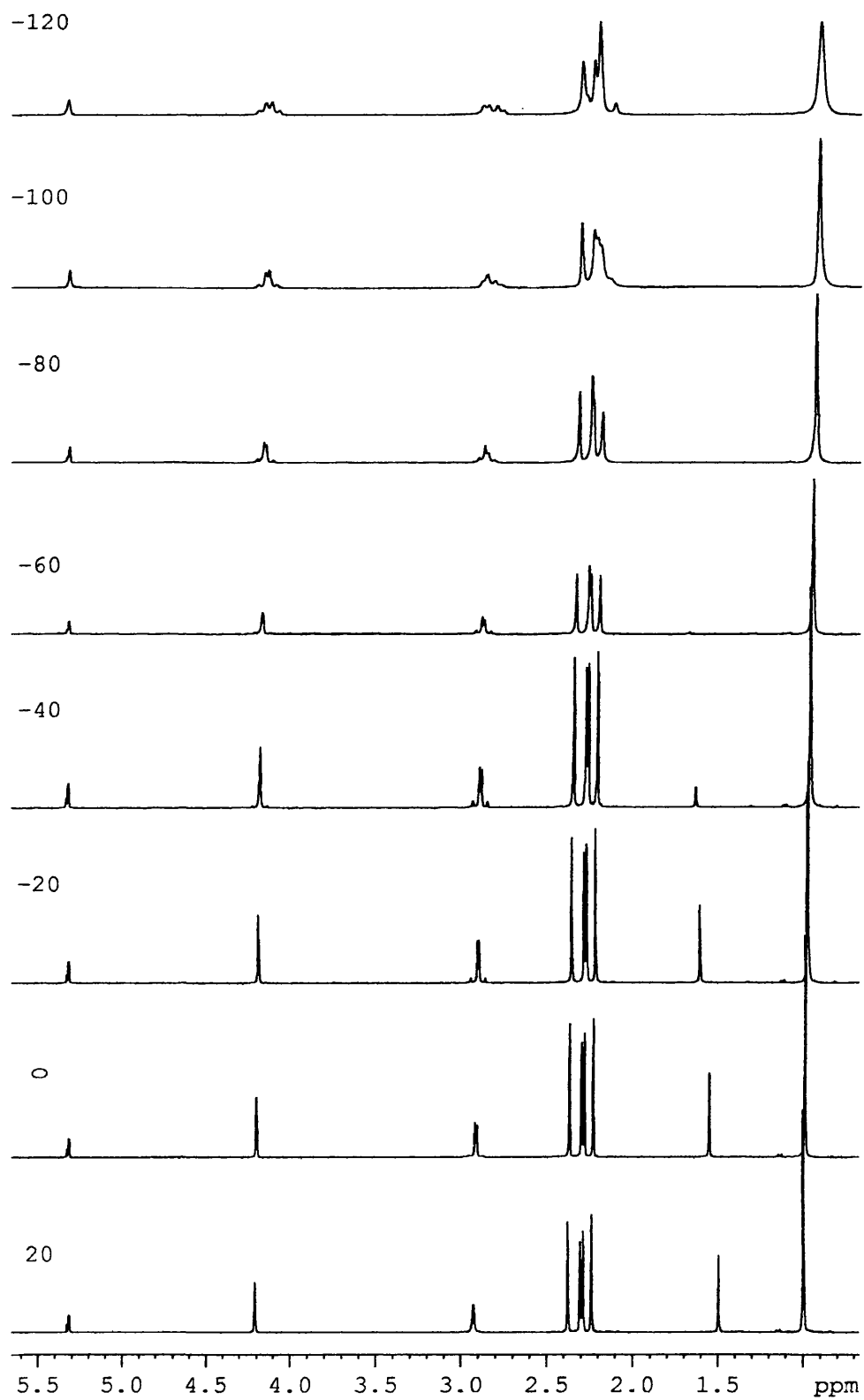


Figure 4.8. The dynamic NMR spectrum of the phenyl-compound (4.7).

On cooling a sample of the α -naphthyl-compound (4.5) in $\text{CHCl}_2\text{F}:\text{CHClF}_2:\text{CD}_2\text{Cl}_2$ (~2:2:1), at about -90°C , the CH_2CMe_3 signal de-coalesces before finally sharpening up at lower temperatures. The ArCH_3 and CH_2CMe_3 regions of the proton NMR spectrum are shown in figure 4.9. The methylene region at -120°C consists of an AB system centred at 2.81 and 2.90 ppm and a singlet at 2.881 ppm of intensity ratio 3.0:1 equating to an energy difference of $0.33\text{ kcal mol}^{-1}$.

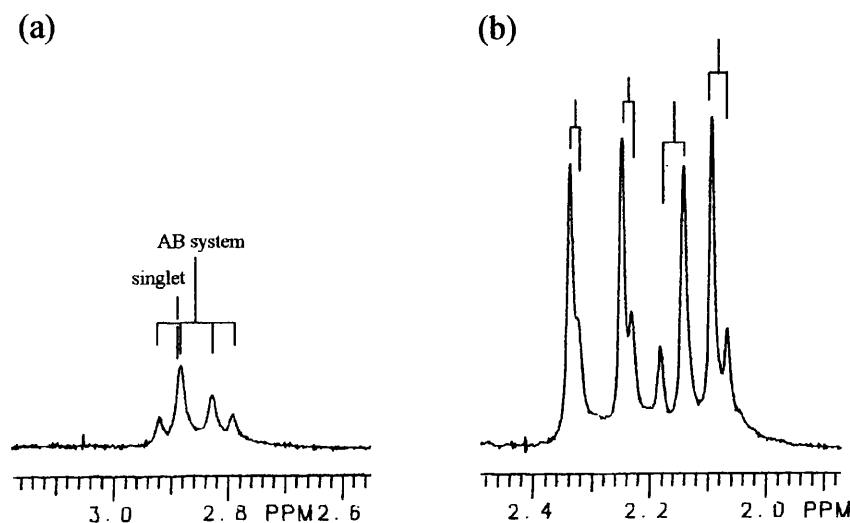


Figure 4.9.

- (a) The CH_2CMe_3 region of the proton NMR spectrum of the α -naphthyl-compound (4.5) at -120°C .
 (b) The ArCH_3 region of the same spectrum each of the four methyl groups has split into two.

As for the β -naphthyl-compound (4.7) in $\text{CHCl}_2\text{F}:\text{CHClF}_2:\text{CD}_2\text{Cl}_2$ (~2:2:1), the proton NMR's CH_2CMe_3 signal de-coalesced at about -90°C . And at -130°C , the signal has split into an AB system and a singlet, with the later resonating marginally upfield the midpoint of the quartet. The methylene region and the ArCH_3 regions of the spectrum are shown in figure 4.10a and b respectively. The proton NMR chemical shifts are summarised in table 4.3.

For compounds 4.5 – 4.7, the pattern observed in the proton NMR signals from the Ar-CH_3 and CH_2CMe_3 protons as regards the relative shift of the major and minor peaks, is similar for the three compounds, see figures 4.7, 4.9a and 4.10a as well as table 4.3. And based on the assumption that in the methylene region, the *anti* signals always resonates downfield the *syn*, it is plausible to suggest that in each of 4.5 – 4.8 the *syn* conformation is the more populated and therefore the more stable.

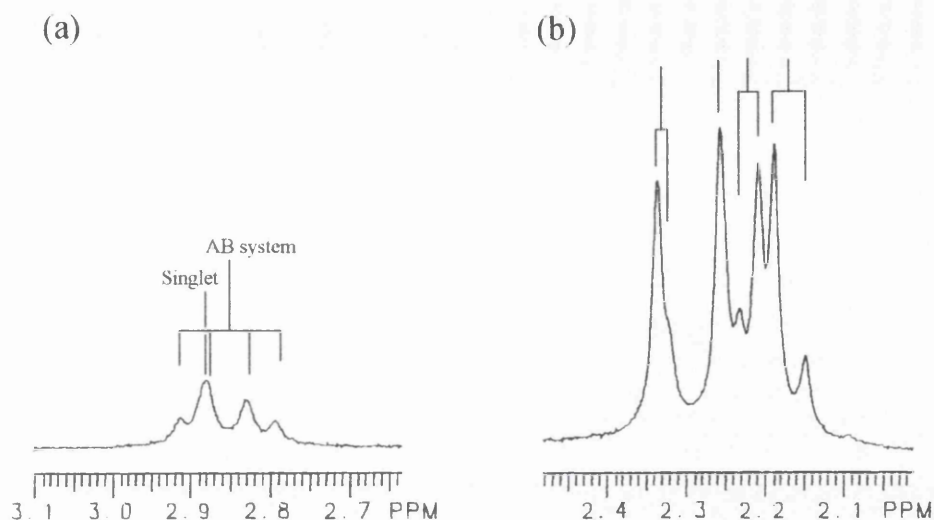


Figure 4.10.

(a) The CH_2CMe_3 region of the proton NMR spectrum of the β -naphthyl-compound (4.6) at -130°C .

(b) The ArCH_3 region of the same spectrum.

Table 4.3. The proton NMR chemical shifts^a for the α -naphthyl- (4.5) and β -naphthyl- (4.6) and phenyl- (4.7) compounds at low temperatures.

Z	Chemical shifts /ppm				
	ArCH_3	ArCH_3	ArCH_3	ArCH_3	CH_2^tBu
α -Naphthyl	2.07	2.14	2.23	2.32	2.81 (AB, $J = 14.2$ Hz); 2.881 (s);
-120°C	2.09	2.18	2.25	2.34	2.90 (AB, $J = 14.2$ Hz);
β -Naphthyl	2.15	2.21	2.25	2.32	2.811 (AB, $J = 14.6$ Hz); 2.880 (s);
-120°C	2.19	2.23		2.34	2.895 (AB, $J = 14.6$ Hz).
Ph	2.12	b			2.78 (AB, $J = 14.4$ Hz); 2.88 (s);
-130°C	2.18				2.86 (AB, $J = 14.4$ Hz).

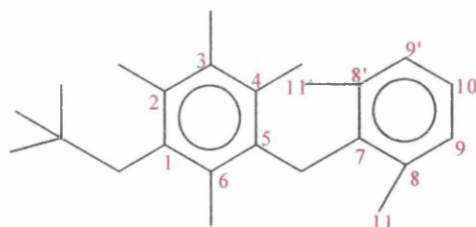
^a The signals in the aromatic region of the spectra are not shown because they are being obscured by the solvent peaks.

^b Too complex to interpret because of strong overlap.

(c) NMR spectra of the xylyl-compound (4.8)

In the proton NMR spectrum of the xylyl-compound in $\text{CHCl}_2\text{F}:\text{CHClF}_2:\text{CD}_2\text{Cl}_2$ ($\sim 2:2:1$), the signals from the xylyl methyl groups together with those from the two groups of methylene protons all appear broad and at the point of de-coalescence at room

temperature. On cooling to 0 °C, the exchange broadened xylyl methyl signal had split into two broad singlets of equal intensity suggesting that rotation about the CH₂-C⁷



bond, presumably, together with the C⁵-CH₂ bond had both become slow on the NMR time scale. At the same time, both signals from the two groups of methylene protons have each split into a single AB system.

In the subsequent spectra taken between -20 and -120 °C, the broad signals sharpened up but there was no sign of the methyl signals from the main benzene ring broadening and splitting, although, rotation about both C⁵-CH₂ and C¹-CH₂ bonds would surely have been stopped at this temperatures. The most likely explanation is that the xylyl compound exists predominantly in a single conformation, this inference is also supported by ¹³C NMR spectroscopy which also shows only one set of signals.

Thus in the ¹³C NMR spectrum at room temperature (+22 °C), the aromatic region consists of ten peaks with those from C-8 and C-9 appearing broad and at the point of de-coalescence. But at -60 °C the signals from C-8 and C-9 had each split into two peaks of equal intensity, supposedly, because rotation about the CH₂-C⁷ bond had been stopped. Furthermore, the carbon atoms in the molecule are in a total of twenty-two different environments and the spectrum at -120 °C contains a total of twenty-two peaks of which twelve are in the aromatic region.

(d) *NMR spectra of 1-ethyl-3-neopentyl-2,4,5,6-tetramethylbenzene (4.9)*

On cooling a sample of the methyl-compound (4.9) in CHCl₂F:CHClF₂:CD₂Cl₂ (~2:2:1), the triplet from the CH₂CH₃ protons de-coalesces at about -100 °C. And at -127 °C, the tert-butyl and one of the ArCH₃ signals has each split into two and the CH₂CH₃ protons now appears as two sets of multiplets with the appearance of triplets. The ArCH₃ region of the spectrum is shown in figure 4.11a. The signal from the CH₂CH₃ was simplified by decoupling at the CH₂Me signal, the resultant spectrum is shown in figure 4.11b. Based on the assumption that the more downfield signal in the methylene region always comes from the anti, using the decoupled spectrum (figure

4.11b), an intensity ratio of 2.6:1, equating to a conformational energy difference of $0.28 \text{ kcal mol}^{-1}$ in favour of the *syn* is obtained.

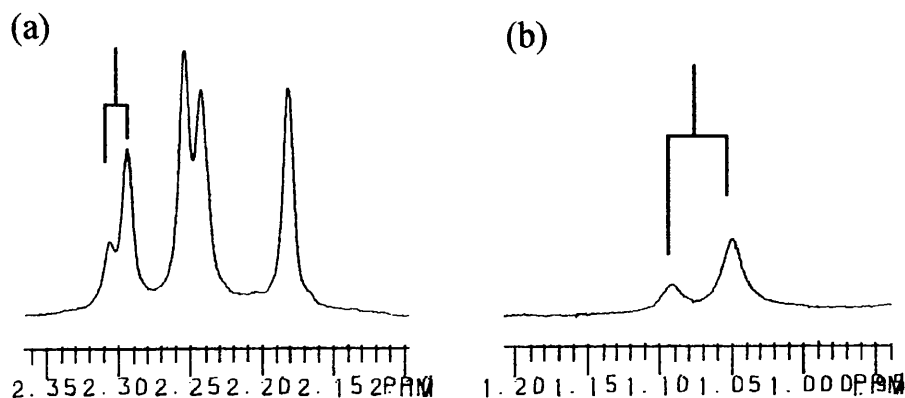


Figure 4.11.

(a) The ArCH_3 region of the proton NMR spectrum of the methyl-compound (**4.9**) at -120°C .

(b) The signal from the CH_2CH_3 protons at -120°C on decoupling at the CH_2Me signal.

(4.1.1-2) MM3 calculation

Calculations were performed on compounds **4.1** – **4.9**. In the first part of the discussion (a), the results for the halides (**4.1** – **4.4**) are presented followed in part (b) by the results for **4.5** – **4.9** are discussed.

(a) Compounds **4.1** – **4.4**

As for the halides **4.1** – **4.4** calculations showed that the *syn* conformations of the iodo- (**4.3**) and bromo-adamantyl- (**4.4**) compounds are slightly more stable relative to the *anti*, the enthalpy differences ($\Delta H_{\text{calc.}}$) being about (**4.3**, -0.03) and (**4.4**, $0.04 \text{ kcal mol}^{-1}$). By contrast the *anti* conformations of the chloro- (**4.1**) and bromo-neopentyl- (**4.2**) compounds were calculated to be more stable than the *syn*, the $\Delta H_{\text{calc.}}$ values being about (**4.1**, 0.14) and (**4.2**, $0.03 \text{ kcal mol}^{-1}$). The results of MM3 calculations are summarised in table **4.4**.

When the sum of the individual atom-atom van der Waals interaction between the X and Z groups in both conformations of **4.1**-**4.4** are being considered, the *syn* conformation benefits by about (**4.1**, 0.11); (**4.2**, 0.16); (**4.3**, 0.21) and (**4.4**, $0.28 \text{ kcal mol}^{-1}$) relative to the *anti*, see table **4.5**. The X-Z steric interactions is as expected greater in the *syn* conformation because, unlike the *anti*, the two groups are closer together and therefore better placed to maximise attractive steric interactions. And the

Chapter Four

Table 4.4. A summary of the steric energy contributions (kcal mol⁻¹) for 4.1 – 4.4

Compound →	Chloride (4.1)		Bromide (4.2) ^a		Iodide (4.3)		Bromide (4.4) ^b	
	<i>Syn</i>	<i>Anti</i>	<i>Syn</i>	<i>Anti</i>	<i>syn</i>	<i>anti</i>	<i>syn</i>	<i>anti</i>
Compression	2.9133	2.9181	2.9544	2.9741	2.9136	2.9422	3.6503	3.6417
Bending	4.1973	4.2430	4.1941	4.2453	4.5656	4.6585	4.3092	4.3182
Bend-bend	-0.2295	-0.2275	-0.2302	-0.2281	-0.3495	-0.3472	-0.2367	-0.2377
Stretch-bend	-0.3104	-0.3144	-0.3116	-0.3146	-0.3052	-0.3059	-0.4152	-0.4158
van der Waals								
1,4 energy	12.5536	12.5995	12.5478	12.5772	12.4080	12.4363	22.7133	22.7659
Other	7.4028	7.4401	7.4378	7.5976	7.2235	7.4091	6.0000	6.2058
Torsional	-7.3508	-7.5867	-7.5288	-7.7870	-12.9250	-13.2077	-0.7279	-1.0020
Torsion-stretch	-0.0033	-0.0024	-0.0033	-0.0024	-0.0033	-0.0024	-0.0038	-0.0037
Dipole-dipole	6.7038	6.6653	6.9003	6.8703	6.9615	6.9360	6.8970	6.8706
Total Steric Energy (H)	25.8767	25.7351	25.9604	25.9323	20.4893	20.5188	42.1861	42.1430
ΔH	0.1416		0.0281		-0.0295		-0.0431	

^a The neopentyl-compound.^b The adamantyl-compound.

increase in magnitude of the X-Z attractive steric interactions on going from chlorine to bromine and to iodine in the neopentyl-compounds reflects the fact that an iodine atom is more polarisable than a bromine atom which in turn is more polarisable than a chlorine atom. And the increase on going from the bromo-neopentyl to the bromo-adamantyl compound is because in the latter more atoms are involved in the X-Z attractive steric interactions.

Table 4.5. The van der Waals energy (kcal mol⁻¹) associated with the pairwise interaction between the atom(s) of the X groups in both conformations of 4.1, 4.2, 4.3 and 4.4.

	Chloro- (4.1)	Bromo-neopentyl- (4.2)	Iodo- (4.3)	Bromo-adamantyl- (4.4)
<i>Syn</i>	-0.1560	-0.2210	-0.2809	-0.3551
<i>Anti</i>	-0.0465	-0.0607	-0.0724	-0.0790
Diff.	-0.1095	-0.1603	-0.2085	-0.2761

In all these compounds, calculations thus show that the steric interactions between X and Z relatively stabilises the *syn* conformation to a greater extent than predicted by the overall enthalpy difference (ΔH_{calc}), suggesting that other factors, presumably gearing, destabilises the *syn* relative to the *anti*. The effect of gearing is in contrast to that predicted for the series of compounds investigated in the preceding chapters, where gearing was found to relatively favour the *syn*.

Calculations also indicate that in neither the *syn* nor *anti* conformation is the successive up and down arrangement of C-Y (Y = X, Z or H) bonds preserved. This conformation is shown, in the literature, to be the most populated in hexamethyl³⁰ and hexaethyl-benzenes³¹. The arrangement of the groups on the ring is illustrated in figure 4.12.

(b) Compounds 4.5 – 4.9

With the exception of the methyl- compound, in the 4.5 – 4.9 series, the *syn* conformation was calculated to be more stable than *anti*, the enthalpy differences being (α -naphthyl-, -0.06); (β -naphthyl-, -0.12); (phenyl-, -0.23); (xylyl-, -0.68); (methyl-, +0.10 kcal mol⁻¹). The contributors to the final steric energies are shown in table 4.6.

Table 4.6 The steric energy contributions (kcal mol⁻¹) for the α -naphthyl- (4.5), β -naphthyl- (4.6), phenyl- (4.7), xyl-yl- (4.8) and methyl- (4.9) compounds

Compound	→	α -Naphthyl- (4.5)		β -Naphthyl- (4.6)		Phenyl- (4.7)		Xyl-yl- (4.8)		Methyl- (4.9)	
		<i>Syn</i>	<i>Anti</i>	<i>Syn</i>	<i>Anti</i>	<i>Syn</i>	<i>anti</i>	<i>syn</i>	<i>anti</i>	<i>syn</i>	<i>anti</i>
Compression		3.7321	3.7229	3.5493	3.5183	3.3573	3.3618	4.0995	4.1637	3.0744	3.0863
Bending		5.1456	5.1614	5.1104	5.1282	4.5704	4.6224	5.6902	5.8080	4.1338	4.2051
Bend-bend		-0.1927	-0.1899	-0.2030	-0.1994	-0.1707	-0.1702	-0.1742	-0.1732	-0.1869	-0.1842
Stretch-bend		-0.5418	-0.5477	-0.5122	-0.5160	-0.4380	-0.4283	-0.5377	-0.5278	-0.3161	-0.3186
van der Waals											
1,4 energy		21.2743	21.3017	21.1512	21.1882	17.5364	175365	19.2382	19.1582	13.6543	13.6768
Other		6.1436	6.3532	5.3639	5.5810	6.2253	6.4506	7.1682	7.7039	7.7393	7.8061
Torsional		-17.2362	-17.4198	-17.2854	-17.3722	-12.1990	-12.2198	-12.4587	-12.4291	-9.6560	-9.9272
Torsion-stretch		-0.0032	-0.0022	-0.0034	-0.0023	-0.0027	-0.0034	-0.0024	-0.0035	-0.0039	-0.0030
Dipole-dipole		12.2119	12.2141	12.3581	12.3238	12.0264	11.9844	12.6678	12.6710	7.7926	7.7888
Total Steric Energy (H)		30.5337	30.5936	29.5289	29.6497	30.9054	31.1337	35.6909	36.3711	26.2314	26.1301
ΔH		-0.0599		-0.1208		-0.2283		-0.6802		0.1013	

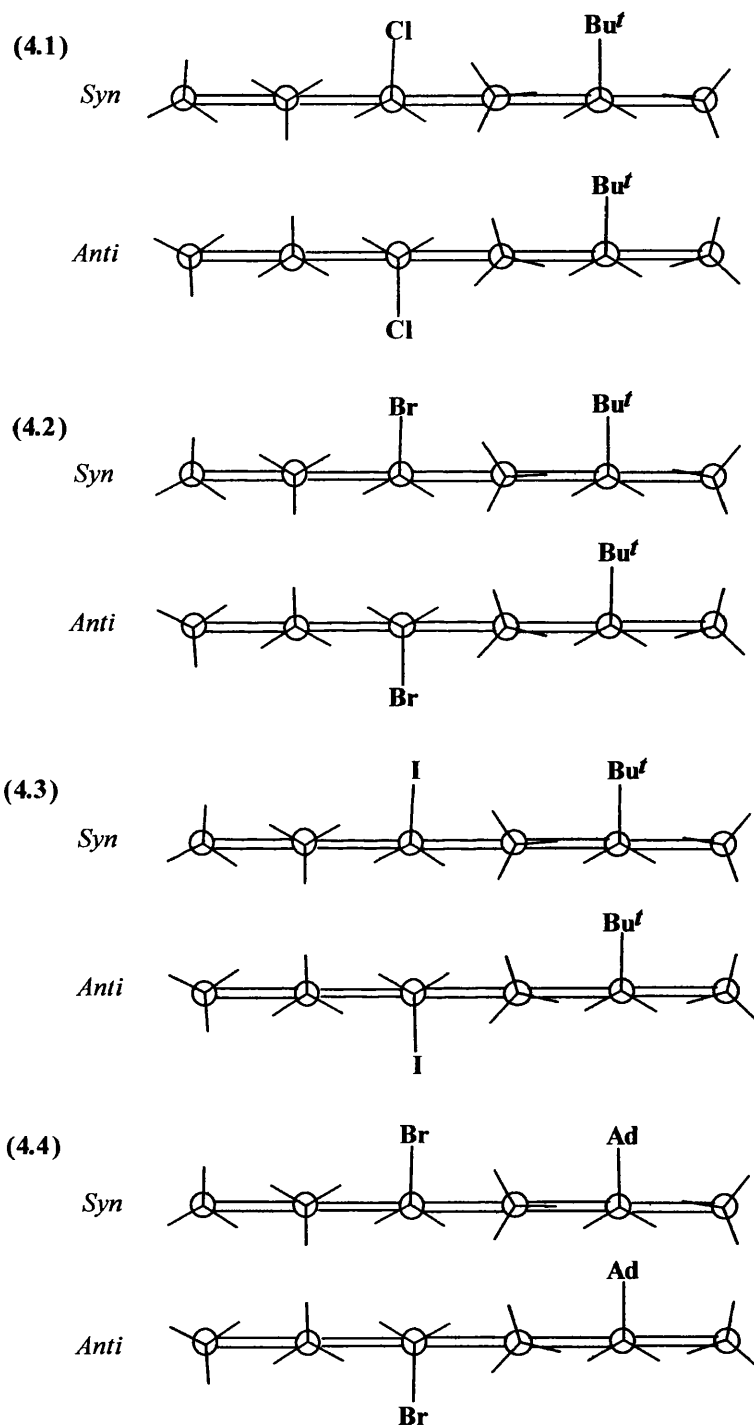


Figure 4.12. The interlocking arrangement of the groups on the main benzene ring. The diagram was constructed using torsional angles from calculations.

When the sum of the atom-atom van der Waals interaction between the X and Z groups in both conformations are being considered, the *syn* conformations gains about (α -

naphthyl-, 0.37); (β -naphthyl-, 0.41); (phenyl-, 0.26); (xylyl-, 0.32); (methyl-, 0.10 kcal mol⁻¹) relative to the *anti*, see table 4.7. It is worth pointing out that in the *syn* conformation of the xylyl-compound, the closest pair of hydrogen atoms, one from the xylyl's methyl group and the other from the *tert*-butyl group, were found to be slightly repelling by about 43 cal mol⁻¹.

Table 4.7 The sum of the X-Z van der Waals contributions for the α -naphthyl- (4.5), β -naphthyl- (4.6), phenyl- (4.7), xylyl- (4.8) and methyl- (4.9) compounds

Compound →	α -Naphthyl- (4.5)	β -Naphthyl- (4.6)	Phenyl- (4.7)	Xylyl- (4.8)	Methyl- (4.9)
<i>Syn</i>	-0.4783	-0.5067	-0.3224	-0.4089	-0.1250
<i>Anti</i>	-0.1040	-0.0920	-0.0654	-0.0858	-0.0294
Diff.	-0.3743	-0.4147	-0.2570	-0.3231	-0.0956

Surprisingly, with the exception of the xylyl-compound, the magnitude of the *syn* advantage originating from X-Z attractive steric interactions in 4.5 - 4.9, is lower than that predicted by the overall enthalpy difference, suggesting that just like in the halides, gearing probably disfavors the *syn* relative to the *anti*. And judging the xylyl-compound on the same basis, gearing seems to slightly favour the *syn* relative to the *anti*.

The interlocking arrangement of the groups on main benzene ring is shown in figure 4.13 and 4.14, like in the halides (4.1 - 4.4), the conformation in which the C-Y (Y = X, Z or H) bonds are arranged more or less in an up and down manner all the way round the ring is not observed for the *syn* and *anti* forms of 4.5 - 4.9.

And finally, it should be known that unlike the methyl-compound, in the phenyl-, naphthyl- and xylyl-compounds, rotation about the C-Z bond may lead to other equally or less stable *syn* and *anti* conformations. The value of the torsional angle (ϕ) which defines the conformation about the C-Z, bonds in 4.5 - 4.8 are summarised in figure 4.13a. For the α -naphthyl-compound (4.5), ϕ is calculated to be (*syn*, -172°); (*anti*, +168°), these values are in close agreement with those obtained from X-ray crystallography, here the corresponding torsional angles are (*syn*, -174.8°); (*anti*, -171.2°). The X-ray structure of the α -naphthyl-compound is shown in figure 4.13b.

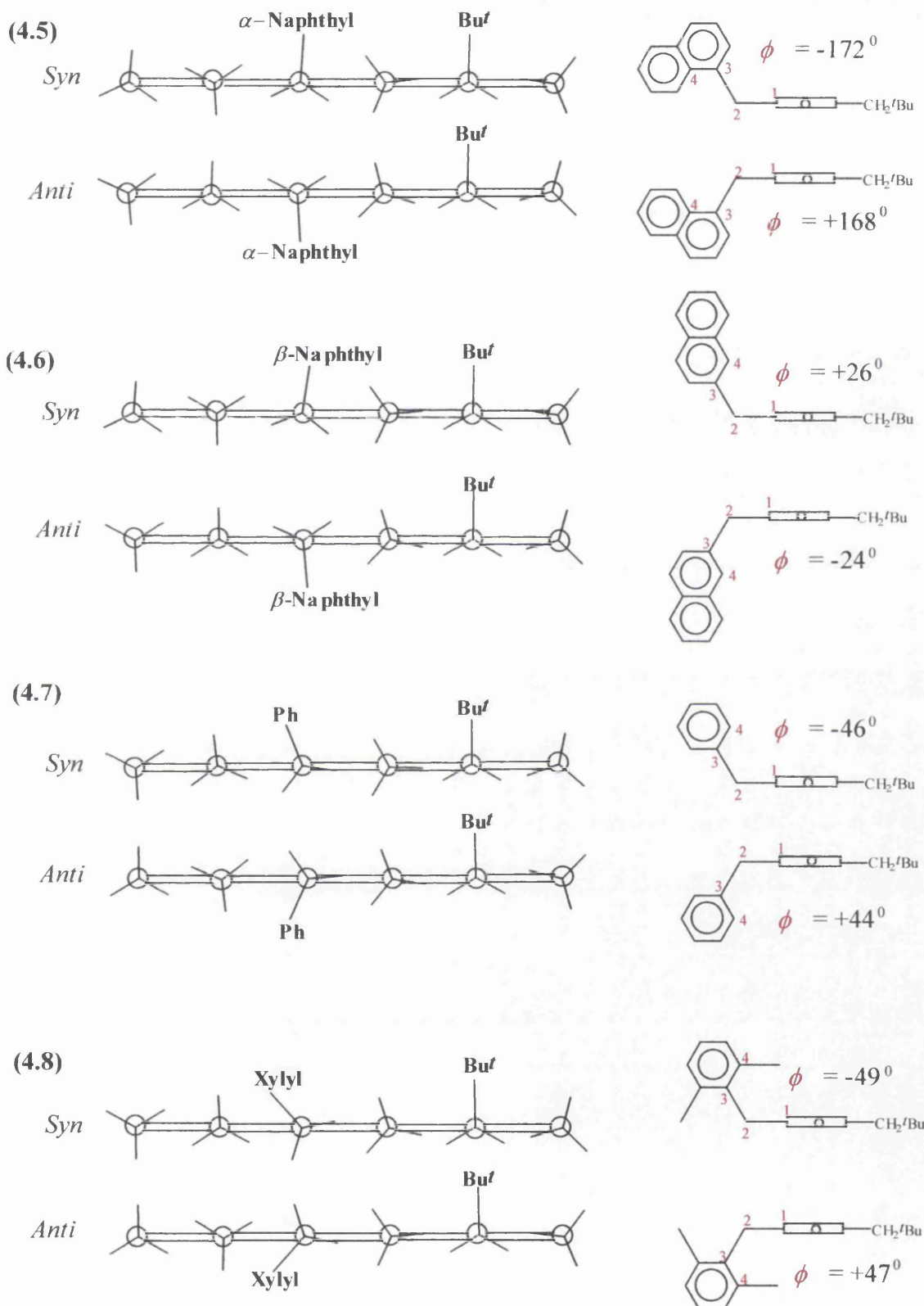


Figure 4.13a. The interlocking arrangement of the groups on the main ring. The diagram was constructed using the torsional angles from calculation. The angle ϕ is the torsional angle defined by C1-C2-C3-C4.

(4.1.1-3) X-ray analysis of 1-(α -naphthyl)-3-neopentyl-2,4,5,6-tetramethylbenzene

The α -naphthyl-compound (4.5) crystallises as a monoclinic system comprising of a 1:1 ratio of *syn* to *anti*, with each unit cell consisting of a total of eight molecules. Part of the unit cell is shown in figure 4.13b.

Crystal data: C₂₆H₃₂

Molecular weight = 344.52; temperature = 100(2) K; wavelength = 0.71073 Å;

Unit cell dimension a = 21.4456(13) Å; $\alpha = 90^\circ$

 b = 21.584(4) Å; $\beta = 94.520(10)^\circ$

 c = 8.730(4) Å; $\gamma = 90^\circ$

Volume = 4028(2) Å³

Density = 1.136 Mg m⁻³

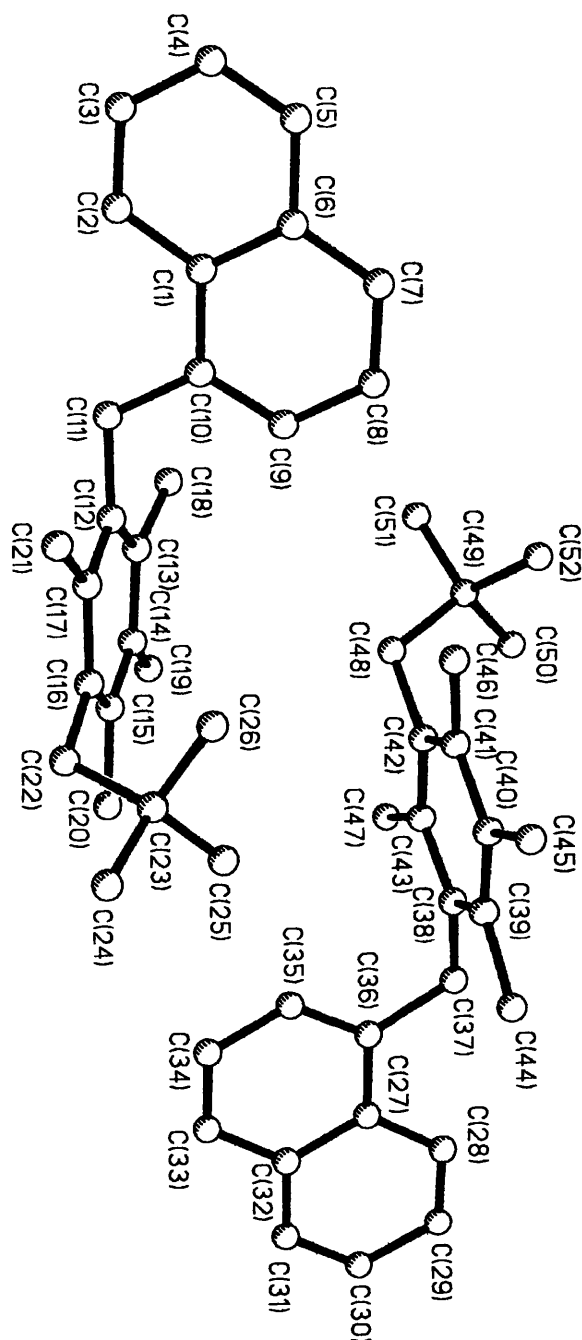


Figure 4.13b. X-ray structure showing the arrangement of the *syn* and *anti* conformations in a unit cell of the α -naphthyl-compound (4.5).

(4.1.2) Conclusion

The energy differences obtained from experiments and calculations are summarised in table 4.8. Initially, we predicted that the *syn* conformations of 4.1 - 4.9 would be more

stable than the *anti* form. The hypothesis is based on the assumption that gearing, like in the series of compounds investigated in the previous chapters, would always preferentially stabilise the *syn* relative to the *anti*. But calculations carried out on 4.1 - 4.9, show that while this may be true for the xylyl-compound, as for the rest of the compounds in the series, gearing destabilises the *syn* form relative to the *anti*. The prediction failed because unlike the other X groups investigated in the two previous chapters, here, the *tert*-butyl group is so demanding of space that it prevents C-H bonds, from adjacent methyl groups, from being orthogonal to the ring plane. The result is that hexasubstituted-benzenes with one or more neopentyl substituents can not be nicely geared and have a successive up and down arrangement of bonds all the way round the benzene ring.

Table 4.8. A summary of the result from dynamic NMR and calculations for 4.1-4.9

X	Z	Solvent	T	K ^a	ΔG_{exp}^c	ΔH_{calc}^c
			^o C		kcal mol ⁻¹	kcal mol ⁻¹
<i>t</i> -Bu	Cl	CD ₂ Cl ₂	-80	0.43	+0.34	+0.14
<i>t</i> -Bu	Br	CD ₂ Cl ₂	-80	0.50	+0.26	+0.03
<i>t</i> -Bu	I	CD ₂ Cl ₂	-65	0.50	+0.28	-0.03
Ad	Br	CD ₂ Cl ₂	-80	0.36	+0.39	-0.04
<i>t</i> -Bu	α -Naphthyl	Freon	-120	3.0	-0.33	-0.06
<i>t</i> -Bu	β -Naphthyl	Freon	-130	3.0	-0.33	-0.12
<i>t</i> -Bu	Ph	Freon	-130	3.1	-0.32	-0.23
<i>t</i> -Bu	Xylyl	Freon		^b		-0.68
<i>t</i> -Bu	Me	Freon	-127	2.6	-0.28	+0.10

^a The conformational population ratio of *syn* to *anti*.

^b It exist predominantly in a single conformation.

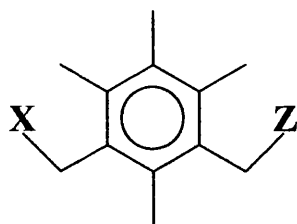
^c When the sign is +ve *anti* is the more stable and when the sign is -ve *syn* is the more stable.

Calculations also show that the contribution from gearing to the overall enthalpy difference in some of these compounds, for example, the bromo-adamantyl, α -naphthyl-, β -naphthyl- and phenyl-molecules, is that the high magnitude of *syn* advantage, originating from Z-X attractive steric interactions, is drastically reduced or completely reversed as in the case of the methyl-compound.

In summary dynamic NMR spectroscopy showed that in the α -naphthyl-, β -naphthyl-, phenyl-, methyl- and perhaps the xylyl- compounds, the *syn* conformation is more stable than the *anti*. And since calculations show that gearing destabilises the *syn* form relative to the *anti*, it is reasonable to conclude that a high proportion of the free energy difference, obtained experimentally, originates from attractive steric interactions between the X and Z groups which as shown by calculations is much higher in the more compact *syn* conformation.

And finally, as for the halides (4.1 - 4.4), NMR spectroscopy showed that the *anti* conformation is more stable than the *syn*. A plausible explanation is that the *syn* advantage originating from attractive steric interactions between the X and Z groups is overwhelmed by the *anti* advantage from gearing.

SECTION TWO

(4.2.1) Results and Discussion of 4.10 – 4.14

	X	Z
4.10	Ph	Cl
4.11	Ph	Br
4.12	Ph	I
4.13	Ph	Me
4.14	<i>p</i> -C ₆ H ₄ NO ₂	<i>p</i> -C ₆ H ₄ NH ₂

(4.2.1-1) Conformational assignment of NMR signals at low temperatures(a) *NMR analysis of 4.10 - 4.12*

Considering the NMR spectra of 4.10 - 4.12 in CHCl₂F:CHClF₂:CD₂Cl₂ (~2:2:1), the features of the aromatic region of the proton decoupled ¹³C NMR spectra on stopping rotation about both CH₂-Z and CH₂-Ph bonds are similar. The ¹³C NMR chemical shifts are summarised in table 4.9.

As for the proton NMR at low temperatures, the signals in the methyl region are complex to interpret and those in the aromatic region are obscured by solvent signals. The methylene protons from the CH₂Z and CH₂Ph groups each appeared as singlets at +22 °C but on cooling to temperatures low enough to slow rotation about the CH₂-Z (Z = Cl, Br or I) bond but not the CH₂-Ph bond, on the NMR time scale, each of the two singlets had split into an AB quartet. When rotation about both the CH₂-X and CH₂-Z bonds had become slow, the features of the methylene region of the three halides are similar, the dynamic NMR of the iodide is now presented.

On cooling a sample of the iodide, the signals in the proton NMR spectrum decoalesce at about -90 °C, and at -130 °C, a temperature low enough to slow rotation about both CH₂-I and CH₂-Ph bonds, an AB system centred at 4.49 ppm (J = 9.3 Hz) and 4.56 ppm together with a singlet resonating at 4.57 ppm are seen in the CH₂I region. Likewise, in the CH₂Ph region, an obscured AB quartet centred at 4.08 ppm (J = 17.7 Hz) and 4.13 ppm together with a singlet at 4.14 ppm are observed. In both regions, the chemical shift of the singlet is marginally downfield the midpoint of the AB system and the later is more intense than the former. The CH₂Ph and CH₂I regions of

Table 4.9. The chemical shifts of the aromatic carbons of compounds 4.10 - 4.14 regions at low temperatures. The major signals that happens to come from the *syn* conformation is shown in red.

X	Z	Chemical shifts /ppm											
Ph	Cl	126.07	128.06	128.71	131.36	133.78	134.49	134.57	134.74	137.53	140.03		
	-130 °C	126.14			131.64	134.11		134.61	135.21	137.59	140.43		
Ph	Br	126.21	128.23	128.84	131.64	133.94	134.72	135.04	137.84	140.10			
	-120 °C	126.26			131.97	134.39	134.82	135.38	137.96	140.76			
Ph	I	126.26	128.29	128.93	132.67	133.36	134.08	134.67	135.14	137.23	140.33		
	-130 °C	126.33			133.13	133.82	134.26		135.33	137.32	140.69		
Ph	Me	125.96	128.10	128.71	132.36	133.27	133.62	133.75	134.42	138.43	140.68		
	-130 °C	126.05			132.51			133.88	134.65	138.73	140.81		

the spectrum are shown in figure 4.14, from the CH_2I signals a conformational population ratio of 2.1:1 which equates to an energy difference of $0.21 \text{ kcal mol}^{-1}$ is observed.

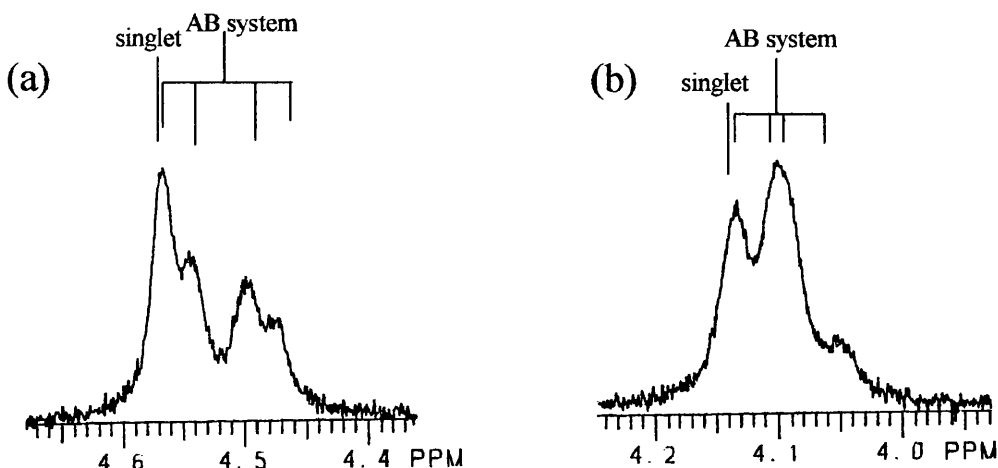


Figure 4.14.

(a) The CH_2I region of the proton NMR spectrum of the iodide (4.12) at -130°C .

(b) The CH_2Ph region of the proton NMR spectrum of the iodide at -130°C

As regards the bromide, the CH_2Br signal at -130°C consists of an AB system (4.65 ppm, $J = 10.1 \text{ Hz}$; 4.72 ppm) and a singlet (4.73 ppm) of intensity ratio 2.9:1 equating to an energy difference of $0.30 \text{ kcal mol}^{-1}$, see figure 4.15a. The CH_2Ph signal of the same spectrum contains a singlet (4.14 ppm) and an unresolved AB system centred at 4.10 ppm, see figure 4.15b.

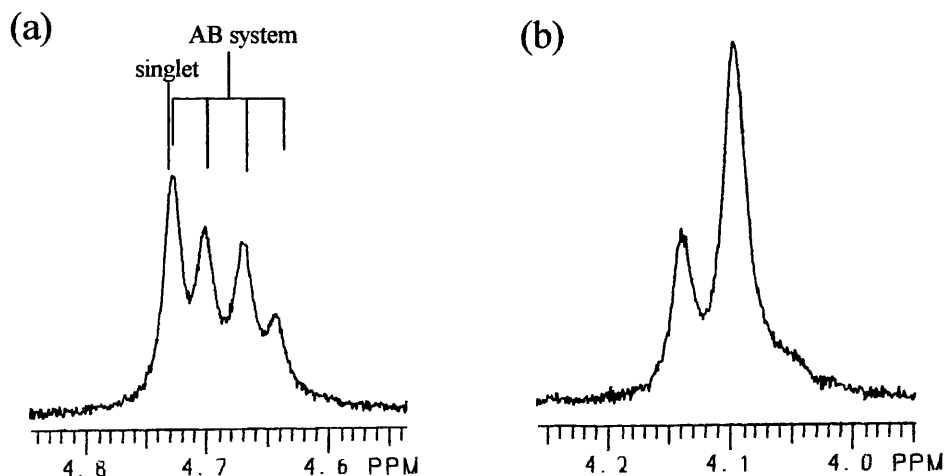


Figure 4.15.

(a) The CH_2Br region of the proton NMR spectrum of the bromide (4.11) at -130°C .

(b) The CH_2Ph region of the proton NMR spectrum of the bromide at -130°C

In the chloride, the CH_2Cl region of the proton NMR spectrum at -130°C , once again consists of an AB quartet (4.75 ppm, $J = 11$ Hz; 4.80 ppm) and a singlet (4.81 ppm). From the most downfield signal in the ^{13}C NMR spectrum of the chloride at -130°C , see figure 4.16, a conformational population ratio of 3.0:1 equating to an energy difference of $0.31\text{ kcal mol}^{-1}$ is observed.

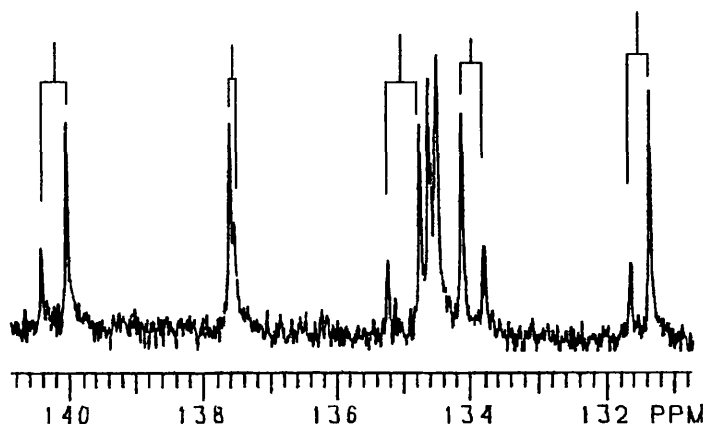


Figure 4.16. Part of the aromatic region of the ^{13}C NMR spectrum of the chloride (4.10) at -130°C .

We have not been able to show unequivocally, which of the two conformations is the more stable in the halides. However, based on the assumption that in the methylene region, the *anti* signals always resonates downfield the *syn* signals, we are able to conclude that the observed population ratio and the energy differences are both in favour of the *syn* conformation.

(b) NMR analysis of 4.13-4.14

For the methyl-compound (4.13) in $\text{CHCl}_2\text{F}:\text{CHClF}_2:\text{CD}_2\text{Cl}_2$ ($\sim 2:2:1$) at -120°C , a temperature low enough to stop rotation about both the $\text{CH}_2\text{-Ph}$ and $\text{CH}_2\text{-Me}$ bonds, the Ar-CH_3 region of the proton NMR spectrum is complex and impossible to interpret. The signals from the CH_2CH_3 and CH_2CH_3 protons are also complex, but by decoupling, in turn, at the CH_2CH_3 and CH_2Me signals, the signals were simplified therefore making it possible to determine the relative position of the major and minor peaks in both regions of the spectrum. The proton NMR chemical shifts are summarised in table 4.10. The CH_2Ph region of the spectrum at -130°C is shown in figure 4.16a, it

consist of two singlets centred at 4.08 and 4.14 ppm, once again the more upfield signal is the more intense.

Part of the ^{13}C NMR spectrum at -130°C is shown in figure 4.16b, from the pair of peaks at 138.43 and 138.73 ppm a conformational population ratio of 1.6:1 is obtained, this corresponds to an energy difference of $0.13\text{ kcal mol}^{-1}$. The chemical shifts of the aromatic carbons at -130°C is summarised in table 4.9.

Table 4.10. The chemical shifts ^a of the proton NMR spectrum of the methyl- compound (4.13) at -130°C .

substituents		Chemical shifts /ppm		
		CH_2CH_3 ^b	CH_2CH_3 ^c	CH_2Ph
Ph	Me	1.07	2.69	4.08
		1.10	2.74	4.14

^a The signals in the methyl region are complex to interpret and are not included.

^b The resultant spectrum after decoupling at the CH_2CH_3 signal.

^c The resultant spectrum after decoupling at the CH_2CH_3 signals.

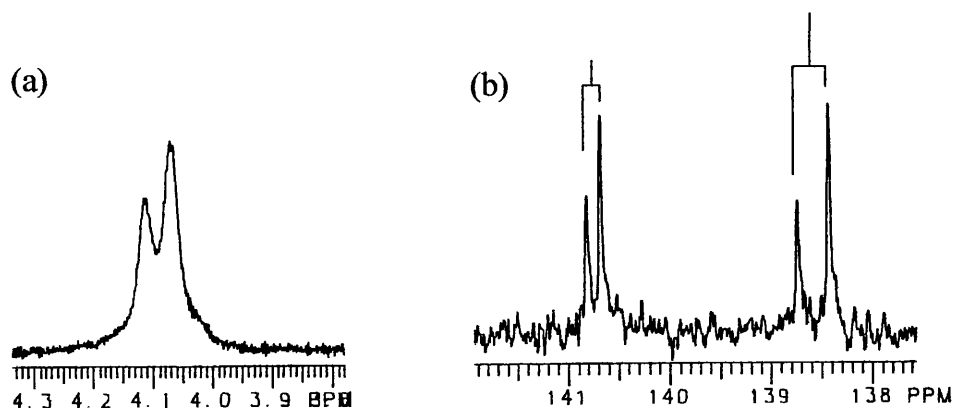


Figure 4.17.

(a) The CH_2Ph region of the proton NMR spectrum of the methyl-compound (4.13) at -130°C .

(b) Part of the aromatic region of the ^{13}C NMR spectrum of the same compound at -130°C .

As regards the nitro-amine-compound (4.14) in $\text{CHCl}_2\text{F}:\text{CHClF}_2:\text{CD}_2\text{Cl}_2$ ($\sim 2:2:1$), the signal from the aromatic protons that are *ortho*- to the NO_2 group, appeared as a doublet at room temperature, but on cooling, the signals broadened and eventually de-coalesced at about -110°C before finally sharpening up at lower temperatures. At -120°C the signal had split into two sets of partially overlapping doublets (see figure 4.18). From these signals a population ratio of $\sim 1.4:1$ corresponding to an energy difference of \sim

0.10 kcal mol⁻¹ is obtained. The methyl and methylene peaks do de-coalesce at low temperatures but strong overlap made them complex and impossible to interpret.

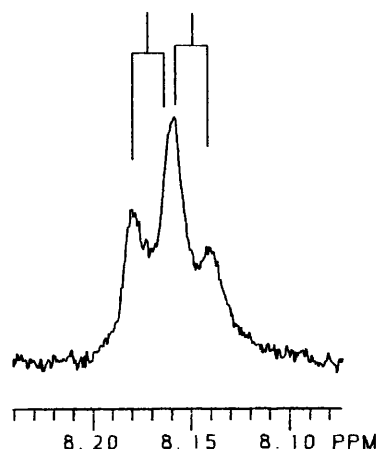


Figure 4.18. Part of the proton NMR spectrum of the nitro-amine compound (4.14) showing the signals from the aromatic proton *ortho* to the NO₂ group at -120 °C. It consists of two partially overlapping doublets.

For the methyl- (4.13) compound, we are able to conclude, based on the assumption that the more downfield signal in the methylene region always comes from the *anti*, that the *syn/anti* free energy difference is in favour of the *syn* conformation.

As for the nitro-amine- (4.14) compound, it was impossible to determine which of the two conformations is the more populated. But in light of the experimental result from other compounds with similar structures, namely the 1,3-bis(benzyl)- (3.7) and 1,3-bis(*p*-nitrobenzyl)- (3.8) 2,4,5,6-tetramethylbenzenes, where the *syn* conformations were proven using shifts reagents to be the more stable, it is reasonable to propose that the observed energy difference in the nitro-amine-compound would also be in favour of the *syn*.

(4.2.1-2) MM3 Calculations

Calculations were performed on the chloride (4.10), bromide (4.11), iodide (4.12) and the methyl-compound (4.13) but as for the nitro-amine-compound (4.14), some of the parameters needed to perform calculations are not available on the MM3 program.

In each of the compounds in the series, 4.10 -4.13, the *syn* conformation was calculated to be more stable than the *anti*, the enthalpy differences being (chloride,

0.46); (bromide, 0.45); (iodide, 0.50) and (methyl-, 0.34 kcal mol⁻¹) in favour of the *syn* form. The contributions to the final steric energy are summarised in table 4.12.

As shown in table 4.11, when the sum of the atom-atom van der Waals interactions between the X and Z groups in both conformations of 4.10 - 4.13 is being considered, the *syn* form is favoured relative to the *anti*. However, the magnitude of the *syn* advantage arising from such steric interactions is small in comparison to the calculated enthalpy difference ($\Delta H_{\text{calc.}}$), suggesting that gearing is once again involved and that a high proportion of $\Delta H_{\text{calc.}}$ may be attributed to gear effect.

Table 4.11. The sum of the X-Z van der Waals contributions (kcal mol⁻¹) for 4.10 - 4.13

Compound →	Chloride- (4.10)	Bromide- (4.11)	Iodide- (4.12)	Methyl- (4.13)
<i>Syn</i>	-0.0980	-0.1364	-0.1812	-0.0596
<i>Anti</i>	-0.0354	-0.0459	-0.0546	-0.0297
Diff.	-0.0626	-0.0905	-0.1266	-0.0299

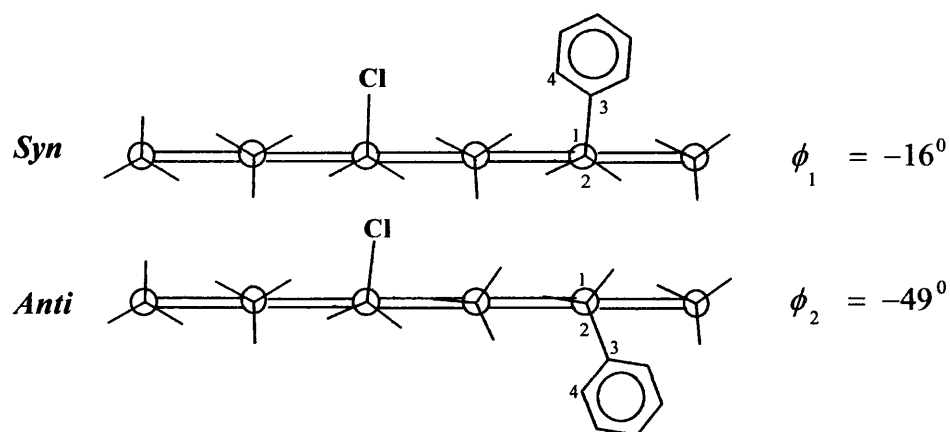
The arrangement of the groups attached to the ring is shown in figure 4.19. Unlike the *anti* form, in the *syn* conformation, these groups are nicely geared with C-Y (Y = H, X or Z) bonds arranged successively in an up and down manner round the ring. Undoubtedly, this arrangement reduces steric repulsion between adjacent groups on the ring in the *syn* conformation in comparison to the *anti*. The values of ϕ_1 and ϕ_2 which defines the conformation about the CH₂-Ph bond in the *syn* and *anti* forms respectively, are also shown in figure 4.19.

Chapter Four

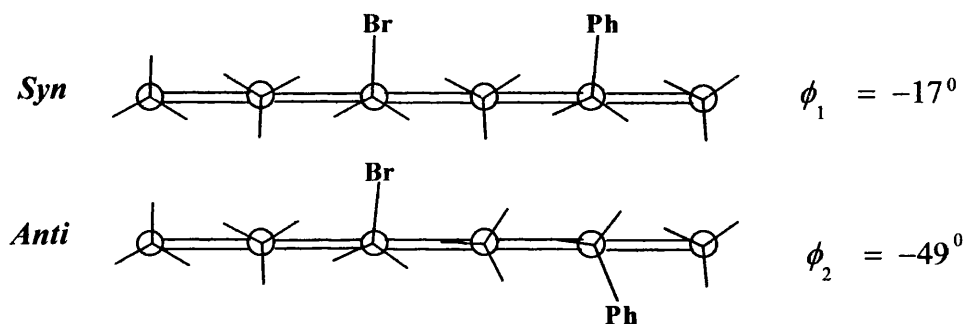
Table 4.12. A summary of the steric energy contributions (kcal mol⁻¹) for 4.10 – 4.14

Compound →	Chloride (4.10)		Bromide (4.11)		Iodide (4.12)		Methyl- (4.13)	
	<i>Syn</i>	<i>Anti</i>	<i>Syn</i>	<i>Anti</i>	<i>syn</i>	<i>anti</i>	<i>syn</i>	<i>anti</i>
Compression	2.2039	2.3379	2.2588	2.3908	2.2290	2.3631	2.4100	2.4838
Bending	3.1424	3.2843	3.1662	3.3063	3.5611	3.7142	3.1520	3.2232
Bend-bend	-0.2456	-0.2487	-0.2456	-0.2482	-0.3669	-0.3724	-0.1925	-0.1938
Stretch-bend	-0.4836	-0.5057	-0.4836	-0.5095	-0.4776	-0.5038	-0.4933	-0.5124
van der Waals								
1,4 energy	14.1204	13.9494	14.1027	13.9436	13.9605	13.7969	15.1445	15.0516
Other	3.8816	4.4299	4.0026	4.5319	3.8080	4.3585	4.3745	4.6775
Torsional	-9.8304	-10.2476	-10.0724	-10.4912	-15.4957	-15.8867	-12.4535	-12.6051
Torsion-stretch	0.0000	0.0000	0.0000	0.0000	0.0000	0.0000	-0.0004	-0.0004
Dipole-dipole	10.6997	10.9565	10.9052	11.1599	10.9777	11.2230	11.9075	12.0735
Total Steric Energy (H)	23.4882	23.9530	23.6339	24.0835	18.1961	18.6926	23.8488	24.1978
ΔH	-0.4648		-0.4496		-0.4965		-0.3490	

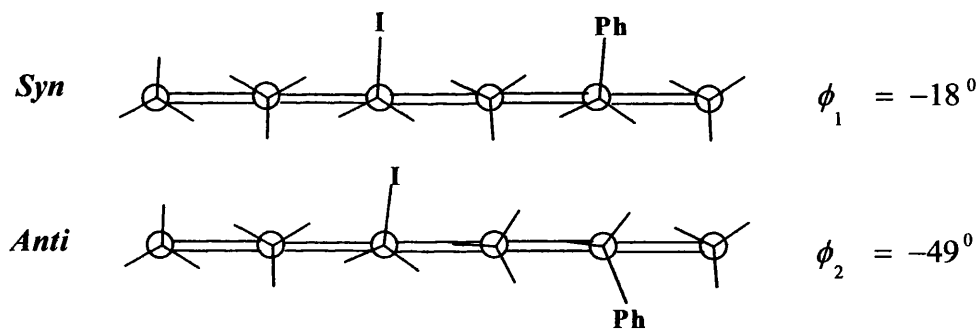
4.10



4.11



4.12



4.13

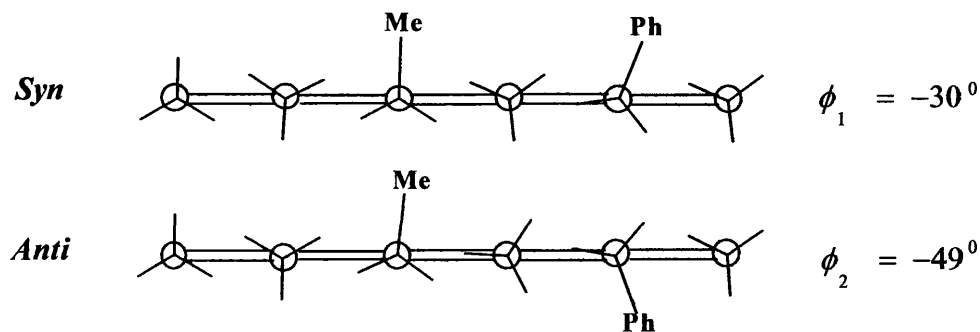


Figure 4.19. Diagram showing the arrangement of the groups attached to the ring as calculated by MM3. ϕ_1 and ϕ_2 are the torsional angles defined by C1-C2-C3-C4 in the *syn* and *anti* conformations respectively.

(4.2.2) Conclusion

Experimental results show that in each of the compounds (4.10 - 4.14) the *syn* conformation is more stable relative to the *anti*, a trend also supported by calculations, see table 4.13. However, we have to be cautious in attributing the free energy differences (ΔG_{exp}) in there entirety to attractive steric interactions between the X and Z groups because calculations also show that a high proportion of the calculated enthalpy difference comes from gearing.

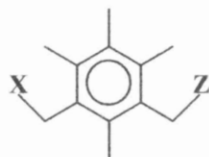
Table 4.13. A summary of the results from dynamic NMR and calculations for 4.10 – 4.14.

	X	Z	Solvent	T	K	$-\Delta G_{exp}$	$-\Delta H_{cal}$
				$^{\circ}\text{C}$	<i>syn/anti</i>	kcal mol ⁻¹	kcal mol ⁻¹
4.10	Ph	Cl	CD ₂ Cl ₂	-130	3.0	0.31	0.46
4.11	Ph	Br	CD ₂ Cl ₂	-130	3.0	0.31	0.45
4.12	Ph	I	CD ₂ Cl ₂	-130	2.1	0.21	0.50
4.13	Ph	Me	Freon	-130	1.6	0.13	0.35
4.14	<i>p</i> -C ₆ H ₄ NO ₂	<i>p</i> -C ₆ H ₄ NH ₂	Freon	-120	~1.4	~0.10	^a

^a Not available.

SECTION THREE

(4.3.1) Results and Discussion of 4.10 – 4.12



	X	Z
4.15	Me	Cl
4.16	Me	Br
4.17	Me	I

(4.3.1-1) Conformational assignment of NMR signals at low temperatures

NMR spectra of 4.15 – 4.17

The proton and ^{13}C NMR spectra of the chloride (**4.15**), bromide (**4.16**) and iodide (**4.17**) are similar. On cooling a sample of the iodide and the bromide (**4.15 – 4.17**) in $\text{CHCl}_2\text{F}:\text{CHClF}_2:\text{CD}_2\text{Cl}_2$ (~2:2:1), when rotation about the $\text{C}_{\text{Ar}}\text{-CH}_2\text{Z}$ bond, but not the $\text{C}_{\text{Ar}}\text{-CH}_2\text{Me}$ bond, became slow on the NMR time, the CH_2Z signals broadened before splitting into a pseudo-triplet. But when the sample is cooled further, the CH_2Z and CH_2Me de-coalesce at about $-100\text{ }^\circ\text{C}$ and in the subsequent spectra taken at $-110\text{ }^\circ\text{C}$ and at temperatures below this, the signals had sharpened. The proton and ^{13}C NMR chemical shifts when rotation about both the $\text{CH}_2\text{-Me}$ and $\text{CH}_2\text{-Z}$ bonds becomes slow on the NMR time scale are summarised in tables **4.14** and **4.15** respectively.

Table 4.14. The proton NMR chemical shifts^a of the chloride (**4.15**), bromide (**4.16**) and iodide (**4.17**). The major signals which happens to come from the *syn* are shown in red.

	Chemical shifts /ppm				
	CH_2CH_3^b	ArCH_3	ArCH_3	ArCH_3	ArCH_3
Cl	1.06	2.20	2.25	2.32	2.36
	1.10	2.22	2.27		2.38
Br	1.04	2.18	2.24	2.31	2.35
	1.09	2.20	2.26		2.37
I	1.05	2.19	2.22 – 2.27 multiplets		2.29
	1.09	2.21			2.32

^a The chemical shifts of the signals in the methylene regions are not shown.

^b Obtained after simplifying the spectrum by decoupling at the CH_2CH_3 signal.

Table 4.15. The Chemical shifts of the aromatic carbons in the chloride (4.15), bromide (4.16) and iodide (4.17). The major signals which happens to come from the *syn* are shown in red.

Compound ↓	Chemical shifts /ppm					
Cl	131.60	132.84	133.97	134.35	136.72	139.10
-120 °C	131.79	132.91	134.30	134.54		139.55
Br	131.41	132.64	133.82	134.42	136.60	138.97
-130 °C	131.71	132.75		134.46	136.76	139.42
I	132.08	132.36	133.23	134.45	136.05	139.10
-130 °C	132.23	132.83	133.30		136.22	139.46

The CH_2CH_3 region of the proton NMR spectrum of the bromide (4.16) at -130°C on decoupling at the CH_2CH_3 signal together with the CH_2Br region are shown in figures 4.20b and 4.20a respectively. The CH_2Br region consists of two sets of AB systems centred at 4.65 ppm and 4.71 ppm whilst the CH_2CH_3 region contains two singlets of intensity ratio 2.5:1 (after decoupling at the CH_2CH_3) equating to an energy difference of $0.26 \text{ kcal mol}^{-1}$. The conformational population ratio is also substantiated by ^{13}C NMR spectroscopy, the aromatic region of the spectrum is shown in figure 4.21.

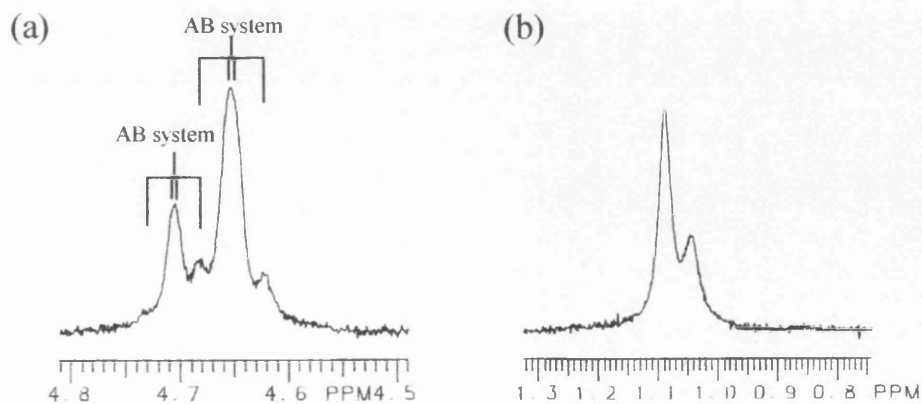


Figure 4.20.

(a) The CH_2Br region of the proton NMR spectrum of the bromide (4.16) at -130°C .

(b) The CH_2CH_3 region of the proton NMR spectrum at -130°C , on decoupling at the CH_2CH_3 signal.

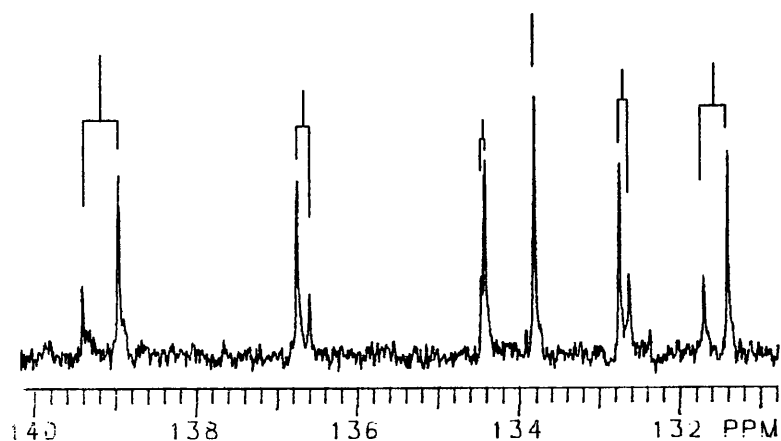


Figure 4.21. The aromatic region of the decoupled ^{13}C NMR spectrum of the bromide (4.16) at -130°C .

The CH_2Cl and CH_2CH_3 regions of the proton NMR spectrum of the chloride (4.15) at -130°C are shown in figure 4.22a and 4.22b respectively. In the CH_2Cl region, each of the CH_2Cl group from the *syn* and *anti* conformations are resolved more or less as singlets. And from the two singlets in the CH_2CH_3 region (on decoupling) a conformational population ratio of 2.8:1 corresponding to an energy difference of $0.31\text{ kcal mol}^{-1}$ is obtained.

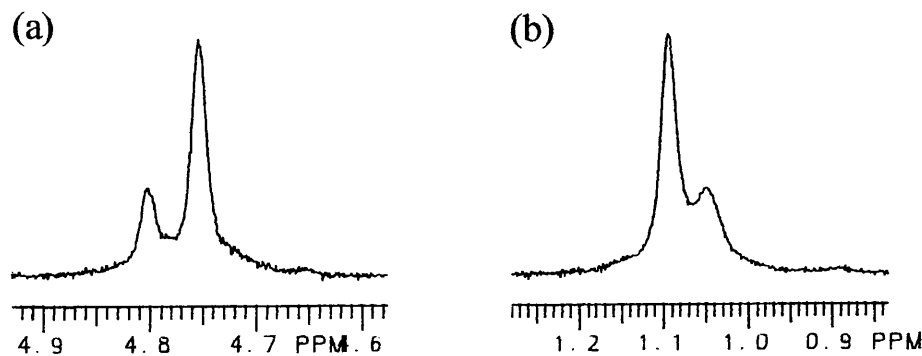


Figure 4.22.

(a) The CH_2Cl region of the proton NMR spectrum of the chloride (4.15).

(b) The CH_2CH_3 region of the proton NMR spectrum at -130°C , on decoupling at the CH_2CH_3 signal.

In the iodide (4.17), the CH_2I region of the proton NMR at -130°C consists of an AB system centred at 4.46 and 4.50 ppm together with a pseudo triplet centred at 4.55 ppm. From the two singlets observed in the CH_2CH_3 region, on decoupling at the CH_2CH_3 signal, a conformational ratio of 2.3:1 which equates to an energy difference of $0.24\text{ kcal mol}^{-1}$ is obtained.

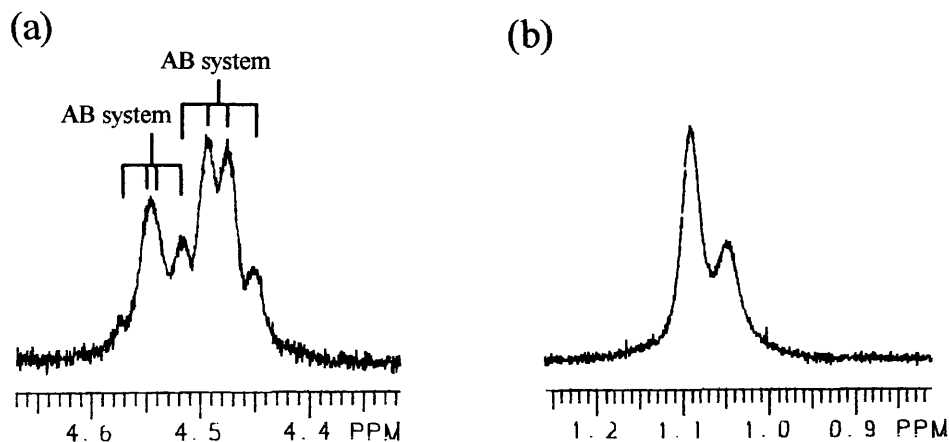


Figure 4.23.

(a) The CH_2I region of the proton NMR spectrum of the iodide at -130°C (4.17).

(b) The CH_2CH_3 region of the proton NMR spectrum at -130°C , on decoupling at the CH_2CH_3 signal.

(4.3.1-2) MM3 Calculation

Calculations were performed on the halides and the results are summarised in table

4.16. In each of the three compounds, the *syn* conformation was found to be

Table 4.16. Contributions to the final steric energies (kcal mol^{-1}) of 4.15 – 4.17

Compound →	Chloride (4.15)		Bromide (4.16)		Iodide (4.17)	
	<i>Syn</i>	<i>Anti</i>	<i>syn</i>	<i>anti</i>	<i>syn</i>	<i>anti</i>
Compression	1.9807	2.0918	2.0340	2.1332	2.0032	2.1101
Bending	2.6926	2.9523	2.7129	2.9780	3.1086	3.3877
Bend-bend	-0.2573	-0.2516	-0.2569	-0.2506	-0.3776	-0.3737
Stretch-bend	-0.3878	-0.3997	-0.3877	-0.4014	-0.3816	-0.3975
van der Waals						
1,4 energy	10.1337	10.0917	10.1158	10.0947	9.9789	9.9226
Other	5.4480	6.1050	5.5940	6.0775	5.4204	5.9448
Torsional	-7.7199	-7.7750	-7.9379	-7.9841	-13.3664	-13.3425
Torsion-stretch	-0.0004	-0.0004	-0.0004	-0.0004	-0.0004	-0.0004
Dipole-dipole	6.6781	6.6837	6.8866	6.8900	6.9512	6.9496
Steric Energy (<i>H</i>)	18.5678	19.4978	18.7604	19.5370	13.3364	14.2007
ΔH	-0.9300		-0.7766		-0.8643	

significantly more stable than the *anti*, the energy differences being Cl, 0.93; Br, 0.78 and I, 0.86 kcal mol⁻¹.

Considering the sum of the atom-atom van der Waals interaction between the halogen atom and the methyl (CH₂CH₃) group, in each of the two conformations, the magnitude of such energies is small in all the halides. Likewise, the benefit of having the halogen atom and the methyl group on the same side rather than on opposite sides of the ring plane is small in magnitude, see table 4.17. In the light of the weak X-Z attractive steric interactions, it is reasonable to suggest that a substantial amount of the calculated enthalpy difference is as a result of a higher degree of self-organisation (i.e. gear effect) amongst the groups attached to the ring in the *syn* form in comparison to the *anti*.

Table 4.17. The sum of the X-Z van der Waals contributions (kcal mol⁻¹) for 4.15 – 4.16

Compound →	Chloride- (4.15)	Bromide- (4.16)	Iodide- (4.17)
<i>Syn</i>	-0.0318	-0.0447	-0.0554
<i>Anti</i>	-0.0160	-0.0214	-0.0268
Diff.	-0.0158	-0.0233	-0.0286

The arrangement of the methyl and halomethyl groups on the benzene ring is shown in figure 4.24. Once again, unlike the *anti*, in the *syn* conformation the methyl, halomethyl and ethyl groups on the ring are arranged in such a way that there is a successive up and down arrangement of C-Y (Y = H, X, or Z) bonds and in addition these bonds are more or less orthogonal to the ring plane.

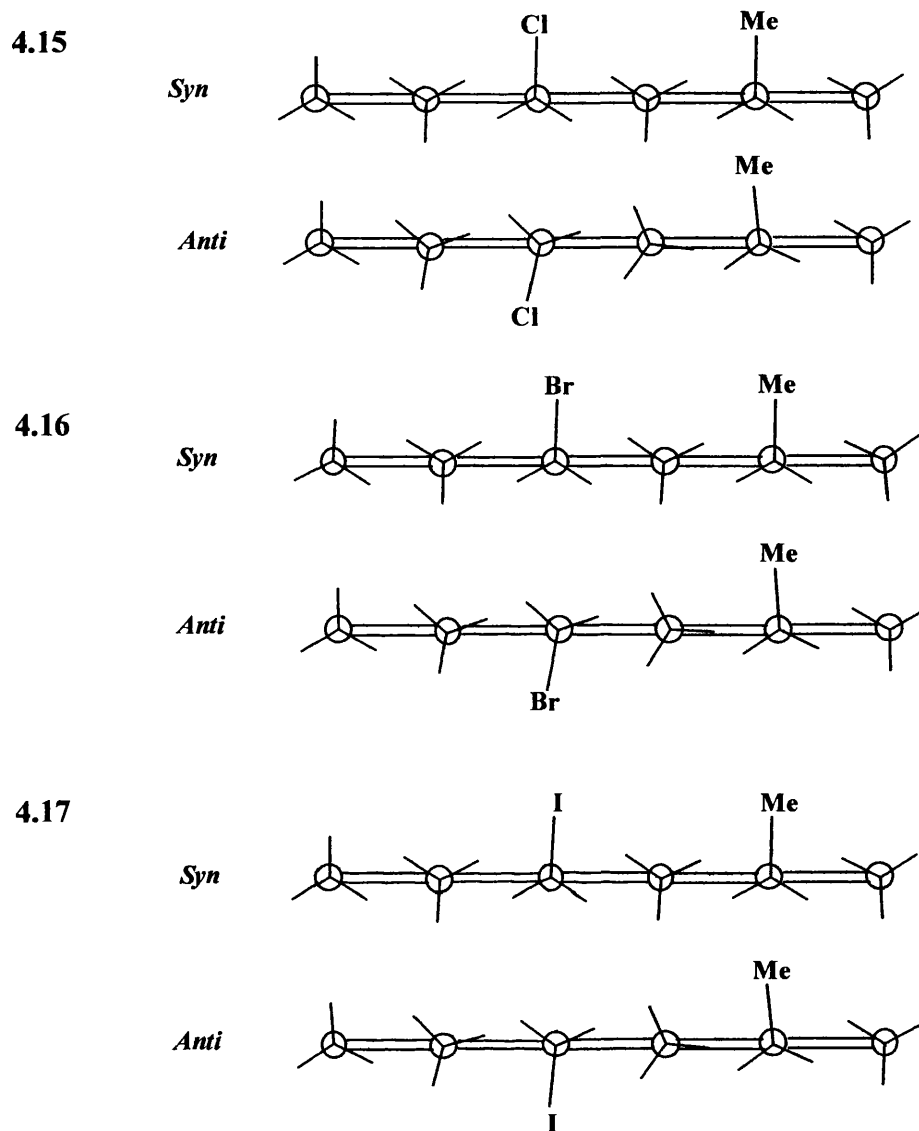


Figure 4.24. The arrangement of the groups attached to the benzene ring as calculated by MM3 program.

(4.3-2) Conclusion

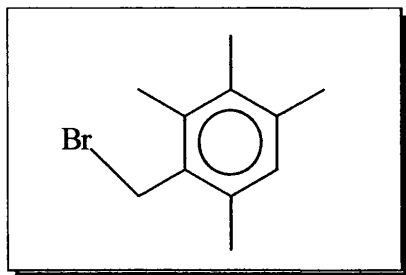
The results from dynamic NMR are summarised in table 4.18. For each of the halides experiments are concluded to show that the *syn* conformation is more stable than the *anti*, this trend is also in agreement with calculations. But once again a substantial amount of the calculated enthalpy difference comes from gearing rather than X-Z attractive steric interactions suggesting that it will be wrong to attribute the free energy differences from experiments entirely to attractive steric interactions between the X and Z groups.

Table 4.18. A summary of the results from dynamic NMR and calculations for 4.15 – 4.17. (In all cases the energy difference is in favour of the *syn*)

	X	Z	Solvent	T	K	$-\Delta G_{exp}$	$-\Delta H_{cal}$
				$^{\circ}\text{C}$	<i>syn/anti</i>	kcal mol ⁻¹	kcal mol ⁻¹
4.15	Me	Cl	Freon	-130	2.8	0.31	0.93
4.16	Me	Br	Freon	-130	2.5	0.26	0.78
4.17	Me	I	Freon	-130	2.3	0.24	0.86

SECTION FOUR**(4.4) Synthesis**

It is worth pointing out that during the synthesis, much effort was put into obtaining the compounds in its purest form rather than maximising the yields.

**1-(Bromomethyl)-2,4,5,6-tetramethylbenzene³⁷ (4.1a).**

The method described for the bromomethylation of isodurene will serve as a general procedure for the bromomethylation of other hydrocarbons. The synthesis of the starting material, isodurene (**3.1b**) is described in chapter three.

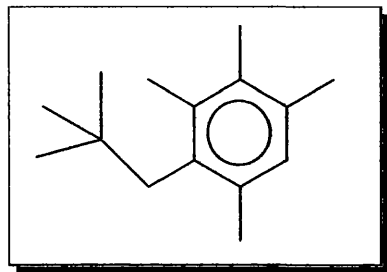
The entire reaction was carried out under argon. To a solution of isodurene (9.6 g, 71.5 mmol) in glacial acetic acid (30 ml) at 50 °C was added paraformaldehyde (2.15 g, 71.5 mmol) and then a solution of hydrogen bromide (13 ml, 5.7 M sol in glacial acetic acid, 74.1 mmol) the mixture was stirred at the same temperature for 5 h.

The mixture was allowed to cool down to room temperature before pouring into water (150 ml). The resultant white emulsion was extracted with dichloromethane (3 x 20 ml) and the extract was washed with water (3 x 30 ml) and then a saturated solution of sodium hydrogencarbonate (2 x 30 ml). The extract was dried over anhydrous magnesium sulfate and the solvent was removed using a rotary evaporator leaving a light yellow oily liquid. The crude product was dried under a vacuum pump at 0.5 mmHg pressure for 20 h.

The crude product (14.1 g) was used in other reactions without any further purification. Trying to purify by chromatography led to loss of material presumably because bromomethyl compounds sticks irreversibly to silica gel.

NMR spectroscopy

300 MHz ^1H NMR (CDCl_3) δ /ppm 2.15, 2.23, 2.31, 2.34 (each s, 3H, CH_3); 4.59 (s, 2H, CH_2Br); 6.84 (s, 1 H, arom.);



1-Neopentyl-2,4,5,6-tetramethylbenzene⁴¹(4.1b)

The reaction was carried out under an inert atmosphere of argon.

A 0.2 M solution of the catalyst, Li_2CuCl_4 , was prepared by adding THF (50 ml) to a stirred mixture of lithium chloride (0.85g, 0.02 mol) and copper (II) chloride (1.35 g, 0.01 mol). The mixture was stirred for 5 min.

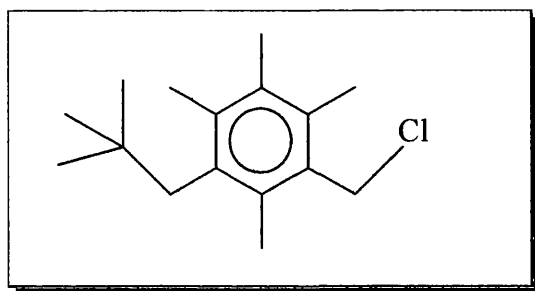
The Grignard was prepared by adding 10 ml of a solution of 2-chloro-2-methylpropane (38.2 ml, 347 mmol) in THF (30 ml), dropwise, *via* a dropping funnel to a stirred mixture of magnesium turnings (8.3 g, 342 mmol) and THF (180 ml). A crystal of iodine was added to initiate the reaction and after an induction period of 25 min the reaction began, causing the mixture to warm up. The remainder of the chloride solution was then added at such a rate that the mixture boiled gently. The mixture was refluxed for 3 h, cooled and then allowed to settle. The Grignard was cannulated into a clean round bottom flask equipped with a mechanical stirrer.

A mixture of the bromide (4.1a) (22.5 g, 99.1 mmol) dissolved in THF (50 ml) and (10 ml) of the catalyst was added dropwise to the Grignard, *via* a dropping funnel whilst stirring. The mixture was stirred at room temperature for 20 h.

The reaction was quenched by adding 3 M hydrochloric acid (100 ml) dropwise. The organic phase was separated from the inorganic phase and the later was extracted with ether (3 x 30 ml). The combined organic phase was dried over anhydrous magnesium sulfate and the solvent was removed using a rotary evaporator leaving a semi-solid white crude product. The crude product was purified by flash column chromatography using petroleum spirit (30-40 $^{\circ}\text{C}$) as the eluting solvent. After several runs, the product (4.74 g) was obtained as a colourless liquid.

NMR spectroscopy

300 MHz ^1H NMR (CDCl_3) δ /ppm 0.92 {s, 9H, $\text{C}(\text{CH}_3)_3$ }; 2.14, 2.21, 2.23, 2.28 (each s, 3H, ArCH_3); 2.69 (s, 2H, CH_2CMe_3); 6.84 (s, 1 H, arom.);

**1-(Chloromethyl)-3-neopentyl-2,4,5,6-tetramethylbenzene⁴²(4.1)**

The reaction was carried out under an inert atmosphere of argon. To a mixture of the bromide (4.2) (0.3 g, 1.01 mmol) and excess lithium chloride (43 mg, 3.03 mmol) was added acetone (15 ml). The mixture was refluxed for 24 h and the solvent was removed on a rotary evaporator.

A 1 M hydrochloric acid solution 20 ml together with dichloromethane (10 ml) were added to the residue. The organic phase was separated from the aqueous phase and the later was extracted with dicholoromethane (3 x 5 ml). The combined organic phases was washed with 0.5 M hydrochloric acid solution (3 x 7 ml) to remove inorganic salts and then dried over anhydrous magnesium sulphate. The solvent was removed using a rotary evaporator leaving a colourless liquid.

Analysis of the proton NMR spectrum of the liquid revealed that only about 50 % of the bromine has been converted hence further reaction was carried out on the product, following the procedure described above. After subjecting the product to three more cycles of reactions, the product was obtained as a colourless liquid (150 mg).

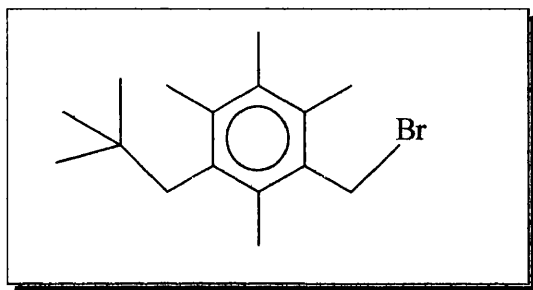
NMR spectroscopy

400 MHz ^1H NMR (CD_2Cl_2) δ /ppm 0.90 {s, 9H, $\text{C}(\text{CH}_3)_3$ }; 2.21, 2.26, 2.35, 2.39 (each s, 3H, ArCH_3); 2.81 (s, 2H, CH_2CMe_3); 4.77 (s, 2H, CH_2Cl).

100.6 MHz ^{13}C NMR (CD_2Cl_2) δ/ppm 16.11, 17.11, 17.79, 19.55 (ArCH_3); 30.29 ($\text{C}(\text{CH}_3)_3$); 34.80 (CMe_3); 41.18 (CH_2CMe_3); 44.04 (CH_2Cl); 131.97, 133.63, 133.83, 134.72, 135.23, 137.73 (arom. C).

Elemental analysis

Found: C, 75.37; H, 9.93; Cl, 14.09 %. $\text{C}_{16}\text{H}_{25}\text{Cl}$ requires C, 76.01; H, 9.97; Cl, 14.02 %.



1-(Bromomethyl)-3-neopentyl-2,4,5,6-tetramethylbenzene (4.2)

The method described for the synthesis of **4.1a** was followed but using neopentyl-tetramethylbenzene (**4.1b**) (1.42 g, 6.96 mmol), paraformaldehyde (0.21 g, 7.0 mmol) and a solution of hydrogen bromide (1.3 ml, 5.7 M sol. in glacial acetic acid, 7.41 mmol).

The product (1.4 g) was obtained as a white solid m.p. 65-67 $^{\circ}\text{C}$.

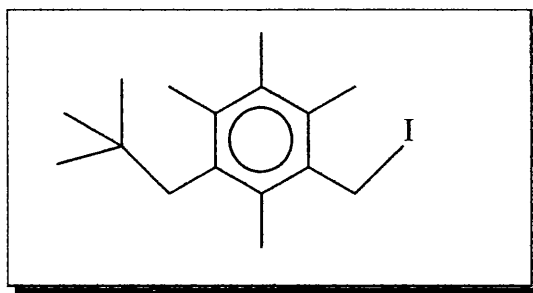
NMR spectroscopy

400 MHz ^1H NMR (CDCl_3) δ/ppm 0.90 {s, 9H, $\text{C}(\text{CH}_3)_3$ }; 2.20, 2.26, 2.33, 2.38 (each s, 3H, ArCH_3); 2.80 (s, 2H, CH_2CMe_3); 4.69 (s, 2H, CH_2Br).

100.6 MHz ^{13}C NMR (CD_2Cl_2) δ/ppm 16.06, 17.10, 17.76, 19.56 (ArCH_3); 30.23 ($\text{C}(\text{CH}_3)_3$); 33.45 (CH_2Br); 34.78 (CMe_3); 41.18 (CH_2CMe_3); 131.85, 133.67, 133.87, 134.80, 135.27, 137.90 (arom. C).

Elemental analysis.

Found: C, 65.31; H, 8.54; Br, 26.82 %. $\text{C}_{16}\text{H}_{25}\text{Br}$ requires C, 64.65; H, 8.48; Br, 26.88 %.



1-(Iodomethyl)-3-neopentyl-2,4,5,6-tetramethylbenzene³⁸(4.3)

Under an inert atmosphere of argon, acetone (15 ml) was added to a mixture of the bromide (4.2) (0.2 g, 0.67 mmol) and excess sodium iodide (0.50 g, 3.33 mmol). The mixture was stirred at 22 °C for 3 h and the solvent was removed using a rotary evaporator. A 0.1 M hydrochloric acid solution (20 ml) was added to the residue and the product was extracted with dichloromethane (3 x 10 ml). The dichloromethane extract was washed firstly with 0.5 M hydrochloric acid (3 x 10 ml) so as to remove the inorganic salts and then saturated sodium sulfite solution (10 ml) in order to remove iodine. The solvent was removed using a rotary evaporator and the solid residue was recrystallised from chloroform to give an off white solid (113 mg) m.p. 58 – 61 °C.

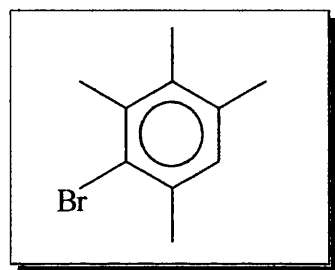
NMR spectroscopy

400 MHz ¹H NMR (CDCl₃) δ/ppm 0.89 {s, 9H, C(CH₃)₃}; 2.20, 2.24, 2.26, 2.31 (each s, 3H, ArCH₃); 2.80 (s, 2H, CH₂CMe₃); 4.57 (s, dynamic broadened, 2H, CH₂I).

100.6 MHz ¹³C NMR (CD₂Cl₂) δ/ppm 8.00 (CH₂I); 16.04, 17.00, 17.69, 19.50 (ArCH₃); 30.19 {C(CH₃)₃}; 34.58 (CMe₃); 40.89 (CH₂CMe₃); 132.10, 132.76, 133.53, 134.91, 135.05, 137.00 (arom. C).

Elemental analysis

Found: C, 56.17; H, 7.36; I, 37.57 %. C₁₆H₂₅I requires C, 65.82; H, 7.31; I, 36.86 %.



1-Bromo-2,3,4,6-tetramethylbenzene⁴⁵(4.4a)

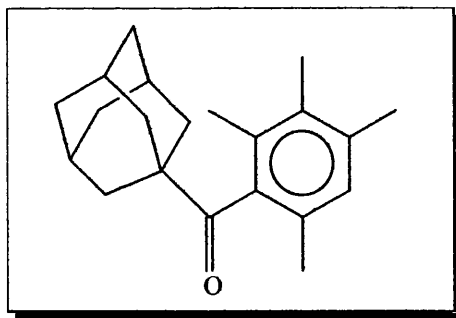
The reaction was carried out under an inert atmosphere of argon. A 1.82 M stock solution of bromine was prepared as follows: - 7.28 g of bromine was weighed out accurately into a volumetric flask. The flask was filled up to the 50 ml mark with glacial acetic acid.

Zinc chloride (1.04 g, 7.63 mmol) dissolved in glacial acetic acid was added to a stirred solution of isodurene (**3.1b**) (1 g, 7.45 mmol) in glacial acetic acid (7 ml). To the stirred mixture was added, dropwise, the solution of bromine (4.19 ml, 1.82 M sol. in acetic acid, 7.63 mmol).

The reaction mixture was poured into water (30 ml) and then extracted with dichloromethane (3 x 15 ml). The combined organic phase was washed firstly with a saturated solution of sodium sulfite (15 ml) so as to remove unreacted bromine and then water (3 x 15 ml). The extract was dried over anhydrous magnesium sulfate and the solvent was removed on a rotary evaporator leaving the product, a colourless liquid (1.35 g).

NMR spectroscopy

300 MHz ^1H NMR (CDCl_3) δ /ppm 2.20 (s, 6H, 2ArCH₃); 2.34, 2.40 (each s, 3H, 2ArCH₃); 6.89 (s, 1H, arom.).



1-(1-Adamantanecarbonyl)-2,3,4,6-tetramethylbenzene⁴⁶ (4.4b)

The reaction was prepared under an inert atmosphere of argon. To prepare the Grignard reagent, 1-bromo-2,3,4,6-tetramethylbenzene (4.4a) dissolved in THF (15 ml) was added to a mixture of magnesium turnings in THF (7 ml). A crystal of iodine was added so as to initiate the reaction and the mixture was refluxed for 3 h during which all the magnesium had reacted.

The Grignard prepared above was added dropwise to a solution of 1-adamantanecarbonyl chloride dissolved in THF (20 ml) at -78°C over a period of 25

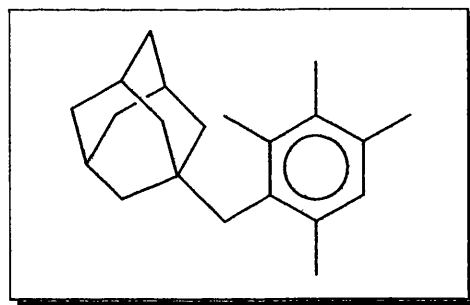
min. the resultant mixture was stirred at the same temperature for 2 h and then allowed to rise to room temperature. The mixture was stirred at room temperature for 15 h.

The reaction was quenched by adding water (20 ml). The mixture was extracted with ether (3 x 15 ml) and the combined extract was dried over anhydrous magnesium sulfate. The solvent was removed on a rotary evaporator. The crude product was purified by flash column chromatography and the product (1.56 g) was obtained as a white solid.

NMR spectroscopy

400 MHz ^1H NMR (CDCl_3) δ /ppm 1.62-1.73, 1.85-1.91 (m, 6H, 3CH_2 from Ad); 1.97-2.01 (m, 3H, 3CH from Ad); 2.08, 2.11, 2.12, 2.23 (each s, 3H, ArCH_3); 6.82 (s, 1H, arom.).

100.6 MHz ^{13}C NMR (CDCl_3) δ /ppm 15.07, 18.90, 20.28, 20.47 (ArCH_3); 28.15 (3CH , from Ad); 36.45, 39.09 (3CH_2 from Ad); 47.27 (CCOAr from Ad); 129.03 (arom. C); 129.47, (arom. C-H); 130.53, 132.67, 135.83, 139.77 (arom. C.); 218.76 ($\text{C}=\text{O}$).



1-(1-Adamantanemethyl)-2,3,4,6-tetramethylbenzene⁴⁷(4.4c)

To a stirred mixture of THF (10 ml) and ammonia (~20 ml) together with a catalytic amount of aluminium powder (~1 mg), was added lithium (120 mg, 17.3 mmol). A solution of the ketone (1.0 g, 3.37 mmol) in THF (10 ml) was then added dropwise to the blue resultant mixture. After allowing the mixture to reflux for 3 h, the reaction was quenched by adding solid ammonium chloride. The ammonia was allowed to boil off by leaving at ambient temperature for 14 h.

Water (20 ml) and ether (10 ml) were added and the organic phase was separated from the inorganic phase. The organic phase was then extracted with ether (3 x 10 ml) and the combined organic phase was dried over anhydrous magnesium sulfate. The

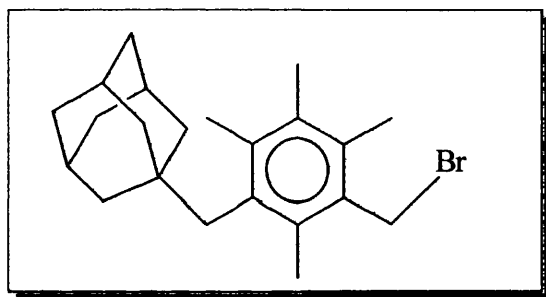
solvent was removed on a rotary evaporator and the crude product was purified by flash column chromatography.

The product (150 mg) was obtained as a colourless liquid.

NMR spectroscopy

400 MHz ^1H NMR (CDCl_3) δ /ppm 1.62-1.73, 1.85-1.91 (m, 6H, 3CH_2 from Ad); 1.97-2.01 (m, 3H, 3CH from Ad); 2.08, 2.11, 2.12, 2.23 (each s, 3H, ArCH_3); 2.55 (br, m, CH_2Ad); 6.82 (s, 1H, arom.).

100.6 MHz ^{13}C NMR (CDCl_3) δ /ppm 16.24, 18.88, 20.54, 22.05 (ArCH_3); 28.90 (3CH , from Ad); 36.74 (quaternary C); 36.96 (3CH_2 from Ad); 42.83 (CH_2Ad); 42.99 (3CH_2 from Ad); 129.51 (arom. C-H); 132.75, 133.13, 133.30, 134.82, 136.46 (arom. C).



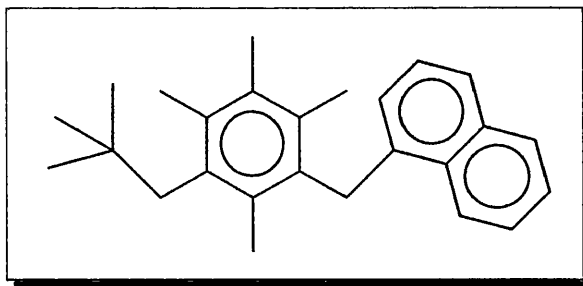
1-(1-Adamantanemethyl)-3-(bromomethyl)-2,4,5,6-tetramethylbenzene (4.4)

The method described for the synthesis of **4.1a** was followed but using **4.4c** (150 mg), hydrogen bromide solution (c.a. 0.2 ml, 5.7 M sol. in glacial acetic acid) and paraformaldehyde (17 mg, 5.67 mmol). The product was obtained as a viscous colourless liquid.

NMR spectroscopy

300 MHz ^1H NMR (CD_2Cl_2) δ /ppm 1.52-1.69, (m, 12H, 6CH_2 from Ad); 1.90(s, br, 3H, 3CH from Ad); 2.21, 2.27, 2.34, 2.39 (each s, 3H, ArCH_3); 2.69 (s, 2H, CH_2Ad); 4.68 (AB, $J = 10.4$ Hz, 1H, CH_2Br); 4.71 68 (AB, $J = 10.4$ Hz, 1H, CH_2Br).

100.6 MHz ^{13}C NMR (CDCl_3) δ /ppm 15.97, 17.02, 17.82, 19.66 (ArCH_3); 28.93 (3CH , from Ad); 32.79 (CH_2Br) 36.69 (quaternary C); 36.98 (3CH_2 from Ad); 42.81 (CH_2Ad); 42.89 (3CH_2 from Ad); 131.39, 133.27, 133.33, 133.81, 134.68, 137.64 (C, arom.).



1-(α -Naphthyl)-3-neopentyl-2,4,5,6-tetramethylbenzene⁴⁴(4.5).

The synthesis of a 0.2 M solution of LiCuCl_4 in THF which acts as a catalyst in the reaction presented below, has been described in the method used to synthesis **4.1b**.

The reaction was carried out under an inert atmosphere of argon. To prepare the Grignard, 1-bromonaphthalene (1.05 g, 5.07 mmol) was added to a stirred mixture of magnesium turnings (0.12 g, 4.94 mmol) in THF (30 ml). A crystal of iodine was added to initiate the reaction. The mixture was then refluxed for 2 h during which time all the magnesium had dissolved.

A mixture of 0.2 M LiCuCl_4 in THF (1 ml) and 1-(iodomethyl)-3-neopentyl-2,4,5,6-tetramethylbenzene (**4.3**) (1.50 g, 4.36 mmol) in THF (9 ml) was added dropwise at 0 °C. The mixture was stirred at the same temperature for 2 h and then at 22 °C for 10 h. The reaction was quenched by adding an aqueous solution of 2 M hydrochloric acid (20 ml). The organic layer was separated and the aqueous phase was extracted with ether (3 x 10 ml). The organic phase was combined and the solvent was removed. The crude product was purified by flash column chromatography using petroleum spirit (b.p. 30-40 °C):dichloromethane (9:1) as the mobile phase. The product (243 mg) was obtained as a white solid m.p. 125-127 °C.

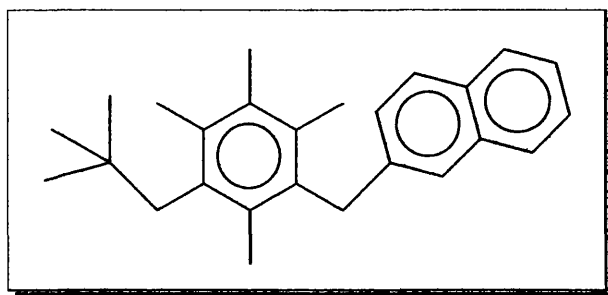
NMR spectroscopy

400 MHz ^1H NMR (CDCl_3) δ /ppm 0.92 {s, 9H, $\text{C}(\text{CH}_3)_3$ }; 2.09, 2.14, 2.24, 2.31 (each s, 3H, ArCH_3); 2.83 (s, 2H, CH_2CMe_3); 4.46 (s, 2H, CH_2 -Naphthyl); 6.67-7.01 (m, 1H, arom. H); 7.19-7.94 (m, 5H, arom. H); 8.22-8.27 (m, 1H, arom. H).

100.6 MHz ^{13}C NMR CDCl_3 δ /ppm 17.18, 17.62, 19.07, 19.89 (ArCH_3); 31.00 ($\text{C}(\text{CH}_3)_3$); 34.34 (CH_2 -Naphthyl); 35.69 (CMe_3); 42.16 (CH_2CMe_3); 124.36, 125.09, 126.70, 126.90, 127.06, 127.55, 129.92 (arom. C-H); 133.64, 134.35, 134.59, 134.97, 135.10, 135.71, 135.95, 135.98, 137.30 (arom. C).

Elemental analysis

Found: C, 89.44; H, 9.32 %. $C_{26}H_{32}$ requires C, 90.62; H, 9.38 %.

1-(β-Naphthyl)-3-neopentyl-2,4,5,6-tetramethylbenzene (4.6).

The method described for the synthesis of 4.4 was followed but using 2-bromonaphthalene (1.05 g, 5.07 mmol) magnesium (0.12 g, 4.94 mmol) and 1-(iodomethyl)-3-neopentyl-2,4,5,6-tetramethylbenzene (4.3) (1.6 g, 4.65 mmol).

The product (324 mg) was obtained as a highly viscous colourless liquid.

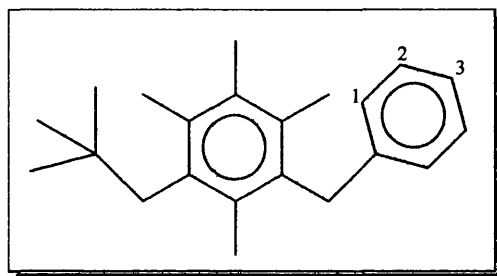
NMR spectroscopy

300 MHz 1H NMR ($CDCl_3$) δ /ppm 0.92 {s, 9H, $C(CH_3)_3$ }; 2.16, 2.21, 2.23, 2.30 (each s, 3H, $ArCH_3$); 2.83 (s, 2H, CH_2CMe_3); 2.84 (s, 2H, CH_2 -Naphthyl); 7.27-7.43 (m, 4H, arom. H); 7.63-7.80 (m, 3H, arom. H).

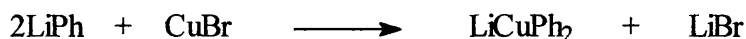
100.6 MHz ^{13}C NMR { $CHCl_2F:CHClF_2:CD_2Cl_2$ (~2:2:1)} δ /ppm 17.40, 17.68, 19.34, 19.93 ($ArCH_3$); 31.04 { $C(CH_3)_3$ }; 35.69 (CMe_3); 37.59 (CH_2 -Naphthyl); 42.16 (CH_2CMe_3); 126.20, 126.69, 126.93, 128.40, 128.63, 128.67, 128.93 (arom. C-H); 133.38, 134.33, 134.36, 135.09, 135.26, 135.48, 135.94, 135.96, 139.67 (arom. C).

Elemental analysis

Found: C, 90.45; H, 9.55 %. $C_{26}H_{32}$ requires C, 90.62; H, 9.38 %.

1-(Phenylmethyl)-3-neopentyl-2,4,5,6-tetramethylbenzene³⁹ (4.7)

The reaction was carried out under an inert atmosphere of argon. Lithium diphenylcuprate was prepared by adding a solution of phenyllithium (2.8 ml, 1.8 M sol. in cyclohexane:ether/7:3, 5.04 mmol) to a stirred mixture of ether (15 ml) and copper (i) bromide (0.36 g, 2.5 mmol) at 0 °C, see equation below. The mixture was stirred at the same temperature for 50 min.



A solution of 1-(bromomethyl)-3-neopentyl-2,4,5,6-tetramethylbenzene (**4.2**) (0.61 g, 2.1 mmol) in ether (20 ml) was added to the lithium diphenylcuprate prepared above. The mixture was stirred at 0 °C for 4h and then at 22 °C for 14 h. the reaction was quenched by adding 3 M hydrochloric acid (30 ml). The organic phase was separated from the aqueous phase and the latter was extracted with ether (3 x 15 ml). The combined organic phase was washed with water (2 x 15 ml) and then dried over anhydrous magnesium sulfate. The solvent was removed using a rotary evaporator and the resultant crude product was purified by flash column chromatography using petroleum spirit (30-40 °C): dichloromethane (9:1) as the eluting solvent. The product (120 mg) was obtained as a white solid m.p. 88-90 °C.

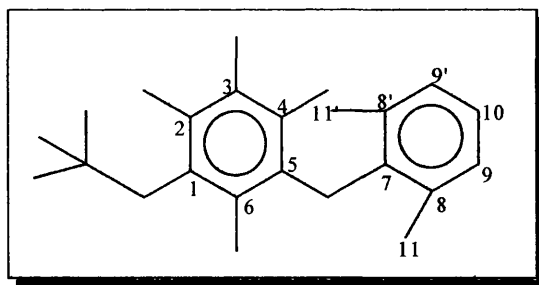
NMR spectroscopy

400 MHz ¹H NMR (CDCl₃) δ/ppm 0.90 {s, 9H, C(CH₃)₃}; 2.14, 2.18, 2.21, 2.27 (each s, 3H, ArCH₃); 2.80 (s, 2H, CH₂CMe₃); 4.10 (s, 2H, CH₂Ph); 6.97-7.01 (m, 2H, arom. H¹); 7.09-7.15 (m, 2H, arom. H³); 7.18-7.23 (m, 2H, arom. H²).

100.6 MHz ¹³C NMR {CHCl₂F:CHClF₂:CD₂Cl₂ (~2:2:1)} δ/ppm 17.37, 17.66, 19.36, 19.92 (ArCH₃); 31.04 {C(CH₃)₃}; 35.69 (CMe₃); 37.37 (CH₂Ph); 42.18 (CH₂CMe₃); 126.73 (arom. C³-H); 129.11, 129.51 (2C, arom. C-H); 134.28, 134.33, 135.41, 135.51, 135.89, 135.95, 142.13 (arom. C).

Elemental analysis

Found: C, 89.96; H, 10.31 %. C₂₂H₃₀ requires C, 89.73; H, 10.27 %.



1-Neopentyl-3-(2-xylyl)-2,4,5,6-tetramethylbenzene (4.8)

The method described for the synthesis of **4.6** was followed but using 2-bromoxylene (0.94 g, 5.08 mmol), magnesium (0.12 g, 4.94 mmol) and 1-(iodomethyl)-3-neopentyl-2,4,5,6-tetramethylbenzene (**4.3**) (1.65 g, 4.80 mmol). The product (142 mg) was obtained as a white solid m.p. 73-75 °C.

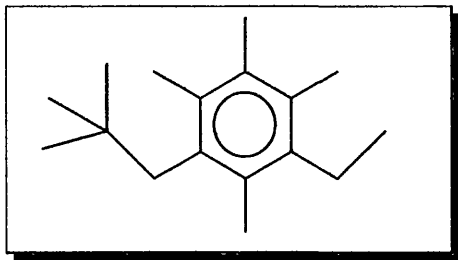
NMR spectroscopy

500 MHz ^1H NMR (CDCl_3) δ/ppm 0.80 {s, 9H, $\text{C}(\text{CH}_3)_3$ }; 1.87-2.20 (dynamic broadened, 6H, CH_3^{11}); 2.00, 2.06, 2.11, 2.19 (each s, 3H, ArCH_3); 2.72 (s, 2H, CH_2CMe_3); 4.05 (s, 2H, $\text{CH}_2\text{-xylyl}$); 6.83-6.92 (dynamic broadened multiplet, 3H, arom. H)

100.6 MHz ^{13}C NMR $\{\text{CHCl}_2\text{F}:\text{CHClF}_2:\text{CD}_2\text{Cl}_2$ (~2:2:1) δ/ppm 17.64, 17.84, 19.84, 19.89 (ArCH_3); 21.68 (C^{11}); 30.97 $\{\text{C}(\text{CH}_3)_3\}$; 34.40 (CH_2C^7); 35.63 (CMe_3); 42.08 (CH_2CMe_3); 126.48 (C^{10}); 129.95 (dynamic broadened, C^9); 134.08, 134.20, 135.08, 135.36, 135.91, 137.58 (arom. C) 138.12 (dynamic broadened, C^8); 140.01 (arom. C).

Elemental analysis

Found: C, 88.93; H, 10.68 %. $\text{C}_{24}\text{H}_{34}$ requires C, 89.35; H, 10.65 %.



1-Ethyl-3-neopentyl-2,4,5,6-tetramethylbenzene (4.9)

The method described for the synthesis of the phenyl-methyl-compound (**4.7**) from the bromide (**4.2**) was followed but using a solution of methyl lithium (2.2 ml, 1.6 M solution in THF, 3.5 mmol), copper (i) iodide (0.34 g, 1.8 mmol) and the bromide (**4.2**)

(0.50 g, 1.7 mmol). The crude product was purified flash column chromatography using petroleum spirit (b.p. 30-40 °C) as the eluent. The product was obtained as a colourless liquid (110 mg).

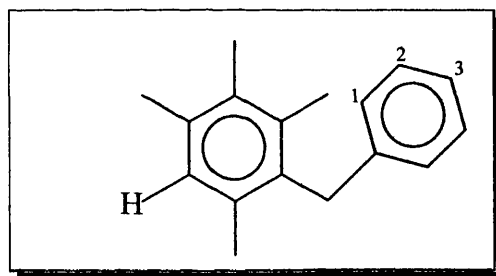
NMR spectroscopy

400 MHz ^1H NMR $\{\text{CHCl}_2\text{F}:\text{CHClF}_2:\text{CD}_2\text{Cl}_2 (\sim 2:2:1)\}$ δ/ppm 1.02 {s, 9H, $\text{C}(\text{CH}_3)_3$ }; 1.19 (t, $J = 7.5$ Hz, 3H, CH_2CH_3); 2.30, 2.35, 2.36, 2.41 (each s, 3H, ArCH_3); 2.84 (q, $J = 7.5$ Hz, 2H, CH_2Me); 2.94 (s, 2H, CH_2CMe_3).

100.6 MHz ^{13}C NMR $\{\text{CHCl}_2\text{F}:\text{CHClF}_2:\text{CD}_2\text{Cl}_2 (\sim 2:2:1)\}$ δ/ppm 14.39 CH_2CH_3 16.63, 17.51, 18.69, 19.81 (ArCH_3); 24.92 (CH_2Me); 31.14 $\{\text{C}(\text{CH}_3)_3\}$; 35.81 (CMe_3); 42.43 (CH_2CMe_3); 133.30, 134.39, 134.62, 135.35, 136.27, 140.19 (arom. C).

Elemental analysis

Found: C, 87.46; H, 12.08 %. $\text{C}_{17}\text{H}_{28}$ requires C, 87.86; H, 12.06 %.



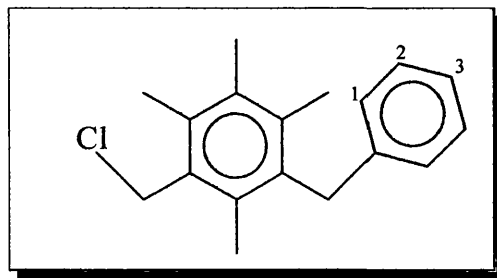
1-(Phenylmethyl)-2,4,5,6-tetramethylbenzene (4.10a).

The method described for the synthesis of 1-(phenylmethyl)-3-neopentyl-2,4,5,6-tetramethylbenzene (4.7) from 1-(bromomethyl)-3-neopentyl-2,4,5,6-tetramethylbenzene (4.2) was followed but using 1-(bromomethyl)-2,4,5,6-tetramethylbenzene (4.1a) (2.07 g, 9.16 mmol), copper (i) iodide (2.82 g, 19.6 mmol) and phenyllithium (10.9 ml, 1.8 M.sol. in cyclohexane:ether/7:3, 19.6 mmol).

After purification by flash column chromatography, the product (0.85 g) was obtained as a white solid.

NMR spectroscopy

300 MHz ^1H NMR (CDCl_3) δ/ppm 2.17, 2.21, 2.23, 2.31 (each s, 3H, ArCH_3); 4.09 (s, 2H, CH_2Ph); 6.88 (s, 1H, arom.); 6.96-7.01 (m, 2H, arom. H^1); 7.12-7.16 (m, 1H, arom. H^3); 7.20-7.23 (m, 2H, arom. H^2);



1-(Chloromethyl)-3-(phenylmethyl)-2,4,5,6-tetramethylbenzene (4.10).

The procedure described for the conversion of 1-(bromomethyl)-3-neopentyl-2,4,5,6-tetramethylbenzene (4.2) to 1-(chloromethyl)-3-neopentyl-2,4,5,6-tetramethylbenzene (4.1) was followed but using the bromide (4.2) (0.38 g, 1.19 mmol) and excess lithium chloride (0.53 g).

The product (185 mg) was obtained as white solid m.p. 103-106 °C.

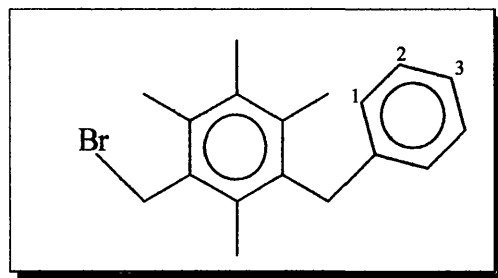
NMR spectroscopy

400 MHz ^1H NMR (CDCl_3) δ /ppm 2.17, 2.23, 2.29, 2.39 (each s, 3H, ArCH_3); 4.10 (s, 2H, CH_2Ph); 4.74 (s, 2H, CH_2Cl); 6.96-7.01 (m, 2H, arom. H^1); 7.12-7.16 (m, 1H, arom. H^3); 7.20-7.23 (m, 2H, arom. H^2);

100.6 MHz ^{13}C NMR $\{\text{CHCl}_2\text{F}:\text{CHClF}_2:\text{CD}_2\text{Cl}_2$ ($\sim 2:2:1$) $\}$ δ /ppm 16.47, 16.65, 17.25, 17.70 (ArCH_3); 37.01 (CH_2Ph); 43.84 (CH_2Cl); 126.93 (arom. $\text{C}^3\text{-H}$); 129.13, 129.59 (2C, arom. C-H); 133.24, 135.00, 135.18, 135.58, 136.18, 138.09, 141.57 (arom. C).

Elemental analysis

Found: C, 78.83; H, 7.79; Cl, 13.35 %. $\text{C}_{18}\text{H}_{21}\text{Cl}$ requires C, 79.25; H, 7.76; Cl, 12.99 %.



1-(Bromomethyl)-3-(phenylmethyl)-2,4,5,6-tetramethylbenzene (4.11).

The method described for the bromomethylation of isodurene in the synthesis of 1-(bromomethyl)-2,4,5,6-tetramethylbenzene (4.1a) was followed but using 1-(phenylmethyl)-2,4,5,6-tetramethylbenzene (4.10a) (0.85 g, 3.79 mmol),

paraformaldehyde (0.12 g, 4.00 mmol) and 30 wt. % hydrogen bromide sol. in acetic acid (0.8 ml).

The crude product was recrystallised from chloroform to give the product (0.84 g) an off white solid m.p. 94-96 °C.

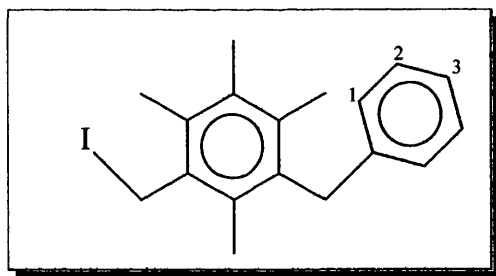
NMR spectroscopy

300 MHz ^1H NMR (CDCl_3) δ /ppm 2.13, 2.20, 2.22, 2.29 (each s, 3H, ArCH_3); 4.09 (s, 2H, CH_2Ph); 4.53 (s, 2H, CH_2I); 6.96-7.01 (m, 2H, arom. H^1); 7.12-7.16 (m, 1H, arom. H^3); 7.20-7.23 (m, 2H, arom. H^2);

100.6 MHz ^{13}C NMR ($\text{CHCl}_2\text{F}:\text{CHClF}_2:\text{CD}_2\text{Cl}_2$ (~2:2:1)) δ /ppm 16.45, 16.60, 17.23, 17.73 (ArCH_3); 32.68 (CH_2Br); 37.06 (CH_2Ph); 127.02 (arom. $\text{C}^3\text{-H}$); 129.22, 129.67 (2C, arom. C-H); 133.34, 135.16, 135.31, 135.69, 136.36, 138.30, 141.67 (arom. C).

Elemental analysis

Found: C, 68.53; H, 6.69; Br, 25.70 %. $\text{C}_{18}\text{H}_{21}\text{Br}$ requires C, 68.14; H, 6.67; Br, 25.19 %.



1-(Iodomethyl)-3-(phenylmethyl)-2,4,5,6-tetramethylbenzene (4.12).

The procedure described earlier for the conversion of 1-(bromomethyl)-3-neopentyl-2,4,5,6-tetramethylbenzene (4.2) to 1-(iodomethyl)-3-neopentyl-2,4,5,6-tetramethylbenzene (4.3) was followed but using the bromide (4.2) (0.17 g, 0.53 mmol) and excess sodium iodide (0.52g).

The product (176 mg) was obtained as an off white solid m.p. 58-61 °C.

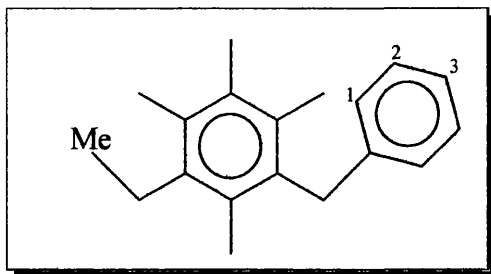
NMR spectroscopy

400 MHz ^1H NMR (CDCl_3) δ /ppm 2.17, 2.23, 2.29, 2.39 (each s, 3H, ArCH_3); 4.10 (s, 2H, CH_2Ph); 4.74 (s, 2H, CH_2Cl); 6.96-7.01 (m, 2H, arom. H^1); 7.12-7.16 (m, 1H, arom. H^3); 7.20-7.23 (m, 2H, arom. H^2).

100.6 MHz ^{13}C NMR CD_2Cl_2 δ/ppm 6.98 (CH_2I); 15.89, 16.15, 16.74, 17.21 (ArCH_3); 35.97 (CH_2Ph); 125.74 (arom. $\text{C}^3\text{-H}$); 127.86, 128.39 (2C, arom. C-H); 132.44, 133.38 (arom. C); 133.67, (2C, arom. C); 134.87, 136.33, 139.97 (arom. C).

Elemental analysis

Found: C, 60.09; H, 5.93; I, 35.39 %. $\text{C}_{18}\text{H}_{21}\text{I}$ requires C, 59.35; H, 5.81; I, 34.83 %.



1-(Ethyl)-3-(phenylmethyl)-2,4,5,6-tetramethylbenzene (4.13).

The method described for the synthesis of 1-(phenylmethyl)-3-neopentyl-2,4,5,6-tetramethylbenzene (4.7) from 1-(bromomethyl)-3-neopentyl-2,4,5,6-tetramethylbenzene (4.2) was followed but using 1-(bromomethyl)-3-ethyl-2,4,5,6-tetramethylbenzene (4.16) (1.7 g, 6.67 mmol), copper (i) bromide (2.07 g, 14.4 mmol) and phenyllithium (8.0 ml, 1.8 M sol. in cyclohexane:ether/7:3, 14.4 mmol).

The product (0.88 g) was obtained as a white solid m.p. 70-71 $^{\circ}\text{C}$.

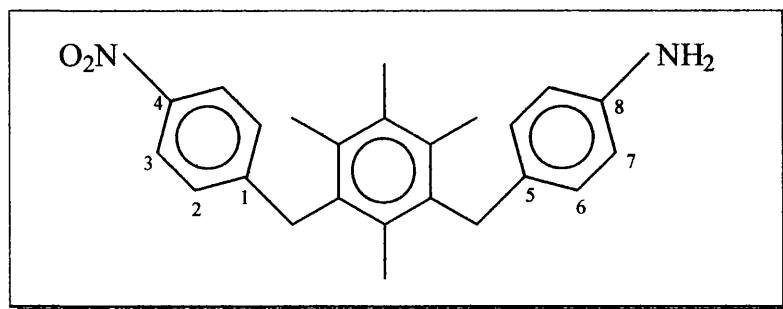
NMR spectroscopy

300 MHz ^1H NMR (CDCl_3) δ/ppm 1.11 (t, $J = 7.5$ Hz, 3H, CH_2CH_3); 2.14, 2.18, 2.22, 2.28 (each s, 3H, ArCH_3); 2.71 (q, $J = 7.5$ Hz, 2H, CH_2CH_3); 4.09 (s, 2H, CH_2Ph); 4.53 (s, 2H, CH_2I); 6.96-7.01 (m, 2H, arom. H^1); 7.12-7.16 (m, 1H, arom. H^3); 7.20-7.23 (m, 2H, arom. H^2);

100.6 MHz ^{13}C NMR $\{\text{CHCl}_2\text{F}:\text{CHClF}_2:\text{CD}_2\text{Cl}_2$ ($\sim 2:2:1$) $\}$ δ/ppm 14.64 (CH_2CH_3), 16.62, 16.80, 17.34, 17.41 (ArCH_3); 24.57 (CH_2CH_3); 37.16 (CH_2Ph); 126.74 (arom. $\text{C}^3\text{-H}$); 129.17, 129.49 (2C, arom. C-H); 133.40, 133.86, 134.28, 134.99, 135.59, 139.85, 142.12 (arom. C).

Elemental analysis

Found: C, 90.38; H, 9.60 %. $\text{C}_{19}\text{H}_{24}$ requires C, 90.40; H, 9.60 %.



1-(*p*-Aminobenzyl)-3-(*p*-nitrobenzyl)-2,4,5,6-tetramethylbenzene⁴⁸(4.14)

The procedure for synthesising the starting reagent, 1,3-bis(*p*-nitrobenzyl)-2,4,5,6-tetramethylbenzene (**3.8**) has been described in the preceding chapter.

The reaction was carried out under an inert atmosphere of argon. To prepare Lalancette's reagent (see equation below), THF (12 ml) was added to sodium borohydride-sulphur (0.99 g, 7.43 mmol) and then stirred at ambient for 10 min.



The di-nitro- (**3.8**) compound dissolved in THF (15 ml) was then added to the Lalancette's reagent and the resultant mixture was refluxed for 30 h. The solvent was removed under reduced pressure leaving a brown solid. The crude product was extracted with dichloromethane (20 ml). After removing some of the solvent using a rotary evaporator, the concentrated crude product was run through a column using dichloromethane as the eluent so as to remove unreacted di-nitro-compound and the corresponding di-amino-compound by-product. An attempt to remove the entire remaining sulfur from the resultant yellow product by sublimation was not successful.

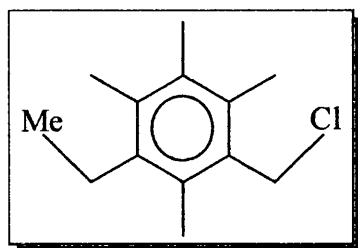
NMR spectroscopy

300 MHz ¹H NMR (CDCl₃) δ/ppm 2.07, 2.15, 2.21, 2.24 (each s, 3H, CH₃); 3.53 (s, 2H, NH₂); 4.00 (s, 2H, CH₂C₆H₄NH₂); 4.19 (s, 2H, CH₂C₆H₄NO₂); 6.58 (d, J = 8.45 Hz, 2H, Ar-H⁶); 6.79 (d, J = 8.45 Hz, 2H, Ar-H⁷); 7.16 (d, J = 8.78 Hz, 4H, Ar-H²); 8.08 (s, J = 8.78 Hz, 4H, Ar-H³).

100.6 MHz ¹³C NMR {CHCl₂F:CHClF₂:CD₂Cl₂ (~2:2:1)} δ/ppm 16.68 (1C, CH₃); 16.95 (3C, CH₃); 35.22 (s, 2H, CH₂C₆H₄NH₂); 36.19 (s, 2H, CH₂C₆H₄NO₂); 115.33 (arom. C⁷); 123.65 (arom. C³); 128.57, 128.60 (arom. C² and C⁶ not necessarily in this order); 130.05, 132.59, 133.32, 133.34, 133.44, 134.69, 135.20, 144.09, 146.23 (arom. C); 148.78 (arom. C-NO₂).

Elemental analysis

Found: C, 75.99; H, 7.09; N, 7.18 %. $C_{24}H_{22}N_2O_2$ requires C, 76.98; H, 7.00; N, 7.48; O, 8.54 %.

1-(Chloromethyl)-3-ethyl-2,4,5,6-tetramethylbenzene (4.15)

The method described earlier for the synthesis of 1-(chloromethyl)-3-neopentyl-2,4,5,6-tetramethylbenzene (4.1) from 1-(bromomethyl)-3-neopentyl-2,4,5,6-tetramethylbenzene was followed but using 1-(bromomethyl)-3-ethyl-2,4,5,6-tetramethylbenzene (4.16) (194 mg, 0.76 mmol) and excess lithium chloride (400 mg).

The product (56 mg) was obtained as a white solid m.p. 53-54 °C.

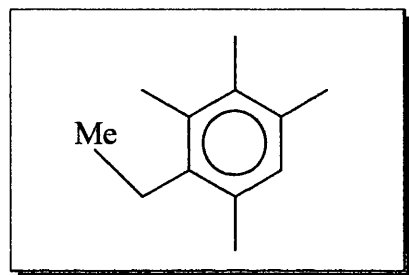
NMR spectroscopy

300 MHz 1H NMR ($CDCl_3$) δ /ppm 1.10 (t, $J = 7.5$ Hz, 3H, CH_2CH_3); 2.20, 2.24, 2.33, 2.37 (each s, 3H, $ArCH_3$); 2.69 (q, $J = 7.6$ Hz, 2H, CH_2CH_3); 4.71 (s, 2H, CH_2Cl).

100.6 MHz ^{13}C NMR $\{CHCl_2F:CHClF_2:CD_2Cl_2$ ($\sim 2:2:1$) $\}$ δ /ppm 14.47 (CH_2CH_3), 15.72, 16.51, 16.98, 17.16 ($ArCH_3$); 24.53 (CH_2CH_3); 43.91 (CH_2Cl); 133.21, 133.90, 134.77, 134.99, 136.95, 140.44 (arom. C).

Elemental analysis

Found: C, 73.81; H, 9.02; Cl, 14.47 %. $C_{18}H_{21}Cl$ requires C, 79.23; H, 7.77; Cl, 12.99 %.

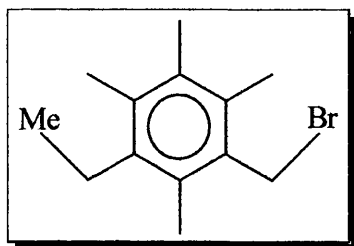
1-Ethyl-2,3,4,6-tetramethylbenzene (4.16a)

The method described for the synthesis of 1-(phenylmethyl)-3-neopentyl-2,4,5,6-tetramethylbenzene (**4.7**) from the bromide (**4.2**) was followed but using a solution of methyl lithium (16.5 ml, 1.6 M solution in THF, 3.5 mmol), copper (i) iodide (2.52 g, 13.2 mmol) and the bromide (**4.2**) (3.0 g, 13.2 mmol).

The product (440 mg) was obtained as a colourless liquid.

NMR spectroscopy

300 MHz ^1H NMR (CDCl_3) δ /ppm 1.09 (t, $J = 7.5$ Hz, 3H, CH_2CH_3); 2.15, 2.22, 2.23, 2.26 (each s, 3H, ArCH_3); 2.64 (q, $J = 7.5$ Hz, 2H, CH_2CH_3); 6.82 (s, 1H, arom. H).



1-(Bromomethyl)-3-ethyl-2,4,5,6-tetramethylbenzene (4.16)

The general method described for the bromethylation of isodurene in the synthesis of 1-(bromomethyl)-2,4,5,6-tetramethylbenzene (**4.1a**) was followed but using 1-ethyl-2,3,4,6-tetramethylbenzene (**4.16a**) (0.44 g, 2.72 mmol), paraformaldehyde (0.09 g, 3.0 mmol) and 30 wt. % hydrogen bromide in acetic acid (0.8 ml).

After recrystallisation from chloroform:petroleum spirit (b.p. 60-80 $^{\circ}\text{C}$) (1:1), the product (460 mg) was obtained as a white solid m.p. (56-58 $^{\circ}\text{C}$).

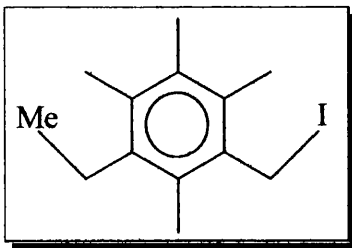
NMR spectroscopy

300 MHz ^1H NMR (CDCl_3) δ /ppm 1.09 (t, $J = 7.5$ Hz, 3H, CH_2CH_3); 2.19, 2.24, 2.31, 2.36 (each s, 3H, ArCH_3); 2.69 (q, $J = 7.6$ Hz, 2H, CH_2CH_3); 4.63 (s, 2H, CH_2Br).

100.6 MHz ^{13}C NMR $\{\text{CHCl}_2\text{F}:\text{CHClF}_2:\text{CD}_2\text{Cl}_2$ ($\sim 2:2:1$) $\}$ δ /ppm 14.46 (CH_2CH_3), 15.68, 16.47, 17.01, 17.15 (ArCH_3); 24.50 (CH_2CH_3); 32.79 (CH_2Br); 133.10, 133.90, 134.46, 134.75, 134.98, 137.20 (arom. C).

Elemental analysis

Found: C, 61.22; H, 7.69; Br, 31.48 %. $\text{C}_{18}\text{H}_{21}\text{Br}$ requires C, 61.18; H, 7.50; Br, 31.31 %.

**1-(Iodomethyl)-3-ethyl-2,4,5,6-tetramethylbenzene (4.17)**

The method described earlier for the synthesis of 1-(iodomethyl)-3-neopentyl-2,4,5,6-tetramethylbenzene (**4.3**) from the corresponding bromide was followed but using 1-(bromomethyl)-3-ethyl-2,4,5,6-tetramethylbenzene (**4.16**) (50 mg, 0.20 mmol) and excess sodium iodide (120 mg).

The product (48 mg) was obtained as an off white solid m.p. 71-72 °C.

NMR spectroscopy

300 MHz ^1H NMR (CDCl_3) δ /ppm 1.09 (t, $J = 7.5$ Hz, 3H, CH_2CH_3); 2.19, 2.22, 2.24, 2.28 (each s, 3H, ArCH_3); 2.68 (q, $J = 7.6$ Hz, 2H, CH_2CH_3); 4.51 (s, 2H, CH_2I).

75.4 MHz ^{13}C NMR CD_2Cl_2 δ /ppm 7.19 (CH_2I); 13.89 (CH_2CH_3), 15.11, 16.04, 16.56, 16.68 (ArCH_3); 23.44 (CH_2CH_3); 131.99, 132.18, 132.83, 133.54, 134.99, 138.93 (arom. C).

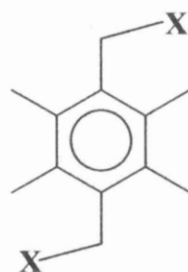
Elemental analysis

Found: C, 51.60; H, 6.51; Br, 41.63 %. $\text{C}_{18}\text{H}_{21}\text{I}$ requires C, 51.67; H, 6.34; I, 41.99 %.

Attractive Steric Interactions in 1,4-
Dineopentyl-2,3,5,6-tetramethylbenzene
and 1,4-bis(Halomethyl)-2,3,5,6-
tetramethylbenzenes

(5.1) Introduction

	X
5.1	^t Bu
5.2	Cl
5.3	Br
5.4	I



In this chapter steric interactions in 1,4-disubstituted-2,3,5,6-tetramethylbenzenes **5.1** - **5.4** are discussed. Rotation about the C-CH₂X bonds, assuming it happens independently, should give rise to four major rotamers *a*, *b*, *c* and *d* (see figure **5.1**). The rotamers *a* and *c* that has the two X groups on the same side of the ring plane (i.e. *syn*) are identical. A 180° rotation about any of the C-CH₂X bonds should give rotamers *b* and *d*, these rotamers are “*anti*” and are identical. In determining which of the two conformations is the more stable we ought to consider the energy contribution from the interaction of the atoms from the two X groups as well as the level of self organisation amongst the groups attached to the benzene ring, in the two conformations.

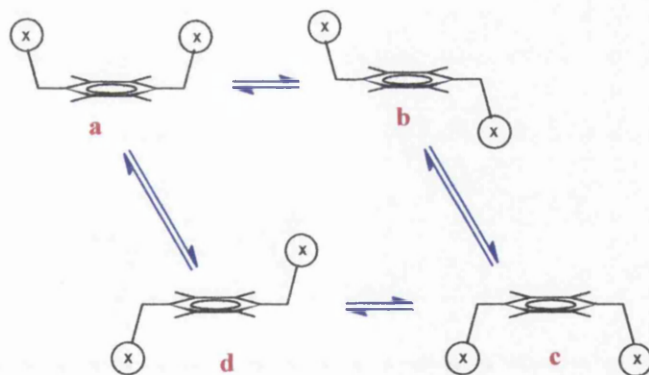


Figure **5.1**. The rotamer interconversion scheme for the 1,4-disubstituted compounds (**5.1** – **5.4**). It is assumed that rotation about the C-CH₂X bonds happens one at a time.

Considering the interaction between the two X groups in the two conformations, these groups are clearly too far apart to be repelling hence they should slightly attract one another and reduce the overall energy of formation of the structures. However, the level of attraction would be expected to be marginally higher in the *syn* conformation because the two X groups are slightly closer together.

NMR spectroscopy

In compounds **5.1** – **5.4**, when rotation about the C-CH₂X bonds is fast on the NMR time scale, as is the case at room temperature for the four compounds, the four methyl groups are in the same chemical environment just as are the two CH₂X groups, therefore both groups should each give rise to a singlet in the proton NMR spectrum. But when rotation about the C_{Ar}-CH₂X bonds becomes slow on the NMR time scale, the peaks which appear at room temperature should each split into two reflecting the fact that both conformations are now distinguishable on the NMR time scale. However, the two sub-spectra from the two conformations are expected to be alike (see figure **5.2**) as

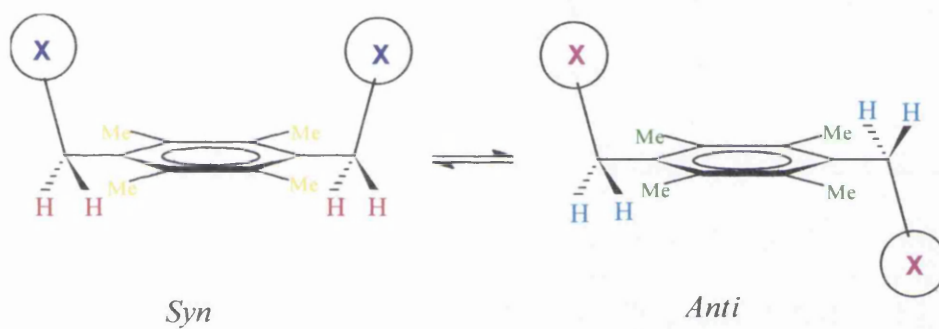


Figure **5.2**. The *syn* and *anti* conformations of **5.1** – **5.4**, different colours are used to depict the different chemical environments of the atoms.

a result of which it would be impossible to assign the signals as *syn* or *anti*. In the case of the neopentyl-compound (**5.1**), using X-ray crystallography in conjunction with dynamic NMR spectroscopy solved the problem.

(5.2) Results and Discussion

(5.2.1) Conformational assignment of NMR signals at low temperatures

(a) *NMR spectra of the dineopentyl-compound (5.1)*

As regards dynamic NMR analysis of the dineopentyl compound (**5.1**) in methylene chloride-*d*₆, at room temperature, three singlets are observed in the proton NMR spectrum with the *tert*-butyl signal appearing broad due to slow dynamic exchange. On cooling, the *tert*-butyl signal de-coalesces at about +10 °C before eventually sharpening

up at lower temperatures. Within the temperature range -7 to -95 $^{\circ}\text{C}$, the conformational population ratio is temperature dependent with the ratio rising from 0.96 (-7 $^{\circ}\text{C}$) to 1.94 (-95 $^{\circ}\text{C}$). The population ratio at various temperatures is shown in table 5.1. It is interesting to know that the more stable conformation between -7 and -13 $^{\circ}\text{C}$ is the less stable at lower temperatures (see figure 5.3a and b).

Table 5.1. The equilibrium constant at various temperatures obtained for the dineopentyl compound (5.4) dissolved in CD_2Cl_2 .

Temperature / $^{\circ}\text{C}$ (K)	Equilibrium Constant (<i>anti/syn</i>)
-7 (266)	0.96
-13 (260)	0.99
-40 (233)	1.21
-60 (213)	1.54
-80 (193)	1.83
-95 (178)	1.94
$\Delta H_{\text{exp}} = -0.81 \pm 0.06 \text{ kcal mol}^{-1}$; $\Delta S_{\text{exp}} = -3.12 \pm 0.34 \text{ cal mol}^{-1} \text{ K}^{-1}$	

An attempt was also made to obtain a snapshot spectrum of the compound in the solid state to help determine which of the two conformations is the more populated in solution. The procedure and the result of the experiment are now presented.

A few crystals of the compound was added to pre-chilled methylene chloride- d_2 at -78 $^{\circ}\text{C}$, in order to freeze the *syn/anti* interconversion process, and the NMR spectrum of the sample was immediately taken in a spectrometer with a pre-cooled probe temperature of -80 $^{\circ}\text{C}$. The *tert*-butyl region of the resultant spectrum observed after about 2 min from the point of adding the solid to methylene chloride- d_2 is shown in figure 5.3c, the intensity ratio of the peaks is 2.6:1. In the subsequent spectrum observed about 5 min later, the *syn/anti* interconversion process seems to have reached the point of equilibrium. The 2.6:1 ratio is much higher than any of the population ratios observed over the temperature range, -7 to -95 $^{\circ}\text{C}$ (see table 5.1), during which time, the process was allowed sufficient time to equilibrate before recording the spectrum.

In light of the time that elapsed before the snapshot spectrum was recorded and the relatively short half-life of the conformers in the *syn/anti* equilibrium, it is reasonable to assume that the conformational population ratio in the solid state is substantially higher

than the 2.6:1 value obtained in the experiment that only a single conformation is populated in the solid. And since the spectrum of figure 5.3c represents a sample on route to equilibrium in solution at -80°C (when $K = 1.83$), it is the conformation with the downfield *tert*-butyl signal that is found in the solid state.

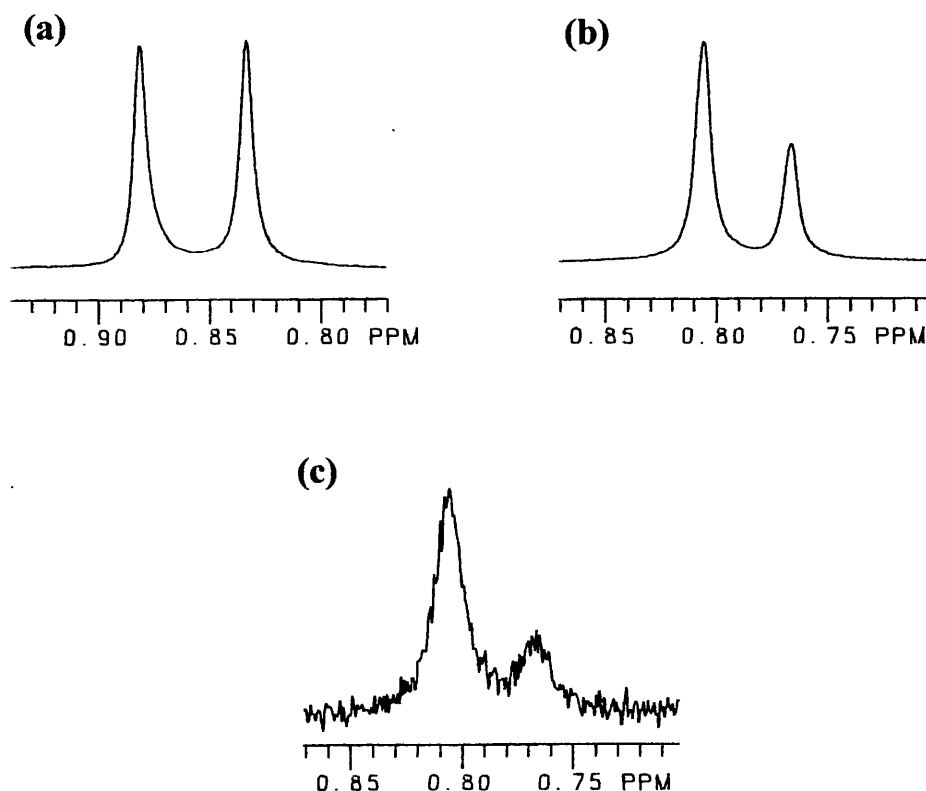


Figure 5.3.

(a) The $\text{C}(\text{CH}_3)_3$ region of the proton NMR spectrum of the dineopentyl compound (5.1) in CD_2Cl_2 at -13°C .

(b) The $\text{C}(\text{CH}_3)_3$ region of the same sample but at -95°C .

(c) The $\text{C}(\text{CH}_3)_3$ region the only partially equilibrated solution of (5.1) dissolved at low temperature.

Now, trying to address the question of which conformation is the more populated and therefore the more stable in solution, well, if we can determine which of the two conformations is found in the solid state by X-ray crystallography, it should be possible to assign the major and minor peaks in the snapshot spectrum of the solid as either *syn* or *anti*.

X-ray crystallography analysis reveals that the dineopentyl-compound (5.1) crystal exists in a single conformation, the *anti* conformation, see figure 5.6. Thus, the more intense of the two *tert*-butyl singlets in the snapshot spectrum (figure 5.3c) and in

the low temperature equilibrium spectrum (figure 5.3b) which happens to be the more downfield, is from the *anti*.

Having assigned the spectra, we are able to reach the conclusion that when the sample of the dineopentyl-compound in methylene chloride- d_2 is cooled, it is the population of the *anti* form, relative to the *syn*, that gradually increases with decreasing temperature. By plotting $\ln k$ vs $1/T$, here k is the equilibrium constant (*anti/syn*) and T is the temperature in Kelvin, the magnitude of the enthalpy difference (ΔH) and the difference in entropy (ΔS) may be obtained from the solution to equation (I).

$$\ln k = - \frac{\Delta H}{R} \left(\frac{1}{T} \right) + \frac{\Delta S}{R} \dots\dots\dots(I)$$

For the conversion of a *syn* conformation to an *anti*, ΔH is $-0.81 \pm 0.06 \text{ kcal mol}^{-1}$ and ΔS is $-3.12 \pm 0.34 \text{ cal mol}^{-1} \text{ K}^{-1}$. It is worth pointing out at this stage that there is the possibility that this ΔH and ΔS value may well not be due to the *syn/anti* interconversion process but to a solvent effect process or a combination of both.

(b) NMR spectra of the halides (5.2–5.4)

The methylene region of the proton NMR spectra of the three halides (5.2 - 5.4), when rotation about the C-CH₂X bonds becomes slow on the NMR time scale are similar, in that they all contain two singlets of unrelated intensity with the major peak resonating upfield the minor. The chemical shifts of the proton NMR spectrum at low temperatures are shown in table 5.2.

Considering the proton NMR spectrum of the chloride (5.2) in methylene chloride- d_2 at room temperature, two singlets, one in the methylene region and the other in the methyl region are observed but on cooling, the signal from the CH₂Cl group broadens before de-coalescing at about -70°C . And at -90°C the signal has split into two singlets resonating at 4.66 and 4.69 ppm of intensity ratio 2.3:1. The methylene region of the spectrum is shown in figure 5.3a. The ratio equates to an energy difference of $0.30 \text{ kcal mol}^{-1}$

As far as the bromide (5.3) is concerned, the dynamic NMR spectrum was carried out in two solvents, methylene chloride- d_2 and acetone- d_6 . In CD₂Cl₂ the signal from the CH₂Br group de-coalesces at about -45°C before eventually splitting into two peaks at lower temperatures. At -80°C , two singlets resonating at 4.57 and 4.60 ppm of intensity ratio 2.0:1 are observed (see figure 5.3b), this represents an energy difference

of $0.26 \text{ kcal mol}^{-1}$. But in the more polar solvent, acetone- d_6 , a slightly lower conformational population ratio of 1.3:1 at -80°C is observed. The ratio corresponds to an energy difference of $0.10 \text{ kcal mol}^{-1}$.

Table 5.2. The proton NMR chemical shifts^a of the chloride (5.2), bromide (5.3) and iodide (5.4) at low temperatures.

Compound (X)	Solvent	Temperature / K	Chemical Shift /ppm		
			$\text{C}(\text{CH}_3)_3$	CH_3	CH_2X
<i>t</i>-Bu	CD_2Cl_2	233	0.806	2.145	2.765
			0.853	2.163	2.775
Cl	CD_2Cl_2	183	-	2.247	4.66
			-	2.253	4.69
Br	CD_2Cl_2	193	-	2.24	4.57
			-		4.60
Br	CD_3COCD_3	188	-	2.25	4.74
			-	2.27	4.80
I	CD_2Cl_2	213	-	2.176	4.43
			-	2.183	4.46

^a The chemical shifts shown in red are the more intense. In the neopentyl-compound the more intense signals are from the *anti*.

On cooling a sample of the iodide dissolved in methylene chloride- d_2 , the CH_2I signal de-coalesces at about -20°C before eventually sharpening up at lower temperatures. At -60°C the two singlets resonating at 4.43 and 4.46 ppm are of intensity ratio 1.9:1 and this equates to an energy difference of $0.27 \text{ kcal mol}^{-1}$. The CH_2I region of the spectrum is shown in figure 5.3c.

As regards the preferred conformation in the halides, if one compares the relative shift of the major and minor signals from the methylene group in the low temperature NMR of the halides with that of the assigned methylene signals in the neopentyl-compound, it is consistent with the *anti* being the more stable. On the other hand, when the same comparison is made using the methyl signals, in contrast, it is consistent with the *syn* being the more stable in the three halides. Though using the

chemical shifts does not shed light on the question of which conformation is the more stable, but since in the neopentyl compound, the *anti* is the more stable and calculations also indicate that the *anti* form of the halides is substantially more stable than the *syn*, it is within reason to presume that the observed energy differences in the halides are in favour of the *anti*.

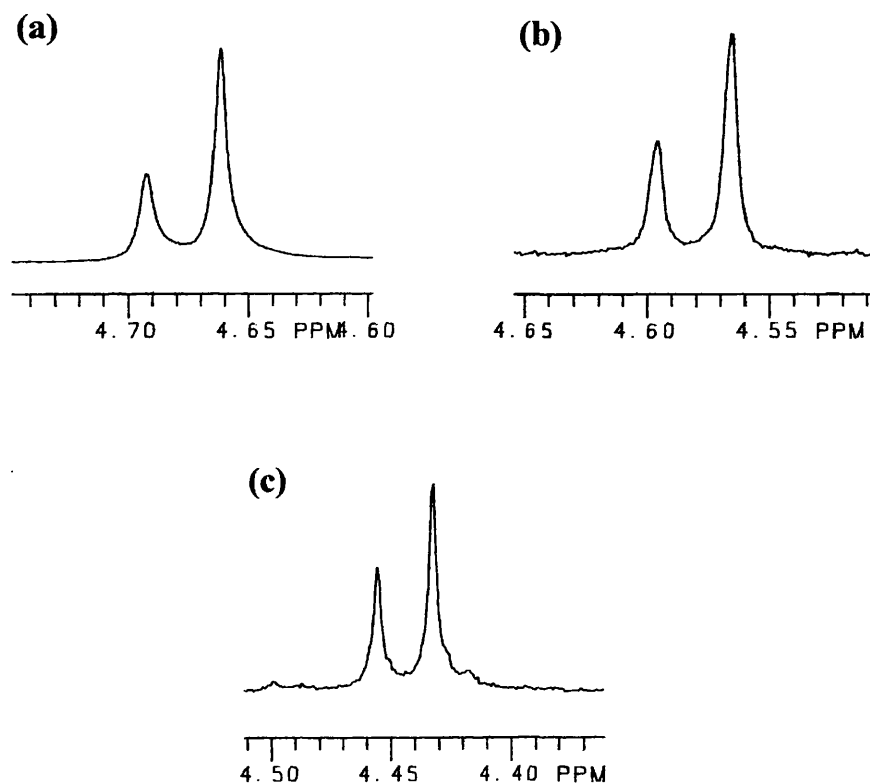


Figure 5.3.

- (a) The CH₂Cl region of the proton NMR spectrum of the chloride (**5.2**) in CD₂Cl₂ at -90 °C.
(b) The CH₂Br region of the NMR spectrum of the bromide (**5.3**) at -80 °C.
(c) The CH₂I region of the NMR spectrum of the iodide (**5.4**) at -60 °C.

(5.2.2) MM3 Calculations

MM3 calculations were performed on compounds **5.1** - **5.4** and the results are summarised in table 5.3. In the dineopentyl-compound the *syn* is slightly more stable than the *anti* whereas in the halides the *anti* is substantially more stable than the *syn*. The calculated enthalpy differences being about (dineopentyl-, -0.11); (chloride, +1.29); (bromide, +0.88) and (iodide, +1.03 kcal mol⁻¹).

In the dineopentyl-compound (**5.1**), the sum of the 13 x 13 pairwise interaction amongst the *tert*-butyl groups in the *syn* conformation is -169 cal mol⁻¹ whereas in the

Table 5.3. The contributions to the final steric energy (kcal mol⁻¹) of the *syn* and *anti* conformations of 5.1 – 5.4

	Dineopentyl comp. (5.1)		Chloride (5.2)		Bromide (5.3)		Iodide (5.4)	
	<i>Syn</i>	<i>Anti</i>	<i>Syn</i>	<i>Anti</i>	<i>syn</i>	<i>Anti</i>	<i>syn</i>	<i>anti</i>
Compression	3.9533	3.9193	1.9984	1.8546	2.0563	1.9447	2.0360	1.8868
Bending	5.7145	5.6726	3.0653	2.7444	3.1008	2.7970	3.9440	3.5980
Bend-bend	-0.1619	-0.1585	-0.3045	-0.3093	-0.3113	-0.3091	-0.5529	-0.5513
Stretch-bend	-0.2591	-0.2595	-0.4000	-0.3855	-0.4024	-0.3855	-0.3943	-0.3722
van der Waals								
1,4 energy	16.1849	16.2044	8.9339	9.0346	8.9574	9.0040	8.6110	8.7094
Other	9.7324	9.7587	6.2343	5.1882	6.0490	5.5259	5.9876	5.2261
Torsional	-9.6884	-9.5394	-5.6787	-5.3653	-5.9443	-5.8509	-16.8993	-16.6911
Torsion-stretch	-0.0064	-0.0047	0.0000	0.0000	0.0000	0.0000	0.0000	0.0000
Dipole-dipole	7.7741	7.7650	5.6926	5.5129	6.0275	5.9280	6.1814	6.0645
Total Steric Energy (<i>H</i>)	33.2435	33.3579	19.5414	18.2547	19.5330	18.6540	8.9136	7.8802
ΔH	-0.1144		1.2867		0.8790		1.0334	

anti the level is much lower at -74 cal mol^{-1} , reflecting the fact that the group of atoms in the two X groups are closer together in the *syn*. There seems to be a correlation between the magnitude of the *syn* advantage (95 cal mol^{-1}) arising from 'Bu-'Bu attractive steric interactions and the calculated enthalpy difference (ΔH_{calc}) (114 cal mol^{-1}). Thus, suggesting that it is reasonable to attribute a high proportion of ΔH_{calc} to attractive steric interactions between the *tert*-butyl.

For the halides, the magnitude of the *syn* advantage, when only the X-X steric interactions are being considered is very small in comparison to the calculated enthalpy difference, the *syn* advantages being (Cl, 7); (Br, 13); (I, 22 cal mol^{-1}), see table 5.4.

Table 5.4. The sum of the X-X attractive steric contributions (kcal mol^{-1}) for 5.1 – 5.4.

Compound →	Dineopentyl- (5.1)	Chloride (5.2)	Bromide (5.3)	Iodide (5.4)
<i>Syn</i>	-0.1688	-0.0168	-0.0306	-0.0478
<i>Anti</i>	-0.0735	-0.0102	-0.0177	-0.0251
Diff.	-0.0953	-0.0066	-0.0129	-0.0221

Accounting for the difference in the total dipole-dipole contributions for the *syn* and *anti* conformations of the halides, is the fact that the situation in the *syn*, where the dipoles from the two C-X bonds (X = Cl, Br or I) lie on the same side of the ring plane, is far more destabilising than the “1 up, 1 down” arrangement of the C-X dipoles in the *anti*. The energy associated with the interaction of the two C-X dipoles in the *syn* and *anti* conformations are summarised in table 5.5.

Table 5.5. The energy (kcal mol^{-1}) associated with the interaction of the two C-X dipoles in the *syn* and *anti* conformations of 5.1 – 5.4.

Compound →	Chloride (5.2)	Bromide (5.3)	Iodide (5.4)
<i>Syn</i>	+0.1673	+0.1183	+0.1091
<i>Anti</i>	+0.0210	+0.0169	+0.0267
Diff.	+0.1463	+0.1014	+0.0824

The magnitude of the *anti* advantage arising from the (C-X) – (C-X) dipole-dipole interactions is very small in comparison to the calculated enthalpy difference, this suggest that other factors presumably, gearing is also involved in preferentially stabilising the *anti* relative to the *syn*.

Hexamethyl-³² and hexaethyl-benzenes³³ have been shown in the literature to exist predominantly in a geared type conformation in which there is a successive up and down arrangement of CH₂-Y bonds (Y = Me or H) and in addition the bonds lie more or less perpendicular to the plane of the benzene ring. This is the conformation in which steric repulsion between the groups on the ring is at its lowest. In the halides (5.2-5.4), the up and down arrangement of bonds is observed in the *anti* but not in the *syn* forms, see figure 5.5.

In contrast to the halides, in the dineopentyl compound (5.1), in neither the *syn* or *anti* conformation is the successive up and down arrangement of bonds observed. This being so because the *tert*-butyl group is so bulky that it prevents C-H bonds from adjacent methyl groups from being orthogonal to the ring plane and the two adjacent methyl groups are not concerned with gearing with each other. Each is concerned with accommodating its *tert*-butyl neighbour.

The experimentally observed entropy difference between the *syn* and *anti* conformations of 1,4-dineopentyl compound (5.1) compared with say the 1,4-diiodomethyl compound (5.4) is significantly high. There are six extra rotamers in the 1,4-dineopentyl-compound in comparison to the 1,4-dibromomethyl compound (5.4). It is difficult to decide whether this or ring methyl group rotation is the seat of the entropy difference between conformations.

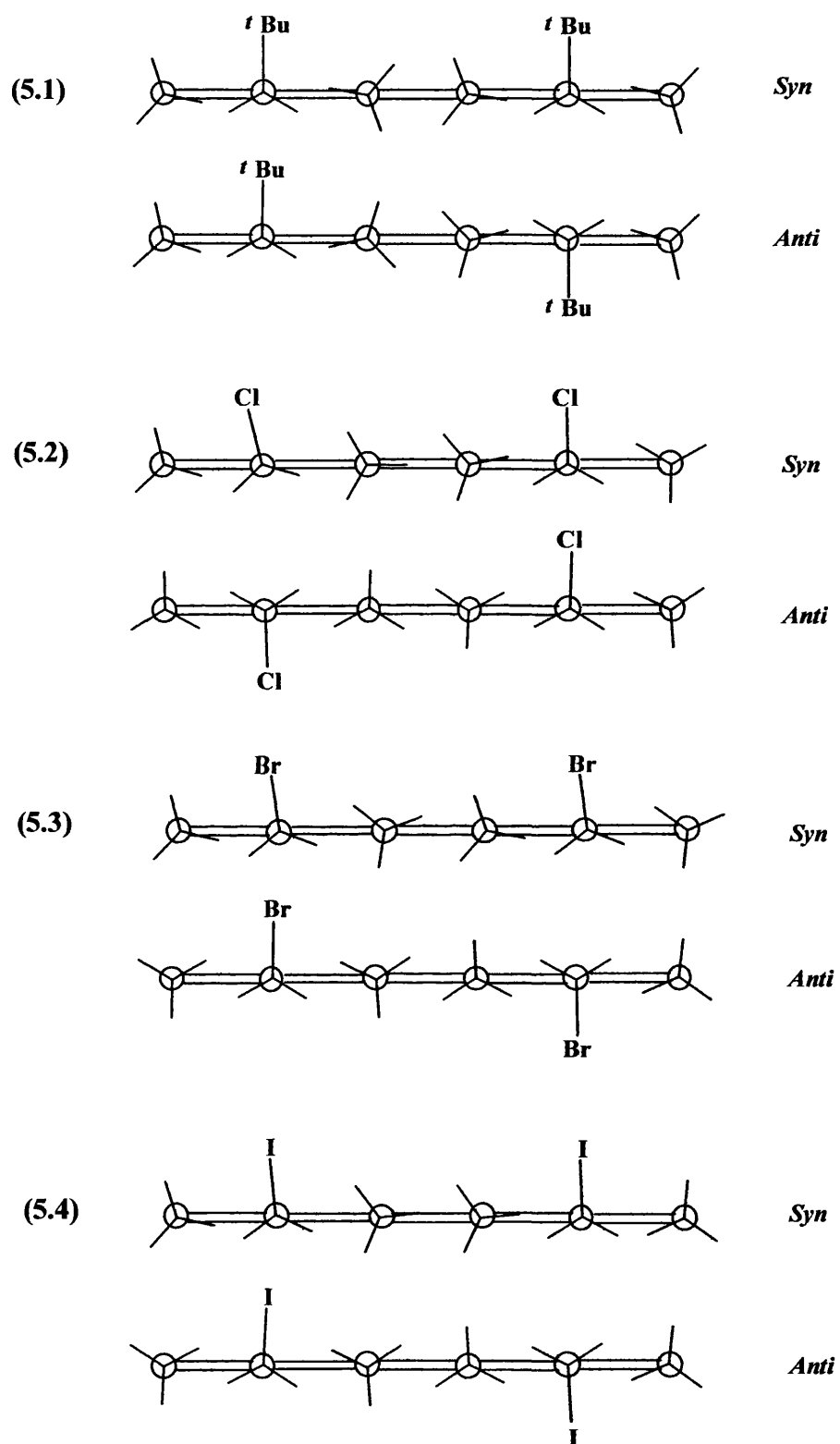


Figure 5.5. The conformation adopted by the groups on the ring as calculated by MM3 calculations.

(5.2.3) X-ray crystallography of the dineopentyl-compound (5.1)

The dineopentyl-compound crystallises as a monoclinic system with each unit cell containing two molecules of the *anti* form. The X-ray structure is shown in figure 5.6.

Crystal data: $C_{20}H_{34}$

Molecular weight = 274.47; temperature = 100(2) K; wavelength = 0.71073 Å;

Unit cell dimension $a = 6.1227(4)$ Å $\alpha = 90^\circ$
 $b = 6.2187(7)$ Å $\beta = 95.738(6)^\circ$
 $c = 23.536(2)$ Å $\gamma = 90^\circ$

Volume = 891.65(14) Å³

Density = 1.022 Mg m⁻³

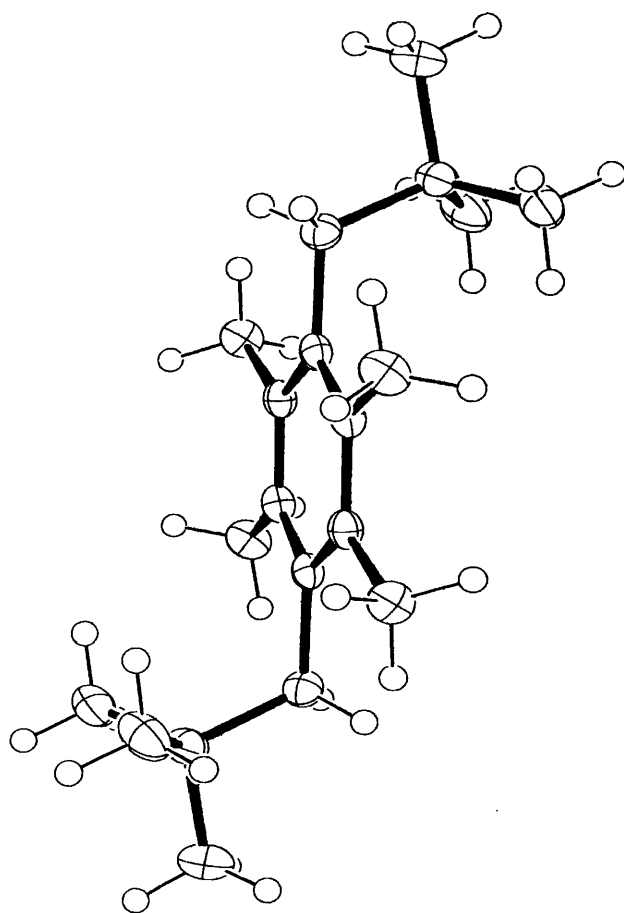


Figure 5.6.

(5.3) Conclusion

In the dineopentyl-compound, dynamic NMR shows that the relative stability of the *anti* for compounds with substituents in the 1 and 4 positions increases with decreasing temperature and the value of ΔH^θ indicate that the *anti* conformation is substantially more stable than the *syn*. X-ray crystallography also reveal that only one conformation, the *anti* form is present in the solid state. But in contrast, calculations indicate that the *syn* conformation is slightly more stable than the *anti*.

The results from experiments and calculations are summarised in table 5.6. As for the halides, experiments show that the *anti* conformation is more stable than the *syn*, a trend also supported by calculations. Although, in contrast to experiments, calculations suggest that the difference in enthalpy in favour of the *anti* conformation, is substantial. The calculated extra stability of the *anti* conformation in the halides seems to be caused predominantly by “gear effect” and to a small extent by dipole-dipole interactions.

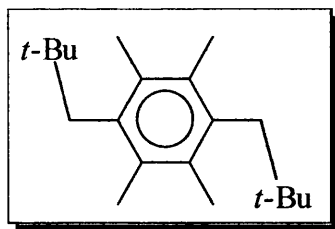
The drop in relative stability of the *anti* conformation on going from a less polar solvent (CD_2Cl_2) to a more polar solvent (acetone- d_6) in the bromide (5.3) is consistent with the results from the “solvent effect experiments” carried out on the 1,3-bis(bromomethyl)-2,4,5,6-tetramethylbenzene (see chapter 3 section one). In chapter three, the trend was explained in terms of the molecules from the more polar solvents being able to form stronger complexes with the *syn* form that has one side of the ring plane free of steric hindrance from bulky groups and in the process stabilise it, relative to the *anti*.

Table 5.6. Summary of the results from experiments and calculations for 5.1-5.4

R	solvent	Temperature	K_{exp} <i>anti/syn</i>	ΔG_{exp}^a	ΔH_{cal}^a
		$^\circ\text{C}$		kcal mol $^{-1}$	kcal mol $^{-1}$
<i>t</i> -Butyl ^b	CD_2Cl_2	-80	1.8	0.22	-0.11
Cl	CD_2Cl_2	-95	2.3	0.30	1.29
Br	CD_2Cl_2	-80	2.0	0.26	0.88
	Acetone d_6	-85	1.3	0.10	
I	CD_2Cl_2	-60	1.9	0.27	1.00

^a +ve value means that the *anti* is the more stable, the reverse is true when it is -ve.

^b The equilibrium constant varies with temperature see table 5.1.

(5.4) Synthesis**1,4-dineopentyl-2,3,5,6-tetramethylbenzene⁴¹ (5.1)**

The reaction was carried out under an inert atmosphere of argon.

A 0.2 M solution of the Li_2CuCl_4 catalyst, was prepared by adding THF (50 ml) to a stirred mixture of lithium chloride (0.85g, 0.02 mol) and copper (II) chloride (1.35 g, 0.01 mol). The mixture was stirred for 5 min.

The Grignard reagent, *tert*-butylmagnesium chloride was synthesised as follows:- Magnesium turnings (4.0 g, 167 mmol) was added to a three neck flask equipped with a mechanical stirrer and a dropping funnel. The magnesium was stirred for 6 h to activate it before adding THF (90 ml). The dropping funnel was loaded with a solution of *tert*-butyl chloride (15.3 g, 165 mmol) dissolved in dry THF (20 ml). A portion (~5 ml) of the *tert*-butyl chloride solution was added to the THF-magnesium mixture via the dropping funnel. A crystal of iodine was added to the mixture to initiate the reaction. After an induction period of 15 min the reaction began causing the reaction mixture to warm. The remainder of the *tert*-butyl chloride was added at such a rate that the THF boils gently. The mixture was refluxed for 3 h, cooled to ambient temperature and allowed to settle. The supernatant liquid was transferred into a clean flask.

A mixture of 1,4-bis(bromomethyl)-2,3,5,6-tetramethylbenzenes (8.84 g, 27.6) dissolved in THF (50 ml) and the catalyst (5 ml) was added to the Grignard at ambient temperature *via* a dropping funnel whilst stirring. The mixture was stirred at the same temperature for 14h.

The reaction was quenched by the addition of 3 M hydrochloric acid (50 ml) dropwise. The organic phase was separated from the inorganic phase and the later was extracted with ether (3 x 20 ml). The combined organic phase was dried over anhydrous magnesium sulfate and the solvent was removed using a rotary evaporator leaving a white semi-solid crude product. The crude product was purified by flash column chromatography using petroleum spirit (30-40 °C) as the eluting solvent. After several runs, the product (1.45 g) was obtained as a white solid m.p. (107-108 °C).

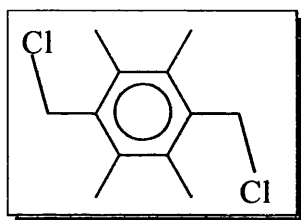
NMR spectroscopy

300 MHz ^1H NMR (CDCl_3) δ /ppm 0.88 {dynamic broadened, s, 18H, $2\text{C}(\text{CH}_3)_3$ }; 2.21 (s, 12H, 4Ar CH_3); 2.60 (s, 4H, CH_2CMe_3).

100.6 MHz ^{13}C NMR (CDCl_3) δ /ppm 19.28 (Ar CH_3); 30.21 (CH_2CMe_3); 34.55 (CMe_3); 40.84 (CH_2^tBu); 133.76 (CCH_2^tBu); 134.01 (CCMe_3). All signals are broad due to dynamic exchange.

Elemental analysis

Found: C, 87.63; H, 12.48 %. $\text{C}_{20}\text{H}_{34}$ requires C, 87.51; H, 12.50 %.

**1,4-bis(chloromethyl)-2,3,5,6-tetramethylbenzene⁴² (5.2)**

Under an inert atmosphere of argon, acetone (25 ml) was added to a mixture of 1,3-bis(bromomethyl)-2,3,5,6-tetramethylbenzene (0.4 g, 1.25 mmol) and lithium chloride (159 g, 3.75 mmol) the mixture was refluxed for 24 h. The solvent was removed using a rotary evaporator. Methylene chloride (15 ml) and water (15 ml) were added to the solid residue. The inorganic phase was then separated and the organic phase collected, the latter was then extracted with methylene chloride (3 x 10 ml). The combined organic extracts was washed with water (3 x 8 ml) to remove inorganic salts before drying over anhydrous magnesium sulfate. The solvent was removed using a rotary evaporator to give the crude product.

Analysis of the proton NMR of the crude product indicated that not all bromine atoms have been substituted, hence the procedure described above was repeated using the crude product and the same amount of lithium chloride. After subjecting the crude product through four more cycles of reaction and work-up, the product (138 mg) was obtained as a white solid m.p. 202-204 $^{\circ}\text{C}$.

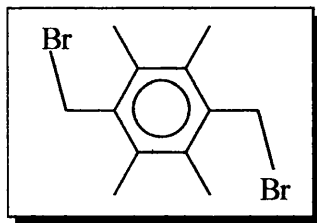
NMR spectroscopy

400 MHz ^1H NMR (CD_2Cl_2) δ /ppm 2.34 (s, 12H, 4Ar CH_3); 4.73 (s, 4H, CH_2Cl).

100.6 MHz ^{13}C NMR (CD_2Cl_2) δ/ppm 15.94 (ArCH_3); 42.25 (CH_2Cl); 134.07 (CCH_3 , arom.); 134.58 (CCH_2Cl arom.).

Elemental analysis

Found: C, 61.98; H, 6.95 %. $\text{C}_{12}\text{H}_{16}\text{Cl}_2$ requires C, 62.32; H, 6.93; Cl, 30.69 %.



1,3-bis(Bromomethyl)-2,3,5,6-tetramethylbenzene³⁷ (5.3)

The reaction was carried out under an inert atmosphere of argon. Durene (6.71 g, 50 mmol) was added to glacial acetic acid (100 ml) and warmed up to 50 $^{\circ}\text{C}$ with stirring. When the durene has dissolved paraformaldehyde (3.4 g, 113 mmol) and then hydrogen bromide (21.1 ml, 5.7 M solution in glacial acetic acid, 120 mmol) were added and the resultant mixture was stirred at 120 $^{\circ}\text{C}$ for 12 h.

The mixture was allowed to cool before pouring into water (200 ml). The solid was collected by suction filtration and then recrystallised from chloroform to give the product (13.11 g) as a white solid m.p. 215-217 $^{\circ}\text{C}$.

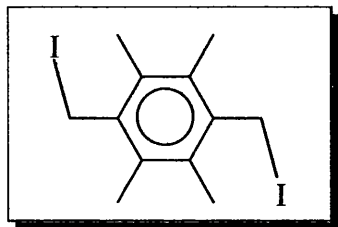
NMR spectroscopy

400 MHz ^1H NMR (CD_2Cl_2) δ/ppm 2.32 (s, 12H, 4 ArCH_3); 4.63 (s, 4H, CH_2Br).

100.6 MHz ^{13}C NMR (CD_2Cl_2) δ/ppm 15.88 (ArCH_3); 30.94 (CH_2Br); 134.10 (CCH_3 , arom.); 134.66 (CCH_2Br , arom.).

Elemental analysis

Found: C, 45.10; H, 4.93; Br, 49.62 %. $\text{C}_{12}\text{H}_{16}\text{Br}_2$ requires C, 44.93; H, 5.04; Br, 49.81 %.



1,4-bis(iodomethyl)-2,3,5,6-tetramethylbenzene³⁸ (5.4)

Under an inert atmosphere of argon, acetone (25 ml) was added to a mixture of 1,3-bis(bromomethyl)-2,3,5,6-tetramethylbenzene (100 mg, 0.31 mmol) and excess sodium iodide (140 mg, 0.93 mmol). The mixture was stirred at ambient temperature for 3 h and the solvent was removed using a rotary evaporator. Dichloromethane (10 ml) and water (18 ml) were added to the solid residue and the organic phase was separated and collected. The aqueous phase was extracted with dichloromethane (3 x 10 ml) and the combined dichloromethane extract was combined and washed with water (3 x 8 ml) and dried over anhydrous magnesium sulfate. The solvent was removed using a rotary evaporator leaving the product (108 mg), an off white solid m.p. 227-228 °C.

NMR spectroscopy

400 MHz ^1H NMR (CD_2Cl_2) δ /ppm 2.24 (s, 12H, 4ArCH₃); 4.51 (s, 4H, CH₂I).

100.6 MHz ^{13}C NMR (CDCl_3) δ /ppm 4.19 (CH₂I); 15.59 (ArCH₃); 30.96 (CMe₃); 134.17 (CCH₃, arom.); 135.99 (CCH₂I, arom.).

Elemental analysis

Found: C, 34.81; H, 3.89 %. $\text{C}_{12}\text{H}_{16}\text{I}_2$ requires C, 34.79; H, 3.90; I, 61.47 %.

Barriers to Rotation in Hexasubstituted- benzenes

(6.1) Introduction

The barriers to rotation obtained from NMR spectroscopy and MM3 calculations are summarised in table 6.1. The barriers quoted in the table for a particular aryl-CH₂X bond with two *ortho* methyl group substituents are expected to be more or less the same regardless of the other substituents on the ring.

Barriers are not reported for CH₂X rotation in every compound studied, since spectral changes are often complex or relative chemical shifts are very small, but at least one barrier is reported for each CH₂X group for the wide range used.

The experimental barriers (ΔG_{exp}) were determined using equation (I)⁴⁹. R is the Gas constant, T_c (K) is the temperature at the decoalescence point and $\Delta\nu$ (Hz) is the frequency of separation of the two peaks well below the decoalescence temperature.

$$\Delta G_{\text{exp}}^{\#} = RT_c [23 + \ln(T_c) - \ln(\Delta\nu)] \quad \dots\dots\dots(I)$$

Because the equation strictly applies to environmental exchange between two equally populated sites, and the two conformations in majority of the compounds investigated, with the exception of the xylyl-compound, are not equally populated, it therefore follows that the barriers quoted in the table are approximations.

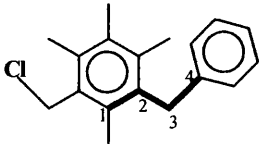
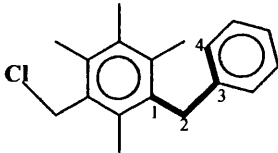
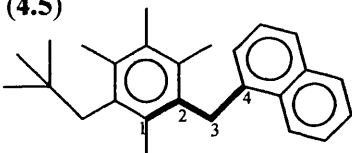
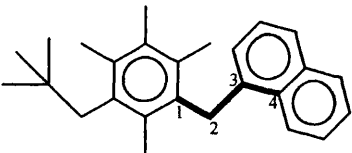
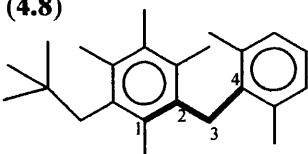
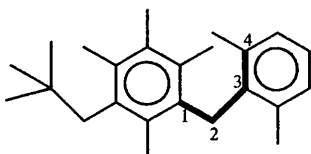
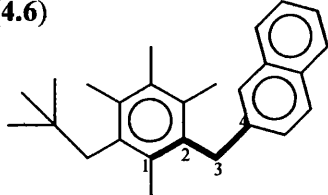
(6.2) ResultsTable 6.1. The barrier to rotation about the C²-C³ bond as determined by experiments ($\Delta G^\#_{exp}$) and calculations ($\Delta H^\#_{calc}$).

Compound ↓	Decoalescence	$\Delta G^\#_{exp}$	$\Delta H^\#_{calc}$	See figure ^a
	Temperature ^b	kcal mol ⁻¹	kcal mol ⁻¹	
(5.2) 	200 K (CH ₂ Cl)	~10.3	7.9	6.1
(5.3) 	228 K (CH ₂ Br)	~11.4	9.4	6.2
(5.4) 	248 K (CH ₂ I)	~13.0	13.0	6.3
(3.6) 	168 K (CCH ₂ Me)	~8.2	8.4	6.4
(3.1) 	268 K {C(CH ₃) ₃ }	~13.9	22.7	6.5
(4.4) 	-	-	23.8	6.6
(3.10) 	< 143 K	-	2.9	6.7

^a See these figures for the potential energy level diagram as calculated by MM3.^b The signals used for determining the barriers to rotation are those from the group in brackets

Table is continued on the next page.

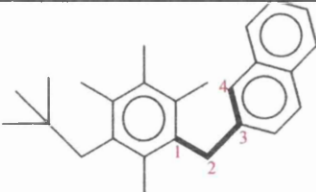
Continuation of Table 6.1.

Compound ↓	Decoalescence	$\Delta G_{exp}^{\#}$	$\Delta H_{calc.}^{\#}$	See figure ^a
	Temperature ^b	kcal mol ⁻¹	kcal mol ⁻¹	
(4.10) 	173 K (CCH ₂ Ph)	~8.4	6.2	6.8
	-	-	2.2 (<i>anti</i>) 3.6 (<i>syn</i>)	6.9 6.9
(4.5) 	173 K (ArCH ₃)	~8.2	6.0	6.10
	-	-	10.1 (<i>anti</i>) 9.0 (<i>syn</i>)	6.11 6.11
(4.8) 	-	-	4.4	6.12
	295 K Xylyl's (CH ₃)	14.2	4.4 (<i>anti</i>) 5.5 (<i>syn</i>)	6.13 6.13
(4.6) 	173 K (ArCH ₃)	~8.2	6.3	6.14

^a See these figures for the potential energy level diagram as calculated by MM3.^b The signals used for determining the barriers to rotation are those from the group in brackets

Table is continued on the next page.

Continuation of Table 6.1.

Compound ↓	Decoalescence Temperature	$\Delta G^{\ddagger}_{exp}$	$\Delta H^{\ddagger}_{calc.}$	See figure ^a
		kcal mol ⁻¹	kcal mol ⁻¹	
	-	-	5.6 (<i>anti</i>)	6.15
			6.3 (<i>syn</i>)	6.15

^a See these figures for the potential energy level diagram as calculated by MM3.

^b The signals used for determining the barriers to rotation are those from the group in brackets

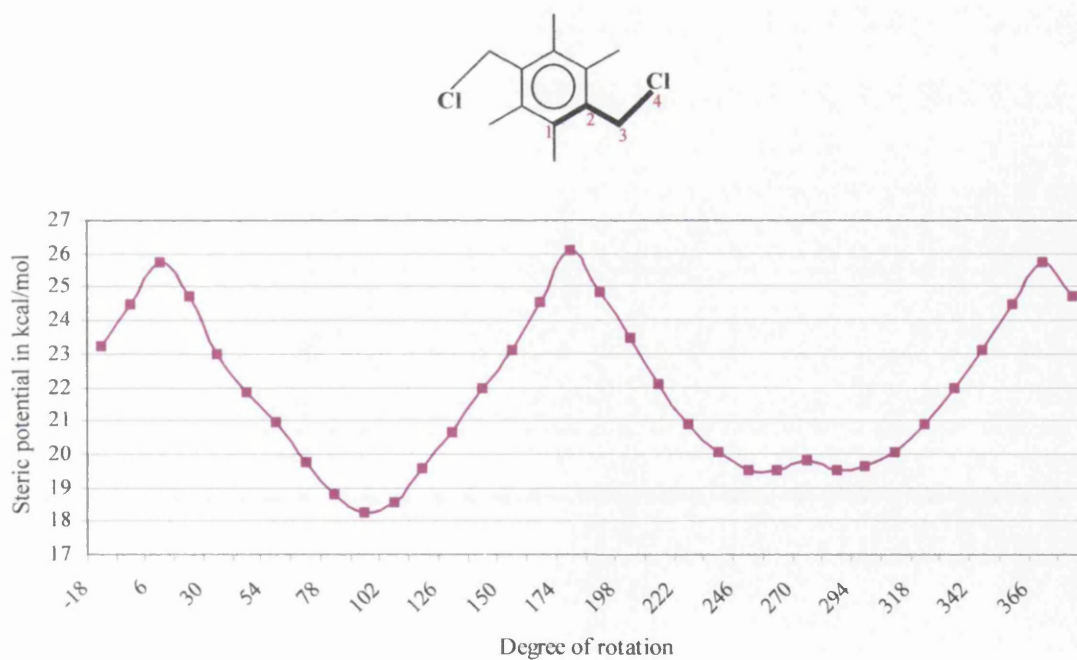


Figure 6.1. The potential-energy diagram calculated for the chloride (5.2) on driving the torsional angle ϕ , defined by C¹-C²-C³-C⁴, from -18 to +378°. When 0 < ϕ < 180° the conformation is *anti*.

$$\text{Calculated rotational barrier} = 7.9 \text{ kcal mol}^{-1}$$

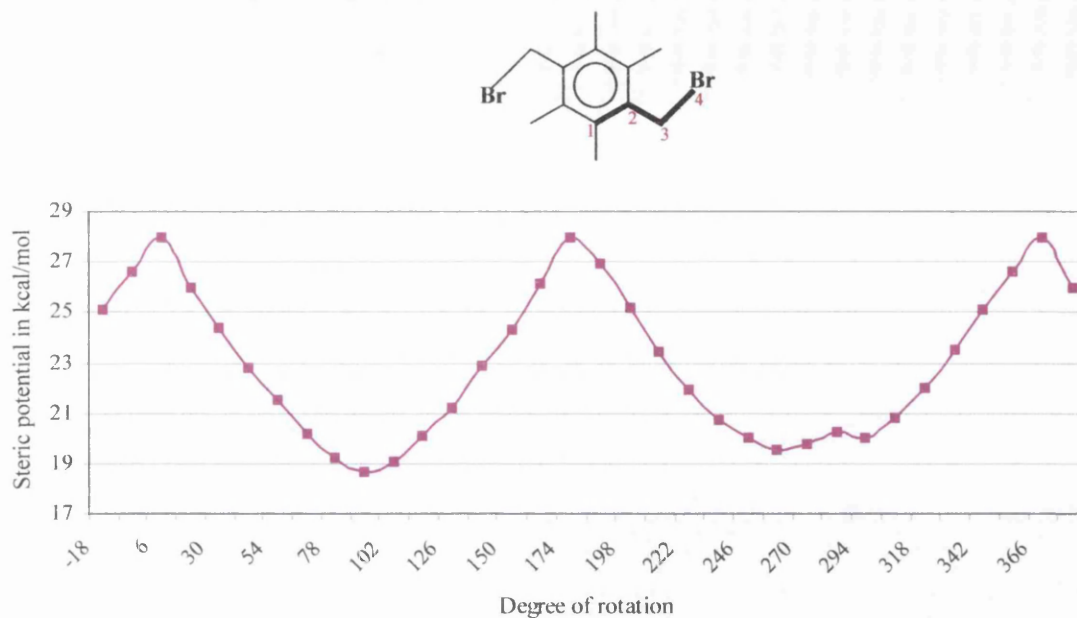


Figure 6.2. The potential-energy diagram calculated for the bromide (5.3) on driving the torsional angle ϕ , defined by C¹-C²-C³-C⁴, from -18 to +378°. When $0 < \phi < 180^\circ$ the conformation is *anti*.

Calculated rotational barrier = 9.4 kcal mol⁻¹

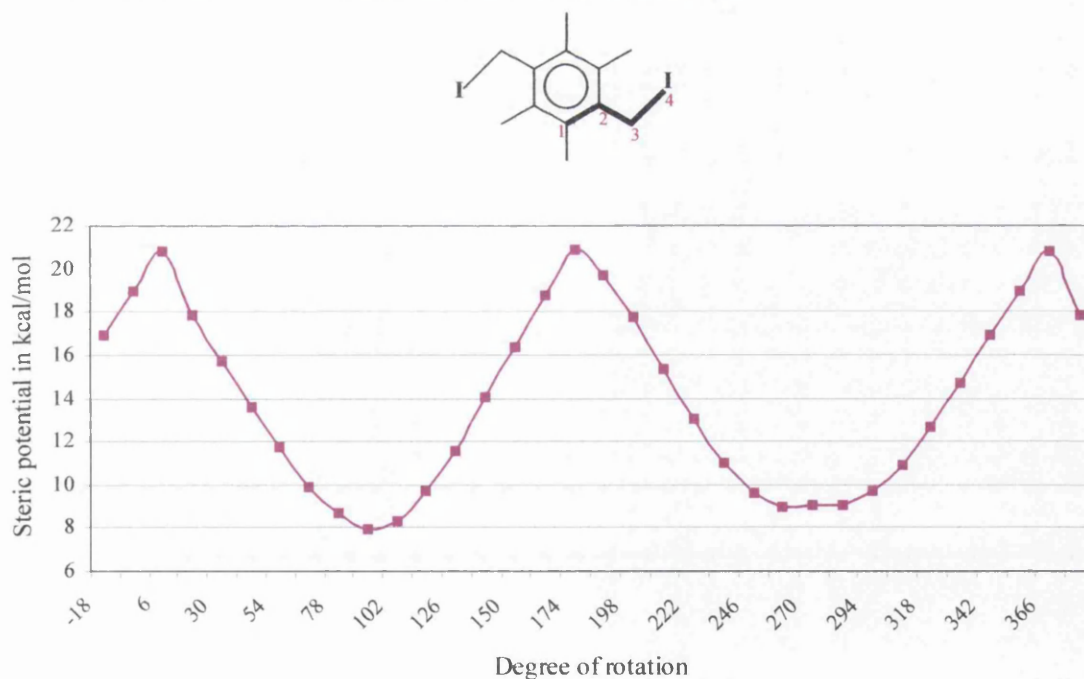


Figure 6.3. The potential-energy diagram calculated for the iodide (5.3) on driving the torsional angle ϕ , defined by C¹-C²-C³-C⁴, from -18 to +378°. When $0 < \phi < 180^\circ$ the conformation is *anti*.

Calculated rotational barrier = 13.0 kcal mol⁻¹

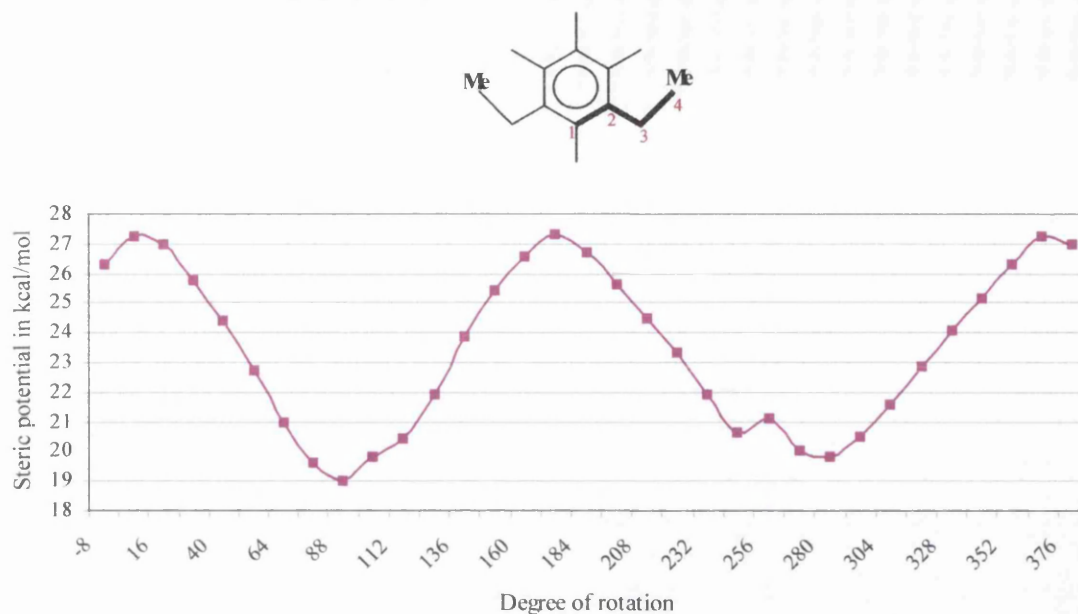


Figure 6.4. The potential-energy diagram calculated for **3.6** on driving the torsional angle ϕ , defined by C¹-C²-C³-C⁴, from -8 to +376°. When $0 < \phi < 180^\circ$ the conformation is *anti*.

Calculated rotational barrier = 8.4 kcal mol⁻¹

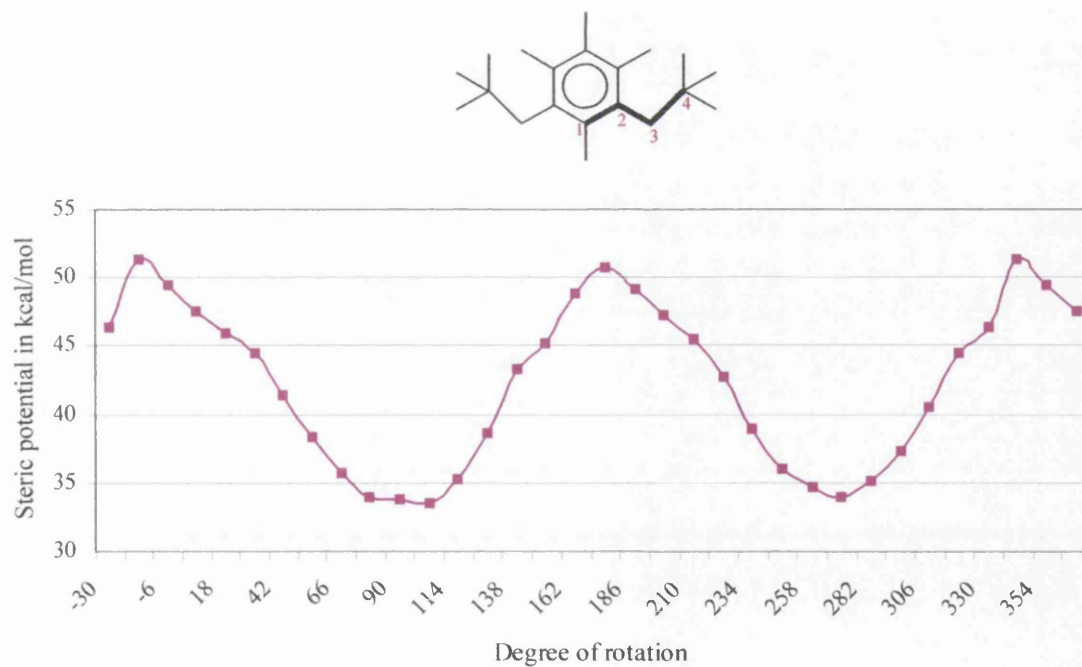


Figure 6.5. The potential-energy diagram calculated for **3.1** on driving the torsional angle ϕ , defined by C¹-C²-C³-C⁴, from -6 to +376°. When $0 < \phi < 180^\circ$ the conformation is *syn*.

Calculated rotational barrier = 22.7 kcal mol⁻¹

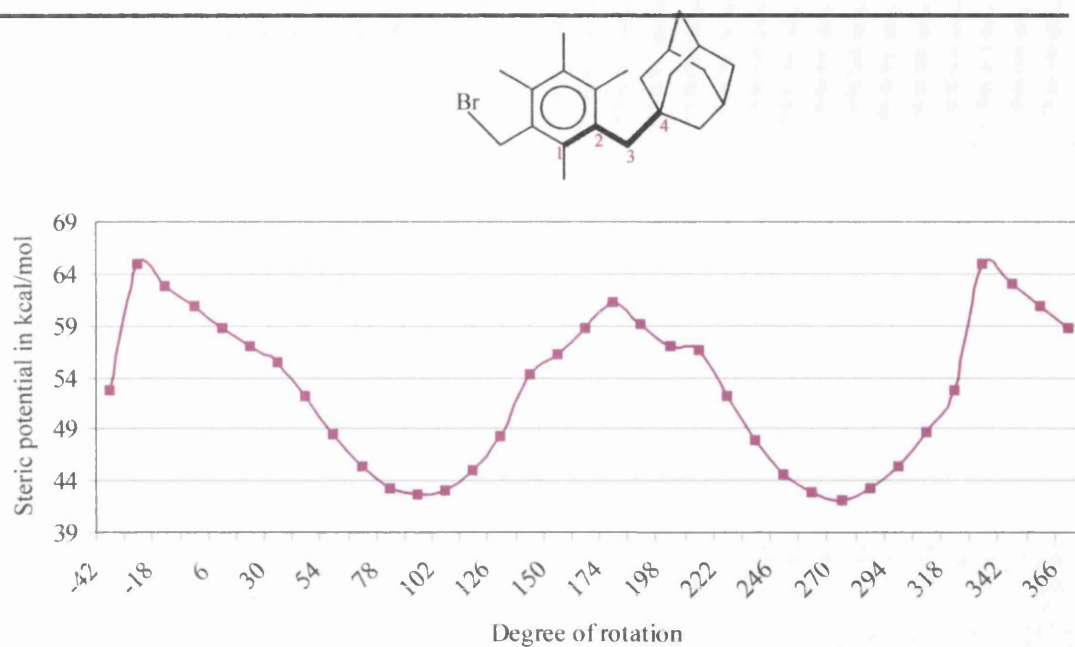


Figure 6.6. The potential-energy diagram calculated for **4.4** on driving the torsional angle ϕ , defined by C¹-C²-C³-C⁴, from -42 to $+366^\circ$. When $0 < \phi < 180^\circ$ the conformation is *syn*.

Calculated rotational barrier = $23.8 \text{ kcal mol}^{-1}$

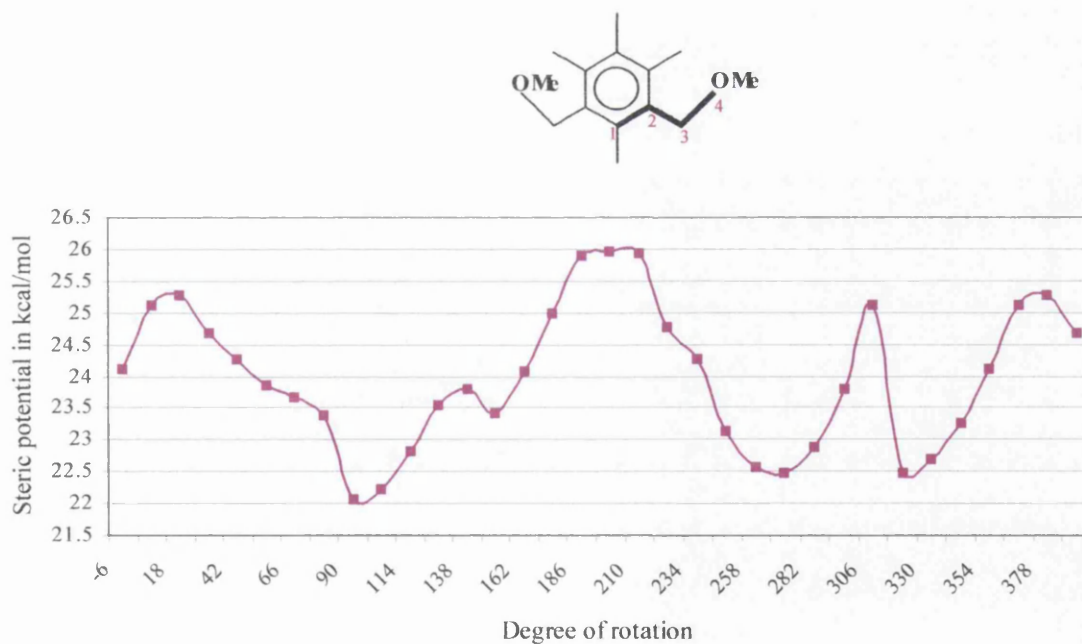


Figure 6.7. The potential-energy diagram calculated for **3.10** on driving the torsional angle ϕ , defined by C¹-C²-C³-C⁴, from -6 to $+390^\circ$. When $0 < \phi < 180^\circ$ the conformation is *syn*.

Calculated rotational barrier = $3.9 \text{ kcal mol}^{-1}$

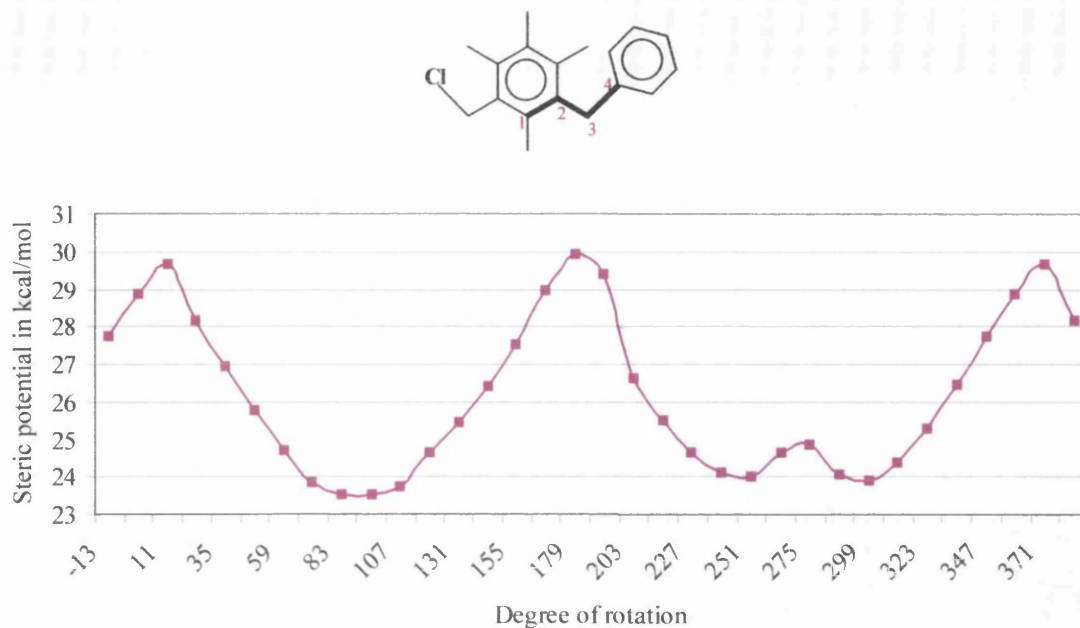


Figure 6.8. The potential-energy diagram calculated for **4.10** on driving the torsional angle ϕ , defined by C¹-C²-C³-C⁴, from -13 to +383°. When $0 < \phi < 180^\circ$ the conformation is *syn*.

Calculated rotational barrier = 6.2 kcal mol⁻¹

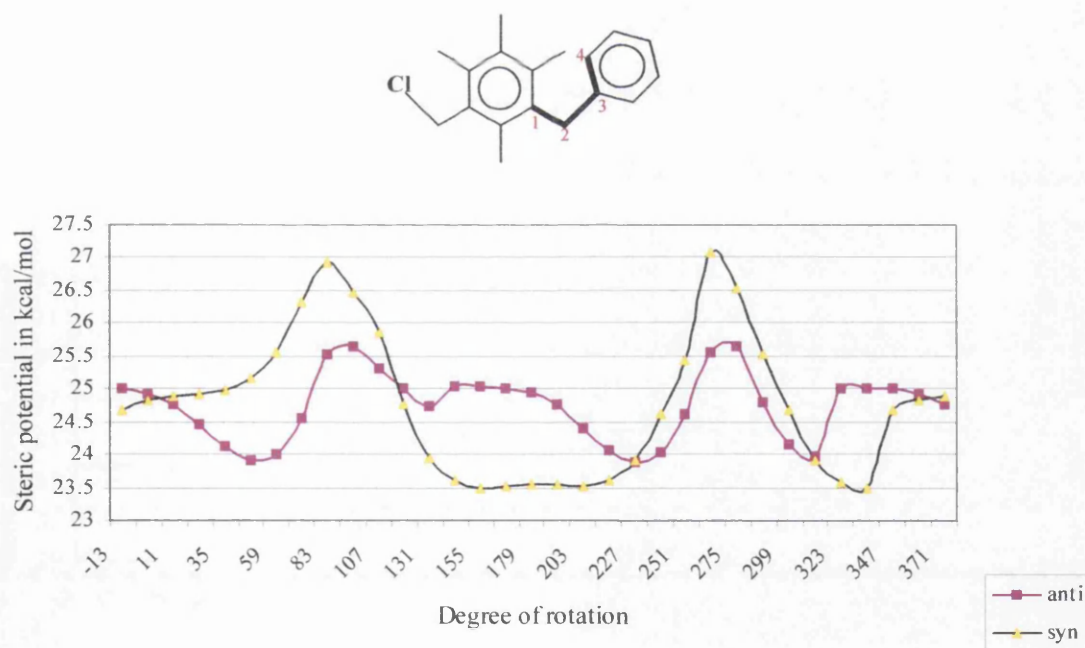


Figure 6.9. The potential-energy diagram calculated for the **4.10** on driving the torsional angle ϕ , defined by C¹-C²-C³-C⁴, from -13 to +371°.

Calculated rotational barrier for *anti* = 2.16 kcal mol⁻¹

Calculated rotational barrier for *syn* = 3.58 kcal mol⁻¹

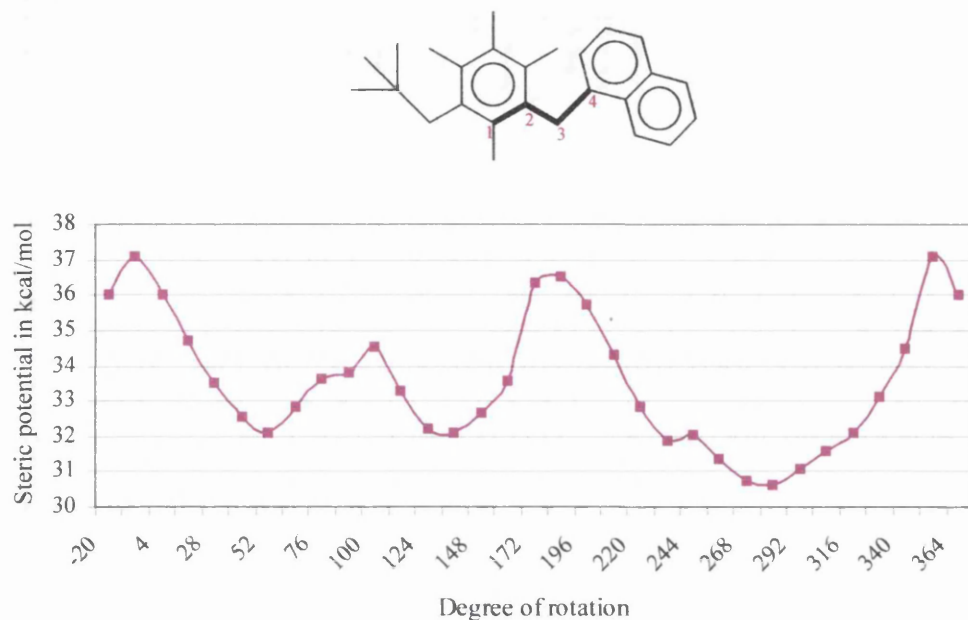


Figure 6.10. The potential-energy diagram calculated for **4.5** on driving the torsional angle ϕ , defined by C¹-C²-C³-C⁴, from -20 to $+364^\circ$. When $0 < \phi < 180^\circ$ the conformation is anti

Calculated rotational barrier = $6.0 \text{ kcal mol}^{-1}$

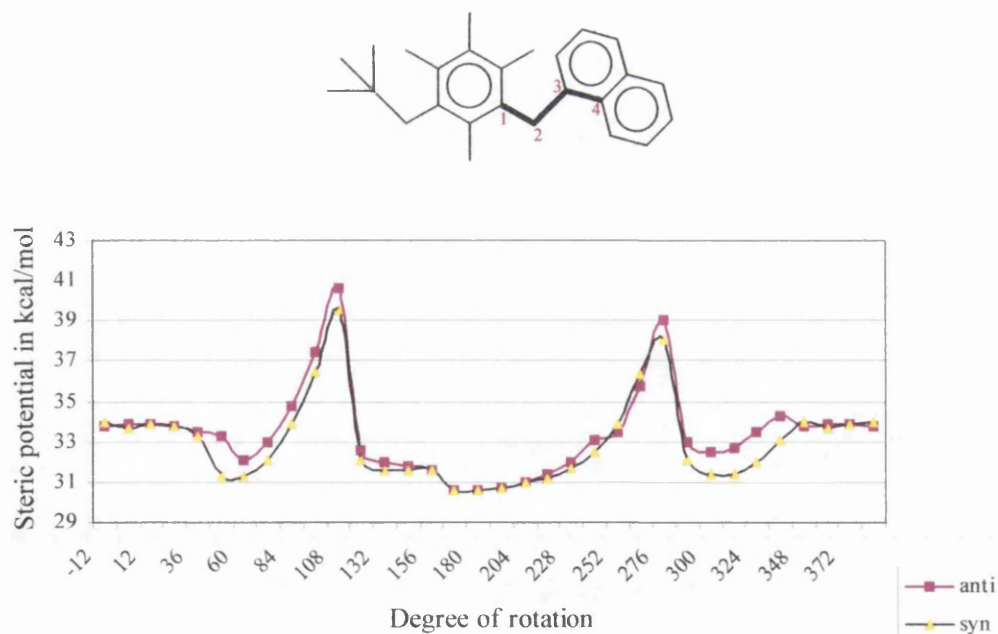


Figure 6.11. The potential-energy diagram calculated for **4.5** on driving the torsional angle ϕ , defined by C¹-C²-C³-C⁴, from -12 to $+384^\circ$.

Calculated rotational barrier for *anti* = $10.1 \text{ kcal mol}^{-1}$

Calculated rotational barrier for *syn* = $9.0 \text{ kcal mol}^{-1}$

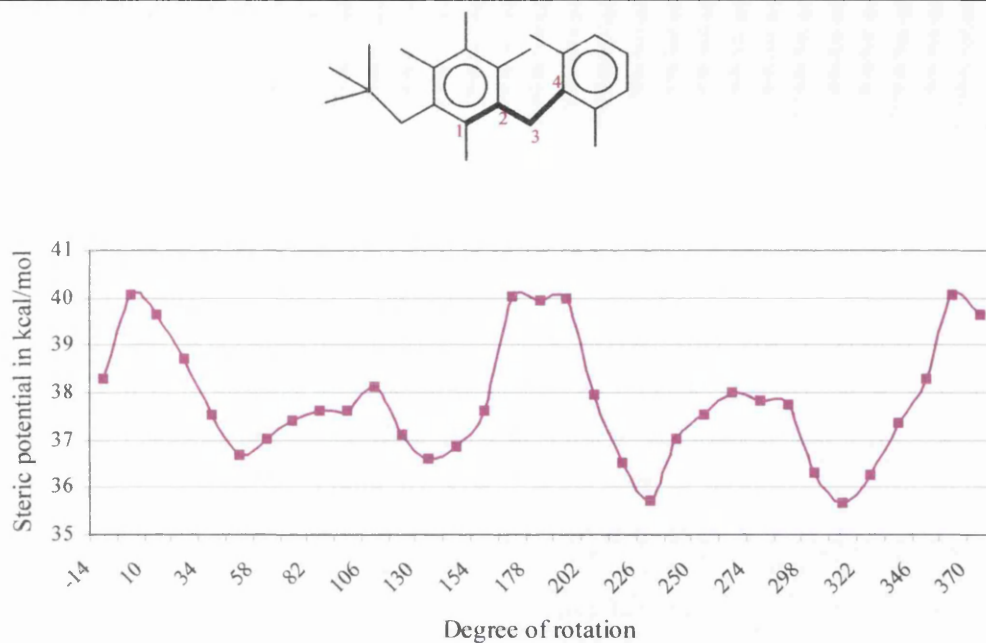


Figure 6.12. The potential-energy diagram calculated for **4.8** on driving the torsional angle ϕ , defined by C¹-C²-C³-C⁴, from -14 to $+384^\circ$. When $0 < \phi < 180^\circ$ the conformation is anti

Calculated rotational barrier = $4.4 \text{ kcal mol}^{-1}$

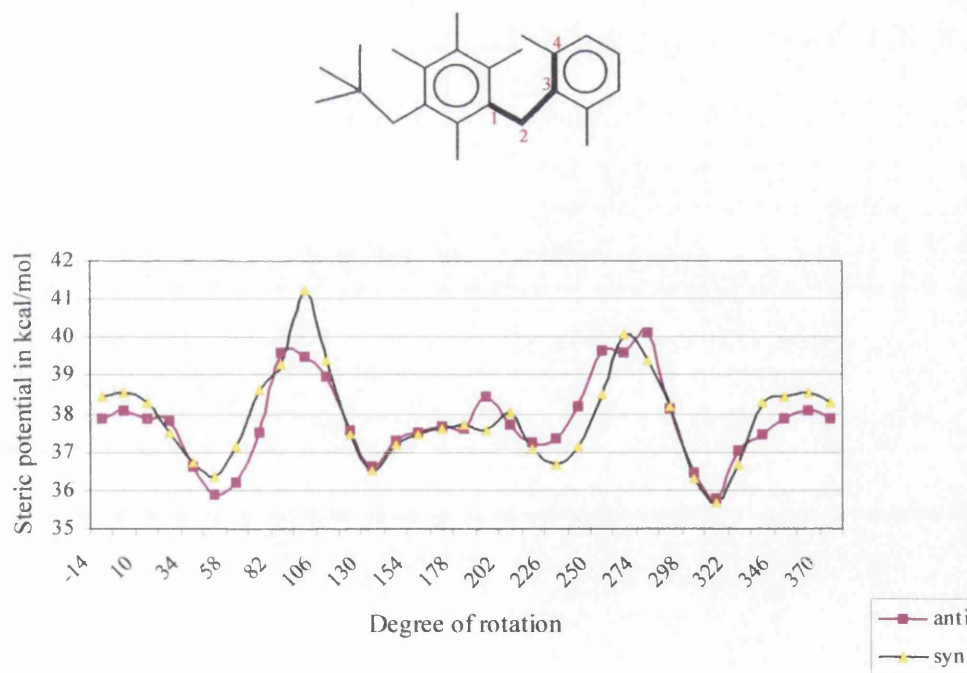


Figure 6.12. The potential-energy diagram calculated for **4.8** on driving the torsional angle ϕ , defined by C¹-C²-C³-C⁴, from -14 to $+384^\circ$.

Calculated rotational barrier for *anti* = $4.4 \text{ kcal mol}^{-1}$

Calculated rotational barrier for *syn* = $5.5 \text{ kcal mol}^{-1}$

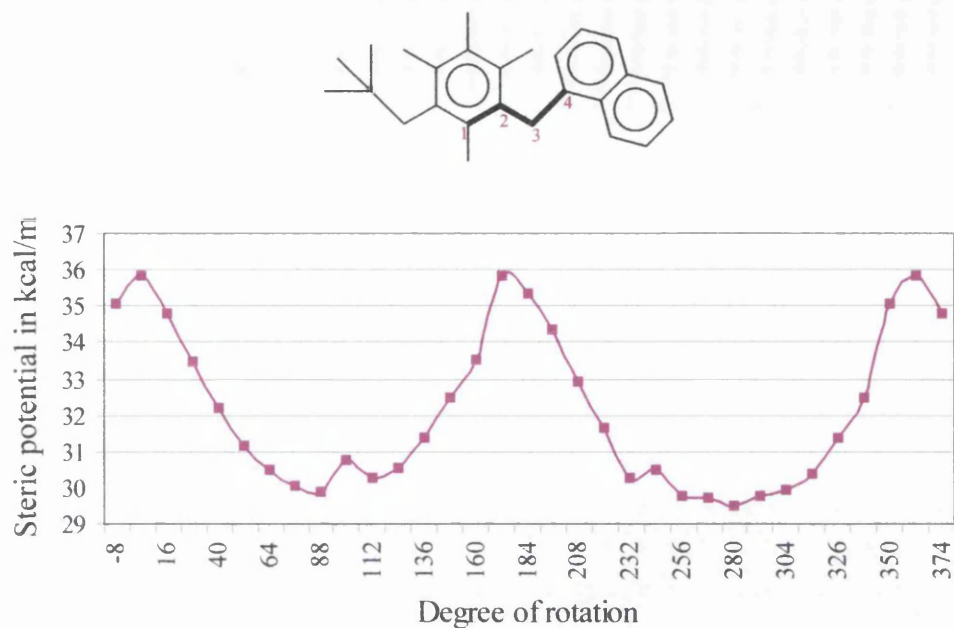


Figure 6.13. The potential-energy diagram calculated for **4.6** on driving the torsional angle ϕ , defined by C¹-C²-C³-C⁴, from -8 to +374°. When $0 < \phi < 180^\circ$ the conformation is anti

Calculated rotational barrier = 6.3 kcal mol⁻¹

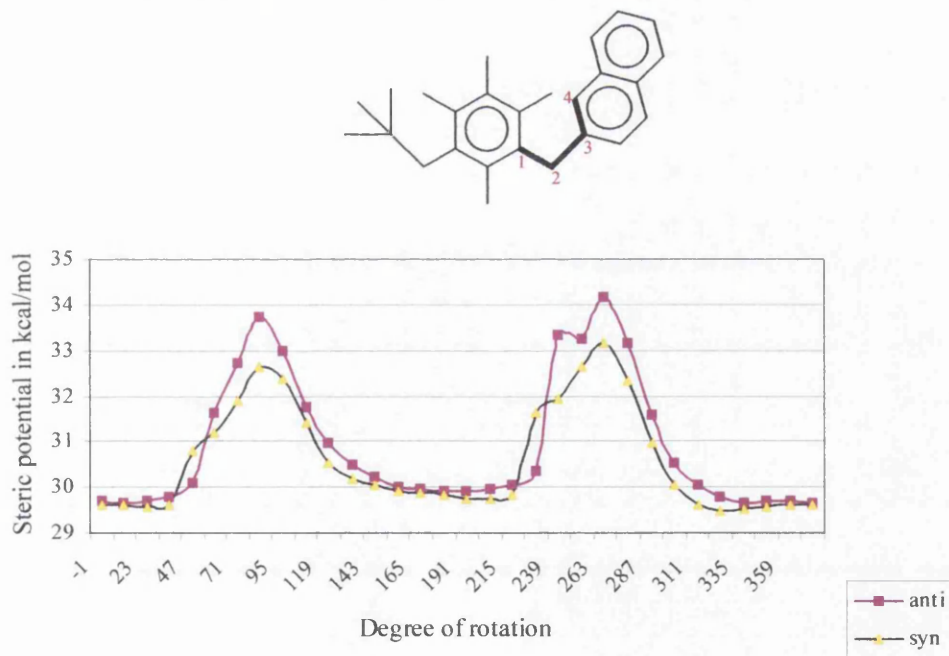


Figure 6.13. The potential-energy diagram calculated for **4.6** on driving the torsional angle ϕ , defined by C¹-C²-C³-C⁴, from -1 to +371°.

Calculated rotational barrier for *anti* = 5.6 kcal mol⁻¹

Calculated rotational barrier for *syn* = 4.2 kcal mol⁻¹

(6.3) Conclusion

The experimentally determined barrier to rotation about the $C^1C^2-C^3X$ bonds, increased in the order, when X is methyl→chlorine→bromine→iodine→*tert*-butyl, the barriers (ΔG^\ddagger) being about 8.2 (168 K), 10.3 (200 K), 11.4 (228 K), 13.0 (248 K) and 13.9 kcal mol⁻¹ (268 K) respectively. In cases, where X is spherical (this is not strictly true when X is CH₃ or a *tert*-butyl), the observed trend in the barriers probably reflects the effective size of the X group. It is also interesting to know that there are other examples in the literature⁵⁰, where the effective size of the methyl group relative to a chlorine or a bromine atom is in agreement with our result. However, other cases where the observed trend is in contradiction with our results are also available⁵⁰. In the contradicting examples, the effective size increases in the order (Cl < Br ≈ CH₃), (CH₃ ≈ Cl < Br) or (Cl < CH₃ < Br). The relative size of the CH₃ group was suggested to depend on the type of molecular system being investigated.

The barriers when X is a phenyl, α -naphthyl or a β -naphthyl group is just about the same as when X is a methyl group.

For the dineopentyl-compound, the experimentally determined barrier to rotation about the $C_{Ar}-CH_2^tBu$ bond is ~13.9 kcal mol⁻¹, a value which is about 8.8 kcal mol⁻¹ lower than calculations predicts. A possible explanation for the discrepancy is that whilst the results from experiment probably points towards a “stepwise rotational process” for rotation of the *tert*-butyl group past an adjacent CH₃, in contrast, calculations takes this rotation to be a “coupled disrotatory process” with the *tert*-butyl group forcing the CH₃ to rotate. Distinction between a stepwise rotational process and a coupled disrotatory process has been made in the literature⁵¹. It is also worth pointing out that the observed barrier of ~13.9 kcal mol⁻¹ is in agreement with that obtained for a *tert*-butyl group rotating past a methyl group in a similar compound, 1,3-dimethyl-2,4,6-trineopentylbenzene⁵⁰, the barrier being 15.4 kcal mol⁻¹.

The magnitude of the calculated barrier to rotation about the $C^1C^2-C^3X$ bond past a methyl group only agrees with experiments when X is a methyl group or an iodine atom. But in cases where X is a chloro-, bromo-, phenyl-, α -naphthyl- or β -naphthyl- group, calculations with respect to experiments underestimates the magnitude of the rotational barrier by about 2 kcal mol⁻¹. In the α -naphthyl-compound calculations predicts that the barrier to rotation about the $CH_2-C_{\alpha\text{-naphthyl}}$ bond is about 10.1 kcal mol

⁻¹, a value that is about 4 kcal mol⁻¹ higher than the calculated barrier to rotation about the C_{Ar}-CH₂C_{α-naphthyl}.

And finally the calculated barriers for the xylyl compound is unrealistically low in light of the results from dynamic NMR analysis (see chapter 4 section one).

Attractive Steric Interactions in Monosubstituted Cyclohexane

(7.1) Introduction

The previous chapters considered attractive steric interactions in hexasubstituted benzenes, in this chapter we report the results from preliminary investigations of attractive steric interactions in monosubstituted cyclohexanes.

In the majority of monosubstituted cyclohexanes, the equatorial conformer is more stable than the axial conformer. This trend is often rationalised in terms of the presence of a relatively higher destabilising 1,3-diaxial interactions in the axial conformer, these interactions are much more reduced in the equatorial conformer.

We aimed to synthesise and investigate monosubstituted cyclohexanes, where the more compact axial conformer might be the more stable. To achieve this the cyclohexane molecule is substituted in such a way that the various groups to be investigated (*R*) are at a distance more than the sum of their van der Waals radii from the cyclohexane ring. Inserting an acetylenic group between the ring and the *R* group did this, see figure 7.1. Since the atom(s) in the *R* group are not in close proximity to those in the cyclohexane ring, one would expect the nature of the interaction between them to be attractive and not repulsive. However, the level of attractive steric interactions between the *R* group and the cyclohexane ring would be expected to be different in the two conformations.

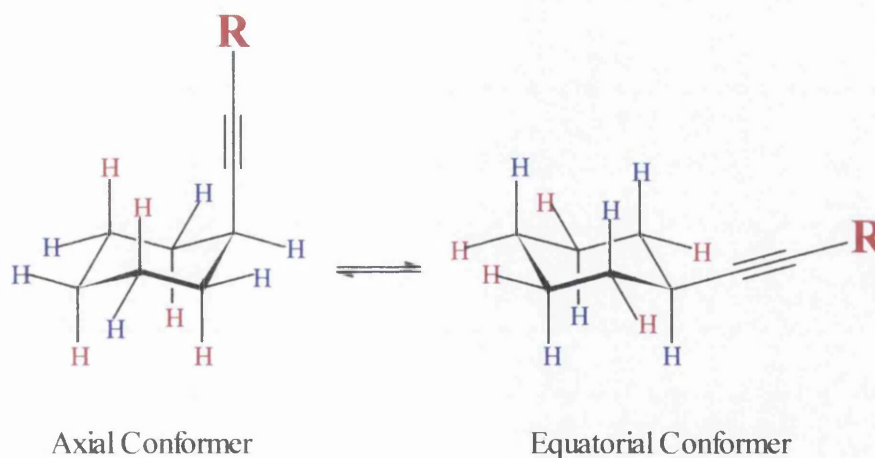


Figure 7.1.

The axial conformer is "L" shaped, with the *R* group positioned above the plane of the ring, in this arrangement, the *R* group and the methylene groups in the cyclohexane ring are much closer together and better placed for maximising mutual attractive steric interaction. By contrast, in the equatorial conformer the structure is almost linear, with the *R* group lying further away from the methylene groups of the ring.

On the basis that attractive steric interactions between the R group and the ring preferentially stabilises the axial conformer relative to the equatorial, we proposed that the bulkier the R group the more stable should be the axial conformer relative to the equatorial. And we foresaw a circumstance where the attractive steric interactions between the R group and the ring would be high enough to surpass the destabilising 1,3-diaxial interaction of the $\text{--C}\equiv\text{C--}$ group in the axial conformation, so the axial conformer would be the more stable.

We intended to synthesise and investigate attractive steric interactions in a series of compounds where the R group is; (7.1, H); (7.2, *t*-Bu); (7.3, Ad) and (7.4, CPh₃).

Determination of conformational population ratio using indirect NMR spectroscopy

The axial-equatorial conformational population ratio was determined by an indirect NMR method using coupling constants. For more on this method of analysis see chapter one.

For each of the compounds in the series (7.1 – 7.4), we hope to measure the methine vicinal couplings, $^3J_{ab}$ and $^3J_{ac}$ (see figure 7.2) from the proton NMR spectrum as well as the $^{13}\text{C}\text{--H}_a$ coupling from the uncoupled ^{13}C NMR spectrum at room temperature. These coupling constants should be a weighted average of the values in the

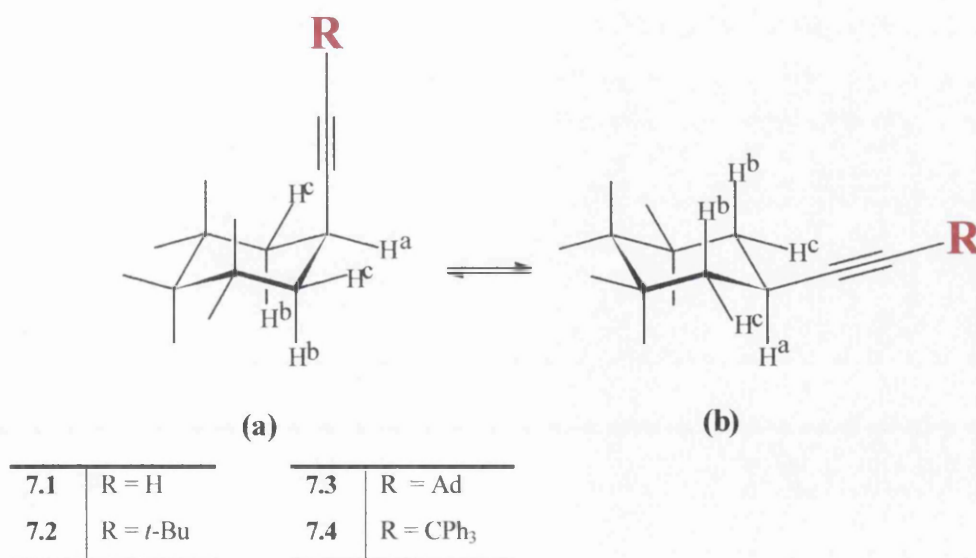


Figure 7.2. The axial and equatorial conformations of 7.1-7.4.

axial and equatorial conformers. We also intend to measure the corresponding $^3J_{ab}$, $^3J_{ac}$ and $^{13}\text{C}\text{--H}_a$ couplings in the conformationally locked model compounds, 7.5 and 7.6, for use as reference. However, in doing this we assume that the *tert*-butyl group has no intrinsic

effect on the coupling constants being measured. The coupling constants in 7.5 are equivalent to 100 % axial and the corresponding couplings in 7.6 are equivalent to 100 % equatorial.

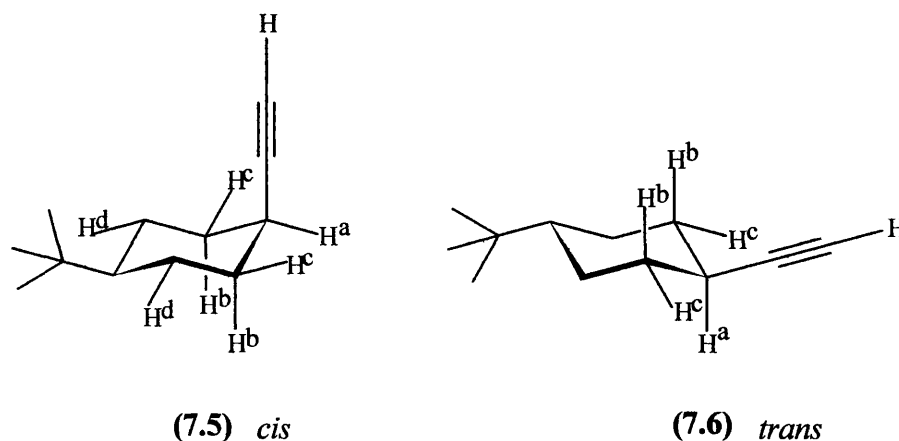


Figure 7.3.

(7.2) Results and Discussion

The compounds 7.1 and 7.2 were synthesised in low yields and attempts to synthesis 7.3 using a similar method, only gave traces of the desired product. All attempts to synthesis 7.4 were unsuccessful. The reference compounds 7.5 and 7.6 were synthesised as a mixture.

The coupling constants from the reference compounds are summarised in table 7.1. In 7.6, the methine proton appeared as triplet of triplets of doublets as a result of being coupled to H^b (12.0); H^c (3.6) and the acetylenic proton (2.5 Hz). As for 7.5, the equatorial methine proton appeared as a broad multiplet signal because of its small couplings to H^b , H^c , the acetylenic proton and H^d . $^3J_{ab}$ and $^3J_{ac}$ were obtained using the Karplus equation (I)⁵² in conjunction with MM3 calculations and NMR spectroscopy. ϕ (57.8°), as

$$^3J_{ac} = J^0 \cos^2 \phi - 0.28 \quad (0^\circ \leq \phi \leq 90^\circ) \quad \dots\dots\dots(I)$$

where J^0 is a constant and ϕ is the torsional angle

calculated by MM3 from 7.6 and $^3J_{ac}$ (3.6 Hz), as determined by NMR spectroscopy for 7.6 were used to determine the value of the constant J^0 (13.66 Hz) in the equation. With

knowledge of J^0 and the torsional angles ($\phi = 53$ and 63.3°), as calculated by MM3 from 7.5, $^3J_{ac}$ and $^3J_{ab}$ were calculated using the Karplus equation to be 4.7 and 2.4 Hz respectively.

Because the margin between the upper and lower limits is much higher in $^3J_{ab}$, in comparison to $^3J_{ac}$, and $^{13}\text{C-H}^a$, only the $^3J_{ac}$ set is used for referencing.

Table 7.1. Coupling constants from the reference compounds (7.5 and 7.6)

	Large coupling	Small coupling	
	$^3J_{ac}$ /Hz	$^3J_{ab}$ /Hz	$^{13}\text{C-H}^a$
(7.6) (<i>trans</i> isomer)	12.0	3.6	125.4
(7.5) (<i>cis</i> isomer)	4.7 ^a	2.4 ^a	122.4

^a The methine coupling constants were obtained using the Karplus equation in conjunction with MM3 calculations and the $^3J_{ac}$ coupling from the axial conformation.

The NMR results for 7.1-7.3 together with the energy differences are summarised in table 7.2. The observed coupling constants corresponds to an *equatorial/axial* substituent population ratio of (7.1, 1.6:1); (7.2, 1.2:1) and (7.3, 1.4:1) that are equivalent to free energy differences of (7.1, 0.27); (7.2, 0.12) and (7.3, 0.19 kcal mol⁻¹).

Table 7.2. The $^3J_{ab}$ coupling constants, the equilibrium constant together with the corresponding energy differences.

R	$^3J_{ab}$ Hz	Equilibrium constant ^a	ΔG_{exp} kcal mol ⁻¹
H (7.1)	9.2	1.6	-0.27
<i>tert</i> -butyl (7.2)	8.7	1.2	-0.12
1-Adamantyl (7.3)	8.9	1.4	-0.19

^a The equatorial/axial substituent population ratio

MM3 Calculations

Calculations show that in each of the three compounds (7.1-7.3), the equatorial conformation is more stable than the axial form. In 7.1, where R = H, the enthalpy difference is relatively high at about 0.29 kcal mol⁻¹ in favour of the equatorial conformation. Presumably, a high proportion of the enthalpy difference comes from the destabilising 1,3-diaxial interactions in the *axial* form. In 7.2 and 7.3, where R is bulky, the enthalpy difference is much lower at (7.2, 0.03) and (7.3, 0.03 kcal mol⁻¹) in favour of the equatorial form. The contributions to the steric energy are summarised in table 7.3.

When one considers the atom-atom pair wise steric interactions between the group of atoms in blue and those in red (see figure 7.4 and table 7.4), unlike in 7.1, the attractive part of the steric interactions in both 7.2 and 7.3 is just high enough to overcome the repulsive part of the interactions. And if a comparison between the set of data for 7.2 and 7.3 in table 7.4 is made, it is noticeable that the attractive steric interactions of an adamantyl group are hardly greater than those of the *tert*-butyl group even though it has twelve more atoms.

Table 7.3. The contributions to the final steric energies (kcal mol⁻¹) in 7.1, 7.2 and 7.3.

R →	H (7.1)		<i>tert</i> -Butyl (7.2)		1-Adamantyl (7.3)	
	<i>Axial</i>	<i>Equat.</i>	<i>Axial</i>	<i>Equat.</i>	<i>Axial</i>	<i>Equat.</i>
Compression	0.3517	0.3243	0.5539	0.5275	1.3122	1.2951
Bending	0.2552	0.1414	0.4143	0.3130	0.7793	0.6683
Bend-bend	-0.0091	-0.0115	-0.0273	-0.0292	-0.0338	-0.0364
Stretch-bend	0.0476	0.0316	0.0831	0.0683	-0.0324	-0.0493
van der Waals						
1,4 energy	6.6696	6.5946	10.0085	9.9247	20.3097	20.2243
Other	-0.5580	-0.6550	-1.4244	-1.2868	-2.3713	-2.1908
Torsional	1.7169	1.7559	1.6545	1.7069	8.1053	8.1269
Torsion-stretch	-0.0098	-0.0054	-0.0095	-0.0055	-0.0111	-0.0066
Dipole-dipole	1.8733	1.8738	2.6504	2.6503	2.6524	2.6518
Total Steric Energy (<i>H</i>)	10.3373	10.0498	13.9034	13.8689	30.7103	30.6833
-Δ<i>H</i>	+0.2875		+0.0345		+0.0270	

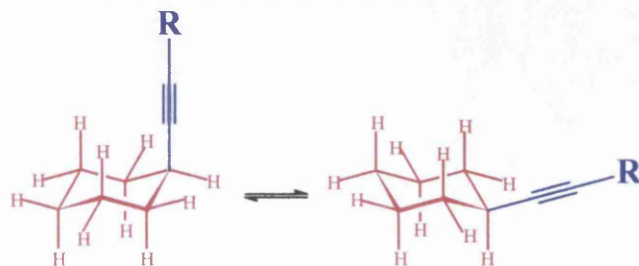


Figure 7.4.

Table 7.4 The atom-atom pair-wise steric interactions (kcal mol^{-1}) between the group of atoms in red and blue, see figure 7.4.

R \rightarrow	H (7.1)		<i>tert</i> -Butyl (7.2)		1-Adamantyl (7.3)	
	<i>Axial</i>	<i>Equat.</i>	<i>Axial</i>	<i>Equat.</i>	<i>Axial</i>	<i>Equat.</i>
Attractive	-0.6820	-0.5370	-1.4006	-0.9877	-1.4760	-1.1269
Repulsive	+1.5878 ^a	+1.2808 ^b	+1.6243 ^a	+1.2914 ^b	+1.5870 ^a	+1.2819 ^b
Sum	+0.9058	+0.7438	+0.2237	+0.3037	+0.1110	+0.1550
Difference	+0.1620		-0.0800		-0.0450	

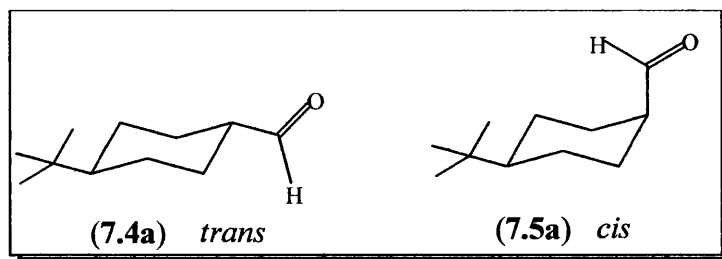
^a Total of 6 pair-wise repulsive steric interactions.

^b Total of 4 pair-wise repulsive steric interactions.

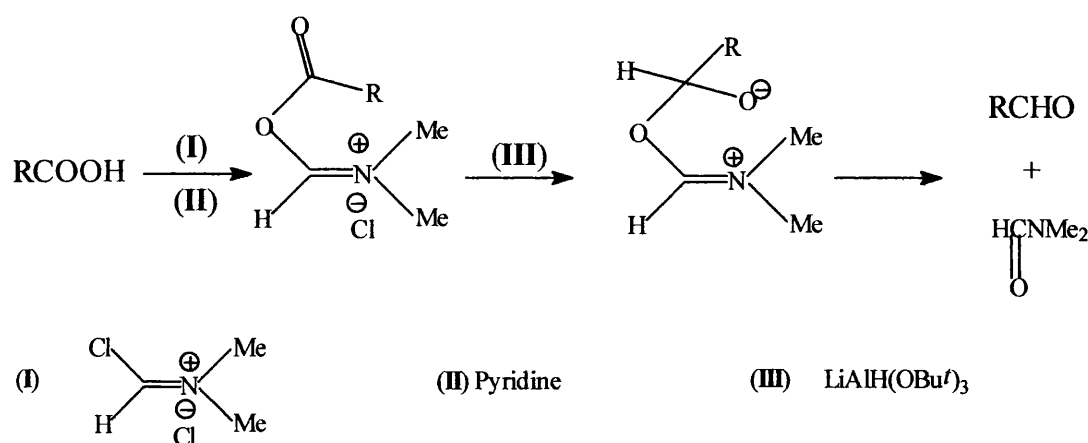
(7.3) Conclusion

Experiments show that in the cyclohexylacetylene compound (7.1), the equatorial conformation is more stable than the axial form in both 7.2 and 7.3. Replacing the acetylenic proton with a *tert*-butyl or an adamantyl group only lead to a slight reduction in the magnitude of the equatorial advantage, suggesting that the attractive steric interactions between these bulky groups and the cyclohexane ring, in the axial conformation, is not high enough to counterbalance the destabilising 1,3-diaxial interactions. NMR also indicates that the magnitude of ΔG_{exp} for a *tert*-butyl or a adamantyl substituent is just about the same and calculation is in agreement with this observation.

Calculations agree with NMR analysis as to which conformation is the more stable and also show that when the acetylenic proton is replaced with the bulky groups a high proportion of the axial 1,3-diaxial interactions in the axial conformation is overcome by attractive steric interactions between the R group and the ring.

(7.4) Synthesis

4-*t*-butylcyclohexanecarboxaldehyde:⁵³ mixture of (7.4a) and (7.5a) (see scheme 1)



Scheme 1.

The reaction was carried out under an inert atmosphere of nitrogen. *N,N*-dimethylchloromethyleniminium chloride salt (I) was synthesised as follows:- Excess oxalyl chloride (19.8 ml of 2 M dichloromethane solution, 39.6 mmol) was added dropwise to a stirred solution of *N,N*-dimethylformamide (0.91 ml, 11.7 mmol) in dichloromethane (2.4 ml) at 0°C. The mixture was stirred at the same temperature for 1h. The solvent was removed under reduced pressure leaving the salt as a white solid.

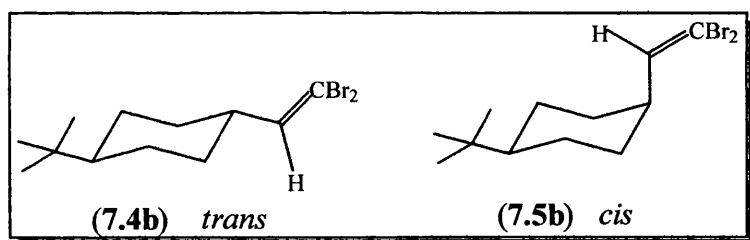
An inert atmosphere of nitrogen was re-established and acetonitrile (18 ml) and THF (30 ml) were added to the salt. The mixture was cooled to -30 °C. A solution of 4-*t*-butylcyclohexanecarboxylic acid (mixture of the *cis* and *trans* isomers) (2.16 g, 11.7 mmol) and pyridine (0.95 ml 11.7 mmol) in THF (18 ml) were added dropwise at -30 °C. The resultant mixture was stirred at the same temperature for 1h.

To the reaction mixture was added a suspension of 10 mol % copper (I) iodide in THF and lithium tri-*tert*-butoxyaluminumhydride (46.0 ml of 0.5 M diglyme solution, 23

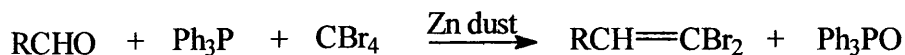
mmol) at -78°C . After stirring at -78°C for 0.5 h the reaction was quenched by the addition of 2 M hydrochloric acid solution (50.0 ml).

The organic layer was extracted with diethyl ether (4 x 40 ml). The ethereal extract was washed with a 4 M sodium hydroxide solution (15.0 ml) and water (4 x 40 ml) before drying over anhydrous magnesium sulfate. The solvent was removed under reduced pressure leaving an oily yellow liquid crude product (1.93 g). The crude product was made purer by flash column chromatography using silica gel as the stationary phase and petroleum spirit 30-60 $^{\circ}\text{C}$: ethyl acetate (8.6:1.4) as the eluting solvent to give the aldehydes (0.91 g).

400 MHz ^1H NMR (CDCl_3) δ /ppm 0.76 {s, 9H, $\text{C}(\text{CH}_3)_3$, *cis* }; 0.82 {s, 9H, $\text{C}(\text{CH}_3)_3$, *trans*}; 2.05-2.15 (ttd, 1H, methine proton, *trans*); 2.34-2.40 (m, 1H, methine proton, *cis*); 9.57 (d, $J = 1.7$ Hz, 1H, *trans* CHO); 9.68 (s, 1H, *cis* CHO); 0.8-2.05 (m, ring methylene protons).



4-tert-butylcyclohexylidenedibromoolefin:⁵⁴ mixture of (7.5b) and (7.6b)

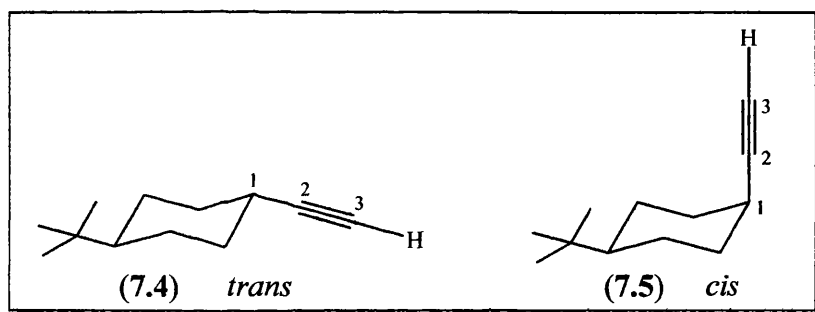


Under an inert atmosphere of nitrogen, a solution of triphenylphosphine (3.00 g, 11.4 mmol) in dichloromethane (12 ml) was added to a stirred mixture of carbon tetrabromide (3.76 g, 11.4 mmol) and zinc dust (1.50 g, 22.7 mmol) in dichloromethane (24 ml). The resultant mixture was stirred at 23°C for 2 days. A solution of 4-tert-butylcyclohexanecarboxaldehyde (**2a**, **2b**) (0.91 g, 5.41 mmol) in dichloromethane (10 ml) was added to the light brown mixture and stirred for 5 h.

The dark brown mixture was poured into petroleum spirit (30-40 $^{\circ}\text{C}$) (180 ml, 4 equivalent) and stirred vigorously until the precipitate harden. The mixture was filtered and the filtrate collected. The residue was reworked with two cycles of dichloromethane extraction and petroleum spirit 30-40 precipitation. The solvent in the combined filtrate

was removed under reduced pressure leaving a liquid-solid mixture. Diethyl ether (30 ml) was added to the mixture, stirred and then filtered. The filtrate was concentrated and the resultant crude product was purified by flash column chromatography using silica gel as the stationary phase and petroleum spirit (40-60 °C) as the eluting solvent to give the product (1.01 g) as a colourless liquid.

400 MHz ^1H NMR (CDCl_3) δ /ppm 0.82 {obs. s, 9H, $\text{C}(\text{CH}_3)_3$, *trans*}; 0.83 {obs. s, 9H, $\text{C}(\text{CH}_3)_3$, *cis* }; 2.15-2.25 (m, 1H, methine proton, *trans*); 2.61-2.72 (m, 1H, methine proton, *cis*); 6.16 (d, $J = 9.2$ Hz, 1H, alkenic proton, *trans*); 6.64 (d, $J = 9.2$ Hz, 1H, alkenic proton, *cis*); 0.8-1.9 (m, ring methylene protons).



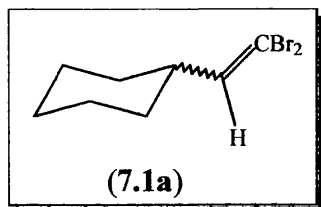
4-*tert*-butylcyclohexylacetylene:⁵⁴

Under an inert atmosphere of nitrogen, a solution of *n*-butyl lithium (2.7 ml, 2.0 M in pentane, 5.4 mmol) was added to a solution of the dibromoolefin (7.4b/7.5b) (0.85 g, 2.6 mmol) in THF (20 ml) at -78 °C. The mixture was stirred at -78 °C for 1h and then at 22 °C for another hour. The reaction mixture containing the acetylide ion was quenched by the addition of water (20 ml).

The organic phase was separated and the aqueous layer was extracted with diethyl ether (3 x 15 ml). The combined organic phase was washed with water and then dried over anhydrous magnesium sulfate. The solvent was removed under reduced pressure leaving a yellow liquid product (0.30 g)

400 MHz ^1H NMR (CDCl_3) δ /ppm 0.83 (s, 9H, $\text{C}(\text{CH}_3)_3$, *trans*); 0.86 (s, 9H, $\text{C}(\text{CH}_3)_3$, *cis*); 2.03 (d, $J = 2.5$ Hz, 1H, acetylenic proton, *trans*); 2.04 (d, $J = 2.5$ Hz, 1H, acetylenic proton, *cis*); 2.08-2.17 (ttd, 1H, methine proton, *trans*); 2.74-2.79 (m, 1H, methine proton, *cis*); 0.8-2.05 (m, ring methylene protons).

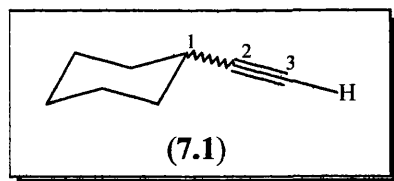
100.6 MHz ^{13}C NMR (CDCl_3) δ/ppm 22.67; 26.57; 26.81; 27.44 $\{\text{C}(\text{CH}_3)_3 \text{ trans }\}$; 27.46 $\{\text{C}(\text{CH}_3)_3 \text{ cis }\}$; 29.48; 31.33; 33.50; 32.39; 32.55; 47.23 (C^1 , *trans*); 48.12 (C^1 , *cis*); 67.33 (C^2 , *trans*); 69.05 (C^2 , *cis*); 87.96 (C^3 , *cis*); 89.25 (C^3 , *trans*).



Cyclohexanedibromoolefin: (7.1a)

The procedure described for the synthesis of 4-*tert*-butylcyclohexanedibromoolefin from the aldehyde was followed but using cyclohexanecarboxaldehyde (0.55 g, 9.0 mmol), triphenylphosphine (2.40 g, 9.15 mmol), carbon tetrabromide (3.03 g, 9.15 mmol) and zinc dust (0.6 g, 9.15 mmol). The product (1.2 g) was obtained as a colourless liquid

200 MHz ^1H NMR (CDCl_3) δ/ppm 0.95-1.46 (m, 6H, β - and γ - CH_2); 1.5-1.84 (m, 4H, α - CH_2); 2.10-2.40 (m, 1H, methine proton); 6.15 (d, 1H, alkenic proton).

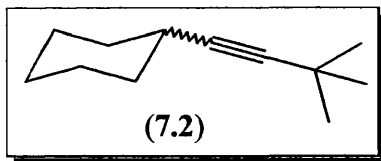


Cyclohexaneacetylene: (7.1)

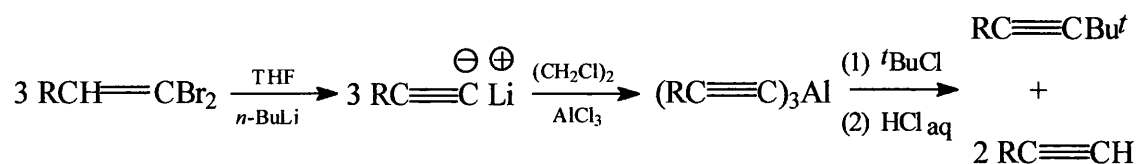
The procedure described for the synthesis of 4-*tert*-butylcyclohexylacetylene was followed but using *n*-butyllithium (6.5 ml, 2.0 M in pentane, 13.0 mmol) and cyclohexanedibromoolefin (1.6 g, 6.0 mmol).

400 MHz ^1H NMR (CDCl_3) δ/ppm 2.06 (d, $J = 2.5$ Hz, 1H, acetylenic proton); 2.43 (m, 1H, methine proton).

100.6 MHz ^{13}C NMR $\{\text{CHCl}_2\text{F}:\text{CHClF}_2:\text{CD}_2\text{Cl}_2 \text{ (c.a. 2:2:1)}\}$ δ/ppm 25.83, 26.82, 29.96 (ring carbons); 33.70 (C^1); 68.38 (C^2); 89.88 (C^3).



Synthesis of (7.2)⁵⁵ see scheme 2



Scheme 2.

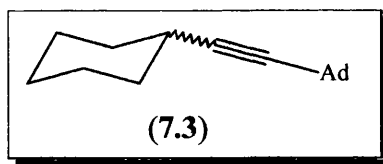
The reaction was carried out under argon. A solution of *n*-butyllithium (23 ml, 2.0 M in pentane, 46 mmol) was added dropwise to a solution of cyclohexyldibromoolefin (6.01 g, 22.4 mmol) in THF (60 ml) at -78 °C. The solution was stirred at -78 °C for 1 h and then at 21 °C for another hour. The solvent was removed under vacuum leaving a white residue.

Hexane (40 ml) was added to the residue and then cooled to 0 °C. Powdered anhydrous aluminium chloride (1.0 g, 7.5 mmol) was added to the white mixture and stirred at the same temperature for 1 h.

The solvent was removed under vacuum leaving a white residue. The residue was dissolved in 1,2-dichloroethane (50 ml) and then cooled to 0 °C. *tert*-Butylchloride (0.70 g, 7.5 mmol) was added to the mixture and stirred at 0 °C for 3 h. The reaction was quenched by pouring the resultant brown mixture into 3 M hydrochloric acid (50 ml) at 0 °C and stirred for 10 min.

The organic phase was separated and the aqueous phase was extracted with ether (3 x 20 ml). The combined organic phase was washed with water and then dried over anhydrous magnesium sulfate. The solvent was removed under reduced pressure leaving a red oily crude product (1.71 g). The crude product was made purer firstly by flash column chromatography using silica gel as the stationary phase and petroleum spirit (40-60 °C) as the eluting solvent and secondly by distillation. The fraction that boiled at 63 °C (10 mmHg pressure) was collected.

400 MHz ¹H NMR (CDCl₃) δ/ppm 1.19 {obs. s, 9H, C(CH₃)₃}; 1.6-1.8 (m, 4H, α-CH₂); 2.25-2.40 (m, 1H, methine proton)

**Synthesis of (7.3)**

The procedure described above was followed but using cyclohexanedibromoolefin (1.02 g 3.78 mmol), *n*-butyllithium (1.89 ml, 2.0 M solution in pentane, 3.78 mmol) 1-bromoadamantane (0.27 g, 1.26 mmol) and aluminium chloride (168 g, 1.26 mmol). A trace of the product was obtained.

400 MHz ^1H NMR (CDCl_3) δ/ppm 2.33 (tt, 1H, methine proton).

General Information

Experimental Considerations

Synthesis

Reagents used for synthesis are commercially available from Aldrich or Fluka. Flash column chromatography was performed using flash silica gel of particle size 0.13-0.25 mm and melting points were taken using an Electrothermal melting point apparatus.

NMR spectroscopy

Dynamic NMR spectra, unless indicated otherwise, were obtained using a Varian VXR-400 spectrometer operating at 400 MHz for ^1H and 100.6 MHz for ^{13}C nucleus. And NMR samples were prepared by dissolving ~12 mg of the substrate in ~1 ml of solvent.

The probe and the interconversion process were giving sufficient time to equilibrate before recording each spectrum at low temperatures. In practice this meant cooling was done initially in steps of 20 $^{\circ}\text{C}$ and then 10 $^{\circ}\text{C}$ or lower, at temperatures close to the decoalescence point. And after cooling the probe to a particular temperature, the sample was given at least ~20 min to equilibrate before recording the spectrum.

For each sample, the deuterated solvent present is used for referencing the chemical shifts.

A delay between pulses of 2 seconds is used when recording the ^{13}C NMR spectra so as to allow sufficient time for relaxation to take place before pulsing.

Before measuring the relative intensity of peaks NMR spectra were properly faced to give a straight baseline. Determination of the relative intensity of two singlet peaks that are well separated was accomplished using one of two methods, by electronic integration and by photocopying the signal on to a "3000 laser copier paper" before cutting out the signal and weighing on a Precisa 125A analytical weighing balance. The errors associated with measuring the equilibrium constant using both methods is lower than ± 0.1 . On the other hand when the signals slightly overlap one another, the relative intensity of the two peaks was obtained by computer simulation of the spectrum using a dynamic NMR simulating program, based on the Mc Cunnell modification⁵⁶ of the Bloch equations. During the simulation, a high rate constant of 1000 s^{-1} was used and the relative intensities of the two peaks is altered until a best fit for the spectrum is obtained. The errors associated with measuring the equilibrium constant using this method is lower than ± 0.2 .

The N.O.E difference spectroscopy experiment was carried out at a temperature well below the coalescence point in order to minimise transfer of N.O.E. from one conformation to another.

Abbreviations

Ad	adamantyl group
Ar	aromatic
arom	aromatic
aq	aqueous
b.p.	boiling point
calc	calculation
d	doublet
exp	experiment
m	multiplet
m.p.	melting point
NMR	Nuclear Magnetic Resonance
obs.	observed
Ph	phenyl
s	singlet
sol.	solution
t	triplet

References

- 1) For a comprehensive discussion of this, see P.W. Atkins; *Physical Chemistry*, Oxford press, (1978) Chap. 23, p. 747. R. A. Alberty and R. J. Silbey; *Physical Chemistry*, First Edition, John Wiley & Sons Inc., (1992), Chap. 12, p. 415.
- 2) R. E. Carter, B. Nilsson, K. Olsson; *J. Amer. Chem. Soc.*, **97**, 6155, (1975).
- 3) B. Nilsson, P. Martinson, K. Olsson and R. E. Carter; *J. Amer. Chem. Soc.*, **96**, 3190 (1974).
- 4) R. E. Carter and P. Stilbs; *J. Am. Chem. Soc.* **98**, 7515, (1976).
- 5) B. Aurivillius and R. E. Carter; *J. Chem. Soc. Perkin Trans. 2*, 1033, (1978).
- 6) M. H. Lyttle, A. Streitweiser, Jr., and R. Q. Klutz; *J. Amer. Chem. Soc.*, **103**, 3232, (1981).
- 7) L. A. Paquette, G. J. Hefferon, R. Samodral and Y. Hanzawa; *J. Org. Chem.*, **48**, 1262, (1983).
- 8) J. E. Anderson, P. A. Kirsch; *J. Chem. Soc., Perkin Trans. 2*, 885 (1990).
- 9) J. E. Anderson, P. A. Kirsch; *J. Chem. Soc., Perkin Trans. 2*, 1951 (1992).
- 10) J. E. Anderson, H. D. Beckaus and C. Ruchardt; *Tetrahedron*, **38**, 2299 (1982).
- 11) J. E. Anderson unpublished results.
- 12) T. Harada, H. Kurokawa, Y. Kagamihara, S. Tanaka, A. Inoue and A. Oku; *J. Org. Chem.*, **57**, 1412, (1992).
- 13) T. Harada, S. Tanaka, A. Inoue, A. Oku, J. Uchimura and I. Wada; *J. Amer. Chem. Soc.*, **115**, 7665, (1993).
- 14) N. S. Angerman, S. S. Danyluk and T. A. Victor; *J. Amer. Chem. Soc.*, **94**, 7137, (1972).
- 15) J. H. van't Hoff; *Bull. Soc. Chim. France* **23**, 295, (1875).
- 16) H. Sachse; *Ber.* **23**, 1363 (1890).
- 17) H. Sachse; *Phys. Chem.* **10**, 203 (1892).
- 18) E. J. Mohr; *J. Prakt. Chem.* **98**, 315 (1918).
- 19) Eusebio Juaristi, "Conformational Behavior of Six-Membered Rings" VCH Publishers, Inc. (1985) chapter. 2, p. 28.
- 20) F. R. Jensen and L. H. Gale; *J. Amer. Chem. Soc.*, **91**, 344 (1969).
- 21) F. R. Jensen, C. H. Bushweller and B. H. Beck; *J. Amer. Chem. Soc.*, **81**, 6337 (1959).

- 22) F. A. L. Anet, J. Krane, W. Kitching, D. Doddrel and D. Praeger; *Tetrahedron lett.* 3255, (1974).
- 23) P. F. Baron, W. Kitching and D. Doddrel; *J. Organometallic Chem.* **139**, 361, (1977).
- 24) K. Kwetkat and W. Kitching; *J. Chem. Soc., Chem. Commun.* 345, (1994).
- 25) E. L. Ernest and S. H. Wilen "*Stereochemistry of Organic Compounds*" A Wiley-Interscience Publication (1994) chapters 10.4 and 11.4.
- 26) E. L. Eliel; *Chem. Ind. (London)*, 1102. (1955).
- 27) E. L. Eliel, E. W. Della, T. H. Williams; *Tetrahedron lett.* 831, (1963).
- 28) P. J. D. Park, R. A. Pethrick and B. N. Thomas; "*Infrared and Raman band intensities and conformational change*", in W. J. Orville-Thomas, Ed., *Internal Rotation in molecules*, Wiley, New York, p. 57.
- 29) D. H. Williams and I. Fleming; "*Spectroscopic methods in organic chemistry*" McGraw-Hill book company, fourth edition, p. 91, (1989).
- 30) U. Burket and N. L. Allinger; *Molecular Mechanics*, ACS Monograph 177 American Chemical Society, Washington (1982). See also N. L. Allinger "*Molecular Mechanics*" in A. Domenicano, I. Harggitai, Eds., *Accurate Molecular Structures*, University Press, New York, p. 336 (1992).
- 31) J. H. Lii, N. L. Allinger; *J. Comput. Chem.* **13**, 1138, (1992).
- 32) L. D. Iroff; *J. Comput. Chem.*, **1**, 76, (1980).
- 33) D. J. Iverson, G. Hunter, J. F. Blount, J. R. Damewood Jr. and K. Mislow; *J. Amer. Chem. Soc.*, **103**, 6073, (1981).
- 34) J. E. Anderson, V. Bru-Capdeville, P. A. Kirsch and J. S. Lomas; *J. Chem. Soc., Chem. Commun.*, 1077 (1994).
- 35) H. J. Schenider and V. Hoppen; *J. Org. Chem.*, **43**, 3866, (1978).
- 36) F. R. Jensen and C. H. Bushweller; *Adv. Alicycl. Chem.*, **3**, 139. (1971)
- 37) A. W. van der Made and R. H. van der Made; *J. Org. Chem.*, **58**, 1262, (1993).
- 38) B. S. Furniss, A. J. Hannaford, P. W. G. Smith and A. R. Tatchell; *Vogel's Textbook of Practical Organic Chemistry*, Fifth Edition, Longman Group UK Limited, p1233 (1989).
- 39) G. M. Whitesides, W. F. Fisher Jr., S. Filippo Jr., R. W. Bashe, and H. O. Howe; *J. Amer. Chem. Soc.*, **91**, 4871, (1969).
- 40) S. Krishnamurthy and H. C. Brown; *J. Org. Chem.*, **47**, 276, (1982).
- 41) M. Bullpit and W. Kitching; *Synthesis*, 316 (1977).

- 42) E. D. Hughes, C. K. Ingold and J. D. H. Mackie; *J. Chem. Soc.*, 3173 (1955).
- 43) G. A. Ola, S. J. Kuhn and S. H. Flood; *J. Amer. Chem. Soc.*, **84**, 1688, (1962).
- 44) J. Novak and C. A. Salemink; *Synthesis*, 597, (1983).
- 45) L. J. Andrews and R. M. Keefer; *J. Amer. Chem. Soc.*, **78**, 4549, (1956).
- 46) F. Sato, M. Inoue, K. Oguro and M. Sato; *Tetrahedron lett.* **44**, 4303, (1979).
- 47) S. S. Hall, S. D. Lipsky, F. J. McEnroe and A. P. Bartels; *J. Org. Chem.*, **36**, 2588, (1971).
- 48) J. M. Lancette and J. R. Brindle; *Can. J. Chem.*, **49**, 2990, (1971).
- 49) D. H. Williams, I. Fleming; “*Spectroscopic Methods in Organic Chemistry*” Fourth edition, McGraw-Hill Book Company Europe, p. 103, (1989).
- 50) B. Nilson, P. Martinson, K. Olsson and R. E. Carter; *J. Amer. Chem. Soc.*, **96**, 3190, (1974).
- 51) U. Berg, T. Lil-Jefors, C. Roussel and J. Sandsrom; *Acc. Chem. Res.* **18**, 80, (1985).
- 52) D. H. Williams, I. Fleming; “*Spectroscopic Methods in Organic Chemistry*” Fourth edition, McGraw-Hill Book Company Europe, p. 92, (1989).
- 53) T. Fujisawa, T. Mori, S. Tsuge and T. Sato, *Tetrahedron lett.*, **24**, 1543 (1983).
- 54) E. J. Corey, P. L. Fuchs, *Tetrahedron lett.*, **36**, 3769, (1972).
- 55) This is a modified version of the procedure described by E. Negishi, S. Baba, *J. Amer. Chem. Soc.*, **97**, 7385 (1975).
- 56) H. M. McCounell *J. Chem. Phys.*, **28**, 430 (1958).